Gas Phase Chemical Physics Program

DOE Principal Investigators'
Abstracts

May, 2018

Chemical Sciences, Geosciences, and Biosciences Division
Office of Basic Energy Sciences
Office of Science
U.S. Department of Energy

The research grants and contracts described in this document are supported by the U.S. DOE Office of Science, Office of Basic Energy Sciences, Chemical Sciences, Geosciences and Biosciences Division.

Foreword

The Gas Phase Chemical Physics program supports fundamental gas phase chemical physics research in four areas: Light-Matter Interactions, Chemical Reactivity, Chemistry-Transport Interactions, and Gas-Particle Interconversion. In addition to its traditional focus on clean and efficient combustion, the program has evolved to support fundamental research that impacts other energy-related areas with an emphasis on understanding, predicting, and ultimately controlling matter and energy at the electronic, atomic, and molecular level. The depth and breadth of this fundamental gas phase chemical physics research is reflected in this collection of abstracts and aligns well with the research objectives of the Department of Energy's Office of Basic Energy Sciences (BES).

We appreciate the privilege of serving in the management of this research program. In carrying out these tasks, we learn from the achievements and share the excitement of the research of the many sponsored scientists and students whose work is summarized in the abstracts published on the following pages.

We thank all of the researchers whose dedication and innovation have advanced DOE BES research. We look forward to our assembly in 2019 for our 39th annual meeting.

Jeff Krause
Wade Sisk

Table of Contents

Table of Contents

Abstracts of Principal Investigator Awards

Molecular Reactivity in Complex Systems

Musahid Ahmed, Martin Head-Gordon, Daniel M. Neumark, David G. Prendergast, Kevin R. Wilson
Lawrence Berkeley National Laboratory, 1 Cyclotron Road, Berkeley, CA-94720.
mahmed@lbl.gov, mhead-gordon@lbl.gov, dmneumark@lbl.gov, dgprendergast@lbl.gov, krwilson@lbl.gov.

Program Scope: We seek to target complex multistep and multiphase chemical transformations that extend beyond elementary unimolecular and excited state reactions. The approach is to build complexity from isolated elementary bimolecular reactions to gas surface reaction dynamics to coupled networks of elementary unimolecular and bimolecular pathways embedded at a gas/solid or liquid interface. In each of these areas, the gas phase is central for controlling reactivity. Activities in this subtask drive new theory and simulation to enrich the molecular level interpretation of experiments. Cross-cutting themes of *Chemistry at Complex Interfaces* and *Reaction Pathways in Diverse Environments* are explored, providing valuable insight into microscopic processes relevant to energy generation, storage and combustion.

Recent Progress: ***Non-covalent Interactions and Molecular Chemistry.*** This research effort investigates proton and charge transfer in hydrogen bonded, π-stacked and solvated systems using synchrotron based molecular beams mass spectrometry coupled with electronic structure calculations of Head Gordon. We have recently developed an experimental strategy for characterizing neutral versus ion-induced growth using in-source ionization of molecular beams with tunable VUV synchrotron radiation.[1] A threshold photoionization of acetaldehyde-water clusters demonstrated that proton transfer occurs between the formyl groups (-CH=O) of one acetaldehyde molecule to another, mediated via a relay-type mechanism with water acting as a bridge.[2] This work was extended to study molecular growth processes in mixed acetylene-ethylene clusters to elucidate ion molecule growth dynamics.[3] Experiments combined with theory suggested that different isomers on the potential energy surface are accessible, it is the isomerization rate that dictates fragmentation. Ahmed and Head-Gordon have formulated an understanding as to how non-covalent interactions can drive chemical reactivity in small acetylene clusters upon photoionization. A dramatic dependence of product distribution on the ionization conditions is observed and interpreted by theory.[4]

Molecular Chemistry of Hydrocarbon Growth & Decomposition. The multistep reaction network of polycyclic aromatic hydrocarbons (PAHs) with indene and naphthalene cores in combustion processes is being examined in collaboration with Ralf Kaiser (Hawaii) and Alex Mebel (Florida International). This is achieved by simulating the combustion relevant conditions (pressure, temperature, reactant molecules) in a high temperature 'chemical reactor'. The reactions of the phenyl radical with oxygen[5] and the reactions of benzyl,[6] and naphthyl[1] radicals with acetylene, shed light on molecular growth mechanisms relevant to soot formation. The reactions of the styrenyl and the *ortho*-vinylphenyl radicals—key transient species of the HACA mechanism—with C_2H_2 does lead to the formation of naphthalene,[7] and the reaction of *ortho*-biphenylyl radical with C_2H_2, also leads to the synthesis of phenanthrene,[8] but not to anthracene. A new mechanism – hydrogen abstraction-vinylacetylene (HAVA) addition is needed in addition to HACA to explain formation of 4 membered rings, demonstrated recently for the 4-phenanthrenyl radical reaction with acetylene.[9] A pathway to a facile pyridine synthesis[5] via the reaction of the cyano vinyl radical with vinyl cyanide, and of (iso) quinoline[5] via the reaction of pyridyl radicals with two acetylene molecules, was demonstrated in the high temperature chemical reactor. The same reactor has also been applied to probe the unimolecular decomposition pathways of jet fuel (decane,[10] dodecane,[11] and *exo*-tetrahydrodicyclopentadiene[12]) decomposition and new radical pathways have been elucidated experimentally and confirmed via theoretical calculations and simulations.

In collaboration with Barney Ellison (Colorado), the photoionization and unimolecular decomposition of cyclopentadienone,[13] and 2,5-dimethylfuran was completed. This work was extended to the furanic ether, 2-methoxyfuran,[14] and a pressure-dependent kinetic model was developed to model the decomposition. A comprehensive pyrolytic and photoionization study on the benzyl radical, $C_6H_5CH_2$,[15, 16] cyclohexanone,[17] (the simplest ketone, which can isomerize to its enol form under thermal conditions) and the thermal decomposition of the simplest carbohydrate, glycolaldehyde, and glyoxal was completed.[18]

Heterogeneous Chemical Reactions: Peroxy Radical Reactions with NO and SO_2. Substantial effort has been dedicated to understanding how gas phase mechanisms of peroxy radicals (RO_2) are modified when they occur at an interface. The reaction of RO_2 + NO was examined[19] for C_{30} branched and n-alkanes as well as a C_{27} ester and no nitrates were produced by heterogeneous reaction in contrast to the gas phase mechanisms. Instead, a substantial acceleration in consumption rate of the alkane or ester in the presence of NO was observed. In a companion study, we examined the analogous reaction albeit with SO_2. In the gas phase, the RO_2 + SO_2 reaction is very slow and is considered an unimportant reaction pathway for peroxy radicals. Extensive measurements failed to detect the formation of organic sulfates and like the NO reaction, we observed dramatic reaction rate enhancements when SO_2 was introduced into the reactor.[20] For both reactions (NO and SO_2) the acceleration mechanisms involves the facile production of alkoxy radicals (RO) from the RO_2 + NO/SO_2 reaction.

In related simulation work with Frances Houle (LBNL), we examined how a previously validated free radical reaction scheme[21, 22] changes as a function of the self-diffusion coefficient of the alkane. We find that diffusive confinement of the reaction to <1 nm of the interface substantially increases the importance of alkoxy radical decomposition reactions, whereas the RO_2+RO_2 pathway is favored in cases where internal mixing of material from the bulk to the interface is rapid compared with the overall OH-surface reaction timescale. In collaboration with Ahmed and Kostko, soft X-ray based velocity map imaging is applied to probe surface chemistry and validate the simulations being performed by Houle.[23, 24]

Another key objective of our work is to understand the molecular mechanism of chemical erosion at simple hydrocarbon interfaces involving the formation and subsequent reaction of Criegee intermediates (CI).[25] To do this, we studied[25] a prototypical ozonolysis reaction using nanoparticles comprised a C_{30} branched alkene with 6 double bonds. The reaction produces substantial quantities of gas phase reaction products leading to the loss of up to 25% of the nanoparticle mass. Kinetic modeling revealed that the molecular mechanisms of erosion is due to the reaction of CI with water which product small molecular weight ketones that evaporate from the interface.

Future Plans: ***Bimolecular gas phase chemistry*** **-** Ahmed in collaboration with Ralf Kaiser plan to understand how larger ring (4 and higher) formation leads to the mass-growth processes from simple PAHs to soot particles utilizing the heated reactor coupled to synchrotron based mass spectrometry. This will be achieved, by preparing the brominated precursor molecules (synthesized by Felix Fischer, LBNL) which can undergo bromine-carbon bond ruptures by pyrolysis leading to radical intermediates that react subsequently with acetylene or vinylacetylene to form coronene, fluoranthene, and/or corannulene. The elucidation of the formation routes of these three key PAHs has the potential to revolutionize the understanding of the underlying mass growth processes from simple precursors via complex PAHs. Alex Mebel has been instrumental in computing reaction mechanisms based upon our observations, and also predicting certain pathways and we will be guided by him in this enterprise. These theoretical and experimental details will be necessary to design and interpret the reaction mechanisms that will no doubt arise as we move towards understanding the 2D and 3 D structures of these carbon growth processes. A new direction is to probe gas phase hydrocarbon reactions in confined spaces such as in zeolites by introducing these species into the heated reactor. We anticipate that our scaled down reactor with chemistry being arrested after microsecond reaction times (typical residence times in our reactor are 20-50 microseconds) will allow for reactive intermediates to be captured in the supersonic expansion of a molecular beam. A key here is that the gas phase chemistry will have been directly probed using the same reactor, to allow a comparison with heterogeneity in the dynamics with an introduction of a surface.

Non-covalent Interactions: Reactions Dynamics in Clusters. We will continue our program on the application of VUV photoionization and theoretical calculations to decipher kinetics, dynamics and photo-induced reactivity in molecular clusters, especially hydrogen-bonded and van der Waals clusters.[26] We will examine glycerol/water and naphthalene/water clusters as prototypical models for hydrophilic and hydrophobic interactions, respectively. Glycerol contains three hydroxyl groups and is miscible with water; we believe that such rich dynamics based upon hydrogen bonding between water and glycerol can become

accessible with a judicious combination of experiments and theory. In contrast to glycerol, naphthalene is moderately hydrophobic and is one of the simplest PAHs. The study of naphthalene-water can also shed light on the understanding of water-graphite and water-graphene interactions, which provide a molecular picture of water confinement of carbon nanotubes. We plan to examine how extending the π cloud across an aromatic ring, moving from benzene, to naphthalene and then to anthracene, is affected by water. Again, a theoretical collaboration with Head-Gordon will be crucial in deciphering the intricate dynamics in these systems.

Gas liquid interface scattering dynamics: Increasing in complexity beyond bimolecular reactive events in clusters, Neumark leads a new direction in gas surface reactions, by examining the elastic, inelastic and most importantly reactive scattering of atoms and free radicals from the liquid interfaces of flat jets. The role of solvent and the surface should affect the dynamics substantially when compared to the analogous dynamics observed in binary gas phase collisions. The incorporation of flat jet technology into Neumark's existing molecular beam scattering instrument will bring a new capability to this program. The proposed experiments will provide unprecedented insights into how the well-understood binary interactions that govern gas phase collision dynamics are modified when one of the scattering partners is a liquid. This approach, which focuses on the "gas side" of the interface, connects to work on multiphase reactions pathways at organic nanoparticles surfaces, examined by Wilson.

Multiphase Reaction Mechanisms: This objective of this effort is to examine how gas phase mechanisms involving the coupling of many elementary steps and reactive intermediates is altered at an interface. Future work will address heterogeneous mechanisms in the OH+alkene, Criegee intermediate + SO_2, and in RO_2 + HO_2 systems. The experimental efforts in gas surface chemistry (Wilson and Neumark) will require new theoretical approaches and simulations techniques (Head-Gordon and Prendergast), which aim to provide new molecular insights into the governing principles that control molecular chemistry at gas liquid/solid surfaces.

Heterogeneous OH + Alkene Reactions: We will extend our work to the examine the heterogeneous reaction mechanisms of alkenes—with a particular focus on understanding the formation and subsequent chemistry of hydroxy-peroxy radicals at interfaces, which are formed by OH addition to C=C. We will build a multiphase kinetic model (in collaboration with F. Houle) and will work with Head-Gordon to obtain theoretical support for pathways that connect hydroxy-peroxy and CI in an effort to further elucidate this potentially important rearrangement step.

Heterogeneous Reactivity of Criegee Intermediates and SO_2: We will extend our studies of Criegee intermediates by examining the role that SO_2 plays in the reaction mechanism. Efforts are underway to develop a fully predictive and quantitative description of this multiphase mechanism. Importantly, this particular example provides new opportunities to examine how reactions at interfaces can be a substantial source of reactive gas phase intermediates.

Heterogeneous RO_2 + HO_2 vs. RO_2 + RO_2 Reaction Pathways: We will elucidate this competition by measuring the heterogeneous kinetics at model hydrocarbon interfaces as a function of both [OH] and [HO_2]. The ratio of RO_2/HO_2 will be altered using established literature methods by adding either gas phase methanol or CO to the reaction vessel, both of which react with OH to form HO_2 in near unity yields as described in the literature.

Interfacial Diffusion of Reactive Species and Resulting Products: As we tackle the more complex aspects of molecular chemistry at interfaces described above, experiments often lack direct insight into the key microscopic processes or elementary steps that govern multistep and multiphase reactions. Prendergast will employ a combination of classical molecular dynamics (MD) modeling of gross molecular assembly, surface structure, and resultant porosity of unsaturated organic molecules (such as squalene), and the rate of infiltration of reactive species (e.g. O_3 or OH) will be explored. Simplified lattice models of kinetics in such systems will be employed to derive the fundamental principles that drive kinetics and depth profiles (i.e. spatial distributions) of products, using inputs from specific quantum mechanical estimates of reaction energetics (based on DFT calculations) and morphology (derived from classical MD).

Work supported by BES-GPCP program (2015-present)

1. D. S. N. Parker, R. I. Kaiser, B. Bandyopadhyay, O. Kostko, T. P. Troy and M. Ahmed, Angew Chem Int Edit **54** (18), 5421-5424 (2015).

2. O. Kostko, T. P. Troy, B. Bandyopadhyay and M. Ahmed, Phys Chem Chem Phys **18** (36), 25569-25573 (2016).

3. B. Bandyopadhyay, T. Stein, Y. Fang, O. Kostko, A. White, M. Head-Gordon and M. Ahmed, J. Phys. Chem. A **120**, 5053–5064 (2016).

4. T. Stein, B. Bandyopadhyay, T. P. Troy, Y. Fang, O. Kostko, M. Ahmed and M. Head-Gordon, Proc. Natl. Acad. Sci. U.S.A. **114** (21), E4125-E4133 (2017).

5. D. S. N. Parker, R. I. Kaiser, T. P. Troy, O. Kostko, M. Ahmed and A. M. Mebel, J Phys Chem A **119** (28), 7145-7154 (2015).

6. D. S. N. Parker, R. I. Kaiser, O. Kostko and M. Ahmed, Chemphyschem **16** (10), 2091-2093 (2015).

7. T. Yang, T. P. Troy, B. Xu, O. Kostko, M. Ahmed, A. M. Mebel and R. I. Kaiser, Angew Chem Int Edit **55** (48), 14983-14987 (2016).

8. T. Yang, R. I. Kaiser, T. P. Troy, B. Xu, O. Kostko, M. Ahmed, A. M. Mebel, M. V. Zagidullin and V. N. Azyazov, Angew Chem Int Edit **56** (16), 4515-4519 (2017).

9. L. Zhao, R. I. Kaiser, B. Xu, U. Ablikim, M. Ahmed, D. Joshi, G. Veber, F. R. Fischer and A. M. Mebel, Nature Astronomy, doi:10.1038/s41550-41018-40399-y (2018).

10. L. Zhao, T. Yang, R. I. Kaiser, T. P. Troy, M. Ahmed, D. Belisario-Lara, J. M. Ribeiro and A. M. Mebel, J. Phys. Chem. A **121** (6), 1261-1280 (2017).

11. L. Zhao, T. Yang, R. I. Kaiser, T. P. Troy, M. Ahmed, J. M. Ribeiro, D. Belisario-Lara and A. M. Mebel, J. Phys. Chem. A **121** (6), 1281-1297 (2017).

12. L. Zhao, T. Yang, R. I. Kaiser, T. P. Troy, B. Xu, M. Ahmed, J. Alarcon, D. Belisario-Lara, A. M. Mebel, Y. Zhang, C. C. Cao and J. B. Zoue, Phys Chem Chem Phys **19** (24), 15780-15807 (2017).

13. G. T. Buckingham, T. K. Ormond, J. P. Porterfield, P. Hemberger, O. Kostko, M. Ahmed, D. J. Robichaud, M. R. Nimlos, J. W. Daily and G. B. Ellison, J Chem Phys **142** (4) (2015).

14. K. N. Urness, Q. Guan, T. P. Troy, M. Ahmed, J. W. Daily, G. B. Ellison and J. M. Simmie, J. Phys. Chem. A **119** (39), 9962-9977 (2015).

15. G. T. Buckingham, T. K. Ormond, J. P. Porterfield, P. Hemberger, O. Kostko, M. Ahmed, D. J. Robichaud, M. R. Nimlos, J. W. Daily and G. B. Ellison, J Chem Phys **142** (4), Artn 044307 (2015).

16. G. T. Buckingham, J. P. Porterfield, O. Kostko, T. P. Troy, M. Ahmed, D. J. Robichaud, M. R. Nimlos, J. W. Daily and G. B. Ellison, J Chem Phys **145** (1), 014305 (2016).

17. J. P. Porterfield, T. L. Nguyen, J. H. Baraban, G. T. Buckingham, T. P. Troy, O. Kostko, M. Ahmed, J. F. Stanton, J. W. Daily and G. B. Ellison, J. Phys. Chem. A **119** (51), 12635-12647 (2015).

18. J. P. Porterfield, J. H. Baraban, T. P. Troy, M. Ahmed, M. C. McCarthy, K. M. Morgan, J. W. Daily, T. L. Nguyen, J. F. Stanton and G. B. Ellison, J. Phys. Chem. A **120** (14), 2161-2172 (2016).

19. N. K. Richards-Henderson, A. H. Goldstein and K. R. Wilson, J. Phys. Chem. Lett. **6** (22), 4451-4455 (2015).

20. N. K. Richards-Henderson, A. H. Goldstein and K. R. Wilson, Environ. Sci. Technol. **50** (7), 3554-3561 (2016).

21. A. Wiegel, M. Liu, W. D. Hinsberg, K. R. Wilson and F. A. Houle, Phys Chem Chem Phys, **19**, 6814-6830 (2017).

22. A. Wiegel, K. Wilson, W. Hinsberg and F. Houle, Phys Chem Chem Phys **17** (6), 4398-4411 (2015).

23. M. I. Jacobs, B. Xu, O. Kostko, N. Heine, M. Ahmed and K. R. Wilson, J Phys Chem A **120** (43), 8645-8656 (2016).

24. M. I. Jacobs, O. Kostko, M. Ahmed and K. R. Wilson, Phys Chem Chem Phys **19** (20), 13372-13378 (2017).

25. N. Heine, F. A. Houle and K. R. Wilson, Environ. Sci. Technol. **51** (23), 13740-13748 (2017).

26. O. Kostko, B. Bandyopadhyay and M. Ahmed, Annu. Rev. Phys. Chem. **67** (1), 19-40 (2016).

Nanoparticle Surface Kinetics and Dynamics by Single Nanoparticle Mass Spectrometry

Scott L. Anderson,
Chemistry Department, University of Utah
315 S. 1400 E.
Salt Lake City, UT 84112
anderson@chem.utah.edu

Program Scope

This project uses a new technique – single nanoparticle mass spectrometry (NPMS) – to enable detailed studies of the surface reaction kinetics of individual laser-heated nanoparticles (NPs) trapped in the gas phase. The initial work is on sublimation and oxidation of carbon NPs, however, the method is broadly applicable to nano-structured refractory materials. The focus is fundamental, specifically on the effects of heterogeneity on NP kinetics. NPMS allows us to characterize the chemical effects of two different types of heterogeneity: 1. NP-to-NP variations in size, shape, and nanostructure that affect reaction kinetics. 2. The distribution of surface sites on *individual NPs*, which cause the NP and its kinetics to evolve with time, as the distribution of sites evolves. In addition to fundamental interest in understanding how heterogeneity affects reaction kinetics, this kind of information is essential to understanding and modeling carbon NP chemistry on a molecular level.

Methodology

The heart of the instrument is the split-ring-electrode quadrupole trap (SRET), shown in Fig. 1.[1] An AC voltage is applied across the trap, with amplitude (V_0) and frequency (F_0), and an NP of mass M and charge Q is injected into the trap. The trapped NP motion can be described as slow "secular" motion, with superimposed micro-motion at frequency F_0.[2] The secular motion is harmonic, with frequencies f_z and f_r, for axial and radial motion, proportional to Q/M. For example, the axial frequency,

$$f_z = \frac{|Q|}{M}\left(\frac{V_0\sqrt{2}}{F_0 z_0^2 4\pi^2}\right),$$

where z_0 is a trap geometric parameter (2.97 mm). The NPMS method is, in essence, to trap a single NP, detecting one or both secular frequencies non-destructively, thereby allowing Q/M to be monitored as a function of time. Q is determined exactly by observing steps in f_z from ±e changes in Q, thus giving M.

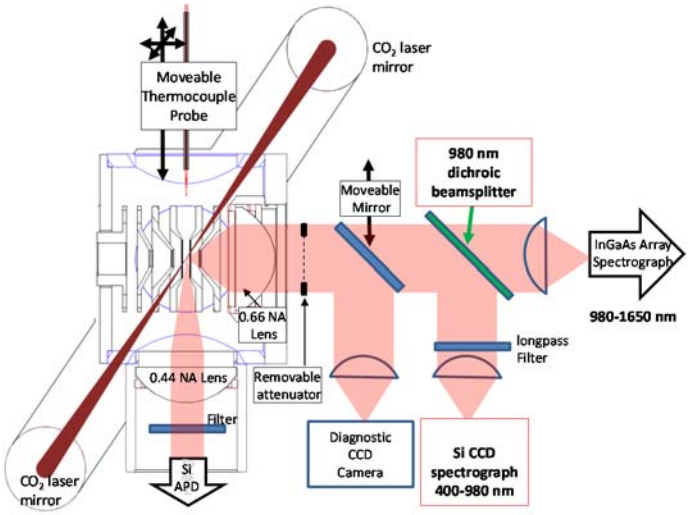

Fig. 1. SRET with optical system

Kinetics for sublimation, addition reactions, and oxidation can be followed over ~5 orders of magnitude by tracking M vs. time, covering a temperature range between 1400 K and 2500 K. NPMS allows the NP-to-NP heterogeneity of particles of different types to be directly measured. In addition, the number of reactive defect and edge sites on each individual NP can be measured using a site titration process, providing NP-by-NP correlations between the number of reactive sites and the kinetics.

Optical emission from the hot NP is used for f_z determination via light detected by an Si avalanche photodiode. In addition, NP temperature (T_{NP}) is determined simultaneously with kinetics, by measuring the emission spectrum from 400 nm to 1650 nm using a pair of array spectrographs. NPs can be heated by a CO_2 laser focused through the trap diagonally, or by 405 nm, 532 nm, or 998 nm lasers focused into the plane of the figure. For graphite, which has been the focus of the work to date, there is no apparent dependence of the kinetics or emission spectra on the excitation wavelength, suggesting that energy randomization is rapid compared to the thermal emission and reaction timescales.

Recent Progress

Prior to the project start in September, we had developed a variety of methods for measuring sublimation and oxidation kinetics in different rate ranges, and for titrating reactive surface sites. Fig. 2 shows a simple oxidation experiment on a graphite NP, initially trapped in 0.3 mTorr of argon buffer gas. A weak drive signal was swept through resonance with f_z (inset), which was ~5.77 kHz initially, corresponding to M/Q of +194 kDa/e. To extract M, a VUV lamp was used to drive ΔQ of ±e, resulting in steps in f_z, shown in the first part of the secular frequency trace (red). The Q values extracted from the step heights are indicated at each step. In this example the initial M (blue trace) was 7.56 MDa (6.29 x 10^5 atoms), equivalent to a 22 nm spherical NP. Initially, the NP slowly sublimed at a rate of dM/dt = 77 Da/minute, or ~0.1 carbon atom/second. When the Ar buffer gas was replaced with O_2 at 0.2 mTorr, the mass loss rate increased to 1.10 kDa/min, increasing with O_2 pressure to 12.71 kDa/min (~18 C atoms/sec) for 9.0 mTorr of O_2. From beam experiments on HOPG, the primary reaction is expected to generate CO, rather than CO_2.[3] Note that the mass loss rates slow noticeably with time at the two higher O_2 pressures, which is attributed to evolution of the surface site distribution as the more reactive edge/defect sites burn away.

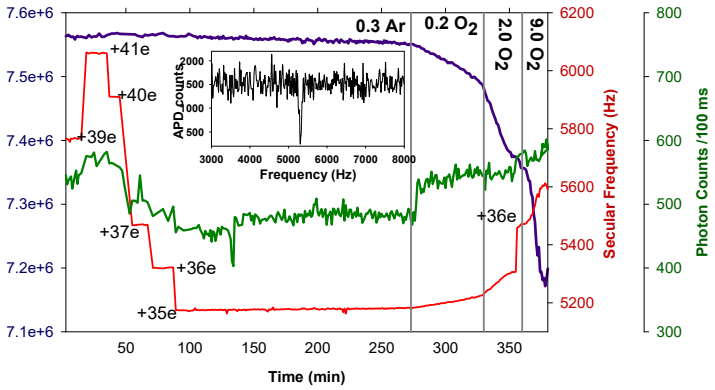

Fig. 2. f_z, APD count rate, and M vs. time for a graphite NP pumped at 532 nm. Q is indicated at each charge step.

Fig. 3 shows a similar experiment in which the oxidative mass loss rate was varied by using the laser intensity to vary T_{NP}. Note that at 92 W/cm^2, the initial oxidative mass loss rate was ~51 kDa/min, but quickly slowed to ~8.2 kDa/min, presumably because a defect/edge-rich region of the NP burned away, leaving a less reactive particle. At 161 W/cm^2, there was initial rapid, steady mass loss, followed by an abrupt event with ΔM = -3.097 MDa and ΔQ = -19e, corresponding to ~40% and ~35%, respectively, of the pre-event M and Q values. Note that Q often *increases* slowly at high T_{NP} due to thermionic electron emission. Here, the NP clearly fissioned.

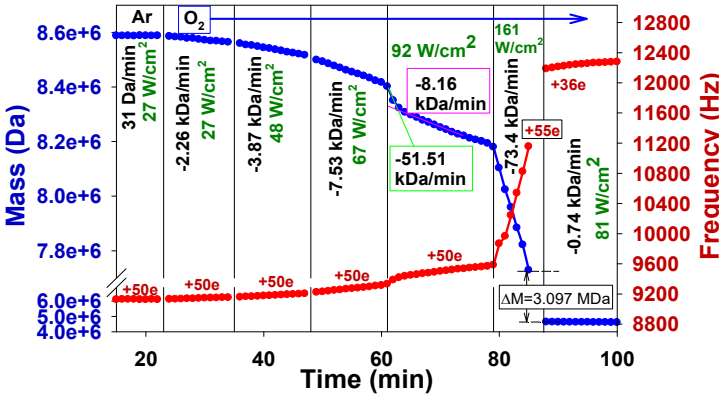

Fig. 3. Graphite NP Oxidation (note ~10x mass scale change)

The observation that oxidation (and sublimation) rates evolve with time for individual NPs points out the desirability of associating kinetics with the number of reactive sites present on the NP surfaces. Graphite basal plane sites are thermodynamically more stable than edge or defect sites, thus the edge/defect sites should sublime and oxidize more quickly. Soot and other carbon NPs also have distributions of surface sites, and this project aims to determine how the heterogeneity of surface sites correlates with sublimation and oxidation kinetics.

Fig. 4 shows how titration can be used to count reactive sites. At the end of an experiment like that in Fig. 2, the NP was trapped in Ar and charge stepped to verify M, then Ar was replaced by 0.25% C_2H_2 in He, leading to an abrupt mass gain of 158 kDa, and when O_2 reintroduced, there was a long induction period for oxidation. The fact that the mass gain was fast, but small and self-limiting, suggests that C_2H_2 added to reactive sites (e.g. edges and defects), C-H terminating them so that they no longer

were reactive toward C_2H_2, and much less reactive toward O_2 as well. The net mass gain, therefore, provides a way to estimate the number of reactive sites on the NP surface, in this case ~12,150.

Current work

Our recent work has been focused on the remaining problem – fast and accurate T_{NP} determination. The approach is to measure emission spectra as the NPs are reacting, then fit them to a Planck-like expression to extract temperature:

$$I(\lambda, T) = \frac{2hc^2}{\lambda^5} \frac{1}{e^{\frac{hc}{\lambda kt}} - 1} \cdot \epsilon(\lambda).$$

From a practical perspective, the problem is calibrating the λ dependence of the detection efficiency of the optical system. It is critical that this be done for the system as a whole under conditions identical to those used for NP measurements, i.e., without disturbing the collection optics, under vacuum, and with similar signal intensities. To provide a broadband calibration source that fits in the trap, we use a micro-thermocouple (75μm wire), mounted on an XYZ manipulator to allow precise positioning in the trap center. The junction is heated by the CO_2 laser, and imaged through apertures onto the spectrograph collection optics, using carefully characterized ND filters to drop the intensity into the same range as that produced by the NPs. We can read the emitter temperature directly from the junction voltage, and since ϵ(λ) is well known for W and Re, we can predict the thermal emission spectrum accurately, and thus determine how detection efficiency varies with λ.

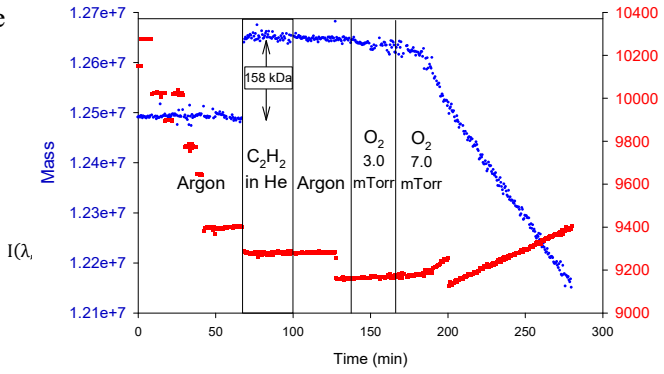

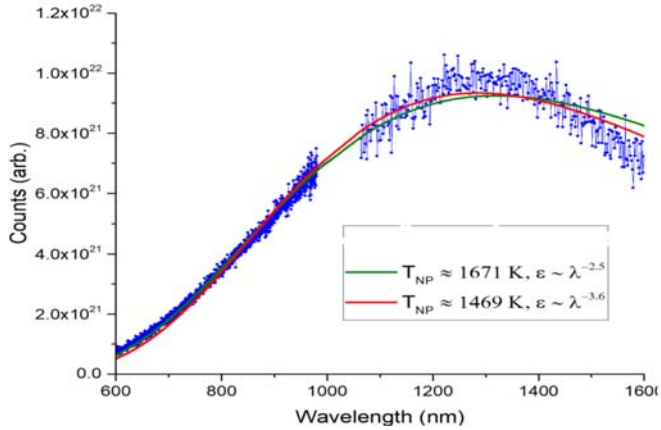

Fig. 5. Single NP emission spectrum

There are also several fundamental points of interest, including how large a single, isolated NP must be to be "thermal", whether surface states or localized sp^2 domains give rise to structured emission, and what should be used for the emissivity, ϵ(λ). From scattering theory, and published graphite optical constants (permittivity), we might expect that ϵ for an NP much smaller than λ should vary roughly like $\lambda^{-2.5}$, however, this does not take into account effects such as temperature effects on electronic band filling. Fig. 5 shows an example single NP spectrum, acquired in 10 seconds. Also shown is a fit to the spectrum assuming $\epsilon(\lambda) \sim \lambda^{-2.5}$. Note that the experimental spectrum shows significantly greater curvature than this simple ϵ(λ) model predicts. The second fit used $\epsilon(\lambda) \sim \lambda^n$, with n variable, but it is not possible to fit the spectrum well with this approximate form for ϵ(λ). This is new scientific territory to a large extent, because existing carbon NP dispersed emission spectra (e.g.[4-5]) have been for ensembles, and covered a narrower wavelength range (e.g. 400 – 900 nm), reducing their sensitivity to the λ dependence of ϵ. We are investigating models to incorporate temperature effects in ϵ(λ).

Fig. 6 shows an example of kinetics measured with simultaneous T_{NP} determination, in this case for sublimation of a graphite NP with initial mass of 28.007 MDa, heated with the CO_2 laser. At present, this experiment is only partly automated, thus T_{NP} is only measured periodically, however, the time scales are such that it is feasible to measure T_{NP} during each mass measurement. In addition, the active stabilization of the CO_2 laser was disabled for this measurement, resulting in some slow T_{NP} drift. During the initial period, T_{NP} drifted from ~1594 to ~1586 K, and the sublimation rate averaged 11 carbon atoms/sec, or ~4 ppm/sec. When T_{NP} was raised to ~1649 K, the rate increase to 50 atoms/sec, and raising the temperature to ~1666 K increased the rate to 63.5 atoms/sec, followed by a drop to 8 atoms/sec

when T_{NP} was returned to 1575 K. When automation of the experiment is complete, the laser stability, frequency of T_{NP} determination, and range of rates that can be studied will increase substantially.

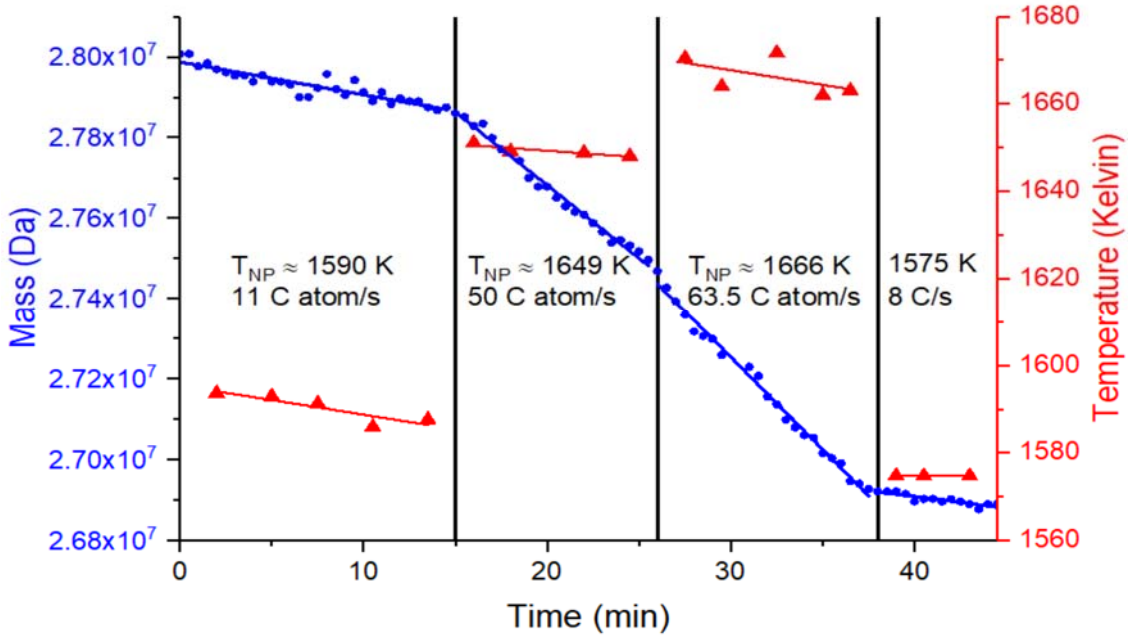

Fig. 6. Sublimation kinetics for a 28 MDa graphite NP as a function of temperature.

Future plans

We are currently working on two fronts – completing automation and integration of the kinetics and T_{NP} determination processes, and carrying out a detailed study of thermal emission spectroscopy of carbon NPs as a function of size, charge, temperature, excitation wavelength, background gas, etc. The latter is necessary to understand the T_{NP} determination process, but will also be of significant interest to research communities that use thermal emission from NP to measure local temperatures in reacting flows or other environments.

Then, we will begin a series of studies of sublimation and oxidation kinetics and dynamics for different types of carbon NPs, including nanodiamonds, c-dots, graphene platelets, graphite. The plan is to first understand the kinetics and structure-reactivity relationships for these relatively simple forms of carbon, and then to transition to more complex, combustion-related carbon such as carbon blacks, and eventually sampled soot.

References

1. Gerlich, D.; Decker, S., Trapping Ions at High Temperatures: Thermal Decay of C_{60}^+. *Appl. Phys. B: Lasers Opt.* **2014,** *114*, 257-266.
2. Schlemmer, S.; Illemann, J.; Wellert, S.; Gerlich, D., Nondestructive High-Resolution And Absolute Mass Determination Of Single Charged Particles In A Three-Dimensional Quadrupole Trap. *J. Appl. Phys.* **2001,** *90* (10), 5410-5418.
3. Murray, V. J.; Marshall, B. C.; Woodburn, P. J.; Minton, T. K., Inelastic and Reactive Scattering Dynamics of Hyperthermal O and O_2 on Hot Vitreous Carbon Surfaces. *J. Phys. Chem. C* **2015,** *119*, 14780-14796.
4. Landstrom, L.; Elihn, K.; Boman, M.; Granqvist, C. G.; Heszler, P., Analysis of ThermalRradiation fromLlaser-Heated Nanoparticles Formed by Laser-Induced Decomposition of Ferrocene. *Appl. Phys. A* **2005,** *81*, 827-833.
5. van de Wetering, F. M. J. H.; Oosterbeek, W.; Beckers, J.; Nijdam, S.; Kovačević, E.; Berndt, J., Laser-induced incandescence applied to dusty plasmas. *J. Phys. D: Appl. Phys.* **2016,** *49*, 295206 (10 pp).

Fundamental Interactions of Kinetics and Transport in Reacting Flows

Robert S. Barlow
Combustion Research Facility
Sandia National Laboratories, MS 9051
Livermore, California 94550
barlow@sandia.gov

Program Scope

This program is directed toward achieving a more complete and quantitative understanding of fundamental interactions of chemical kinetics, molecular transport, and turbulent mixing in gas-phase reacting flows. Simultaneous line imaging of spontaneous Raman scattering, Rayleigh scattering, and two-photon laser-induced fluorescence (LIF) of CO is applied to obtain spatially and temporally resolved measurements of temperature, all major species, mixture fraction, and reaction progress, as well as gradients in these quantities in hydrocarbon flames. The instantaneous three-dimensional orientation of the reaction zone is also measured by imaging of OH LIF in two crossed planes, which intersect along the laser axis for the multiscalar measurements. These combined data characterize both the thermo-chemical state and the instantaneous flame structure, such that the influence of turbulent mixing and molecular transport on flame chemistry may be quantified. Innovations in both hardware and methods of data analysis have achieved unmatched spatial resolution and precision of multiscalar measurements. Our experimental work is closely coupled with international collaborative efforts to develop and validate advanced predictive models for reacting flows. This is accomplished through our visitor program and through the TNF Workshop series.

Recent Progress

Novel Method to Determine Heat Release Rate and Chemical Mode from Raman/Rayleigh Data

Over the past year we have realized a significant breakthrough in developing experimental tools to better understand the fundamental structure and dynamics of partially premixed flames that exhibit multiple modes of combustion. That is, local reaction zones within the overall flame can have structures that are dominantly premixed (propagating front), dominantly nonpremixed (controlled by inter-diffusion of initially separated reactants), or combinations of both types of reaction zones. In collaboration with researchers at the Technical University of Darmstadt, Germany (S. Hartl, C. Hasse, D. Geyer, and A. Dreizler), we have demonstrated that the local heat release rate and chemical explosive mode (Lu et al., *J.Fluid Mech.* 2010, Shan et al., *Combust. Flame* 2012) can be determined from Raman/Rayleigh measurements of major species (N_2, O_2, CH_4, CO_2, H_2O, CO, and H_2) and temperature. This is done by taking the measured scalars for each instantaneous, spatially-resolved sample as initial conditions for a constrained, constant temperature, constant pressure, homogeneous batch reactor calculation (Hartl et al., *Combust. Flame*, 2018). As the calculation proceeds, radicals and minor species build up to reach a steady state consistent with the constrained major species and temperature, yielding an approximation of the full thermochemical state of the sample. The chemical mode, which is calculated from the chemical Jacobian, and heat release rate are then calculated from this approximate full state.

As reported in our 2017 abstract, the method was developed and validated using measurements and simulations of laminar counterflow methane/air flames. More recently, the method was applied to measurements within the stabilization region of lifted turbulent methane jet flames and to simulations of laminar triple flames, as illustrated in Fig. 1 (Hartl et al., *Combust. Flame* 2018). These flames stabilize where there is a transverse gradient in mixture fraction, such that the leading edge has lean and rich premixed branches and a trailing nonpremixed flame aligned along the stoichiometric contour (orange line). The green contour in Fig. 1 marks that chemical mode (CM) zero crossing, which has been shown by Lu and coworkers (*Combust. Flame* 159, 2012) to be an effective marker of a premixed reaction zone or autoignition front.

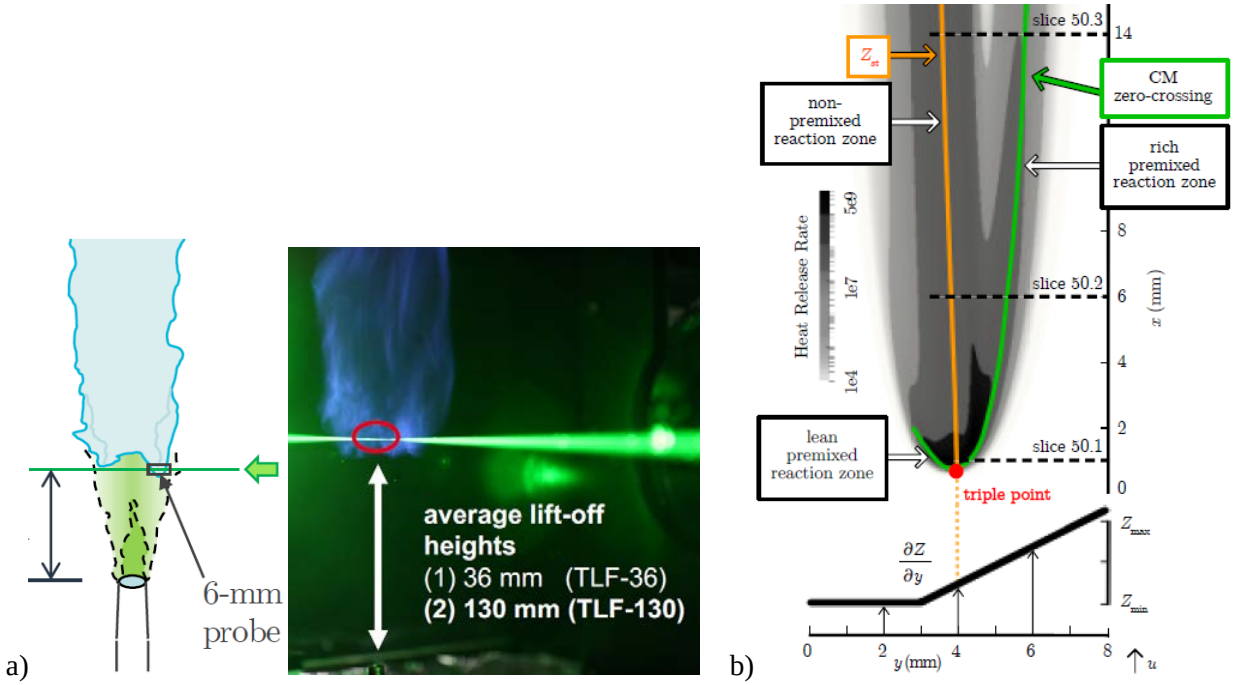

Fig. 1. a) Experimental lifted flame configuration and photo showing flame TLF-130.
b) Illustration of a laminar triple flame simulation with heat release rate shown in gray, CM zero crossing in green, and stoichiometric contour in orange.

The experimental results in Fig. 2 from the turbulent flames show strong correlations among the heat release rate at the CM zero crossing, HRR_{CM}, the change in magnitude of the chemical mode at the zero crossing, ΔCM, and the mixture fraction at the CM zero crossing, Z_{CM}. Briefly, results show that when the when the CM zero crossing occurs within the most reactive range of mixture fraction ($0.05 < Z_{CM} < 0.065$), the maximum heat release rate occurs at the location of the zero crossing, the magnitude of change in CM is large ($\Delta CM < 6$), and reaction zone can be characterized as dominantly premixed. As the CM zero crossing moves outside this most reactive range, HRR_{CM} and ΔCM both decrease rapidly, and the location of the maximum heat release rate separates spatially and in mixture fraction from the CM zero crossing, such that the overall structure become dominantly nonpremixed. (Note that HRR_{max} is evaluated separately on lean and rich sides of the stoichiometric mixture fraction.) Trends in the experimental results are consistent with those from the simulations across more than three orders of magnitude in heat release rate. Furthermore, numerical tests have shown that the accuracy of the heat release rate can be significantly improved if OH is included as an input to the homogeneous reactor calculation along with major species and temperature.

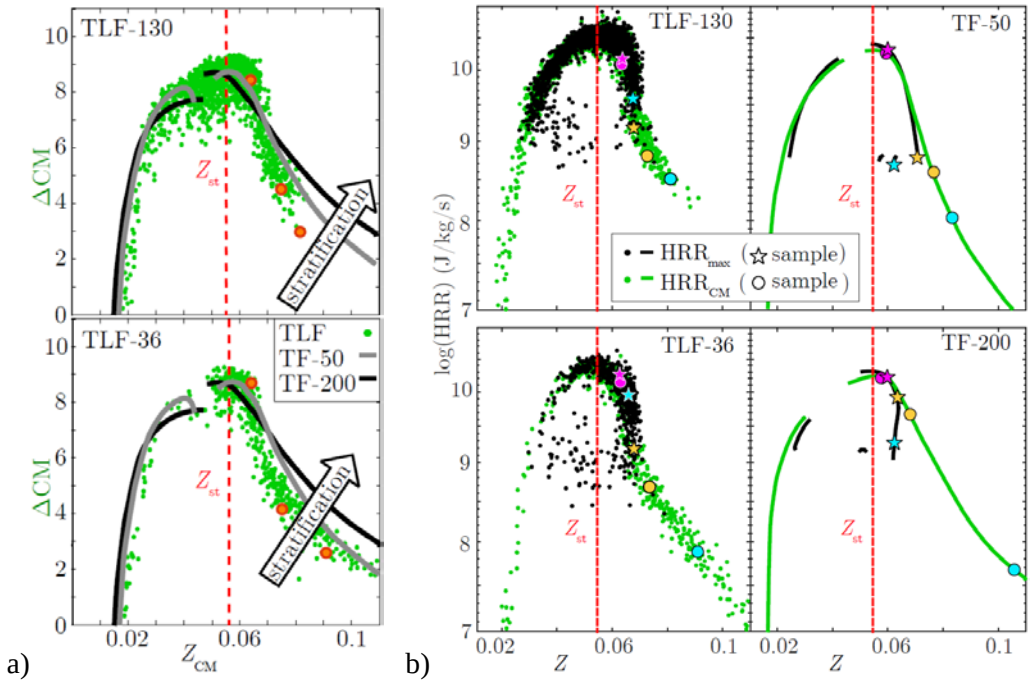

Fig. 2. a) ΔCM plotted as a function of Z_{CM} for both turbulent lifted flames and both laminar triple flame simulations. b) HRR_{max} and HRR_{CM} each plotted against the corresponding mixture fraction. The large symbols (star and circle) correspond to example profiles used in Ref [23] and in Fig. 6.

Figure 3 illustrates the potential benefit of experiments that combine quantitative OH LIF with high-precision, line-imaged Raman/Rayleigh measurements. The instantaneous profiles of CM and HRR are derived from a direct numerical simulation (DNS) of a lean premixed methane/air jet flame (Wang et al. *Proc. Combust. Inst.* 2017), with red curves corresponding to the full DNS, black to the approximation starting from DNS values for major species and temperature, and green to the approximation with OH added as an input to the constrained homogeneous reactor calculation. Differences in CM come mainly from CM being set to zero for T < 1000 K in the approximation approach. Inclusion of OH yields approximated HRR results in close agreement with the original DNS results. Sensitivity of the approximation to experimental uncertainty is being evaluated.

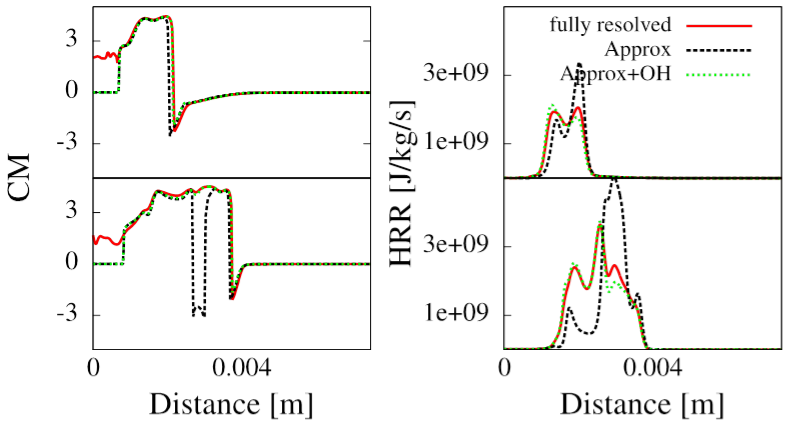

Fig. 3. Comparison of 1D profiles of CM and HRR in a turbulent premixed flame calculated directly from DNS (red), from the approximation starting with temperature and major species (black), and from the approximation with OH included as a constrained input (green).

Other Progress

Papers were published or accepted during the past year on turbulent stratified combustion (Stahler et al.; Straub et al.; Schneider et al.), dual-resolution Raman measurements of six hydrocarbon species and twelve species overall, including N_2, O_2, H_2O, CO_2, CO, H_2, CH_4, DME, CH_2O, C_2H_2, C_2H_4, and C_2H_6 (Magnotti et al.), and scalar dissipation measurements in partially premixed methane and DME flames (Cutcher et al.; Fuest et al.). Experimental data from this program continues to play a central role in focusing efforts of many international experimental and computational research groups toward development of predictive simulation capabilities for complex gas-phase reacting systems for chemical energy conversion.

Future Plans

As directed by BES, research on turbulent combustion at Sandia under this program will be terminated by the end of FY18. After the TNF14 Workshop (Dublin, July 27-28, 2018), the Technical University of Darmstadt, Germany will assume the leadership role for future TNF workshops.

BES Supported Publications (2016 - present)

Kamal, M.M.; Barlow, R.S.; Hochgreb, S., Scalar structure of turbulent stratified swirl flames conditioned on local equivalence ratio, *Combust. Flame* **2016**, *166*, 76–79.

Cutcher, H.C.; Magnotti, G.; Barlow, R.S.; Masri, A.R., Turbulent Flames with Compositionally Inhomogeneous Inlets: Resolved Measurements of Scalar Dissipation Rates, *Proc. Combust. Inst.* **2017**, *36*, 1737–1745.

Stahler, T.; Geyer, D.; Magnotti, G.; Trunk, P.; Dunn, M.J.; Barlow, R.S.; Dreizler, A., Multiple conditioned analysis of the Turbulent Stratified Flame A, *Proc. Combust. Inst.* **2017**, *36*, 1947–1955.

Magnotti, G.; Barlow, R.S., Dual-Resolution Raman Spectroscopy for Measurements of Temperature and Twelve Species in Hydrocarbon-Air Flames, *Proc. Combust. Inst.* **2017**, *36*, 4477–4485.

Barlow, R.S.; Magnotti, G.; Cutcher, H.C.; Masri, A.R, On defining progress variable for Raman/Rayleigh experiments in partially-premixed methane flames, *Combust. Flame* **2017**, *179*, 117–129.

Fuest, F.; Barlow, R.S.; Magnotti, G.; Sutton, J.A., Scalar dissipation rates in a turbulent partially-premixed dimethyl ether/air jet flame, *Combust. Flame* **2018**, *188*, 41–65.

Hartl, S.; Geyer, D.; Dreizler, A.; Magnotti, G., Barlow, R.S.; Hasse, C., Reaction zone detection and characterization from Raman/Rayleigh line measurements in partially premixed flames, *Combust. Flame* **2018**, *189*, 126–141.

Hartl, S.; Van Winkle, R.; Geyer, D.; Dreizler, A.; Magnotti, G.; Hasse, C.; Barlow, R.S., Assessing the relative importance of flame regimes in Raman/Rayleigh line measurements of turbulent lifted flames, *Proc. Combust. Inst.* (accepted).

Scheider, S.; Geyer, D.; Magnotti, G.; Dunn, M.J.; Barlow, R.S.; Dreizler, A., Structure of a stratified CH_4 flame with H_2 addition, *Proc. Combust. Inst.* (accepted).

Straub, C.; Kronenburg, A.; Stein, O.; Barlow, R.S.; Geyer, D., Modelling stratified flames with and without shear using multiple mapping conditioning, *Proc. Combust. Inst.* (accepted).

TNF Workshop Information: http://www.sandia.gov/tnf
TNF13 Workshop Proceedings: http://www.sandia.gov/TNF/13thWorkshop/TNF13.html

Predictive Large-Eddy Simulation of Supercritical-Pressure Reactive Flows in the Cold Ignition Regime

Josette Bellan
Mechanical and Civil Engineering Department, California Institute of Technology
Pasadena, CA 91125
Josette.Bellan@jpl.nasa.gov
DOE Award Number: **02_GR-ER16107-14-00**
STRIPES award number: **SC0002679/0009**

I. Program Scope

This study addresses issues highlighted in the Basic Energy Needs for Clean and Efficient Combustion of 21st Century Transportation Fuels (DOE BES, 2006) under the topic of Combustion under Extreme Pressure. It is there noted that "the most basic concepts of thermal autoignition" are "based on experience and theory at near atmospheric pressures" and that "as pressure increases significantly…, many of these conceptual pictures begin to change or disappear". It is also stated "A better description of the coupling and interaction of high pressure flow and molecular transport processes with chemistry is also necessary", particularly because "Ignition and flame propagation of alternative and renewable fuels, as well as of the changing feed stocks of conventional fossil-based fuels, are very likely to be much different at very high pressures than under the more familiar, lower pressure conditions of current engines." Recognizing that "Under such *(increasing pressure)* conditions distinctions between gas and liquid phases become moot, new equations of state must be used…", it is immediately apparent that there must be "a re-examination of the basic assumptions that govern the physics and chemistry related to combustion; and the need for this type of re-examination increases as the combustion pressure increases." This recognition is also stated under the topic of Multiscale Modeling since due to the new equations of state "The combination of unexplored thermodynamic environments and new physical and chemical fuel properties results in complex interactions among multiphase *(according to the above, the multiphase distinction becomes moot with increasing pressure)* fluid dynamics, thermodynamic properties, heat transfer, and chemical kinetics that are not understood even at a fundamental level." From the theoretical viewpoint for "systems at high pressure, fluid dynamic time scales can be comparable to chemical time scales." and therefore "completely diffusion-controlled reactions … can become important".

Thus, the objective of this study is the investigation of the coupling among thermodynamics, transport properties, intrinsic kinetics and turbulence under the high-pressure and the relatively (with respect to combustion) low-temperature conditions typical of the auto-ignition regime, with particular emphasis on the manifestation of this coupling on the effective kinetic rate. Our collaboration with Dr. Joseph Oefelein is continuing, and we also had past interactions with Drs. A. Wagner and S. Klippenstein of Argonne National Laboratory.

II. Recent Progress

This report contains results obtained during the previous year of funding. The focus of the research during that year was on obtaining an accurate model of the turbulent reaction rate under high-pressure (high-p) conditions and on examining the influence of the simplified representation of a mixture composition as far as the behavior of each species. To this effect we conducted **(1)** an analysis of our Direct Numerical Simulations (DNS) high-p reactive flow database [i] using the Conditional Source-term Estimation (CSE) method [ii], and **(2)** DNS of

increasingly complex mixtures, adding trace species to major species which represented the simplest representation of a complex composition.

(1) The DNS database considered is of a temporal three-dimensional mixing layer having coordinates (x_1,x_2,x_3) and the analysis is performed at the time station of the domain-integrated peak pressure. In CSE [iii], it is assumed that (a) conditional fluctuations can be neglected, (b) the probability density function (pdf) of the conditioning variable can be modeled as a function of only its mean and variance and (c) the conditional averages of the reactive scalars have modest gradients in space. One of the most important assumptions, which is a consequence of applying the first moment Conditional Moment Closure (CMC) approximation is that the conditioned and filtered reaction rate has a value close to that of the reaction rate computed as a function of the filtered and conditioned thermodynamic variables. For high-p turbulent reactive flows this assumption appears problematic since the non-linearity of the chemical source term is compounded by the highly non-linear equation of state. Figure 1(left) illustrates the CSE results obtained using no modeling of the conditional averages and using several mixture fraction pdfs including the exact pdf; the lack of success shows that the CSE method, as applied, is not valid for high-p flows. Thus, the pdf cannot be considered responsible for the lack of accuracy; the suspicion is that single-conditioning cannot sufficiently minimize the conditional fluctuations in this very non-linear problem. Figure 2(right) shows that the agreement between the DNS values and DCSE using the DNS information as inputs is excellent; this is a significant improvement over using CSE. Also, the β pdf combined with DCSE does not perform well, indicating that when the region of modeling is narrowed down through a second conditioning, the deficiency of the β pdf becomes apparent. While the statistical independence between mixture fraction and temperature may also be problematic, we believe that the β pdf form is the largest source of discrepancy, requiring further investigation on the modeling of its exact form provided by the DNS.

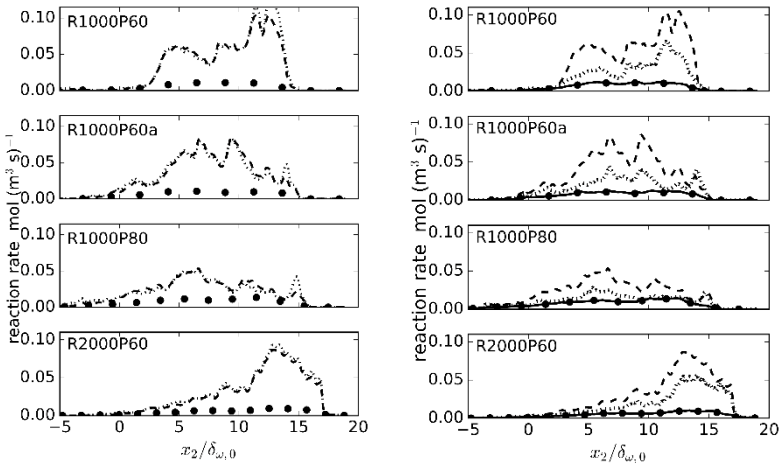

Figure 1. Homogeneous-plane averaged filtered reaction rate obtained for the four DNS cases with (left) CSE by only conditioning over the mixture fraction (dashed lines denote the CSE closure with the exact DNS pdf; dotted lines label the CSE closure with the β pdf), and (right) CSE double conditioning (DCSE) over mixture fraction and temperature (dashed line denotes CSE with the β pdf; dotted line labels DCSE using the product of the two β pdfs; full line denotes DCSE with the exact DNS extracted pdf). Symbols identify the DNS target values; $\delta_{\omega,0}$ is the initial momentum thickness.

(2) The behavior of species in a complex mixture has been studied by creating a DNS database of increasingly complex mixtures -- 2, 3, 5 and 7 species – in a three-dimensional temporal mixing layer configuration at different initial Reynolds number values, and at same free-stream temperature and pressure for all simulations. Each simulation was conducted past a time at which the layer had turbulence characteristics, and the analysis was performed at that time station. Because the species had very disparate initial mass fractions, a normalization was performed to bring this new normalized mass fraction Ξ within the [0,1] interval. This normalization reveals (Fig. 2 top left) that whereas the major species (i.e. n-heptane and oxygen)

experience normal diffusion as their Ξ pdfs varies between 0 and 1, all minor species exhibit uphill diffusion and their Ξ pdfs assume negative values and values larger than 1. This means that regions of concentrated species (α) will form, however, at no time did we detect these species present with mass fraction of unity, meaning that species do not segregate. The effective mass diffusion coefficients (Fig. 2 top right) entirely support the physics of minor species undergoing uphill diffusion and additionally show that H2, the lightest molecule, is that undergoing the most severe uphill diffusion, as also supported by the widest tails in the corresponding pdf of Ξ. We attribute this H_2 prevalence of uphill diffusion over the entire mixing layer to a combination of the light and small aspects of the H_2 molecule, conferring to it greater mobility. Examination of the effective Schmidt and Lewis numbers of these species shows that none of them behaves as species do under perfect gas conditions. Indeed, the most probable value of $Sc_{Hep,eff} \approx Sc_{Oxy,eff} \approx 1.2$ rather than 0.7 as in perfect gas, and these mean values are very statistically significant. $Sc_{\alpha,eff}$ for the minor species are between 1.5-2 for CO, CO_2 and H_2O, whereas it is approximately 0.7 for H_2 for which heavier tails are observed than for all other minor species; these mean values for the minor species are less representative than for the major species. No species has a mean $Le_{\alpha,eff}$ of 1, thus invalidating one of the most commonly used assumptions in combustion simulations. In fact, the most probable $Le_{\alpha,eff}$ values are ≈0.45 for n-C_7H_{16} and O_2, ≈0.75 for CO, CO_2 and H_2O, and ≈0.35 for H_2. Thus, the diffusional properties of species having a crucial role in combustion are greatly different, and this aspect must be taken into account in combustion simulations.

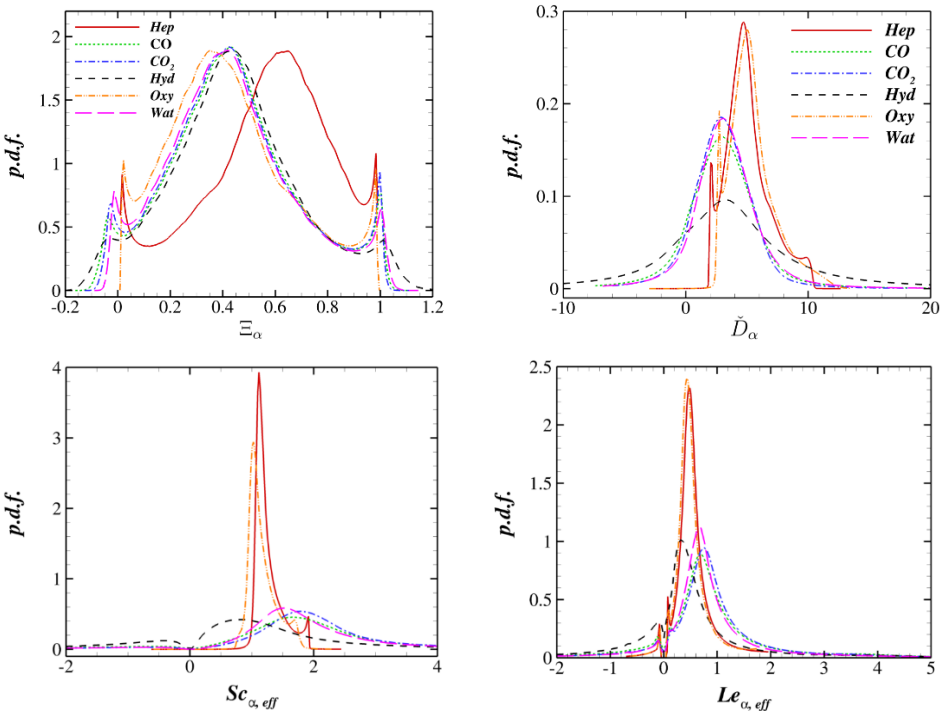

Figure 2. Probability density functions (pdfs) obtained over a mixing layer portraying seven-species mixing; the pdfs are shown at the transitional state. (top left) normalized mass fraction; (top right) effective diffusion coefficient in 10^{-7} m^2/s; (bottom left) effective species-specific Schmidt number; and (bottom right) effective species-specific Lewis number.

The PI has continued the collaboration with Dr. Oefelein and has interacted when warranted with researchers at Argonne National Laboratory.

III. Future Plans

The following activities are planned:

- Develop a model for the mixture fraction pdf in the presence of differential diffusion.
- Develop a DNS database for seven species undergoing two reactions, to study the combustion characteristics compared to those obtained for one reaction among 5 species.

IV. References

i. Bellan, J., *Combust. Flame.*, **2017** *176* 245
ii. Bellan, J., *Combust. Flame.*, **2017** *179* 253
iii. Bushe, W. K and Steiner, H., *Phys. Fluids.* **1999** *11(7)* 1896

V. Publications, presentations, submitted articles supported by this project 2015- 2018

[1] Borghesi, G.; Bellan, J., Irreversible entropy production rate in high-pressure turbulent reactive flows, *Proc. of the Comb. Inst.*, 35, 1537-1547, 2015

[2] Borghesi, G.; Bellan, J., *A priori* and *a posteriori* analysis for developing Large Eddy simulations of multi-species turbulent mixing under high-pressure conditions, *Phys. Fluids*., 27, 035117 (35 pages), 2015

[3] Bellan, J., Direct Numerical Simulation of a high-pressure turbulent reacting mixing layer, *Combust. Flame*, 176, 245-262, 2017

[4] Gnanaskandan, A.; Bellan, J., Numerical Simulation of jet injection and species mixing under high-pressure conditions, in print *Journal of Physics*, Institute of Physics Conference Series: Materials Science and Engineering, 2017

[5] Bellan, J., Evaluation of mixture-fraction-based turbulent-reaction-rate model assumptions for high-pressure reactive flows, *Combust. Flame*, 179, 253-266, 2017

[6] Gnanaskandan, A.; Bellan, J., Large Eddy Simulations of high pressure jets : Effect of subgrid scale modeling, submitted to the *AIAA Progress Series* book titled *High Pressure Flows for Propulsion Applications* (Ed. J. Bellan), 2017

[7] Christopher, N.; Hickey, J.-P.; De Graaf, S.; Bellan, J.; Bushe, W. K.; Devaud C. B., Assessment of Conditional Source-term Estimation for High Pressure Turbulent Combustion Modeling, submitted to the *Proceedings of the Combustion Institute*

[8] Gnanaskandan, A.; Bellan, J., Side-jet effects in high-pressure turbulent flows: Direct Numerical Simulation of nitrogen injected into carbon dioxide, revised version submitted to the *J. Supercritical Fluids*

[9] Bellan, J., Modeling and numerical simulations of multi-species high-pressure reactive flows, **Invited Plenary Lecture**, Summer Program of the SFBTRR40, Institute of Aerodynamics and Fluid Mechanics Technische Universität München, Garching, Germany, August 3, 2015

[10] Bellan, J., Modeling and numerical simulations of multi-species high-pressure reactive flows, **Invited Seminar**, Purdue University, West Lafayette, IN., October 22, 2015

[11] Bellan, J., Reduced models for the simulation of multi-scale problems in physics and chemistry, **Invited Seminar**, Cornell University, Ithaca, NY., November 17, 2015

[12] Bellan, J., Modeling and Numerical Simulations of Multi-Species High-Pressure Turbulent Mixing and Combustion, **Invited Seminar,** SpaceX, Hawthorne, CA., 12/14/2016

[13] Borghesi, G.; Bellan, J., Models for the LES equations to describe multi-species mixing occurring at supercritical pressure, paper 2014-0823 presented at the 52nd Aerospace Sciences Meeting, New Harbor, MD, January 13-17, 2014 Borghesi, G. and Bellan, J., Irreversible entropy production rate in high-pressure turbulent reactive flows, *Proc. of the Comb. Inst.*, 35, 1537-1547, 2015

[14] Borghesi, G.; Bellan, J., *A priori* and *a posteriori* analyses of multi-species turbulent mixing layers at supercritical-*p* conditions, paper 2015-0162 presented at the 53rd Aerospace Sciences Meeting, Kissimmee, FL., January 5-9, 2015; also presented at the 9th US National Combustion Meeting, Cincinnati, OH., May 17-20, 2015

[15] Bellan, J., The mixture fraction for high-pressure turbulent reactive flows, paper 2016-1686 presented at the 54th Aerospace Sciences Meeting, San Diego, CA, January 4-8, 2016

[16] Gnanaskandan, A.; Bellan, J., Large Eddy Simulations of high pressure jets: Effect of subgrid scale modeling, paper 2017-1105 presented at the 55th Aerospace Sciences Meeting, Grapevine, TX, January 9-13, 2017

[17] Sciacovelli, L.; Bellan, J., Mixing in high pressure flows: the influence of the number of species, paper 2018-1189, presented at the 56th Aerospace Sciences Meeting, Kissimmee, FL., January 8-12, 2018

Dynamics of Product Branching from Radical Intermediates in Elementary Combustion Reactions

Laurie J. Butler (PI) and David A. Mazziotti
The University of Chicago, The James Franck Institute
929 E 57th St, Chicago, IL 60637
l-butler@uchicago.edu and damazz@uchicago.edu

I. Program Scope

While the total rate constant for many elementary reactions is well-characterized, understanding the product branching in complex reactions presents a formidable challenge. To gain an incisive probe of such reactions, our experiments investigate the dynamics of the product channels that arise from transient radical intermediates along the bimolecular reaction coordinates. Our recent published work[1-8] uses the methodology developed in my group in the last fifteen years, using both imaging and scattering apparatuses. The experiments generate a particular isomeric form of an unstable radical intermediate along a bimolecular reaction coordinate and study the branching between the ensuing product channels of the energized radical as a function of its internal rotational and vibrational energy under collision-less conditions.

The experiments use a combination of: 1) measurement of product velocity and angular distributions in a crossed laser-molecular beam apparatus, with electron bombardment detection in my lab in Chicago or 2) with tunable vacuum ultraviolet photoionization detection at Taiwan's National Synchrotron Radiation Research Center (NSRRC), and 3) velocity map imaging using state-selective REMPI and single photon VUV ionization of radical intermediates and reaction products. We also employ tunable VUV photoionization detection in our imaging apparatus, using difference frequency four-wave mixing to produce photoionization light tunable from 8 to 10.8 eV. This year of support funded our work to photolytically generate the radical intermediate important in the OH + propene reaction when OH adds to an end carbon. We describe our results on the product channels of the photolytic precursor and some of the dissociation channels of the radical intermediate in Section II.A below. Our other major result this past year was on the photoionization detection of vinoxy radicals. Our experiments at the NSRRC definitively show that vinoxy dissociatively ionizes to both CH_3^+ and HCO^+, and establishes the absolute partial photoionization cross section of vinoxy to CH_3^+ at 10.5 and 11.44 eV. This should allow experimentalists detecting vinoxy radicals produced in bimolecular reactions such as OH + propene to get good branching fractions to that product channel. Finally we initiated studies of the photodissociation of 1-bromo-2-chloroethane and 1,1-bromochloroethane at 193 nm at the NSRRC.

II. Recent Progress

A. OH + Propene: The CH_3CHCH_2OH radical intermediate

The theoretically predicted product channels of the OH + propene reaction depend on whether the products are formed from direct H atom abstraction dynamics, or addition of the OH to the C=C double bond at either the end C atom or the center C atom. We sought to generate exclusively the radical intermediate formed from the addition of OH to an end carbon atom by photodissociating an isomerically pure precursor, 2-chloro-1-propanol. Our prior experiments on the OH + propene reaction produced a mixture of the two radical intermediates by photodissociating a 70/30 mixture of 1-bromo-2-propanol (producing the C_3H_6OH radical intermediate from OH addition at the center carbon) and 2-bromo-1-propanol (producing the radical intermediate from OH addition at the end

carbon). Although those experiments detected the methyl + acetaldehyde and ethyl + formaldehyde product channels from the addition intermediates, they were not able to confirm the radical intermediate responsible for each. Furthermore the enol product channels were not investigated nor was a possible roaming channel to produce H_2O + allyl from the radical intermediate rather than from direct abstraction. Our March 2016 experiments at the NSRRC were able to selectively produce the CH_3CHCH_2OH radical intermediate and study its product channels. Our conclusions from analysis of the data follows.

We photodissociated 2-chloro-1-propanol at 157 nm to generate the CH_3CHCH_2OH intermediate of the OH + propene reaction without interference from the radical intermediate from OH addition to the center carbon atom. Select predicted products from the addition of OH to the end C=C carbon atom are shown in Figure 1. The ethyl + H_2CO product channel should result from this intermediate, but not CH_3CHO + CH_3. The figure shows the lowest barrier pathway giving an enol product from this intermediate, propenol + H.

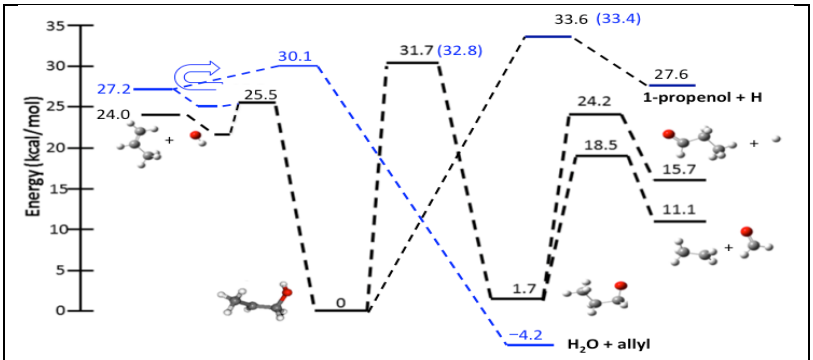

Figure 1. Selected transition states for the OH + propene reaction from Truong[1] (black) and Zádor[2] (blue). The blue arrow is added to hypothesize that trajectories en route to OH + propene might re-cross and result in an H-atom abstraction to form H_2O + allyl.

Our study first detected three photodissociation channels of 2-chloro-1-propanol. They are C-Cl photofission to form the CH_3CHCH_2OH radical intermediate of interest, an HCl photoelimination channel, and a C-C bond photofission channel analogous to that observed in 2-chloroacetaldehyde. Figures 2-4 show that data.

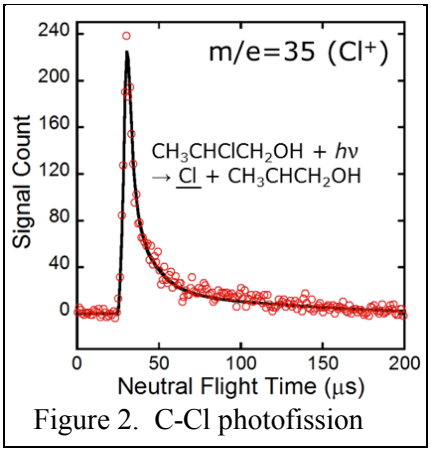

Figure 2. C-Cl photofission

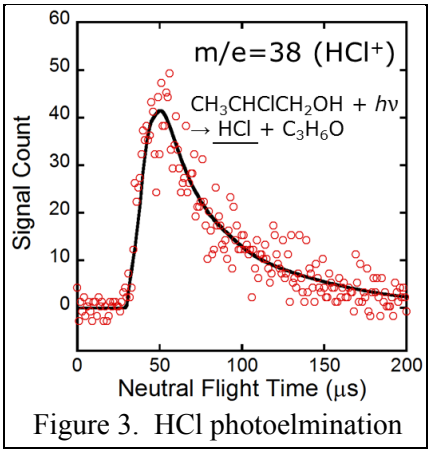

Figure 3. HCl photoelmination

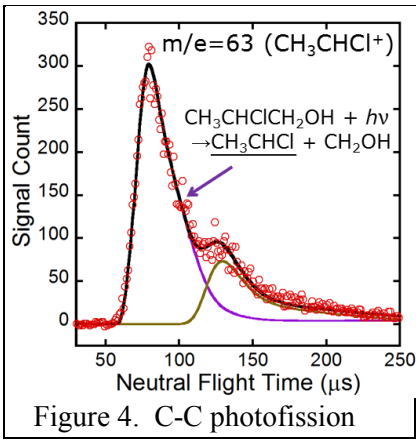

Figure 4. C-C photofission

We sought to detect not only the ethyl + H_2CO product channel from the CH_3CHCH_2OH radical, but also the H + propenol channel predicted by theory and a possible dissociation channel to H_2O + allyl resulting from a non-IRC pathway. (An analogous non-IRC channel occurred from the CH_2CH_2OH radical intermediate of the OH + ethene reaction.) No signal was detected at m/z = 18 (H_2O^+) upon integrating for one million laser shots, so we conclude that the non-IRC channel is not important from this OH + propene radical intermediate. We did detect the H + propenol

product channel (the lowest barrier enol product channel in Figure 1). Our data is shown in Figure 5. Although propenol can also result as a co-fragment of HCl photoelimination, the HCl photoelimination channel leaves the propenol with so much internal energy that it undergoes unimolecular dissociation to CH_2CHCH_2 + OH. In contrast, propenol from the dissociation of the CH_3CHCH_2OH radical intermediate to H + propenol is formed stable to subsequent dissociation. We observed it at the m/z=41 $CH_2CHCH_2^+$ daughter ion, as it undergoes efficient dissociative photoionization. The TOF of this product, shown by the green-line fit in Figure 5, is well predicted from the velocity of the CH_3CHCH_2OH radical intermediates that dissociate to H + propenol (the loss of an H atom does not change the velocity significantly).

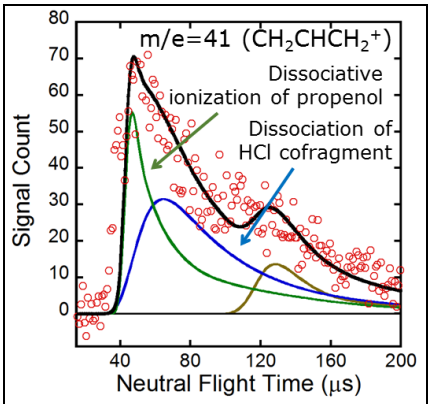

Figure 5. Propenol products

B. Photoionization Detection of Vinoxy Radicals at m/z=15 and m/z=29

Despite its importance in combustion, the photoionization detection of vinoxy radicals has eluded high-resolution spectroscopists for decades. Two experiments on bimolecular reactions producing vinoxy radicals (J. D. Savee et al, *Phys. Chem. Chem. Phys.* **2012**, *14*, 10410-10423 and S-H Lee et al, *Chem. Phys. Lett.* **2007**, *446*, 276-280) detected vinoxy radicals with photoionization at m/z=15, though they were unable to determine the partial photoionization cross section. Recent work by Scrape et al. (J. Phys. Chem. A, 10.1021/acs.jpca.5b12669) detected the very small signal from vinoxy radicals at parent ion, in addition to signal from its dissociative ionization to m/z=15.

In order to determine the partial photoionization cross section of vinoxy radicals, our experiments in March 2016 at the NSRRC formed vinoxy radicals from the photodissociation of 2-chloroacetaldehyde at 157 nm. Though the majority of the vinoxy radicals are formed with enough energy to dissociate to H + ketene and CH_3 + CO, 21% of the C-Cl bond fission events form Cl in conjunction with stable vinoxy radicals. This portion of the C-Cl bond fission $P(E_T)$ is shown in grey dashed line in Figure 6. Any signal from dissociative ionization of vinoxy radicals would then have a sharp TOF distribution that is easily predicted from this portion of the C-Cl fission $P(E_T)$. In contrast to velocity map imaging experiments, the scattering experiments at the NSRRC detect the velocity of the neutral stable vinoxy products, with a precalibrated ion flight time, whether the vinoxy is detected at parent ion or at CH_3. Calibrating with the signal from the momentum matched Cl product, our measured partial photoionization cross section of vinoxy to form CH_3^+ is 1.9 Mb at 10.5 eV and 2.2 Mb at 11.44 eV.

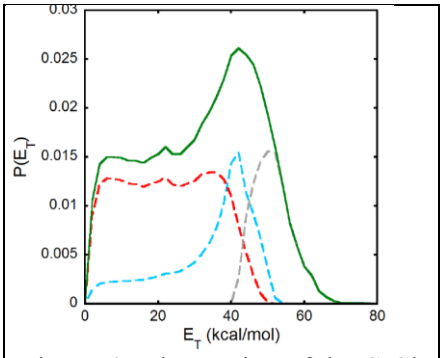

Figure 6. The portion of the C-Cl photofission $P(E_T)$ producing stable vinoxy is in grey dashed line.

C. 2-RDM Theory for Radical Chemistry (with D. A. Mazziotti)

The description of radical structure and processes in chemistry often require a non-trivial treatment of electron correlation. Two-electron reduced density matrix (2-RDM) methods, which directly compute the 2-RDM without the wave function, can provide an accurate

description of multi-reference electron correlation with polynomial cost. The unexpected abundance of HNO in the photodecomposition of the radical CH_2CH_2ONO was recently investigated by calculations of the potential energy surface by the anti-Hermitian contracted Schrödinger equation method (ACSE), which directly generates the 2-electron reduced density matrix (2-RDM). The ACSE, which is able to balance single-reference (dynamic) and multi-reference correlation effects, reveals some subtle correlation effects along the intrinsic reaction coordinate (IRC) en route to NO + oxirane, an IRC which offers a bifurcation to the HNO + vinoxy product channel. These effects were not fully captured by either single-reference techniques, such as coupled cluster, or multi-reference techniques, such as second-order multi-reference perturbation theory. These correlation effects reveal small to moderate energy changes in key transition states, which have implications for the HNO-production mechanism.

III. Publications Acknowledging DE-FG02-92ER14305 (2015 to present)

1. Predicting the effect of angular momentum on the dissociation dynamics of highly rotationally excited radical intermediates, M. D. Brynteson and L. J. Butler, J. Chem. Phys. 142, 054301 (2015). (Joint funding with NSF.)

2. Two HCl-Elimination Channels and Two CO-Formation Channels Detected with Time-Resolved Infrared Emission upon Photolysis of Acryloyl Chloride [$CH_2CHC(O)Cl$] at 193 nm, P.-W. Lee, P. G. Scrape, L. J. Butler, and Y.-P. Lee, J. Phys. Chem. A, DOI 10.1021/jp512376a (2015).

3. Dissociation Pathways of the CH_2CH_2ONO Radical: NO_2 + Ethene, NO + Oxirane and a non-Intrinsic Reaction Coordinate HNO + Vinoxy Pathway, P. G. Scrape, T. D. Roberts, S.-H. Lee and L. J. Butler, J. Phys. Chem. A, 10.1021/acs.jpca.5b12669 (2016).

4. The Onset of H + Ketene Products from Vinoxy Radicals Prepared by Photodissociation of Chloroacetaldehyde at 157, Chow-Shing Lam, Jonathan D. Adams, and Laurie J. Butler, J. Phys. Chem. A, 10.1021/acs.jpca.6b01256 (2016).

5. Primary Product Branching in the Photodissociation of Chloroacetaldehyde at 157 nm, Jonathan D. Adams, Preston G. Scrape, Shenshen Li, Shih-Huang Lee and Laurie J. Butler, J. Phys. Chem. A, 10.1021/acs.jpca.7b05318 (2017).

6. Dissociative Photoionization of the Elusive Vinoxy Radical, Jonathan D. Adams, Preston G. Scrape, Shih-Huang Lee and Laurie J. Butler, J. Phys. Chem. A, 10.1021/acs.jpca.7b04730 (2017).

7. A Measurement of the Photoionization Cross Section of CH_2Cl via Photofragment Translational Spectroscopy of Dichloromethane, Preston G. Scrape, Rosalind J. Xu, Jonathan D. Adams, Shih-Huang Lee and Laurie J. Butler, Chem. Phys. Lett. 687 284-289 (2017).

8. Using reduced density matrix techniques to capture static and dynamic correlation the energy landscape for the decomposition of the CH2CH2ONO radical, and support for a non-IRC pathway, Scott E. Smart, Preston G. Scrape, Laurie J. Butler, and David A. Mazziotti, submitted (2018).

---

[1] Kinetics of Enol Formation from Reaction of OH with Propene, L. K. Huynh, H. R. Zhang, S. Zhang, E. Edding, A. Sarofim, M. E. Law, P. R. Westmoreland, and T. N. Truong, J. Phys. Chem. A 113, 3177–3185 (2009).

[2] The Reaction between Propene and Hydroxyl, J. Zádor, A. W. Jasper and J. A. Miller, Phys. Chem. Chem. Phys. 11, 11040–11053 (2009). Note that Fig. 1 in this reference accidentally reversed the labels on the $CH_2CH_2CH_2OH$ and $CH_3CH_2CH_2O$ wells at -20.9 and -24.9 kcal/mol. Also Zádor informed us that the H-atom abstraction barrier shown in Fig. 3 of the paper is incorrect while the barrier given in the text, 2.9 kcal/mol, is correct.

Chemical Dynamics Methods and Applications

David W. Chandler
Combustion Research Facility
Sandia National Laboratory
Livermore, CA 94551-0969
Email:chand@sandia.gov

Program Scope:

My research focuses on the field of chemical dynamics of gas phase molecular species. Chemical dynamics is the detailed study of the motion of molecules and atoms on inter- or intra- molecular potential energy surfaces in order to learn about the details of the surface as well as the dynamics of their interactions. We have tested simple bimolecular potential energy surfaces by the careful study of collisional energy transfer processes in crossed molecular beam arrangements utilizing Velocity Mapped Ion Imaging techniques. Two years ago we reported on our study of electronically excited state collisions of NO(A). This year we report on an extension of these studies: the study of rotational energy transfer of aligned NO(A). Last year experiments began to use circularly polarized laser light to state-selectively excite the NO and detect the products of collisional energy transfer processes. We do this with high velocity resolution and with single quantum-state resolution of the product molecules. This work is reported below and is in Press at Nature Chemistry. Last year we reported the one-color study of the alignment of hydrogen produced in a single mixed quantum states of the electronically excited E, F state. This work has been extended to using two colors, one for mixing and alignment and one for dissociation and detection. In the future work we plan on studying the photochemistry of small phenolic systems that show branching between dissociation and internal conversion of photon energy. We also are continuing our development of a the dual-etalon frequency-comb technique for the study of molecules strongly coupled by light to a resonance cavity.

Recent Progress and ongoing experiments:

Alignment of H_2 utilizing double resonance techniques: We previously utilized the *E,F* electronic state to study alignment at relatively low laser intensities where we can better observe and quantify the photo-physics. The unusual shape of the *E,F* electronic potential curve has two minima resulting from the avoided crossing of the $(1s\sigma_g)$ $(2s\sigma_g)$, *E* state, and $(2p\sigma_u)^2$, *F* state, potential energy curves. Last year we published a study of the 532-nm alignment of the E,F state of H2. The E, F state was prepared by a two-photon absorption. An intense 532-nm laser beam was focused on the hydrogen molecules in the E,F state. This light mixed the E,F state with nearby B and C states creating a very polarizable excited state that acted to align the nuclei in the laser field. This same 532-nm light also dissociated the H_2 creating H atoms in the N=3 Rydberg state. These were subsequently ionized and imaged by the same 532-nm laser. This one-color experiment suffered from the ambiguity about which step in the process was causing the change in the angular distribution of the N=3 H atoms formed. This year we performed a two-color experiment where low intensity 532-nm light was used for the dissociation and detection steps and intense 1064-nm laser light was used to align the EF state. The ring associated with 532-nm dissociation was then recorded as a function of 1064-nm laser light intensity. The results are shown in Figure 1.

In Figure 1 is shown the angular distribution of H^+ atoms formed from alignment, dissociation and ionization of H_2 initially excited to the H_2(E,F, V=0, J=0) state. The left panel shows the image of the H^+ after dissociation and ionization of H_2 (E,F) with low intensity 532-nm light alone. The middle panel shows the image of the H^+ after dissociation and ionization of H_2 (E,F) with high intensity 1064-nm light alone. The right panel shows the image with both low-intensity 532-nm light and high-intensity 1064-nm light exciting the H_2(E,F) at the same time. One can observe how the equal angular intensity ring associated with the 532-nm only image on the left has changed intensity pattern from being uniformly intense to having more intensity along the laser polarization axis of the 1064-nm laser beam.

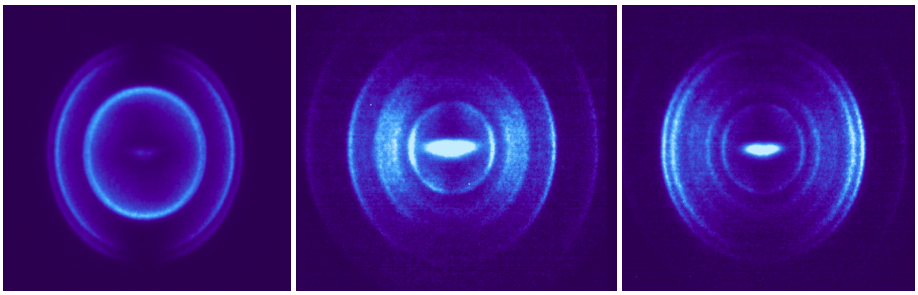

532-nm light only 1064-nm light only 1064 and 532-nm light

Figure 1: H+ images from laser alignment, dissociation and ionization processes following H2 excitation to the E, F V=0, j=0 state. See text for details.

By analyzing the intensity pattern of the ring associated with dissociation of the neutral H2 to form H + H(N=3) we can determine the delta polarizability of the H2 (E,F) state (difference in the polarizability along the internuclear axis and perpendicular to the internuclear axis)[1] Our initial one-color, 532-nm laser beam only experiments indicate a delta polarizability of close to 312 ± 82 a.u. – much smaller than calculations indicate for the polarizability induced by a static electric field and of the opposite sign but much larger than either ground state or pure E, F state hydrogen (~0.7 a.u.)[2]. The new two-color experiments fall on basically the same line and predict a very similar value for the delta polarizability.

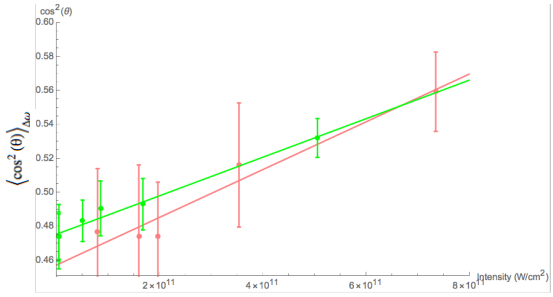

532-nm (Green) or 1064-nm (Red) Laser Intensity

Figure 2: Plots of calculate average cos 2 parameter as a function of laser intensity. The slope is providing the delta polarizability.

This makes H_2 excited to the E, F state the most easily aligned molecule ever produced. The large error bars associated with this data are an indication of the difficulty overlapping consistently the 532 and 1064-nm laser beams and reflect the non-linearity pf the process with laser intensity. For comparison, a difference in the polarizability of 312 a.u. is almost 46 Å^3, by comparison, CS_2 has 10 Å^3, I_2 has 7 Å^3, and hydrochlorothiazide ($C_7H_8ClN_3O_4S_2$) has about 25 Å^3. The 1064-nm alignment is even greater at 419 ± 59 a.u. but certainly within the error bars of the previous one color (532-nm) measurements. This work was performed in collaboration with Dr. Peter Rakitzis of University of Crete and with the assistance of postdoctoral fellows Justin Jankunas, Martin Fournier and Gary Lopez and is being readied for submission.

Collisions with Aligned NO(A) molecules: The correlations among vector quantities in molecular collisions are sensitive reporters on the accuracy of theoretical descriptions of the collisional interactions,

especially on the anisotropic part of the intermolecular potential.[3] Laser-preparation of the NO(A) state to align the NO molecules angular momentum axis toward or against the collision vector; an arrangement that specifically focuses on anisotropic interactions was built. These experiments excited the NO to the A state using circularly polarized light creating an oriented NO (A, J=1.5) molecule, rotating clockwise or counterclockwise relative to the collision vector with a Ne atom depending upon the handedness of the light. The data for the measured differential cross sections for collisional energy transferred into the NO N=3 state. After the oriented NO(A) molecules undergo a collision their final quantum state and orientation was measured by 1+1' resonant ionization through the E state using circularly polarized light and VMII. From the data, one can see that the probability of transfer to NO(A, N=3) that is co-rotating with the original NO(A, N=1) molecule is much more probable.

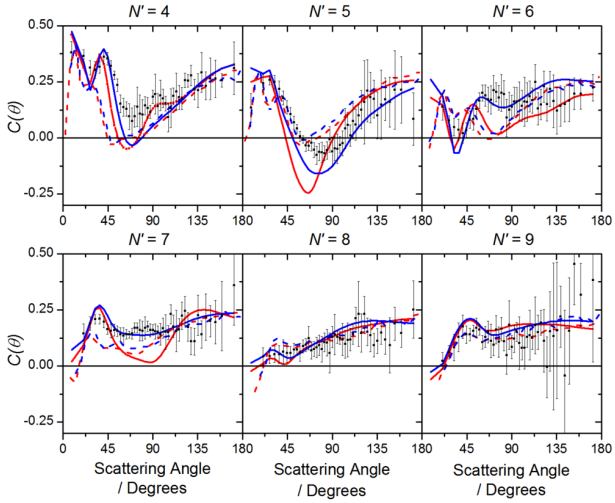

Figure 3: Measured and calculated values of $C(\theta)$ for each N' final state, revealing the variation of the orientation transfer efficiency with scattering angle. Mean experimentally measured values (black squares) with error bars indicating twice the standard error of the mean. Quantum Scattering calculations (solid lines) and Quasi Classical Trajectory(QCT) (dashed lines) calculations on two PESs. Calculations on the CF PES are in red while those on the PRRH PES are in blue.

This work was done in collaboration with Dr. Matt Costen and Dr. Ken McKendrick at Heriot–Watt University in Scotland and Javier Aoiz in Madrid Spain.

Dual Etalon Spectrometer: Fourier Transform spectroscopy is a technique for monitoring multiple frequencies simultaneously by analyzing how they interfere with each other on a single detector. Frequency combs are light sources that have multiple frequencies that are equally spaced. We utilized this fact in the past to patent a new concept for a spectrometer where two transient frequency combs are formed by confocal etalons outputs and interfered. A new set of experiments is being prepared utilizing this unique set up of interfering confocal etalons. By introducing a strongly absorbing and emitting molecule to the cavity such as Iodine perpendicular to the etalon axis during the cavity ring down will couple the molecule with the resonant cavity. In the direction of the cavity emission will be limited to being on a cavity mode and this coupling should split the resonance cavity mode as it mixes with the molecule. This quantum electro dynamic[4] effect will be monitored by time resolved Fourier transform of the interferogram. Recent experiments have shown that one can manipulate the photo-physics of the molecule, including its reactivity by such coupling to an external cavity providing a new method of control of chemical and physical of molecules.

Photochemistry of substituted aromatic molecules: Phenol is the chromophore of the amino acid Tyrosine as well as an early precursor of soot in combustion environments. As such its photochemistry has been

studied expensively. It has a strong UV absorption with a ππ* nature. This state crosses with a πσ* the potential surface for which cuts through both the excited state and the ground state. This leads to very interesting and not well quantified photochemistry. After excitation in the ultraviolet region the molecule can either loose an H atom or return to the ground electronic state as a vibrationally hot molecule. This competition in many similar systems is dictates such things as your DNA and RNA's ability to withstand UV radiation[5]. We are preparing a new set of photochemistry experiments to measure this branching ratio. Many groups have measured the direct H atom coming from phenol and phenol like molecules but it is much more challenging to measure the amount of initially excited molecules that internally convert back to the ground electronic state. We will excite the phenol in the UV near 275 nm. The molecules will either dissociate or internally convert in a matter of several picoseconds. We will come in a few nanoseconds later with tunable IR laser that will be tuned to the red of the OH stretching mode of cold phenol. The hot phenol will have an enhanced absorption cross section and absorb many photons heating the molecule to a point where it RRKM dissociation rate will be on the nanosecond time scale. We will then image all of the H atoms generated from the initially excited phenol. Direct dissociation has been studied by the Ashfold group[6] and produces energetic H atoms, RRKM dissociation should produce very low energy H atoms that are easily distinguished by the velocity mapped ion imaging.

References:

1) J. Komasa, Adv. Quant. Chem. **48**, 151 (2005).
2) G. V. Lopez, M. Fournier, J. Jankunas, A. K. Spiliotis, T. P. Rankisis, D. W. Chandler, J. Chem. Phys. Volume 147, # 13948, 2017.
3) Steill, J. D.; Kay, J. J.; Paterson, G.; Sharples, T. R.; Klos, J.; Costen, M. L.; Strecker, K. E.; McKendrick, K. G.; Alexander, M. H.; Chandler, D. W., *J. Phys. Chem. A* **2013,** *117*, 8163-8174.
4) S. Haroche and D. Kleppner Physics Today Vol.1, 24-30 (1989).
5) S. Boldissar and M. S. de Vries, PCCP, DOI: 10.1039, 2018
6) M. G. D. Nix, A. L. Devine, B. Cronin, R. N. Dixon, and M. N. R. Ashfold, J. of Chem. Phys. **125**, 133318, 2006

Publications acknowledging BES support for DWC, 2016 –

1) Chemical Physics: Quantum Control of light-induced reactions. D. W. Chandler, Nature (2016) Vol 535 pages 42-44.
2) Editorial: The Future of Chemical Physics Conference 2016, A. Michaelides, D. E. Manolopoulos, C. Vega, P. Hamm, D. W. Chandler, E. Brigham, M. I. Lester, J. of Chemical Physics (2016) Vol 145 # 220401
3) Alignment, Dissociation and Ionization of H2 Molecule in Intense Laser Fields using Velocity Mapped Imaging, G. V. Lopez, M. Fournier, J. Jankunas, A. K. Spiliotis, T. P. Rankisis, D. W. Chandler, J. Chem. Phys. Volume 147, # 13948, 2017.
4) Perspective: Advanced Particle Imaging, D. W. Chandler, D. H. Parker and P. H. Houston, J. Chem. Phys. Vol 147 # 013601, 2017 for special Issue on Advanced Particle Imaging.
5) Imaging Spectroscopy: A Novel Use for the Velocity Mapped Ion Imaging Technique, J. Guzman, L. Culberson, K. E. Strecker, J. D. Steill, C. Montcrieffe, and D. W. Chandler, J. Chem. Phys. submitted Phys Rev. (2018).
6) Non-Intuitive Molecular Collision Dynamics from Direct Measurement of Four Vector Correlation, T. Sharples, J. G. Leng, T. Luxford, K. G. McKendrick, P.G. Jambrina, F. J. Aoiz, D. W. chandler and M. L. Costen. Submitted Nature Chem. (2018)

Direct Numerical Simulation of Spontaneous Ignition of Heterogeneous Mixtures

Jacqueline H. Chen (PI) Alex Krisman and Giulio Borghesi
Sandia National Laboratories, Livermore, California 94551-0969
Email: jhchen@sandia.gov

Program Scope

In this research program we have developed and applied massively parallel three-dimensional direct numerical simulation **(**DNS) of canonical flows that reveal fundamental chemistry-transport interactions associated with spontaneous ignition of aliphatic hydrocarbons. The simulation benchmarks are designed to expose and emphasize the coupling between low-temperature chemistry and scalar gradients generated by turbulent mixing. The simulations address fundamental issues associated with 'chemistry-transport' interactions that occur during high pressure multi-stage autoignition with negative temperature coefficient (NTC) chemistry.

Recent Progress

In the past year, we have investigated the role of molecular and turbulent transport on low-temperature spontaneous ignition in n-dodecane mixtures at high pressure (25 bar), and identified distinct regimes of reaction front propagation in the presence of autoignitive mixtures. We also devised a new method to compute reference flame speed(s) for hybrid deflagration/autoignition reaction fronts based on the peak sensitivity of the flame position with respect to variations in inlet velocity in a one-dimensional domain. Highlights from these DNS studies are presented. This is followed by a discussion of future work on understanding the role on non-thermalized chemistry on low-temperature ignition and reaction front propagation.

Cool flame propagation and turbulent mixing effects on low-temperature spontaneous ignition of fuel-lean n-dodecane /air mixtures in the NTC regime at 25 bar

DNS of a temporal jet between n-dodecane and diluted air undergoing spontaneous ignition at elevated pressure was performed and showed two-stage ignition in the negative temperature coefficient regime [1]. A 35 species n-dodecane chemical model including both low- and high-temperature oxidation pathways was used. Stratification of the mixture composition and temperature due to intense turbulent mixing resulted in the formation of localized regions of ignition progress called 'kernels' whose development was initially inhibited due to turbulent dissipation relative to the low-temperature homogeneous ignition delay. Once ignited, low-temperature ignition fronts at near stoichiometric conditions, *i.e.* the mixture fraction at which the homogeneous ignition delay is shortest, propagate towards even more fuel rich mixtures. The propagation into fuel rich regions is due to a combination of laminar cool flame propagation and spontaneous ignition. The cool flame propagation is attributed to a balance between reaction and molecular diffusion of low-temperature intermediates such as ketohydroperoxide. Figure 1b shows the fraction of fluid parcels in the computation undergoing cool flame propagation versus spontaneous ignition as a function of time as defined by a local Damköhler number, Da, based on the ratio of the magnitudes of the maximum value of the reaction rate to the maximum value of diffusion rate of ketohydroperoxide. Premixed cool flames exhibit a balance between chemistry and diffusion terms; ignition, on the other hand, is dominated by reaction. Note that over 50% of the reaction fronts are due to flame propagation (Da<5) and that the percentage increases in time as richer, more difficult to ignite mixtures are encountered.

Low-temperature ignition, especially for very lean or very rich mixtures, is also assisted by turbulent diffusion of enthalpy and radicals. This is shown in Fig. 1c by the conditional means of ketohydroperoxide mass fraction, conditioned on both mixture fraction and mixing intensity represented by the scalar dissipation rate. The figure shows that ignition occurs fastest in regions with low mixing rates and composition closest to the most reactive mixture fraction. It is also evident that for the rich mixtures that have yet to ignite, high radical concentrations are found in regions of very high mixing rates. Note that the profile becomes broad with increasing mixing intensity. Conceptually, turbulent transport inhibits low-temperature ignition by diffusing radicals and heat away from ignition kernels to neighboring regions.

For very rich or very lean conditions with high mixing intensity the radicals present are, in fact, due to turbulent diffusion and not self-ignition which is much slower.

The combination of transport effects, *i.e.* laminar cool flame propagation and turbulent diffusion ultimately results in a shorter ignition delay than homogeneous ignition delay, and ignition occurs at richer conditions comparatively, as shown in Figure 1b. Hence, overall ignition is highly sensitive to the strong coupling between transport and low-temperature chemistry.

The laminar cool flames observed in the temporal n-dodecane turbulent jet propagate into reactive mixtures that are spontaneously igniting, and not into inert reactants. Motivated by the desire to calculate a reference flame speed at autoignitive conditions, calculations were performed for the flame position in a one-dimensional computational domain with inflow-outflow boundary conditions, as a function of the inlet velocity and for a given equivalence ratio of a fuel–air premixture [2,3]. The response of the flame position to a given inlet velocity shows distinct stabilization regimes. For single-stage ignition fuels, at low inlet velocity the flame speed exceeds the inlet velocity and the flame becomes attached to the inlet. Above a critical inlet velocity value, the flame detaches from the inlet and flame position becomes extremely sensitive to the inlet velocity until, for sufficiently high inlet velocity, the sensitivity decreases and the flame position corresponds to the location expected from a purely autoignition stabilized flame. The transition from the attached to the autoignition regimes has a corresponding peak in the change in flame position with respect to the inlet velocity value which is proposed to be a unique reference flame speed for single-stage ignition fuels. For two-stage ignition fuels, there is an additional stable regime where a high-temperature flame propagates into a pool of intermediate species generated by the first stage of autoignition. This results in two peaks in the change in flame position with respect to changes in inlet velocity and therefore two reference flame speed values. The lower value corresponds to the definition of reference speed for single-stage ignition fuels, while the higher value exists only for two-stage ignition fuels and corresponds to a high temperature flame propagating into the first stage of autoignition. With the reference speed definition we plan to analyze the statistics of the normalized propagation speed of the cool flames in the DNS of the turbulent n-dodecane jet.

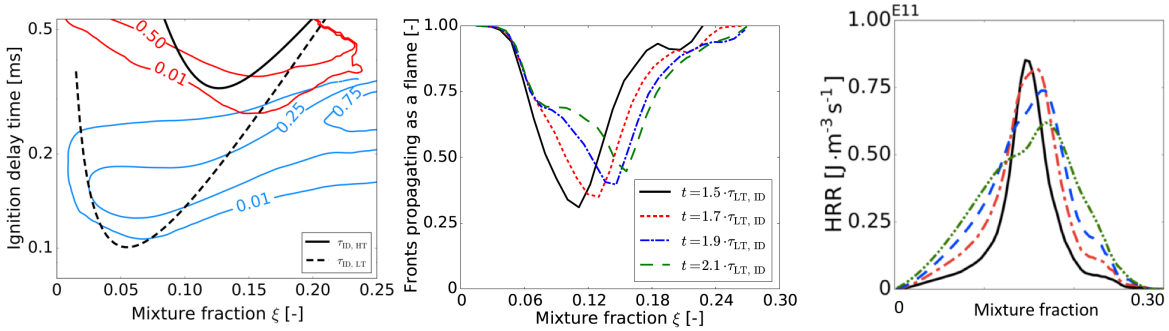

(a) (b) (c)

Figure 1. a) blue lines (red lines): fraction of fluid parcels that have undergone low-temperature (high-temperature) ignition. Black dashed (solid) lines: homogeneous ignition delay for low- (high) temperature ignition; b) fraction of low-temperature reaction fronts that propagate as a laminar cool flame as a function of mixture fraction at select times relative to the homogeneous low-temperature ignition delay; c) doubly conditional means of ketohydroperoxide mass fraction (conditioned on mixture fraction and mixing rate) during low-temperature ignition where the most intense cumulative mixing rates are depicted by the green dashed-dotted line and the lowest mixing rates by the black line. [1]

Future Work:

The Effect of Nonthermalized Chemistry on Low-Temperature Spontaneous Ignition

We plan to examine an auto-ignition system, where hot radicals, e.g., QOOH* radicals, formed in an R + O_2 reaction are expected to react at different rates compared to thermalized QOOH radicals. BES researchers at Sandia and Argonne have created a comprehensive low-temperature propane oxidation sub-

mechanism. Nonequilibrium rate coefficients were parameterized for several important reactions in a sub-model by Burke et al. [4]. The parameterization shows an effective second-order dependence on O_2 concentration for these hot radical reactions. The importance of the aforementioned non-equilibrium effects (hot radical bimolecular reactions) decreased both with temperature and pressure. At higher temperatures the thermal reactions are faster, and the enhancement from hot radicals becomes proportionally less important, while at higher pressures thermalization itself is faster, decreasing the concentration of hot radicals. However, in a turbulent flow at higher pressures the spatial gradients in temperature and composition are greater and the chemical time scales are shorter, which may have important consequences. The thermo-chemical conditions of adjacent fluid parcels may be different, and therefore a hot QOOH radical towards the edge of a given parcel may experience a collisional environment distinct from the one it was created in. If this environment is colder than the one it originated from then the enhancement of chain propagation and chain branching could be significant even at high pressure, as shown by the homogeneous calculations of Burke et al. [4] Hence, we propose to parameterize the rate parameters calculated by Burke et al. [4] to be evaluated in a turbulent simulation of propane undergoing spontaneous ignition at high pressure. This simulation will let us assess the importance of non-Boltzmann reactions in low-temperature oxidation.

References:

1. G. Borghesi, Alex Krisman, Tianfeng Lu and J. H. Chen, "A DNS investigation of turbulent n-dodecane / air mixing layer autoignition," in press *Combustion and Flame* (2018).
2. A. Krisman, Evatt Hawkes, and J. H. Chen, "The structure and propagation of laminar flames under autoignitive conditions," *Combustion and Flame* (2018) **188**:399-411.
3. A. Krisman, C. Mounaim-Rousselle, R. Savaramakrishnan, J.A. Miller, and J. H. Chen, "Reference natural gas flames at nominally autoignitive engine relevant conditions," in press Proc. Comb. Inst. 37 (2018).
4. M. Burke, C. Goldsmith, Y. Georgievskii, S. Klippenstein, "Towards a quantitative understanding of the role of non-Boltzmann reactant distributions in low temperature oxidation," *Proc. Comb. Inst.* 35:205-213.

BES Publications (2016-2018)

1. Zhao, X., Bhagatwala, A., Chen, J. H., Haworth, D. C., Pope, S. B., "An a priori DNS study of the shadow-position mixing model," *Combustion and Flame* (2016) **165**:223-245.
2. Karami, S., Hawkes, E. R., Talei, M., Chen, J. H. "Edge flame structure in a turbulent lifted flame: a direct numerical simulation study," *Combustion and Flame* (2016), 169:110-128.
3. Gao, Y., Shan, R., Lyra, S., Li, C., Wang, H., Chen, J. H., Lu, T., "A lumped-reduced reaction model for combustion of liquid fuels," *Combustion and Flame* (2016),, **163:**437-446.
4. Y. Gao, H. Kolla, J. H. Chen, N. Swaminathan, and N. Chakraborty, "A comparison of scalar dissipation rate transport between simple and detailed chemistry based on direct numerical simulations," in press *Combustion Theory and Modeling* (2016).
5. Kolla, H., Zhao, X., Chen, J. H., Swaminathan N., "Velocity and Reactive Scalar Dissipation Spectra in Turbulent Premixed Flames," *Combustion Science and Technology* (2016), **188**:1424-1439.
6. Y. Minamoto and J. H. Chen, "DNS of a turbulent lifted di-methyl ether jet flame," *Combustion and Flame* (2016), **169**:38-50.
7. F. Salehi, M. Talei, E. Hawkes, A. Bhagatwala, J. H. Chen, S. Kook, "Doubly conditional moment closure modeling for HCCI with temperature inhomogeneities," *Proc. Combust. Inst.* (2017), **36**:3677-3685.
8. A. Krisman, E. R. Hawkes, M. Talei A. Bhagatwala, J. H. Chen, "A DNS of a cool-flame affected autoignition in diesel engine-relevant conditions," *Proc. Combust. Inst.* (2017), **36**:3567-3575.
9. H. Wang, E. R. Hawkes, B. Zhou, J. H. Chen, Z. Li, M. Alden, "A comparison between DNS and experiment of the turbulent burning velocity-related statistics in a turbulent methane-air premixed jet flame at high Karlovitz number," *Proc. Combust. Inst.* (2017), **36**:2045-2053.
10. S. Karami, M. Talei, E. R. Hawkes, and J. H. Chen, "Local extinction and reignition mechanism in a turbulent lifted flame: a DNS study," *Proc. Combust. Inst.* (2017), **36**:1685-1692.
11. E. S. Richardson and J. H. Chen, "Analysis of turbulent flame propagation in equivalence ratio-stratified flow," *Proc. Combust. Inst,* (2017), **36**:1729-1736.

12. H. Wang, E. R. Hawkes, J. H. Chen "Turbulence-Flame Interactions in DNS of a Laboratory High Karlovitz Premixed Turbulent Jet Flame," *Physics Fluids* (2016), **28**, 095107.
13. H. Wang, E. R. Hawkes, B. Zhou, J. H. Chen, Z. Li, M. Alden, "Petascale direct numerical simulations of a high Ka laboratory premixed jet flame," *J. Fluid Mech*. (2017) 815:511-536.
14. M. Kuron, Z. Ren, H. Zhou, E. Hawkes, J. Tang, J. H. Chen, and T. Lu, "Performance of transported PDF mixing models in a turbulent premixed flame," *Proc. Combust. Inst.* (2017), **36**:1987-1995.
15. M. Kuron, Z. Ren, E. R. Hawkes, H. Zhou, H. Kolla, J. H. Chen, T. Lu, "A mixing timescale model for TPDF simulations of turbulent premixed flames," *Combust. Flame* (2017), **177**:171-183.
16. A. Krisman, E. R. Hawkes, M. Talei A. Bhagatwala, J. H. Chen, "Characterisation of two-stage ignition in diesel engine-relevant thermochemical conditions using DNS," *Combust. Flame*, (2016), **172**:326-341.
17. A. Krisman, E. R. Hawkes, and J. H. Chen, "Autoignition and edge flames in a turbulent jet at diesel engine relevant thermochemical conditions," *J. Fluid Mech*. (2017) 824:5-41.
18. C. Han, D.O. Lignell, E. R. Hawkes, J. H. Chen, H. Wang, "Examination of differential molecular diffusion in DNS of turbulent non-premixed flames, *International Journal of Hydrogen Energy* (2017), http://dx.doi.org/10.1016/j.ijhydene.2017.01.094.
19. S. Chaudhuri, D. Simanshu, H. Kolla, H. Dave, E.R. Hawkes, J. H. Chen, C.K. Law, "Flame thickness and conditional scalar dissipation rate in a premixed temporal turbulent reacting jet," in press *Combust. Flame* (2017).
20. H. Wang, E. R. Hawkes, J. H. Chen, "A direct numerical simulation study of flame structure and stabilisation of an experimental high Ka CH_4/air premixed jet flame," *Combust. Flame* 180:110-123 (2017).
21. H. Pouransari, H. Kolla, J. H. Chen, A. Mani, " Spectral analysis of energy transfer in turbulent flows laden with heated particles," *J. Fluid Mech.* (2017), **813**:1156-1175.
22. Z. Ren, M. Kuron, X.Zhou, T. Lu, H. N. Kolla, and J. H. Chen, "Micromixing models for PDF simulations of premixed flames," review article submitted to *Combustion Science and Technology* (2017).
23. A. Krisman, Evatt Hawkes, and J. H. Chen, "The structure and propagation of laminar flames under autoignitive conditions," *Combustion and Flame* (2018) **188**:399-411.
24. G. Borghesi, Alex Krisman, Tianfeng Lu and J. H. Chen, "A DNS investigation of turbulent n-dodecane / air mixing layer autoignition," in press *Combustion and Flame* (2018).
25. H. Wang, E. R. Hawkes, B. Savard, and J. H. Chen, "Direct numerical simulation of a high Ka CH4/air stratified premixed jet flame," in press *Combustion and Flame* (2018).
26. H. Zhou, Z. Ren, M. Kuron, T. Lu and J. H. Chen, (2018) "An investigation of reactive scalar mixing in transported PDF simulations of turbulent premixed methane-air Bunsen flames" submitted to *Physical Review Fluids*.
27. C. Xu, M. Muhsin, S. Som, J. H. Chen, Z. Ren and T. Lu, "Dynamic adaptive combustion modeling of spray flames based on chemical explosive mode analysis," submitted to *Combust. Flame* (2018).
28. K. Aditya, A. Gruber, C. Xu, T. Lu, A. Krisman, M. Bothien, J. H. Chen, "Direct numerical simulation of flame stabilization assisted by autoignition in a reheat gas turbine combustor," in press *Proc. Comb. Inst.* 37 (2018).
29. A. Krisman, C. Mounaim-Rousselle, R. Savaramakrishnan, J.A. Miller, and J. H. Chen, "Reference natural gas flames at nominally autoignitive engine relevant conditions," in press *Proc. Comb. Inst*. 37 (2018).
30. D. H. Shin, E. S. Richardson, V. Aparace-Scutariu, Y. Minamoto, and J. H. Chen, "Residence time-based analysis of a lifted turbulent dimethyl ether jet flame," in press *Proc. Comb. Inst.* 37 (2018).
31. A. Krisman, E.R. Hawkes, and J. H. Chen, "A parametric study of ignition dynamics at ECN Spray A thermochemical conditions using 2D DNS," in press *Proc. Comb. Inst*. 37 (2018).
32. W. Han, H. Wang, G. Kuenne, E. R. Hawkes, J. H. Chen, J. Janicka, and C. Hasse, "Large-eddy simulation/dynamic thickened flame modeling of a high Karlovitz number turbulent premixed jet flame," in press *Proc. Comb. Inst*. 37 (2018).
33. S. Trivedi, R. Griffiths, H. Kolla, J. H. Chen, R. S. Cant, "Topology of pocket formation in turbulent premixed flames," in press *Proc. Comb. Inst*. 37 (2018).

Dynamics and Energetics of Elementary Combustion Reactions and Transient Species
Grant DE-FG03-98ER14879

Robert E. Continetti (rcontinetti@ucsd.edu)
Department of Chemistry and Biochemistry, University of California San Diego
9500 Gilman Drive, La Jolla, CA 92093-0340

I. Program Scope

This research program continues to provide benchmark experimental results to underpin fundamental advances in our understanding of chemical phenomena through the development of accurate methods for the calculation of potential energy surfaces (PESs) and the dynamics of molecular collisions. The research program involves the development and application of advanced experimental techniques that enable the use of photodetachment and dissociative photodetachment of anionic precursors to prepare energized radicals and collision complexes and study the subsequent lifetimes and dissociation dynamics of these species. Kinematically complete measurements of dissociative photodetachment (DPD) processes provide a novel measure of the dynamics of unimolecular and bimolecular reactions and allow the identification of long-lived reaction resonances. These measurements involve the detection of photoelectrons, stable photoneutrals and photofragments in coincidence, using photoelectron-photofragment coincidence (PPC) spectroscopy. During the last year we published an experimental advance production of cold anions in the laboratory, examining the photochemistry of O_3^- and demonstrating a dramatic suppression of an $O + O_2^-(v)$ channel with the quenching of parent anion vibration through buffer gas cooling (DOE pub. 2).[1] We continued our ongoing collaboration with Hua Guo in a study of benchmarks for multidimensional quantum dynamics, in an examination of the dynamics of overtone-excited $F^-(H_2O)$ via IR excitation (DOE pub. 3),[2] expanding on the experimental-theoretical study of the $F + H_2O \rightarrow HF + OH$ reaction in *Science*.[3] Finally, we reported on an experimental-theoretical study with John Stanton that examined the low-lying electronic states of ethylenedione, C_2O_2 (DOE pub. 5). This study resulted in a reassignment of spectra reported in the literature to the oxyallyl radical anion, $C_3H_5O^-$, showing that the long-sought, long-lived states of C_2O_2 have not yet been observed.[4, 5] Ongoing efforts currently include characterization of increasingly complex hydroxyl radical reactions $OH + CH_4/CD_4 \rightarrow H_2O + CH_3/CD_3$ and $OH + C_2H_4$, using photodetachment of the OH^--hydrocarbon complexes. We have also studied the photodissociation of $N_2O_2^-$ and the complex dissociation/autodetachment dynamics exhibited by that system in the near-UV. In the following sections, recent progress will be discussed in more detail, followed by a brief review of future work on concerted elimination of OH from the oxyallyl radical, and other hydroxyl radical complexes by dissociative photodetachment.

II. Recent Progress

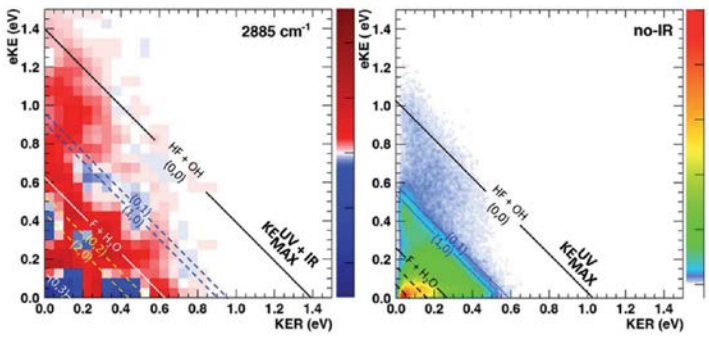

Figure 1. Left Frame: Difference PPC spectrum (IR on – IR off) for $F^-(H_2O)$ with IR = 2885 cm^{-1} and photodetachment at 4.80 eV. Blue regions show depletion, red regions enhancement, and the energetic limits have been shifted up by 2885 cm^{-1} relative to the right frame to reflect the total available energy. Right Frame: PPC spectrum for no-IR (unexcited) $F^-(H_2O)$. Black lines indicate the energetic limits for dissociation to ground state products. Dashed lines indicate vibrationally excited product states.

A. Effects of vibrational excitation on the $F + H_2O \rightarrow HF + OH$ reaction: dissociative photodetachment of overtone-excited [F-H-OH]

The $F + H_2O \rightarrow HF + OH$ reaction is an important benchmark system for reaction dynamics.[6] In the past year, the analysis of the effects of IR excitation for this was reported, in a comparison of theory with high-level quantum dynamics calculations by Guo and co-workers.[2] The effect of excitation of the overtone of the F-H-OH ionic hydrogen bond (IHB, $2\nu_{IHB}$) in $F^-(H_2O)$ compared to the reaction without vibrational excitation was examined. The data shown in Figure 1 shows unambiguous

evidence for an effect of vibrational excitation. In the left frame, the difference PPC spectrum first shows significant signal above the (eKE,KER) = (1.0,1.0) eV diagonal line that constitutes the maximum total kinetic energy (KE_{max}) for unexcited anions. This corresponds to the production of rotationally excited HF(v=0) + OH(v=1) products (denoted (0,1)), where the excess vibrational energy in the parent anion appears in kinetic energy release (KER). The left frame also shows an increase in intensity for the region where (1,0) + (0,1) is energetically allowed and the F + H_2O channel opens. There is a significant depletion of signal at low eKE, corresponding to rotationally excited (2,0) + (0,2) and F + H_2O products. These results are of interest as F^- (H_2O) ($2\nu_{IHB}$) probes a different portion of the neutral potential energy surface. Theory and experiment concur on the channeling of vibrational energy into translation in the (0,0) region at high eKE, as well as the increase in the F + H_2O channel. Experiment indicates an increase in rotational excitation that is not seen in theory. However, the theory doesn't account for the complexity of the vibrational spectrum in $F^-(H_2O)$, with a bending overtone lying close by, as well as potential IVR in the $F^-(H_2O)$ target anion on the 50 ms timescale of these experiments.

B. Internal energy dependence of the photodissociation dynamics of O_3^- using cryogenic photoelectron-photofragment coincidence spectroscopy

The first PPC study using a radio frequency (RF) cryogenic octopole accumulation trap (COAT) to collisionally cool precursor anions with helium buffer gas was reported in a study of the photodissociation of O_3^- .[1] This study showed the production of two ionic dissociation pathways, (1) $O_2(^1\Delta_g)$ + $O^-(^2P)$ and (2) $O_2^-(^2\Pi_g)$+ $O(^3P)$, as well as photodetachment, (3) O_3 + e^- at a photon energy of 3.20 eV. The coldest anions were produced at 17 K COAT temperature with 80 ms trapping using a He/H_2 buffer gas mix. A significant decrease in the 1_1^0 hot bands from photodetachment channel (3) and suppression of the sequential autodetachment of $O_2^-(v'' < 4)$ produced by channel (2) was observed. These measurements revealed further details about the competing ionic photodissociation channels, namely channel (2), in the low-lying $^2A_2$ excited state of O_3^- formed by photon absorption. Examination of the dynamics of autodetachment of $O_2(v'=0)$ + e^- ← $O_2^-(v''=4)$ showed that the parent anion has 1-2 quanta of symmetric stretch excitation with the resulting energy partitioned to KER in the production of $O(^2P)$ + $O_2^-(v''=4)$. The results suggest that bending and asymmetric stretch excitation in the anion greatly enhance the decay of the $^2A_2$ state into $O_2^-(v''=4)$ + $O(^2P)$. These results have been published (DOE pub. 2) and demonstrate how the addition of COAT to the PPC spectrometer greatly enhanced our control over cooling precursor anions as demonstrated by studying the dissociation dynamics of O_3^-.

C. Hydroxyl radical reactions: OH + $CH_4/CD_4/C_2H_4$ → H_2O + $CH_3/CD_3/CHCH_2$

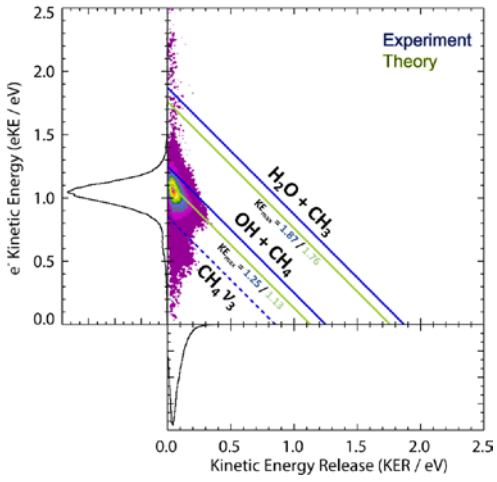

Figure 2. Photoelectron-photofragment coincidence plot of the OH-CH_4 system with experimental KER_{max} and theoretical values from Guo and co-workers.

The OH + CH_4 → H_2O + CH_3 reaction is an elementary step involved in the oxidation of methane in combustion and atmospheric chemistry, so we have endeavored to study this and other hydroxyl radical reactions using clusters with OH^-. A key implementation on to the PPC spectrometer crucial to the rational synthesis of precursor anions for studying these hydroxyl reactions is a dual pulsed valve ion source.[7] PPC measurements were carried out on $OH^-(CH_4)$ at a photon energy of 3.20 eV. Figure 2 shows a coincidence plot with two distinct diagonal features. Using *ab initio* energetics provided by Guo and co-workers, the main channel accessed is OH + CH_4 with a CH_4 asymmetric stretch contribution appearing ~0.40 eV below the diagonal KE_{max} for the OH + CH_4 channel. The events occurring below the hydrogen abstraction barrier beyond the KE_{max} for the OH + CH_4 channel suggests tunneling dissociation might play a role in the formation of H_2O + CH_4, as well as contributions from false coincidences and the isobaric anion HO_2^-. Results for the OD-CD_4 system showed

substantially fewer events beyond the OD + CD_4 KER_{max} as expected for a decrease in tunneling probability because of the larger reduced mass of the isotopologue and elimination of isobaric contamination. Recently, PPC data has also been recorded for the $OH^-(C_2H_4)$ system since electrophilic addition of OH to ethylene serves as a benchmark for fundamentally understanding the reactions of olefins and OH.[8] Preliminary results show evidence of vibrational excitation in the resulting fragments corresponding to C-H asymmetric stretching in ethylene as well as possible O-H stretch excitation in the OH + C_2H_4 channel. Further analysis and characterization of the dissociation dynamics for this 8-atom system, with 18 degrees of freedom, is currently in progress and will represent a significant challenge for theory.

D. Photodissociation and Autodetachment of $N_2O_2^-$

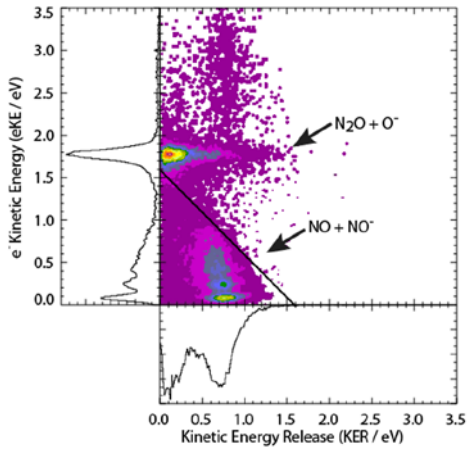

Figure 3: PPC spectrum for $N_2O_2^-$ at 3.20 eV. Three distinct processes can be seen: the vibrational progression at low eKE is the autodetachment of NO^-, the eKE peak at ~1.7 eV is the photodetachment of O^- after photodissociation, and the intensity at high eKE is the photodetachment of NO^- (v=0).

The N_2O_2 system, an important intermediate in atmospheric and combustion chemistry, is known for its various dissociation pathways.[9,10, 11] These are dependent on both the photon energy used to study this system as well as the precursor anion state accessed. Using PPC spectroscopy, these reaction pathways were disentangled to obtain distinct spectra based on different neutral product fragmentation. Three channels were observed through ionic photodissociation followed by anion product photodetachment or autodetachment at 3.2 eV (388 nm), which can be seen in Figure 3. These channels are assigned to $N_2O_2^- + h\nu \rightarrow N_2O + O^- + h\nu \rightarrow N_2O + O + e^-$, via a two photon process, $N_2O_2^- + h\nu \rightarrow NO + NO^-(v=0) + h\nu \rightarrow NO + NO + e^-$, and $N_2O_2^- + h\nu \rightarrow NO + NO^-(v>0) \rightarrow NO + NO + e^-$, with $NO^-(\nu>0)$ undergoing autodetachment due to the low electron affinity of NO. These coincidence measurements provide the first state-resolved data on the autodetachment of the highly vibrationally and rotationally excited NO anion product, and observation of an asymmetric dissociation from the ground state $N_2O_2^-$ anion. The broad feature above eKE=2.0 eV is the first detection of the NO + $NO^-(\nu=0)$ photodissociation channel via photodetachment of $NO^-(\nu=0)$ by a second photon. The results indicate that the ground state *trans* anion is the precursor being accessed. These measurements were carried out with COAT to internally cool the precursor anions to their ground states at 17K, allowing for the *trans* anion to be studied in isolation. These results are currently being prepared for publication and will provide a new piece of the puzzle for the photochemistry of $N_2O_2^-$ with the addition of this detailed data at a photon energy of 3.2 eV.

E. Spectroscopy of Ethylenedione and Ethynediolide: A Reinvestigation

Ethylenedione, C_2O_2, is a transient species whose discovery was claimed by Sanov and co-workers recently via anion photoelectron spectroscopy.[12] The spectra reported the first observation of both ethylenedione, and its analog ethynediolide, HC_2O_2, with the precursor anions produced using a pulsed discharge of glyoxal vapor and N_2O. The ethylenedione spectrum had features that were attributed to a long-lived ground triplet state, as well as two higher energy singlet states that dissociate into CO ($^1\Sigma^+$) + CO ($^1\Sigma^+$). A vibrational progression observed in the ground state triplet was used to infer a lifetime of ~0.5 ns. The predicted dissociation dynamics of the neutral low-lying electronic states make this an ideal system to study using PPC spectroscopy. A detailed account of this study has been published in DOE pub. 5.[5] Reproducing the glyoxal/N_2O anion preparation with PPC spectroscopy indicated that only stable neutrals were produced after photodetachment for anions m/z 56 and 57, a contradictory observation to the theory for this system, as well as the predictions of the neutral dissociations from Sanov and co-workers. The information about the stable neutral products led to the reassignment of the

OCCO and HOCCO spectra reported by Sanov and co-workers, to the oxyallyl diradical, C_3H_4O[13] and acetone enolate radical, C_3H_5O.[14] The reassignments of these spectra were the direct result of the ability of PPC spectroscopy to measure both the photoelectron spectrum as well as the resulting neutral dissociations or stable products.

III. Future Work

In the coming months we will finalize studies of the $OH^-(C_2H_4)$ system as well as characterize a related and very interesting previously unobserved concerted dissociation channel resulting from DPD of the oxyallyl anion, $C_3H_4O^-$ yielding $CO + C_2H_4$. Following this we will work with the negative ion sources to synthesize new precursors including $O^-(CH_4)$ for studies of the $O + CH_4 \rightarrow OH + CH_3$ radical-radical reaction as well as prepare for studies of other relevant hydroxyl radical systems through association reactions in the RF trap including $OH^-(C_2H_2)$, $OH^-(NO)$, $OH^-(H_2)$, and $OH^-(NH_3)$. With this new synthetic method, we can then return to studies of a range of vibrationally excited anions for control of product branching ratios, starting with the HCO_2^- and $HOCO^-$ anions we have previously used to study the formyloxyl radical, HCO_2,[15] and hydroxycarbonyl radical HOCO.[16] This will pave the way for future studies of transient species with controlled internal excitation, providing benchmark data for fundamental understanding of chemical phenomena.

IV. DOE-supported publications by this project 2016-2018

1. A.W. Ray, J. Agarwal, B.B. Shen, H.F. Schaefer, III and R.E. Continetti, *Energetics and transition-state dynamics of the F + $HOCH_3$ → HF + OCH_3 reaction*, Phys. Chem. Chem. Phys. **18**, 30612-30621 (2016).
2. B. Shen, Y. Benitez, K. G. Lunny, R. E. Continetti, *Internal energy dependence of the photodissociation dynamics of O_3^- using cryogenic photoelectron-photofragment coincidence spectroscopy,* J. Chem. Phys., **147,** 094307 (2017).
3. A. W. Ray, J. Ma, R. Otto, J. Li, H. Guo, R. E. Continetti, *Effects of vibrational excitation on the F + H_2O → HF + OH reaction: dissociative photodetachment of overtone-excited [F-H-OH] ¯, Chem. Sci.,* **8,** 7821-7833 (2017).
4. R.E. Continetti and H. Guo, *Dynamics of transient species via anion photodetachment*, Chem. Soc. Rev. **46**, 7650-7667 (2017).
5. K. G. Lunny, Y. Benitez, Y. Albeck, D. Strasser, J. F. Stanton, R. E. Continetti, *Spectroscopy of Ethylenedione and Ethynediolide: A Reinvestigation,* Angew. Chemie. Int. Ed. **57**, (In Press) (2018), doi:/10.1002/anie.201801848.

References

1. B. B. Shen, Y. Benitez, K. G. Lunny and R. E. Continetti, J. Chem. Phys. **147**, 094307 (2017).
2. A. W. Ray, J. Ma, R. Otto, J. Li, H. Guo and R. E. Continetti, Chemical Science **8**, 7821-7833 (2017).
3. R. Otto, J. Ma, A. W. Ray, J. S. Daluz, J. Li, H. Guo and R. E. Continetti, Science **343**, 396-399 (2014).
4. A. R. Dixon, T. Xue and A. Sanov, Angew. Chem. Int. Ed. **54**, 8764-8767 (2015).
5. K. G. Lunny, Y. Benitez, Y. Albeck, D. Strasser, J. F. Stanton and R. E. Continetti, Angewandte Chemie, Int. Ed. **57** (2018) (in press).
6. R. Otto, J. Ma, A. W. Ray, J. S. Daluz, J. Li, H. Guo and R. E. Continetti, Science **343**, 396 (2014).
7. Y.-J. Lu, J. H. Lehman and W. C. Lineberger, J. Chem. Phys. **142**, 044201 (2015).
8. E. E. Greenwald, S. W. North, Y. Georgievskii and S. J. Klippenstein, The Journal of Physical Chemistry A **109**, 6031-6044 (2005).
9. D. W. Arnold and D. M. Neumark, J. Chem. Phys. **102**, 7035 (1995).
10. D. L. Osborn, D. J. Leahy and D. R. Cyr, J. Chem. Phys. **104**, 5026 (1995).
11. R. J. Li and R. E. Continetti, Journal of Physical Chemistry A **106**, 1183-1189 (2002).
12. A. Dixon, T. Xue and A. Sanov, Angew. Chem. Int. Ed. **54**, 8764-8767 (2015).
13. T. Ichino, S. Villano, A. Gianola, D. Goebbert, L. Velarde, A. Sanov, S. Blanksby, X. Zhou, D. Hrovat, W. T. Borden and W. C. Lineberger, J. Phys. Chem. A **115**, 1634 (2011).
14. L. Alconcel, H. J. Deyerl and R. E. Continetti, J. Am. Chem. Soc. **123**, 12675-12681 (2001).
15. A. W. Ray, B. B. Shen, B. L. J. Poad and R. E. Continetti, Chem. Phys. Lett. **592**, 30-35 (2014).
16. C. J. Johnson, R. Otto and R. E. Continetti, Physical Chemistry Chemical Physics **16**, 19091-19105 (2014).

Theory and simulation of far-from-equilibrium gas-phase chemical dynamics at high pressures and under extreme thermodynamic gradients

Rainer N. Dahms
Combustion Research Facility, Sandia National Laboratories
Livermore, CA 94551-0969
Rndahms@sandia.gov

I. Program Scope

This theoretical and simulation effort on gas-phase chemical dynamics at high pressure and under extreme thermodynamic gradients is based on three primary objectives. The first is to establish a physically-based understanding of far-from-equilibrium conditions within multi-component gas-liquid interfaces and between interactions of molecular transport processes and chemical kinetics. Research of this program focuses on certain high-pressure conditions where characteristic length and time scales of molecular transport become much smaller than corresponding scales of gas-liquid interfaces or low-temperature kinetics. Then, imposed extreme thermodynamic gradients can distinctively alter characteristic physical features such as interfacial thicknesses and reactivity. Sophisticated theoretical frameworks and high-fidelity molecular dynamics simulations have to be developed to understand and quantify the relation between the strength of thermodynamic gradients and their ability to alter physical properties of interest. A comprehensive understanding of the underlying relevant phenomena is required to predict and control the stability of the system in order to harness tailor-made physical properties. In this context, a major focus is the development of a more complete set of non-dimensional parameters for generalized regimes that incorporate extreme thermodynamic gradients when they can couple to gas-phase chemical dynamics. The second objective is to develop techniques and methods to interpret data sets obtained from small-scale measurements such as those performed in the Advanced Imaging Laboratory or at the APS of Argonne National Laboratory. Such measurements typically quantify a selected set of certain physical features that, if combined with theory and simulation, can provide even more comprehensive and more direct physical insights into the governing physics. In this context, another focus is the development of methods to directly couple such measurements to the theoretical and simulation efforts which are inherently limited in their ability to represent the exact conditions and physics as encountered in experiments. Such coupling is imperative, however, to fully utilize the unique and diverse capabilities in a concerted manner. The fundamental issues of comparing, validating, and understanding advanced data sets will become even more important as we attempt to understand data sets that capture the temporal evolution of far-from-equilibrium gas-phase chemical dynamics. The third objective is to understand the implications of the conclusions obtained from well-controlled experiments in the context of relevant natural and industrial processes including evaporation, respiration, atmospheric chemistry, deep-ocean hydrothermal vents, multi-phase catalysis, synthesis of rare carbon hydrogen molecules, and modern combustion chamber design. The objective builds on the developed theoretical framework, which establishes a meaningful set of major scaling parameters. Combined with the identification of relevant ranges of far-from-equilibrium regimes and non-dimensional parameters, the framework will serve the general objective of this program to accelerate the development and validation of science-based, predictive computational models for general gas-phase chemical dynamic systems.

II. Recent Progress

Understanding and quantifying gas-phase chemical dynamics at high pressures and under extreme thermodynamic gradients addresses the BES Grand Challenge of characterizing and controlling matter far

away from equilibrium and of understanding the critical role of interfaces[1] and also addresses priority research directions (PRD) that were recently identified in several BES Workshops. This research furthers the goal to achieve "mechanistic control of interfaces and transport in complex and extreme environments", which was identified as a PRD in the BRN report for "Energy and Water."[2]

Gas-liquid interfaces are important in many natural and industrial processes spanning a wide range from evaporation, respiration, atmospheric chemistry, multi-phase catalysis, synthesis of rare carbon hydrogen molecules, formation mechanisms of gas clathrate hydrates in extreme thermodynamic gradients, deep-ocean hydrothermal vents, and fuel spray injection in internal combustion engines. Imaging (such as those performed by Mayer *et al.*[3]) has long shown that under some high-pressure conditions, the presence of discrete two-phase flow dynamics may become diminished. Then, the characteristic processes of primary and secondary atomization, multi-component evaporation, and liquid ligament and drop formation do not occur. As a consequence, the widely acknowledged drop formation and breakup regimes (see Lasheras and Hopfinger[4]), which establish the conceptual foundations of most spray simulation models, do not apply anymore. Modern theory has long lacked a first-principle explanation to understand and quantify the observed phenomena (see a recent review by Cheroudi[5]). Recently, such a theory has been developed that established that the development of such mixing layers is initiated when multicomponent two-phase molecular interfaces become part of the continuum regime (see Dahms *et al.*[6]). This theory demonstrated that fuel injection processes in diesel engines are not determined, contrary to conventional wisdom, by classical spray atomization but by diffusion-dominated dense-fluid mixing dynamics without the presence of surface tension at many relevant conditions (see Dahms *et al.*[7]).

Recent studies aimed to understand the initiation of the transition process from a distinct molecular gas-liquid interface to a far-from-equilibrium transitional layer. The performed analysis was built on the previously developed comprehensive framework, based on theories of extended corresponding states, capillary flows, vapor-liquid equilibrium, and Gradient Theory (see for example the pioneering work of van der Waals[8] and Cahn and Hilliard[9]) to facilitate the calculation of two-phase molecular interface structures close to thermodynamic equilibrium.

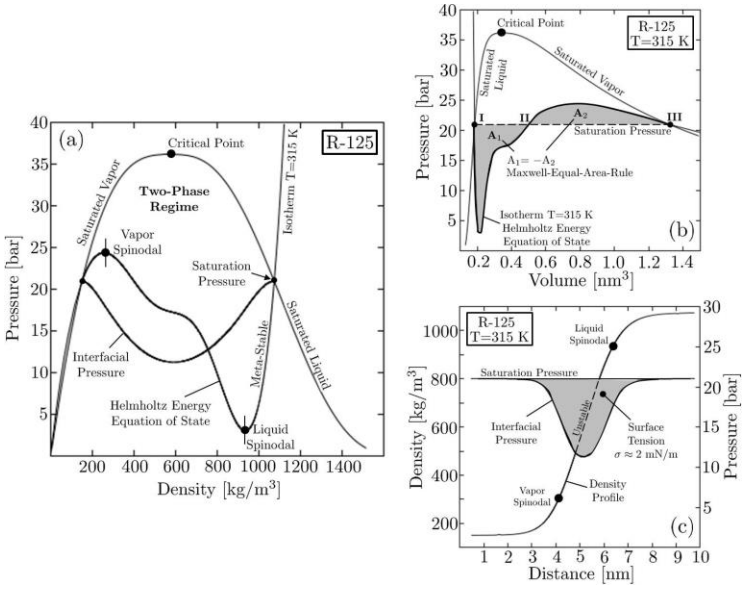

Figure 1: *Classic molecular mean-field relations within thermally equilibrated gas-liquid interfaces. (a) Intense interfacial molecular gradients significantly alter the tangential pressure distribution compared to a homogeneous solution, which is also highlighted in (b). The spatial interfacial density profile, shown in (c), demonstrates the exact relation between surface tension and the tangential pressure distribution. It also shows the locations of the vapor and liquid spinodal along an isotherm. (see Dahms[10]).*

Figure 1 illustrates common molecular mean-field relations within classic and widely-accepted gas-liquid interfacial structures. Illustrated on the tangential pressure distribution, which is exactly related to the directly measurable surface tension force, Fig. 1 shows how the strength of interfacial molecular gradients

significantly alter interfacial thermodynamic and transport properties in comparison to a homogeneous solution without such gradients. The steepness of the molecular gradients and their efficiency to alter interfacial properties are a direct consequence, according to conventional wisdom, of the implicitly applied assumption of a thermally equilibrated gas-liquid interfacial system. This fundamental assumption is valid as long as thermal gradients cannot manifest in gas-liquid interfaces. Hence, thermal collision length scales, above which thermal gradients can exist, must be wider than the interfacial thickness.

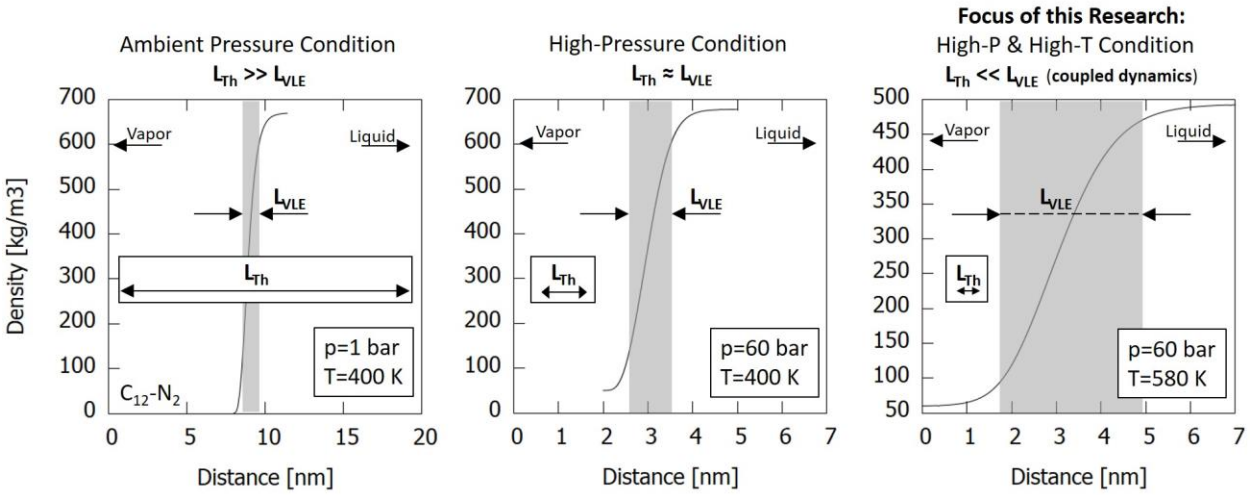

Figure 2: *Gas-liquid interface mean-field density profiles, thicknesses (shaded area) and vapor phase thermal collision length scales (insets) at (left) ambient pressures, (middle) high-pressure conditions, and (c) the targeted high-pressure high-temperature conditions, calculated using Non-Linear Gradient Theory and ab-initio molecular dynamics, where extreme thermodynamic gradients can couple with the interfacial dynamics.*

Figure 2 (left) and (middle) show that this fundamental assumption is supported at ambient and high-pressure conditions where vapor phase thermal collision length scales remain wider than interfacial thicknesses. Contrary to conventional wisdom, however, thermal gradients can manifest across the interfacial region at certain combinations of high-pressure, high-temperature conditions and multiple chemical constituents, as illustrated in Fig.2 (right). The resulting departure from thermal equilibrium distinctively alters the strength of the molecular gradients within the evolving far-from-equilibrium interfacial layer. Those departures can be estimated if the present extreme thermodynamic gradients are considered within the mean-field equations. As a consequence, these previously unrecognized, far-from-equilibrium gas-liquid interfaces can exhibit unique combinations of temperature, density, composition, and their gradients with near-critical physical, transport, and chemical properties.

III. Future Work

Driven by this theoretical framework, future research is aimed to develop a molecular-level understanding of far-from-equilibrium gas-liquid interfaces through a combination of high-fidelity molecular dynamic simulations and continued efforts on theory. Research goals revolve around understanding and quantifying far-from-equilibrium interfacial properties such as permeability, solubility, molecular orientation and dephasing, interfacial thickness, and molecular transport in such unexplored environments as functions of the strength of imposed extreme thermodynamic gradients. New insights gained through these investigations will advance our understanding of interfaces and provide a scientific foundation for controlling matter far away from equilibrium.

IV. Literature Cited

1. BESAC Advisory Committee: Challenges at the Frontiers of Matter and Energy: Transformative Opportunities for Discovery Science (November 2015).
2. Basic Research Needs for Energy and Water (2017), https://science.energy.gov/~/media/bes/pdf/brochures/2017/Energy_and_Water_Brochure.pdf
3. W. Mayer and H. Tamura. Propellant injection in a liquid oxygen/gaseous hydrogen rocket engine. *Journal of Propulsion and Power* **12**:1137-1147, 1996.
4. J.C. Lasheras and E.J. Hopfinger. Liquid jet instability and atomization in a coaxial gas stream. *Annu. Rev. Fluid Mech*. **32**:275-308, 2000. doi: 10.1146/annurev.fluid.32.1.275
5. B. Chehroudi. Recent experimental efforts on high-pressure supercritical injection for liquid rockets and their implications. *Intl. J. Aerospace Engineering* **2012**:1-31, 2012. doi: 10.1155/2012/121802
6. R.N. Dahms, J. Manin, L.M. Pickett, and J.C. Oefelein. Understanding high-pressure gas-liquid interface phenomena in diesel engines. *Proc. Combust. Inst.* **34**:1667-1675, 2013. doi: 10.1016/j.proci.2012.06.169
7. R.N. Dahms and J.C. Oefelein. On the transition between two-phase and single-phase interface dynamics in multicomponent fluids at supercritical pressures. *Phys. Fluids* **25**, 092103, 2013. doi: 10.1063/1.4820346
8. J.D. van der Waals. Square gradient model. *Verhandel Konik Akad Weten Amsterdam* **1**:8-15, 1893.
9. J.W. Cahn and J.E. Hilliard. Free energy of a nonuniform system. I. Interfacial free energy. *J. Chem. Phys*. **28**:258-267, 1958
10. R. N. Dahms. Gradient Theory simulations of pure fluid interfaces using a generalized expression for influence parameters and a Helmholtz energy equation of state for fundamentally consistent two-phase calculations. *J. Colloid Interface Sci*., **445**:48–59, 2016. doi:10.1016/j.jcis.2014.12.069

V. BES Sponsored Publications (2016-2018)

11. R. N. Dahms, G. A. Paczko, S. A. Skeen, and L. M. Pickett. Understanding the ignition mechanism of high-pressure spray flames. *Proc. Combust. Inst*., **36**:2615-2623, 2017. doi:10.1016/j.proci.2016.08.023
12. R. N. Dahms. Understanding the breakdown of classic two-phase theory and spray atomization at engine-relevant conditions. *Phys. Fluids*, **28**:042108, 2016, doi:10.1063/1.4946000

Dynamics of Combustion Reactions

H. Floyd Davis
Department of Chemistry and Chemical Biology
Cornell University, Ithaca, NY 14853-1301
hfd1@cornell.edu

I. Program Scope:

Bimolecular and unimolecular reactions of gas-phase polyatomic free radicals usually involve multiple reaction intermediates and transition states, leading to competing product channels. We are carrying out experimental studies of reactions involving polyatomic free radicals using a crossed molecular beams apparatus to gain insight into the topography of the relevant ground electronic state reactive potential energy surfaces. Bimolecular studies include oxidation reactions of hydrocarbon free radicals with O_2, as well as reactions of OH radicals with alkenes. A new research direction for the group involves studies of the unimolecular decomposition of polyatomic free radicals on ground electronic state surfaces induced by C-H vibrational overtone excitation.

II. Recent Progress:

Our DOE-supported research at Cornell employs Endstation 1 (ES1), a rotatable source crossed molecular beams apparatus originally utilizing synchrotron radiation for "soft" photoionization of products from photodissociation and bimolecular reactions. As discussed in our PCCP perspective article,[1] high intensity pulsed tabletop VUV light sources[2] provide several advantages over quasicontinuous synchrotron radiation in experiments employing pulsed radical beams. The following recent developments form the foundation for our future experiments:

a) A windowless beamline has been developed and installed on ES1, extending the range of photoionization energies to 8.5-11.9 eV using tabletop high-intensity pulsed VUV lasers. This opens up our ability to detect most primary products from bimolecular and C-H vibrational overtone induced unimolecular reactions of interest, including HO_2 (I.E. = 11.4 eV), a primary product from alkyl radical + O_2 reactions. Photoionization energies of 9.5, 9.9, 11.0, and 11.9 eV can be readily and conveniently selected during the course of an experiment with only minor adjustment of the lasers using the configuration shown in Fig. 1. Note that this approach employs unfocussed lasers, allowing us to reach significantly higher VUV/XUV intensities than a method reported earlier by us employing a laser vaporization source, which involved frequency mixing of focused noncollinear beams.[3] The use of unfocussed pulsed lasers with nonlinear frequency conversion into the VUV and XUV

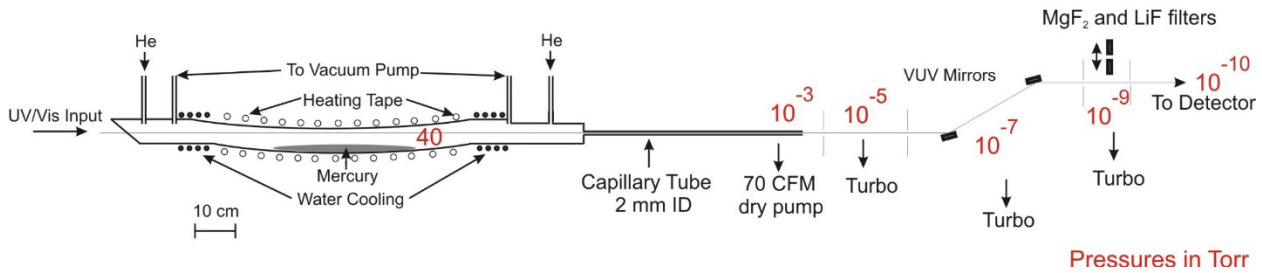

Fig. 1: Windowless Light Source now installed on ES1 at Cornell.

represents a lower-cost alternative to synchrotron- or free electron laser-based approaches for true "universal" photoionization detection.

b) As part of our development and characterization of pulsed hydrocarbon free radical sources, we have studied the UV photodissociation dynamics of three related alkyl iodides: 1-iodopropane, 2-iodopropane, and t-butyl iodide.[4] In contrast to methyl iodide, where only C-I bond fission is operable at 266 nm, we have found that HI elimination plays an important role in secondary and tertiary compounds, forming the corresponding alkenes. The HI yield is smallest (zero) for 1-iodopropane, increasing in the order of $1^o << 2^o < 3^\circ$ iodoalkanes. An interesting observation is that the polarization angular distributions for the HI elimination channels are strongly anisotropic, like the I atom elimination channels, with the β-parameters approaching the limiting values of +2.0 in all cases. This suggests that HI elimination occurs fast on an electronically excited surface, rather than via internal conversion. Another interesting observation is that the translational energy distributions for the HI channels are nearly identical to those for I*, despite the much larger available energy. The excess energy is primarily deposited into the HI, with most formed in $v \geq 4$. Although I* is by far dominant for 1-iodopropane, it is minor for 2-iodopropane. In the case of 1- and 2- iodopropane, the C_3H_7 products are produced with levels of internal excitation below the energetic thresholds for decomposition to C_3H_6 + H. For t-butyl iodide photodissociation at 266 nm, the I* channel is also minor (<5%), and the HI channel contributes to an even greater extent than in the 2-iodopropane case. From our observation of essentially *no* HI from 1-iodopropane, we suggest the HI yields reflect the energy dependence of a curve crossing, most likely between potential energy surfaces correlating with alkene + HI and those for heterolytic bond fission forming ion pairs, the latter more energetically favored with increasing degrees of branching at the α-carbon atom.

c) Flash pyrolysis of azo compounds (R-N=N-R, where R = CH_3, C_2H_5, 1-C_3H_7 and 2-C_3H_7) using a short (~1cm) heated SiC tube (1000-1300^{o}C) attached to a pulsed valve nozzle provides intense beams of alkyl radicals. Using this approach, we have carried out preliminary studies of the 248 nm photodissociation of 1- and 2-propyl radicals (C_3H_7).[5] Previous studies by others showed that H atom elimination forming propene plays an important role in the UV photodissociation dynamics. Fission of a C-H bond can occur from either C_3H_7 isomer via a small barrier in excess of the bond dissociation energy on the ground electronic surface (Fig. 2). However, C-C bond fission producing CH_3 + C_2H_4 is actually a thermodynamically more favorable channel, but has not been detected in previous studies. These C-C fission channels also possess barriers along the reaction pathways, even in the case of 1-C_3H_7, where C-C bond fission can produce methyl radicals + ethylene. Production of CH_3 directly from C-C bond fission in the 2-propyl radical produces the high-energy singlet ethylidene isomer, ($CHCH_3$) lying ~70 kcal/mol above ground state singlet ethylene. The TOF data in Fig 3 were simulated using a P(E) for the CH_3+ C_2H_4 channel peaking at 5 kcal/mol, extending to a maximum of

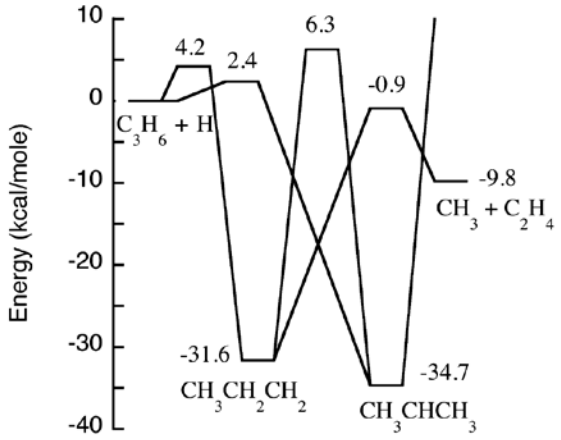

Fig. 2: Simplified ground state PES for dissociation of 1- and 2-propyl radicals, Miller & Klippenstein, *J.Phys.Chem. A.* 117, 2718 (2013).

~18 kcal/mol. This $CH_3 + C_2H_4$ P(E) differs from that for the 1-propyl radical, which was much broader, and extending to nearly 50 kcal/mol. Clearly, a much larger fraction of excess energy appears as internal excitation of the C-C bond fission products for the 2-propyl case, suggesting that the ethylidene isomer is likely produced. In order to check and confirm these observations, we are currently studying the photodissociation dynamics of alkyl radicals produced by photolytic sources, with iodoalkanes (266 nm) and alkyl nitrites (266 nm) examined so far. The primary issue in these cases is interference from photodissociation of the parent compounds, which, like the alkyl radicals, absorb quite strongly in the 240-250 nm range. For these reasons, photolysis of alkyl bromides at 213 nm (Nd:YAG 5th harmonic) or azo compounds at 355 nm appear to be promising, and are currently under investigation.

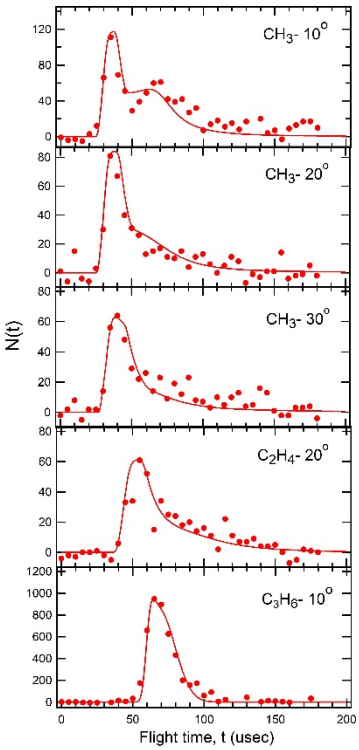

Fig. 3: TOF spectra for the products from 248 nm photodissociation of 2-propyl radicals.

III. Future Plans:

a) Oxidation Reactions of Hydrocarbon Radicals:

The reactions of alkyl radicals with molecular oxygen are extremely important in combustion chemistry. The $C_2H_5 + O_2$ system is the simplest prototype, for C_2H_5 is the smallest saturated hydrocarbon radical in which formation of HO_2 and OH are both thermodynamically accessible elementary channels. Although the ethyl radical reaction is attractive because only two chemical channels are present, in experiments carried out to date in our laboratory on ES1 prior to installation of our windowless beamline (previously limited to <10.2 eV photoionization), we focused on reactions involving 1- and 2- propyl radicals, because the products could be readily ionized, unlike those from ethyl radical reactions, which have ionization energies above 10.2 eV. The propyl radicals have been produced primarily by 266 nm photodissociation of 1- and 2- propyl iodide or by pyrolysis of the appropriate azoalkanes synthesized via a 3-step procedure. The primary issue that has been encountered to date is the presence of aldehyde or ketone impurities in the azoalkane samples, which interfere with the observation of the primary product channel leading to OH production. Recent efforts towards purification of the azoalkane sample using column chromatography appear to be successful. Similarly, detection of the alkene products correlating with HO_2 product channel is subject to interference by dissociative ionization of nonreactively scattered alkyl radical reactants. This was one major driving force towards our recent development of a high-intensity 11.9 eV pulsed photoionization light source, which facilitates direct photoionization detection of the HO_2 product. This should allow us to surmount this significant experimental difficulty.

b) Reactions of OH Radicals with Alkenes

The reactions of hydroxyl radicals (OH) with alkenes are of considerable interest in combustion chemistry. In 2005, substantial levels of two, three and four- carbon enols (compounds having adjacent C=C and OH moieties) were observed in flames burning representative compounds in modern fuel blends. One primary mechanism for enol formation involves bimolecular addition of OH to ethylene followed by H atom elimination: $OH + C_2H_4 \rightarrow C_2H_4OH \rightarrow C_2H_3OH + H$. Theoretical

studies have been able to reproduce most of the experimental data, and they confirm that the vinyl alcohol channel is significant (>10%) above 800K. In addition to the H atom elimination channel forming ethenol via a substantial exit channel barrier, rearrangement of the initially-formed intermediate can lead to formation of a number of additional products including the lower energy acetaldehyde isomer or production of $H_2CO + CH_3$ or $C_2H_3 + H_2O$. We plan to map out these reaction dynamics through crossed beam studies.

Because of the large 193 nm absorption cross section, photolysis of nitric acid was used for OH production in previous reactive scattering studies. However, the HONO + O channel is actually dominant, with ground (^3P_J) and singlet ($^1D_2$) excited oxygen atom production, leading to possible interfering reactions. Although 248 nm photolysis of HNO_3 yields exclusively $OH + NO_2$, the absorption cross section is too small ($2 \times 10^{-20} cm^2$) to make this source viable. By frequency mixing of the fourth harmonic of a Nd:YAG (266 nm) with the fundamental (1064 nm) in the nonlinear crystal CLBO, we can generate intense (>20 mJ) pulses at 213 nm. Since the HNO_3 absorption is significant ($\sigma = 7 \times 10^{-19}$ cm^2) at 213 nm, this appears to be an excellent source of OH. Since HNO_3 photodissociation has not been characterized previously at 213 nm, we have recently begun undertaking studies of this primary photochemistry at this wavelength.

c) U*nimolecular dissociation of vibrationally excited ground state radicals:*

We plan to initiate studies of the unimolecular decomposition of vibrationally-excited ground state hydrocarbon radicals. Our first experiments will focus on the 1- and 2- propyl radicals. As already noted, we have considerable experience generating these species and both C-H and C-C bond fission is expected to occur at low energies on the ground electronic state surfaces (Fig 2). Our first set of experiments will involve pumping the fourth overtone (v=5) of the C-H stretching region near 750 nm. Since H atoms are produced by C-H bond fission, after mapping out the dynamics by monitoring the heavy C_3H_6 fragment (as well as studying C-C bond fission producing $CH_3 + C_2H_4$), we can move our existing Rydberg tagging TOF detector to ES1 to do Rydberg tagging TOF measurements. This would allow us to obtain much better translational energy resolution for the alkene channels, it should be possible to observe product vibrational structure.

IV. Publications from 2013-2018 citing DOE support:

1. D.R. Albert and H.F. Davis "Experimental Studies of Bimolecular Reaction Dynamics Using Pulsed Tabletop VUV Photoionization Detection", invited perspective article, *Phys. Chem. Chem. Phys.* 15, 14566-14580 (2013).

2. D.R. Albert, D.L. Proctor, and H.F. Davis, "High-Intensity Coherent Vacuum Ultraviolet Source Using Unfocussed Commercial Dye Lasers", *Rev. Sci Instrum.* 84, 063104 (2013).

3. M.A. Todt, D.R. Albert, H.F. Davis, "High Intensity VUV and XUV production by noncollinear mixing in laser vaporized Media", *Rev. Sci. Instrum.* 87, 063106 (2016).

4. Competing Pathways from the UV Photodissociation of Primary, Secondary and Tertiary Alkyl Iodides, M. A. Todt, A. Rose, K. Leung, A. H. F. Davis, *J. Chem. Phys.*, submitted for publication.

5. M.A. Todt and H.F. Davis, "Photodissociation dynamics of 1- and 2- propyls radical at 248 nm: the $CH_3 + C_2H_4$ channels", in preparation.

Exploration of chemical-kinetic mechanisms, chemical reactivity, and thermochemistry using novel numerical analysis

Michael J. Davis

Chemical Sciences and Engineering Division
Argonne National Laboratory
Argonne, IL 60439
Email: davis@tcg.anl.gov

The work involves exploration of chemically reactive systems using novel numerical analyses. One focus of the work is exploration and theoretical validation of chemical-kinetic mechanisms, combining global sensitivity analysis with the exploration of the characteristics of the sensitivity analysis over physical and chemical parameters. An important aspect of this part of the work is the use of state of the art methods in numerical analysis, statistics, and signal processing for making the global sensitivity analysis efficient for large-scale chemical mechanisms. An effort on reaction pathway analysis has also been undertaken. The global sensitivity and reaction pathway analyses are used to pinpoint chemical reactions that need to be studied accurately to improve the accuracy of chemical mechanisms. The expertise developed in that work has led to a second focus: the implementation of these techniques for studying problems in chemical reactivity, including isolated chemical kinetics and dynamics. Key features of this focus are regression analysis, optimal sampling, power transformations, and subset selection. There is a major effort underway for using these techniques for fitting potential energy surfaces, where it is difficult to scale existing methods to larger molecular systems. Generating accurate potential surfaces is important for developing fundamental understanding of chemical reactivity.

Recent Progress

Progress has continued in three main areas in the past year. The first is the application of sparse regression to select the most sensitive reactions in engine simulations. It is a collaboration between our group (Davis, Sivaramakrishnan *et al*) and the Engines and Emission group at Argonne (Magnotti, Som, *et al*). The second focus has been the application of a new version of reaction pathway analysis to the low-temperature ignition of propane, a collaboration between University of Colorado (Bai and Skodje) and our group (Sivaramakrishnan and Davis). The third and main focus of the progress in the last year is the development of optimal sampling strategies for fitting with basis functions and its application to the fitting of potential energy surfaces, a collaboration with Jasper in our group.

We studied the sensitivity of the ignition delay time of a mixture of n-heptane and methylbutanoate to uncertainties in the chemical reaction rates in realistic simulations of compression-ignition engines (e.g., diesel engines). This required 800 simulations, each taking a few processor weeks to complete. Each simulation used a different set of rate coefficients for the chemical reactions, as sampled from the range of uncertainties of each chemical reaction in the chemical mechanism (there are 914 reactions in the reduced model used). Sparse regression facilitated the calculation, reducing the number of simulations from 2500 needed in our best previous method (Ref. 10), which was itself considerably reduced from 36,000, which would have been needed in earlier algorithms, based on 40 simulations per reaction. The sparse global sensitivity analysis identified 13 reactions, as described in Ref. 11.

In order to effectively study under what conditions these 13 reactions occurred in the engine cylinder, a comparison was made between the sensitivity rankings of these 13 reactions in the engine cylinder to sensitivity results for homogeneous, constant pressure simulations. A set of 50 constant pressure cases were run, each of which included 50,000 simulations. The cases

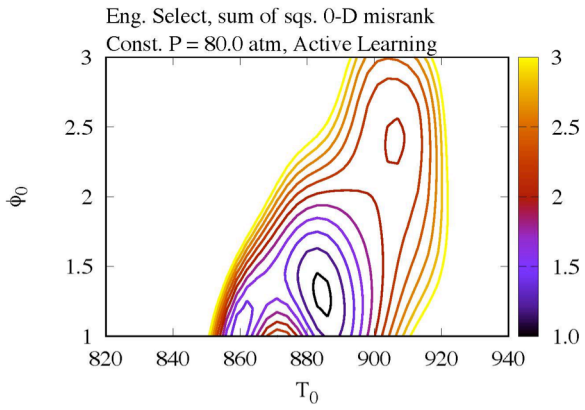

Fig. 1. Selection mismatch between the engine case and the homogeneous case is shown.

were sampled over a range of pressures, initial temperatures, and initial equivalence ratios using Latin Hypercube sampling. A three-dimensional surface was generated using the Gaussian Process Model to describe the rms difference between chemical reaction selection for constant pressure simulations and the engine simulations. An additional two sets of simulations were run to approximately locate the minimum, an example of active learning. Figure 1 is a two-dimensional slice of this three-dimensional surface at P = 80 atm (the range of pressures was 70 – 90 atm). It demonstrates that there is selection agreement between the engine and constant pressure simulations over a relatively narrow range of temperature, and the strongest agreement occurs for a nearly stoichiometric equivalence ratio, as the lowest point on the plot is near ϕ_0 = 1.2, T_0 = 890 K.

We investigated a subset of the 800 engine simulations based on the selection rankings in Fig. 1 and optimal experimental design, with a representative visualization shown in Fig. 2, for the two species that participate in the most sensitive reaction as calculated from the global

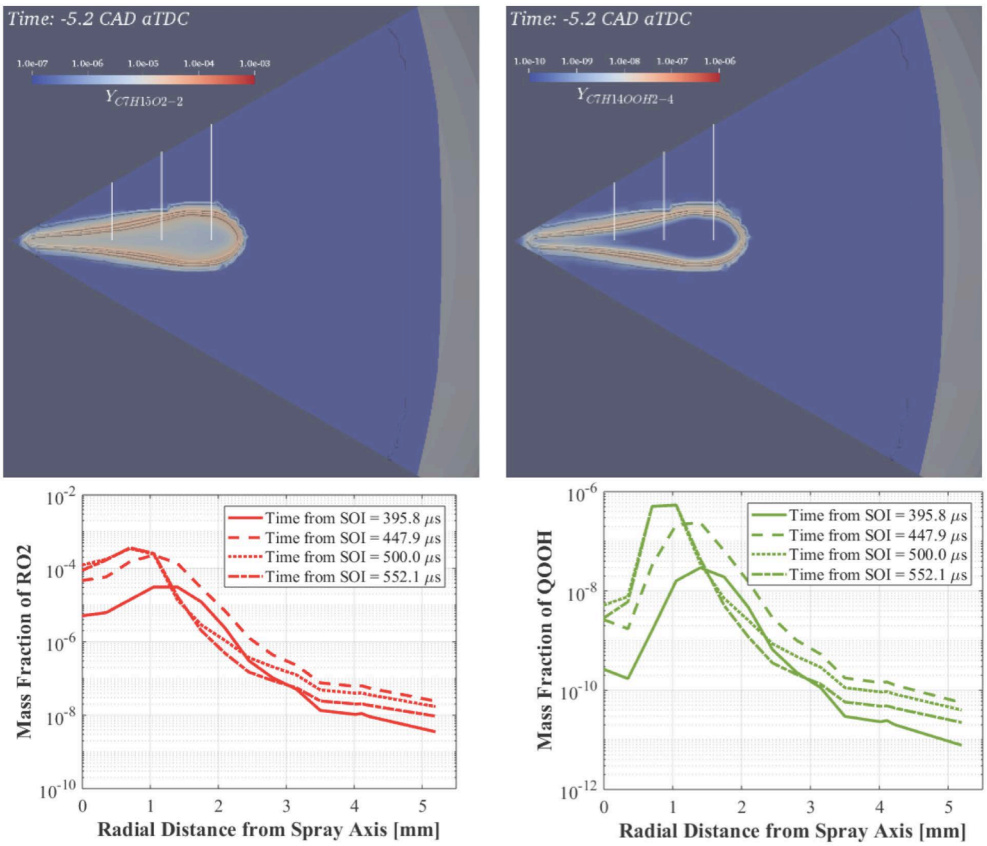

Fig. 2. Visualizations of the RO_2 and QOOH species for the most sensitive reaction are shown and described in detail in the text. Time from start of fuel injection is shown on the bottom panels in physical units. Times to ignition for these cases are 0.16 ms, 0.10 ms, 0.05 ms, and 0.0 ms. Time units in the top panels are crank angle degrees from maximum compression.

sensitivity analysis. The top panels show the location of each species and are color-coded for their mass fractions. Each panel has four temperature contours: 800 K, 850 K, 900 K, and 950 K, from innermost to outermost. These contours demonstrate that most of the concentration of the QOOH species, which is always small, is present in the temperature range suggested by Fig. 1.

There are 3 white vertical lines on each of the two top panels that emanate from the center of the spray. We investigated the species along these lines to better visualize where the RO_2 = QOOH reaction occurred. One-dimensional plots of the two species along the first of these lines is shown in the bottom two panels at the same time as in the top panel, plus three additional times. The legend in the bottom panels indicates time from start of injection and the caption of the figure also includes the time to ignition for these cases. The bottom panel indicates that while the RO_2 species increases by factors of 2 – 4, the QOOH species increases by up to several orders of magnitude as one moves way from the center of the spray. Both species peak around 1 mm from the center of the spray and then decrease from there.

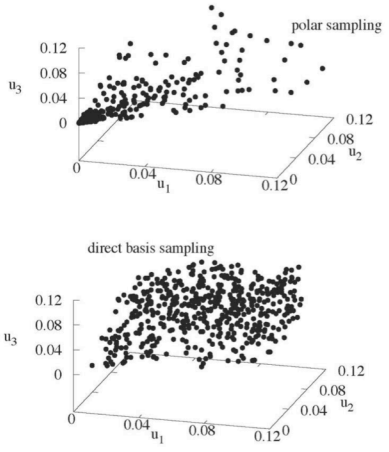

Fig. 3. Random sampling in polar coordinates leads to the basis sampling in the top panel and direct basis sampling leads to the sample in the bottom panel

The numerical methods used in the sensitivity analysis work, particularly Ref. 10, have been applied to the fitting of potential energy surfaces. The potential energy surfaces are fit with direct product basis functions using Morse type functions. It is clear from our work on regression analysis that efficient sampling should be based on these basis functions and a three-dimensional example is shown in Fig. 3 for fitting a surface describing the collision of He with HO_2. The distances in this problem are defined as r_1, r_2, r_3 and are in angstroms. The expansion of the potential surface is done in basis sets consisting of products of u_k^m, $u_k \equiv e^{-r_k}$. A random sample starting in polar coordinates is shown in the top panel after conversion to the u-coordinates and is compared to random sampling in the u-coordinates in the bottom, which obviously covers the function space more uniformly. The sampling method is named "direct basis sampling" and can only be applied in three dimensions (a random set of distances will not yield a physically realizable set of coordinates in more than three dimensions). We have developed an indirect method that can be used in higher dimensional systems and are in the process of applying it to higher dimensional potential energy surfaces. Our goal in this work is to develop sampling methods that will lead to accurate potential energy surface fits with a small number of points.

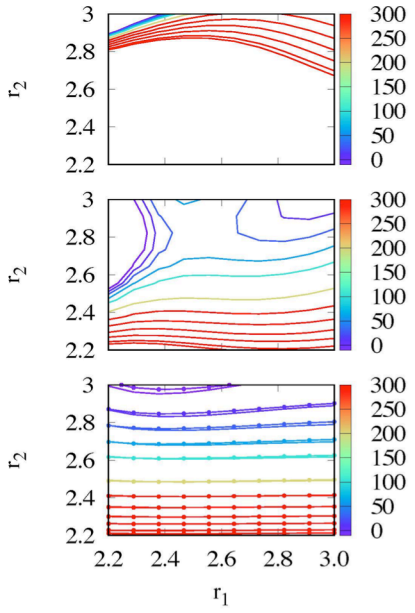

Fig. 4. Three fits are shown for the potential surface of He + HO_2. The r's are distances in angstroms.

The basis set sampling is the start of an optimal sampling procedure using algorithms developed in the optimal experimental design and

machine learning literatures. Figure 4 compares results for the He-HO_2 potential at fixed values of the second He-O distance, r_3, for an extremely small number of fitting points, 21 points for 20 basis functions. The top panel shows a fit with points chosen by polar sampling and is a catastrophically poor fit, as expected. When 21 points are used from basis-set sampling the accuracy of the potential surface fit increases significantly, but not until optimal sampling is used in conjunction with the basis set sampling does good agreement result, as shown in the bottom panel, where the solid line is the fit compared to the exact surface shown as solid lines with dots (the exact potential is a nonlinear fit to *ab initio* quantum chemistry computations). The optimal sampling used for the bottom panel is called a G-optimal design, a common design in the optimal experimental design literature. The algorithm used to generate the optimal sampling is the Fedorov exchange algorithm, a form of point exchange algorithm.

Future Plans

The work on optimal sampling for fitting potential energy surfaces will be extended to larger systems in collaboration with Jasper. It will also be extended to the fitting of force fields for materials in collaboration with Jasper and M. Chan (Center for Nanoscale Materials at Argonne). Work will continue on reaction pathway and sensitivity analyses, as well as a continued search for novel algorithms to apply to problems in chemical dynamics.

Publications

1. S. Bai, D. Zhou, M. J. Davis, and R. T. Skodje, "Sum over Histories Representation for Chemical Kinetics", J. Phys. Chem. Lett., 6, 183–188 (2015).
2. D. M. A. Karwat, M. S. Wooldridge, S. J. Klippenstein, and M. J. Davis, "Effects of New Ab Initio Rate Coefficients on Predictions of Species Formed during *n*-Butanol Ignition and Pyrolysis", J. Phys. Chem. A 119, 543-551 (2015).
3. Y. Pei, M. J. Davis, L. M. Pickett, S. Som, "Engine Combustion Network (ECN): Global sensitivity analysis of Spray A for different combustion vessels", Combustion and Flame 162, 2337-2347.
4. S. Som, Z. Wang, G. M. Magnotti, W. Liu, R. Sivaramakrishnan, and M. J. Davis, "Application of Sparse Sensitivity Analysis to Detailed Chemical Kinetics in High Fidelity Compression-Ignition Engine Simulations", Proceedings of the 9th US National Technical Meeting of the Combustion Institute (2015).
5. F. G. Sen, A. Kinaci, B. Narayanan, S. K. Gray, M. J. Davis, S. K. R. S. Sankaranarayanan, and M. K. Y. Chan, "Towards Accurate Prediction of Catalytic Activity in IrO2 Nanoclusters Via First Principles-Based Variable Charge Force Field", J. Mater. Chem A 3, 18970-18982 (2015).
6. S. Bai, M. J. Davis, and R. T. Skodje, "The Sum Over Histories Representation for Kinetic Sensitivity Analysis: How Chemical Pathways Change When Reaction Rate Coefficients Are Varied", J. Phys. Chem A 119, 11039-11052 (2015).
7. B. Narayanan, A. Kinaci, F. G. Sen, M. J. Davis, S. K. Gray, M. K. Y. Chan, and S. K. R. S. Sankaranarayanan, "Describing the Diverse Geometries of Gold from Nanoclusters to Bulk—A First-Principles-Based Hybrid Bond-Order Potential", J. Phys. Chem. C. 120, 13787-13800 (2016).
8. B. Narayanan, K. Sasikumar, Z.-G. Mei, A. Kinaci, F. G. Sen, M. J. Davis, S. K. Gray, M. Chan, and S. K. Gray, M. K. Y. Chan, and S. K. R. S. Sankaranarayanan, "Development of a Modified Embedded Atom Force Field for Zirconium Nitride Using Multi-Objective Evolutionary Optimization", J. Phys. Chem. C 120, 17475–17483 (2016).
9. A. Kinaci, B. Narayanan, F. G. Sen, M. J. Davis, S. K. Gray, M. Chan, and S. K. Gray, M. K. Y. Chan, and S. K. R. S. Sankaranarayanan, "Unraveling the Planar-Globular Transition in Gold Nanoclusters through Evolutionary Search", Scientific Reports 6, online in November, 2016.
10. M. J. Davis, W. Liu, and R. Sivaramakrishnan, "Global Sensitivity Analysis with Small Sample Sizes: Ordinary Least Squares Approach", J. Phys. Chem. A 121, 553-570 (2017).
11. G. M. Magnotti, Z. Wang, W. Liu, R. Sivaramakrishnan, S. Som, and M. J. Davis, "Sparsity Facilitates Chemical Reaction Selection for Engine Simulations", to be submitted.
12. S. Bai, R. Sivaramakrishnan, M. J. Davis, and R. T. Skodje, "A Chemical Pathway Perspective on the Kinetics of Low-Temperature Ignition of Propane", to be submitted.
13. A. W. Jasper and M. J. Davis, "Parameterization Strategies for Intermolecular Potentials for Trajectory-Based Collision Parameters", to be submitted.

Theoretical and Experimental Studies of Elementary Hydrocarbon Species and Their Reactions (DE-SC0018412)

Gary E. Douberly and Henry F. Schaefer III
University of Georgia, Center for Computational Quantum Chemistry and Department of Chemistry, 1004 Cedar St., Athens, GA 30602-1546
douberly@uga.edu

Program Scope

The objective of this research is to isolate and stabilize transient intermediates and products of prototype combustion reactions. This will be accomplished by Helium nanodroplet isolation (HENDI) spectroscopy, a novel technique where liquid helium nanodroplets freeze out high energy metastable configurations of a reacting system, permitting infrared spectroscopic characterizations of products and intermediates that result from hydrocarbon radical reactions with molecular oxygen and other small molecules relevant to combustion environments. A major aim of this work is to directly observe the elusive hydroperoxyalkyl radical (QOOH) and its oxygen adducts (O2QOOH), which are important in low temperature hydrocarbon oxidation chemistry.

Recent Projects

Helium Nanodroplet Isolation of the Cyclobutyl, 1-Methylallyl and Allylcarbinyl Radicals: Infrared Spectroscopy and Ab Initio Computations

Gas phase cyclobutyl radical ($\cdot C_4H_7$) is produced *via* pyrolysis of cyclobutylmethyl nitrite ($C_4H_7(CH_2)ONO$). Other $\cdot C_4H_7$ radicals, such as 1-methylallyl and allylcarbinyl, are similarly produced from nitrite precursors. Nascent radicals are promptly solvated in liquid He droplets, allowing for the acquisition of infrared spectra in the CH stretching region. For the cyclobutyl and 1-methylallyl radicals, anharmonic frequencies are predicted by VPT2+K simulations based upon a hybrid CCSD(T) force field with quadratic (cubic and quartic) force constants computed using the ANO1 (ANO0) basis set. A density functional theoretical method is used to compute the force field for the allylcarbinyl radical. For all $\cdot C_4H_7$ radicals, resonance polyads in the 2800-3000 cm^{-1} region appear as a result of anharmonic coupling between the CH stretching fundamentals and CH_2 bend overtones and combinations. Upon pyrolysis of the cyclobutylmethyl nitrite precursor to produce the cyclobutyl radical, an approximately two-fold increase in the source temperature leads to the appearance of spectral signatures that can be assigned to 1-methylallyl and 1,3-butadiene. On the basis of a previously reported $\cdot C_4H_7$ potential energy surface, this result is interpreted as evidence for the unimolecular decomposition of the cyclobutyl radical *via* ring opening, prior to it being captured by helium droplets. On the $\cdot C_4H_7$ potential surface, 1,3-butadiene is formed from cyclobutyl ring opening and H atom loss, and the 1-methylallyl radical is the most energetically stable intermediate along the decomposition pathway. The allylcarbinyl radical is a higher energy $\cdot C_4H_7$ intermediate along the ring opening path, and the spectral signatures of this radical are not observed under the same conditions that produce 1-methylallyl and 1,3-butadiene from the unimolecular decomposition of cyclobutyl.

Infrared Spectroscopy of the Entrance Channel Complex Formed Between the Hydroxyl Radical and Methane in Helium Nanodroplets

The entrance channel complex in the exothermic OH + $CH_4 \rightarrow H_2O + CH_3$ reaction has been isolated in helium nanodroplets following the sequential pick-up of the hydroxyl radical and methane. The *a*-type OH stretching band was probed with infrared depletion spectroscopy, revealing a qualitatively similar spectrum to that previously reported in the gas phase, but with additional substructure that is due to the different internal rotation states of methane (j_{CH4} = 0, 1, or 2) in the complex. We fit the spectra by assuming the rotational constants of the complex are the same for all internal rotation states; however, subband origins are found to decrease with increasing j_{CH4}. Measurements of deuterated complexes have also been made (OD-CH_4, OH-CD_4, and OD-CD_4), the relative line widths of which provide information about the flow of vibrational energy in the complexes; vibrational lifetime broadening is prominent for OH-CH_4 and OD-CD_4 for which the excited OX stretching state has a nearby CY_4 stretching fundamental (X,Y=H or D).

Sequential Capture of O(^{3}P) and HCN by Helium Nanodroplets: Infrared Spectroscopy and Ab Initio Computations of the $^3\Sigma$ O−HCN Complex

Catalytic thermal cracking of O_2 is employed to dope helium droplets with O(^{3}P) atoms. Mass spectrometry of the doped droplet beam reveals an O_2 dissociation efficiency larger than 60%; approximately 26% of the droplet ensemble is doped with single oxygen atoms. Sequential capture of O(^{3}P) and HCN leads to the production of a hydrogen-bound O−HCN complex in a $^3\Sigma$ electronic state, as determined *via* comparisons of experimental and theoretical rovibrational Stark spectroscopy. *Ab initio* computations of the three lowest lying intermolecular potential energy surfaces reveal two isomers, the hydrogen-bound ($^3\Sigma$) O−HCN complex and a nitrogen-bound ($^3\Pi$) HCN−O complex, lying 323 cm^{-1} higher in energy. The HCN−O to O−HCN interconversion barrier is predicted to be 42 cm^{-1}. Consistent with this relatively small interconversion barrier, there is no experimental evidence for the production of the nitrogen-bound species upon sequential capture of O(^{3}P) and HCN.

Ongoing Work and Future Plans

Infrared Laser Spectroscopy of the n-propyl and i-propyl Radicals: Stretch-bend Fermi Coupling in the Alkyl CH Stretch Region

According to Smith *et al*. [Smith, I. W. M.; Sage, A. M.; Donahue, N. M.; Herbst, E.; Quan, D. *Faraday Discuss.* **2006**, 133, 137.], for molecule + radical reactions, the energetic difference between the molecule's ionization energy (IE) and the radical's electron affinity (EA) can provide insight into the nature of the reaction barrier, either *above* or *below* the reactant asymptote. They propose that a difference (IE − EA) greater than 8.75 eV indicates a real barrier above the asymptotic limit, whereas a value below 8.75 eV indicates a submerged barrier. Indeed, this difference for the O(^{3}P) + HCN system is 12.2 eV. Accordingly, the barrier to oxygen insertion into the CN π system is ~10 kcal/mol above the reactant asymptote, and a van der Waals complex is observed when these species are brought together in a 0.4 K helium nanodroplet. However, O(^{3}P) reactions with *alkenes* are predicted to cross the postulated 8.75 eV threshold as the alkene substitution pattern evolves from ethene (no substitution) to propene (methyl group substitution)

to butene (dimethyl substitution, of which there are four different isomers), and this trend was tested by Sabbah *et al.* [Sabbah, H.; Biennier, L.; Sims, I. R.; Georgievskii, Y.; Klippenstein, S. J.; Smith, I. W. *Science* **2007**, 317, 102.]. Their findings corroborated the behavior predicted by Smith *et al.* The HCN + O(^{3}P) results presented here demonstrate the feasibility for analogous alkene + O(^{3}P) spectroscopic studies, in which O(^{3}P) and alkenes of varying substitution are combined in helium droplets *via* the sequential capture scheme. As the *real* reaction barrier (*i.e.* for the ethene and propene reactions) evolves to being *submerged* below the asymptotic limit (*i.e.* for the butene reactions), one might expect that strongly bound reaction intermediates, such as triplet biradicals, will be observed in helium droplets, rather than van der Waals complexes. Given the fact that a 10,000 atom helium droplet can dissipate 140 kcal/mol, it should be possible to quench the internal energy of these reaction intermediates and probe them for the first time spectroscopically.

Publications acknowledging DOE support (2013-present):

1. Paul L. Raston, Tao, Liang and Gary E. Douberly, "Infrared Spectroscopy and Tunneling Dynamics of the Vinyl Radical in ^{4}He Nanodroplets" *Journal of Chemical Physics*, **138**, 174302 (2013). Published: May 7, 2013.

2. Paul L. Raston, Jay Agarwal, Justin M. Turney, Henry F. Schaefer III and Gary E. Douberly, "The Ethyl Radical in Superfluid Helium Nanodroplets: Rovibrational Spectroscopy and Ab Initio Computations" *Journal of Chemical Physics*, **138**, 194303 (2013). Published: May 21, 2013.

3. Alexander M. Morrison, Paul L. Raston and Gary E. Douberly, "Rotational Dynamics of the Methyl Radical in Superfluid ^{4}He nanodroplets" *Journal of Physical Chemistry A* **117**, 11640-11647 (2013). Published: November 21, 2013.

4. Christopher P. Moradi, Alexander M. Morrison, Stephen J. Klippenstein, C. Franklin Goldsmith and Gary E. Douberly, "Propargyl + O_2 Reaction in Helium Droplets: Entrance Channel Barrier or Not?" *Journal of Physical Chemistry A* **117**, 13626-13635 (2013). Published: December 19, 2013.

5. Christopher M. Leavitt, Christopher P. Moradi, Bradley W. Acrey and Gary E. Douberly, "Infrared Laser Spectroscopy of the Helium-Solvated Allyl and Allyl Peroxy Radicals" *Journal of Chemical Physics* **139**, 234301 (2013). Published: December 21, 2013.

6. Christopher M. Leavitt, Christopher P. Moradi, John F. Stanton and Gary E. Douberly "Communication: Helium Nanodroplet Isolation and Rovibrational Spectroscopy of Hydroxymethlyene" *Journal of Chemical Physics* **140**, 171102 (2014). Published: May 5, 2014.

7. Bernadette M. Broderick, Laura McCaslin, Christopher P. Moradi, John F. Stanton and Gary E. Douberly "Reactive Intermediates in ^{4}He Nanodroplets: Infrared Laser Stark Spectroscopy of Dihydoxycarbene" *Journal of Chemical Physics* **142**, 144309 (2015). Published: April 14, 2015.

8. Christopher P. Moradi and Gary E. Douberly "On the Stark Effect in Open Shell Complexes Exhibiting Partially Quenched Electronic Angular Momentum: Infrared Laser

Stark Spectroscopy of OH-C_2H_2, OH-C_2H_4, and OH-H_2O" *Journal of Molecular Spectroscopy* **314**, 54-62 (2015). Published: June 22, 2015.

9. Bernadette M. Broderick, Christopher P. Moradi and Gary E. Douberly "Infrared Laser Stark Spectroscopy of Hydroxymethoxycarbene in ^{4}He Nanodroplets" *Chemical Physics Letters* **639**, 99-104 (2015). Published: September 7, 2015.

10. Christopher P. Moradi, Changjian Xie, Matin Kaufmann, Hua Guo and Gary E. Douberly "Two-center Three-electron Bonding in $ClNH_3$ Revealed via Helium Droplet Infrared Laser Stark Spectroscopy: Entrance Channel Complex along the Cl + NH_3 → $ClNH_2$ + H Reaction" *Journal of Chemical Physics*, (2016), Accepted: April 5, 2016.

11. Christopher P. Moradi, Changjian Xie, Matin Kaufmann, Hua Guo and Gary E. Douberly "Two-center Three-electron Bonding in ClNH3 Revealed via Helium Droplet Infrared Laser Stark Spectroscopy: Entrance Channel Complex along the Cl + NH3 → ClNH2 + H Reaction" *Journal of Chemical Physics*, **144**, 164301 (2016). Published: April 2016.

12. Matin Kaufmann, Daniel Leicht, Martina Havenith, Bernadette M. Broderick, Gary E. Douberly "Infrared Spectroscopy of the Tropyl Radical in Helium Droplets" *Journal of Physical Chemistry A*, **120**, 6768-6773 (2016). Published: August 16, 2016.

13. Joseph T. Brice, Tao Liang, Paul L. Raston, Anne B. McCoy, Gary E. Douberly "Infrared Stark and Zeeman spectroscopy of OH-CO: The Entrance Channel Complex along the OH + CO → *trans*-HOCO Reaction Pathway" *Journal of Chemical Physics*, **145**, 124310 (2016). Published: September 2016.

14. Peter R. Franke, Daniel Tabor, Christopher P. Moradi, Gary E. Douberly, Jay Agarwal, Henry F. Schaefer, Edwin L. Sibert "Infrared Laser Spectroscopy of the *n*-propyl and *i*-propyl Radicals: Stretch-Bend Fermi Coupling in the Alkyl CH Stretch Region" *Journal of Chemical Physics*, **145**, 224304 (2016). Published: December 2016.

15. Paul L. Raston, Emmanuel I. Obi, Gary E. Douberly "Infrared Spectroscopy of the Entrance Channel Complex Formed Between the Hydroxyl Radical and Methane in Helium Nanodroplets" *Journal of Physical Chemistry A*, **121**, 7597-7602 (2017). Published: September 2017.

16. Alaina R. Brown, Peter R. Franke, Gary E. Douberly "Helium Nanodroplet Isolation of the Cyclobutyl, 1-Methylallyl and Allylcarbinyl Radicals: Infrared Spectroscopy and Ab Initio Computations" *Journal of Physical Chemistry A*, **121**, 7576-7587 (2017). Published: September 2017.

17. Joseph T. Brice, Peter R. Franke, Gary E. Douberly "Sequential Capture of O(^{3}P) and HCN by Helium Nanodroplets: Infrared Spectroscopy and Ab Initio Computations of the $^3\Sigma$ O-HCN Complex" *Journal of Physical Chemistry A*, **121**, 9466-9473 (2017). Published: November 2017.

Spectroscopic and Dynamical Studies of Highly Energized Small Polyatomic Molecules

Robert W. Field
Massachusetts Institute of Technology
Cambridge, MA 02139
rwfield@mit.edu

I. Introduction

The goal of this research program is to develop simple models that describe complex dynamical chemical processes, including isomerization, predissociation, multi-photon dissociation, and vibronic coupling. This effort proceeds via the combination of new experimental techniques and assignment strategies, and requires a quantitative representation of the physical systems under study. Current efforts focus on atmospherically relevant problems and the dynamics of acetylene, HCCH, as a prototype system for other compounds.

II. Recent Progress

A. Progress Toward Complete Assignment of S_1 Acetylene Vibration-Rotation States up to 47,200 cm^{-1}

We are pursuing a complete vibration-rotation assignment of the S_1 electronic state of acetylene to high energies, as a window into the dynamics of this state. We are interested both in an expanded study of S_1 cis-trans isomerization and the employment of currently unassigned S_1 vibrational states as intermediates in Stimulated Emission Pumping (SEP) schemes to populate high-lying *local-bender* states on the S_0 electronic surface. These local-bender states sample the acetylene-vinylidene isomerization pathway. Previous attempts at mapping the energy levels of S_1 acetylene are impeded by

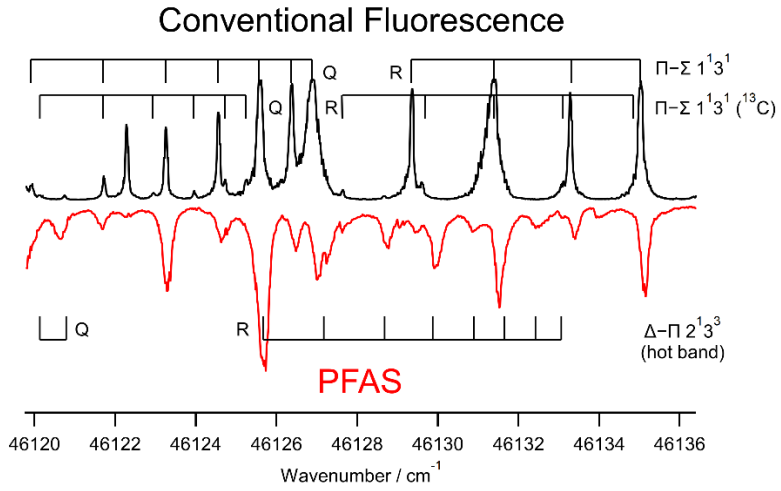

Fig. 1 A comparison of spectra collected in our lab using conventional fluorescence techniques and PFAS. Our new PFAS technique reveals many more discernable lines, particularly in the sparser region of the spectrum. Note that there is a cost in both noise level and line width to PFAS, in comparison to more well-established techniques.

predissociation-shortened lifetimes. Traditional LIF techniques are incompatible with such short lifetimes (shorter than 10 ns), and many essential states have not yielded to our efforts to observe, assign, and exploit them. We have developed a new technique that circumvents these difficulties, Photofragment Fluorescence Action Spectroscopy (PFAS). In PFAS, a focused ultraviolet laser beam (approx.. 220 nm) is used to photodissociate acetylene. This photodissociation is resonance-enhanced at the one-photon level by rotation-vibration states of the S_1 electronic surface of acetylene. The photofragments formed by multiphoton dissociation, C_2 and C_2H, fluoresce in the visible. PFAS is useful in our studies for two reasons; first, it allows the detected radiation to be far removed in frequency from that of the excitation

laser, reducing background, and second, the signal is not significantly reduced by the use of short-lifetime S_1 states, unlike previously-used techniques. Utilizing PFAS, we have extended our search for previously unobserved states to progressively higher energies. In order to fully understand the vibrational dynamics of S_1 acetylene, a variety of observations are required, including double resonance and vibrational hot-band spectra. Currently, we are working on more extensive and specifically targeted observations of hot-bands in this energy region.

Early hot-band PFAS spectra have already shown marked improvement in the signals obtained from hot-band transitions into high lying states. By tuning experimental parameters, namely nozzle position and temperature, hot-band intensities can be enhanced while maintaining low rotational temperatures. These conditions have proven to be effective in concert with PFAS spectroscopy, and data collection and spectra assignments in this area are ongoing.

An additional reason that we have pursued PFAS spectroscopy is the possibility that it could become a probe for many different alkynes, not limited to acetylene. Unfortunately, thermochemical calculations by Professor Barney Ellison of the University of Colorado, Boulder indicate that acetylene is energetically a special case, thus this technique will not be applicable to other alkyne molecules.

B. Determination of Electronic Population Differences in C_2 Formed by Multi-Photon Dissociation of Acetylene

Combining techniques previously used and developed in our lab, we have formulated and demonstrated the effectiveness of a method to determine the sign of the population difference between two probed states in a frequency-modulation (FM) experiment. In an FM experiment, the signal is detected in the form of a frequency beating between two unequally-attenuated sidebands, $\omega_0 \pm \omega_{FM}$ and a center carrier frequency, ω_0. When the carrier frequency is scanned to a resonance, the beat-amplitudes are equivalent on either side of line-center, but the signals from the opposite sides differ in phase by π. The phase pattern of an absorption transition is opposite that of an inverted transition, where the detected beating is due to unequal amplification (stimulated emission), rather than attenuation (absorption). A scan of the carrier frequency over a resonance determines the sign of the population difference, when the phase of the FM signal is detected.

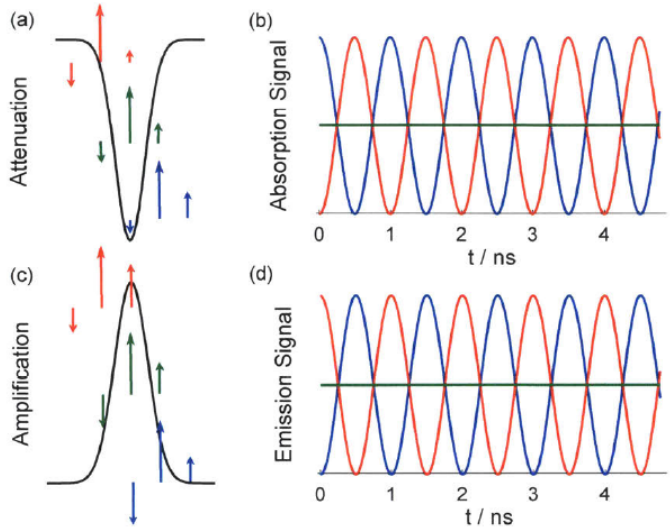

Fig. 2 Phase of the FM signal collected from absorption and stimulated emission events. The color green is a depiction of the center carrier frequency and 2 sidebands when the carrier frequency is on resonance, and red and blue depict red- and blue-detuned carrier frequencies. (a) and (c) depict the relative amplitudes of the two FM sidebands and the carrier frequency, with the direction of the sideband arrow representing the phase of the detected beating. (b) and (d) show the signal collected from the situations outlined in (a) and (c), including the zero signal (green) when the carrier frequency is at the line center and the two out-of-phase sidebands interfere destructively.

This technique was applied to the products of Photofragment Fluorescence Action Spectroscopy (PFAS) of acetylene, HCCH. Analysis of the photofragments via phase-sensitive FM spectroscopy revealed that the photodissociation does not create an inverted electronic band system of C_2, but rather a smaller amount of electronically excited C_2 than is created in the electronic ground state.

C. Investigation into Anomalous Isotope Ratios of Sulfur in the Rock Record

Anomalous sulfur isotope ratios, called sulfur mass independent fractionation (S-MIF), appear in rock records older than 2.45 billion years but are absent in more recent samples. The disappearance of these anomalies is thought to be correlated with The Great Oxygenation Event, the introduction of oxygen into the atmosphere via photosynthesis, an important signpost in the development of life on Earth. However, the mechanism for generation of S-MIF in an anoxic atmosphere has eluded explanation for nearly 20 years. In our model for the origin of S-MIF, we exploit the model of the B-X UV spectrum of S_2, based on a deperturbation of all bound vibration-rotation states in the B/B" system, performed by Green and Western. We also employ a steady state master equation kinetic model to account for electronically and rotationally inelastic collisions between S_2 in the mixed B/B" states and inert species, primarily N_2, in the atmosphere.

A key feature of this model is the difference in average lifetime between the B electronic state (30 ns) and the perturbing B" state (4 μs). We hypothesize that isotopologues of S_2 with longer average excited state lifetimes will have a greater propensity to undergo the requisite reactions that lead to their eventual preservation in the rock record. Our model shows that B~B" perturbations restrict the regions of the spectrum with very long lifetime states. As a result, the differences in average lifetime are especially pronounced when comparing symmetric (e.g. ^{32}S-^{32}S) and asymmetric (e.g. ^{34}S-^{32}S) S_2 isotopologues, as half of the rotational states in symmetric isotopologues are missing, due to nuclear permutation symmetry. Furthermore, inelastic collisions are more effective at moving population out of long-lived states in asymmetric species, due to smaller energy gaps between adjacent rotational states. Current work focuses on identifying features of the B/B" system in S_2 that are most effective in enabling it to produce significant isotope effects. Examples include the difference in rotational constants between the B and B" states; the B-X (v_B, v_X=0) Franck-Condon progression; and the onset of predissociation above v_B=9 in the B state. We also identify the cause of smaller isotope effects – differences among the asymmetric isotopologues. This level of analysis is only possible with our unique combination of master equation modeling, in which the energy gap law is embedded, and a complete spectroscopic deperturbation model.

III. Future Work

The Field Group has recently acquired an Even-Lavie style heated pulsed valve, which allows solid samples to be heated up to 200° C pre-nozzle and seeded in He, resulting in an ultra-cold (<0.5 K), high intensity (10^{21}-10^{23} atoms/m^3) gas expansion that has been shown to be nearly free from clustering. The E-L valve produces an intense and collimated jet expansion with both on-axis beam intensity and speed ratio 10 times larger than a conventional supersonic jet nozzle. We plan to exploit this nozzle for the study of the putative "triple whammy" mechanism of UV photolysis of sym-triazine into three HCN fragments, using Chirped Pulse Fourier transform millimeter wave spectroscopy. For a concerted, symmetric, three-body dissociation ($C_3H_3N_3 \rightarrow 3HCN$) in which the three-fold symmetry of s-triazine is retained during the dissociation, all three HCN fragments are expected to exhibit identical vibration-rotation population distributions. In contrast, for sequential dissociation ($C_3H_3N_3 \rightarrow C_2H_2N_2 + HCN$, $C_2H_2N_2 \rightarrow 2\ HCN$), two mechanisms are possible: a concerted, symmetric dissociation and an asymmetric dissociation. HCN fragments released during the first vs. the second dissociation steps will exhibit two distinct HCN internal state distributions (symmetric). However, if the lifetime of the $C_2H_2N_2$ fragment is substantially longer than the rotational period, the two HCN fragments generated in the second dissociation step may recoil with different velocities resulting in three distinct HCN internal state distributions overall (asymmetric). Using a broadband (>10 GHz) chirped pulse, the populations of all significantly populated vibrationally excited states of HCN can be measured simultaneously via the same selected J' ← J rotational transition. Given that only a few low-J transitions of HCN can be monitored in Chirped Pulse-millimeter Wave experiments, the photolysis must occur in the cooling region of the gas where the photoproducts will be translationally and rotationally cooled very efficiently while vibrations

are cooled less efficiently, providing a "near nascent" measure of the vibrational population distribution. Under similar "near nascent" photolysis conditions, we have observed more than 30 vibrational satellites of the J=1 ← 0 transition of HCN/HNC photofragments from the 193 nm photolysis of vinyl cyanide.

IV. Publications supported by this project 2015-2018

1. J. Jiang, C. A. Saladrigas, T. J. Erickson, C. L. Keenan, R. W. Field, "Probing the predissociated levels of the S_1 state of acetylene via H-atom fluorescence and photofragment fluorescence action spectroscopy" (In preparation).
2. J. A. DeVine, M. L. Weichman, B. Laws, J. Change, M. C. Babin, G. Balerdi, C. Xie, M. L. Malbon, W. C. Lineberger, D. R. Yarkony, R. W. Field, S. T. Gibson, J. Ma, H. Guo, and D. M. Neumark, "Encoding of Vinylidene Isomerization in its Anion Photoelectron Spectrum, *Science* **358**, 336-339 (2017).
3. G. B. Park and R. W. Field, "Perspective: The first ten years of broadband chirped pulse Fourier transform microwave spectroscopy" *J. Chem. Phys.* **144**, 200901 (2016).
4. (a) G. B. Park, J. Jiang, C. A. Saladrigas and R. W. Field, "Observation of b_2 symmetry vibrational levels of the SO_2 SO_2 $\tilde{C}$ $^1B_2$ state: Vibrational level staggering, Coriolis interactions, and rotation-vibration constants" *J. Chem. Phys.* **144**, 144311 (2016).
(b) J. Jiang, G. B. Park and R. W. Field, "The rotation-vibration structure of the SO_2 $\tilde{C}$ $^1B_2$ state explained by a new internal coordinate force field" *J. Chem. Phys.* **144**, 144312 (2016).
(c) G. B. Park, J. Jiang and R. W. Field, "The origin of unequal bond lengths in the $\tilde{C}$ $^1B_2$ state of SO_2: Signatures of high-lying potential energy surface crossings in the low-lying vibrational structure" *J. Chem. Phys.* **144**, 144313 (2016).
5. G. Barratt Park, C. C. Womack, A. R. Whitehill, J. Jiang, S. Ono and R. W. Field, "Millimeter-wave optical double resonance schemes for rapid assignment of perturbed spectra, with applications to the $\tilde{C}$ $^1B_2$ state of SO_2" *J. Chem. Phys.* **142**, 144201-1 – 144201-12 (2015).
6. J. H. Baraban, P. Bryan Changala, G. C. Mellau, J. F. Stanton, A. J. Merer and R. W. Field, "Spectroscopic Characterization of Transition states" *Science* **350**, 1338-1342 (2015).
7. R. W. Field, "Spectra and Dynamics of Small Molecules, Alexander von Humboldt Lectures" Springer Heidelberg (2015).
8. R. Fernando, C. Qu, J. Bowman, R. W. Field, and A. Suits, "Does Infrared Multiphoton Dissociation of Vinyl Chloride Yield Cold Vinylidene?" *J. Phys. Chem. Lett.* **6**(13), 2457 (2015).
9. A. H. Steeves, H. A. Bechtel, J. H. Baraban and R. W. Field, "Communication: Observation of local-bender eigenstates in acetylene," *J. Chem. Phys.* **143**, 071101 (2015).
10. G. B. Park and R. W. Field. "Edge effects in chirped-pulse Fourier transform microwave spectra", *J. Mol. Spectroscopy*. **312**, 54-57 (2015).
11. C. C. Womack, M.-A. Martin-Drumel, G. G. Brown, R. W. Field and M. C. McCarthy, "Observation of the smallest Criegee intermediate CH_2OO in the gas phase ozonolysis of ethylene", *Science Advances* **1**(2), e1400105 (2015).
12. P. B. Changala, J. H. Baraban, A. J. Merer and R. W. Field, "Probing *cis-trans* isomerization in the S_1 state of C_2H_2 via H-atom action and hot band-pumped IR-UV double resonance spectroscopies," *J. Chem. Phys.* **143**, 084310 (2015).
13. G. B. Park, J. H. Baraban, A. H. Steeves and R. W. Field "Simplified Cartesian basis model for intrapolyad emission intensities in the bent-to-linear electronic transition of acetylene." *Journal of Physical Chemistry A*, **2015**, 857 (2015).
14. K. Prozument, Y. V. Suleimanov, B. Buesser, J. M. Oldham, W. H. Green, A. G. Suits, R. W. Field, "A signature of roaming dynamics in the thermal decomposition of ethyl nitrite: Chirped pulse rotational spectroscopy and kinetic modeling" *J. Phys. Chem. Lett.* **5**(21), 3641-3648 (2015).
15. C. Abeysekera, L. Zack, G. B. Park, B. Joalland, J. Oldham, K. Prozument, N. Ariyasingha, I. Sims, R. Field, and A. Suits, A Chirped-Pulse Fourier-Transform Microwave /Pulsed Uniform Flow Spectrometer: II. Performance and applications for reaction dynamics," *J. Chem. Phys.* **141**(21), 214203 (2015).
16. C. Abeysekera, B. Joalland, N. Ariyasingha, L. N. Zack, I. R. Sims, R. W. Field and A. G. Suits, "Product branching in the low temperature reaction of CN with propyne by chirped-pulse microwave spectroscopy in uniform supersonic flows," *J. Phys. Chem. Lett.* **6**(9), 1599 (2015).
17. R. Fernando, C. Qu, J. Bowman, R. W. Field, and A. Suits, "Does Infrared Multiphoton Dissociation of Vinyl Chloride Yield Cold Vinylidene?" *J. Phys. Chem. Lett.* **6**, 2457-2462 (2015).

Quantitative Imaging Diagnostics for Chemically Reacting Systems

Jonathan H. Frank
Combustion Research Facility
Sandia National Laboratories
Livermore, CA 94551-0969
jhfrank@sandia.gov

Program Scope

In the coming year, the scope of this program will transition to include fundamental studies in a broader range of chemically reacting systems to align with changes in the research emphasis of the BES program and the de-emphasis of reacting flows research. For many years, this program has focused on the development and application of quantitative laser-based imaging diagnostics for studying the interactions of fluid dynamics and chemical reactions in reacting flows. Imaging diagnostics provide temporally and spatially resolved measurements of species, temperature, and velocity distributions over a wide range of length scales. Multi-dimensional measurements are necessary to determine spatial correlations, scalar and velocity gradients, flame orientation, curvature, and connectivity. The investigation of flow-flame interactions is of fundamental importance in understanding the coupling between transport and chemistry in turbulent flames. Diagnostic development includes efforts to expand measurement capabilities to a broader range of reacting systems as well as to perform high-repetition rate and three-dimensional measurements. Recent studies have focused on understanding the interaction between flames and the structure of turbulent flows by combining three-dimensional measurements of the velocity field with laser-induced fluorescence of the OH radical.

Recent Progress

Alignment of strain-rate eigenvectors in turbulent flames

We have continued to develop and apply tomographic particle image velocimetry (TPIV) measurements to understand the dynamics and structure of turbulence-chemistry interactions. The TPIV technique provides volumetric, three-component velocity measurements that enable determination of key fluid dynamic quantities such as vorticity and strain rate. Fluctuations in the fluid dynamic strain rate affect the progress of chemical reactions, which leads to variations in heat release rates. The heat release from chemical reactions in turn introduces changes in density, viscosity, and diffusivity that can have important effects on the turbulence, thus creating feedback between chemical reactions and fluid dynamics.

The dynamics of the flame-strain rate interaction is a function of the magnitude of the strain rate tensor eigenvectors, s_i, and their alignment with the flame normal direction, n [1, 2]. The effects of an imposed bulk strain rate on preferential s_i-n alignment could be very pronounced and affect the accuracy of modeling turbulent reacting flows in realistic environments. We investigated the effects of an imposed bulk strain rate field on the local s_i-n alignment in turbulent premixed counterflow flames using simultaneous TPIV and OH-LIF imaging for strain rate measurements and flame front detection, respectively, as shown in Fig. 1. In the counterflow, opposed streams of reactants and combustion products flow from the top and bottom nozzles, respectively.

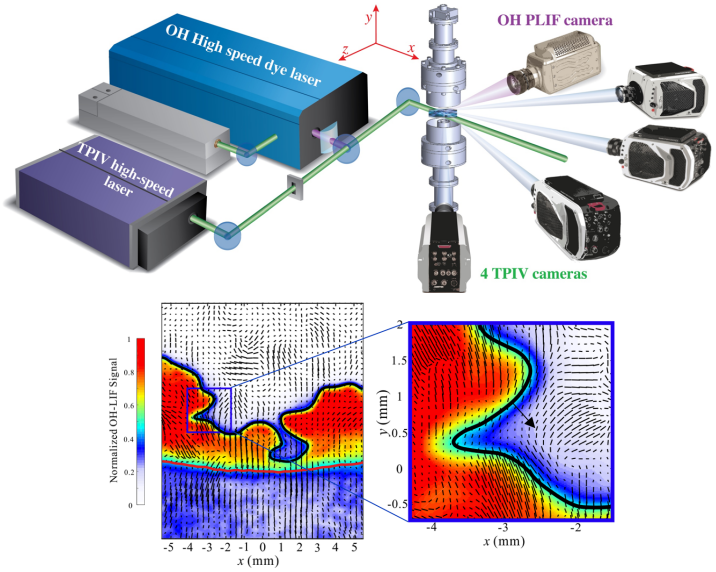

Figure 1: (Top) Experimental apparatus for simultaneous tomographic PIV and OH-LIF imaging at 10 kHz. (Bottom) Single-shot data from counterflow flame with reactant mixture ($CH_4/O_2/N_2$) from top nozzle and product mixture from bottom nozzle. OH-LIF image used to identify the flame front (black curve) and mixing layer interface (red curve) between product stream and local flame-generated products. Projections of the most compressive strain-rate eigenvectors, s_3, are superimposed (1 out of 9 eigenvectors displayed). Large vector on far-right image indicates local flame-front normal.

Turbulent counterflow flames are subject to large streamwise compressive strain rates. This bulk strain introduces a preferential alignment of the most compressive principal strain rate, s_3, with the flame normal, n, through their mutual preferential alignment with the burner axis. However, dilatation induced by heat release is a competing effect that promotes the alignment of the most extensive principal strain rate, s_1, with n. The impact of heat release is identified by comparisons of probability density functions of strain rate alignment in turbulent non-reacting counterflows and flames. In the flames, the preferential s_3-n alignment prevails and remains dominant across almost the entire flame. This alignment stands in stark contrast to observations from previous studies in turbulent Bunsen flames of similar Karlovitz number, indicating the significance of the bulk strain in determining local strain field alignment. The effects of increasing turbulence intensity on strain rate alignment are twofold; The impact of heat release is reduced and preferential s_3-n alignment is enhanced approximately 1 mm ahead of the flame front, similar to non-reacting turbulent flows in which compressive strain preferentially aligns normal to scalar isosurfaces. In addition, turbulence diminishes the geometry-imposed s_3-n preferential alignment by increasing flame surface wrinkling. As a result of this interplay between heat release, turbulence, and bulk strain, the flame-tangential strain rate is on average extensive, and the flame-normal strain rate is dominantly compressive except for an approximately 1 mm region near the flame front where it is extensive due to dilatation. Results are important for developing turbulent flame models to accommodate the effects of externally imposed strain fields.

Particle clustering in two-phase turbulent flows

We began a collaboration with Prof. Gus Nathan and Dr. Timothy Lau (University of Adelaide) to study the dynamics of particle-laden turbulent flows using our high-speed tomographic PIV capability. In particle-laden turbulent flows, non-uniform distributions of

particles are known to form, even in isotropic turbulence. Clusters of higher particle concentration can affect heat transfer, mass transfer, radiation, and chemical reactions. The interactions of particles with the strain rate and vorticity fields are known to play a key role in producing non-uniform particle distributions [3]. However, the dynamics of these processes remain poorly understood, particularly in densely seeded, shear-driven, turbulent flows that are relevant to many two-phase systems. While experimental measurements of particle clustering have been reported (e.g. [4-7]), there is a need for new capabilities to enable detailed, non-intrusive, three-dimensional, in-situ measurements of densely-seeded flows in the two-way coupling regime to provide a more comprehensive understanding of particle clustering. Our initial experiments demonstrated the feasibility of using tomographic particle imaging to provide quantitative, spatially-resolved, three-dimensional measurements of instantaneous particle distributions within a particle-laden turbulent flow. This method extracts particle positions from volume reconstructions of the particle distributions in conjunction with removal of reconstruction artifacts using thresholding and temporal correlation. Initial experiments in a turbulent, particle-laden round jet demonstrated this capability by measuring particle cluster distributions for a particle Stokes number of 1.4. Coherent clusters appeared in long filaments and were detected starting at the jet exit, indicating that they were formed inside of nozzle, which is consistent with previous measurements. Further measurements on different size particles identified the range of conditions for which clusters were formed in the turbulent jet. Additional analysis of the cluster structure and dynamics are ongoing.

Data assimilation of high-speed imaging measurements in large-eddy simulations

The growing use of imaging and high-speed diagnostics for studying chemically reacting systems has created a need for the development of methods for coupling multi-dimensional measurements with simulations. Currently, the modeling community has not taken full advantage of available high repetition rate imaging measurements in analyzing model performance or improving model accuracy. Recently, we began collaborating with Prof. Matthias Ihme (Stanford Univ.) to investigate data assimilation methods for coupling high-speed multi-dimensional imaging measurements of reacting flows with large-eddy simulations (LES). Data assimilation provides methodologies for integrating measurements into numerical simulations [8]. This approach has been used extensively to produce initial conditions for weather prediction models [9] and to provide representations of the spatio-temporally evolving atmospheric state [10]. These assimilation techniques are used to obtain an estimate of the state of a complex, spatio-temporally evolving system based on observations and a model of the dynamics of the system [11]. However, data assimilation has had very limited application in research of turbulent reacting flows. We investigated how data assimilation could be used to integrate multi-dimensional measurements with simulations of chemically reacting flows. High-speed, high-resolution experimental data obtained in a turbulent partially-premixed dimethyl ether/air jet flame is assimilated to evaluate the performance of a LES combustion model for improving the short-term prediction of extinction and reignition events. In this initial study, the ensemble Kalman filter technique was used to locally assimilate time resolved measurements of the 3D velocity field from TPIV and inferred OH concentrations from OH-LIF imaging into the LES. Resulting comparisons of the short-term predictions and time evolution data can potentially be employed in isolating weaknesses in the modeling approach and in understanding underlying phenomena responsible for extinction and reignition.

Future Plans

The investigation of the structure and dynamics of flow-flame interactions will wind down during the remainder of the current fiscal year. Near-term plans for diagnostic development include building a capability for 3D-LIF imaging measurements using a custom-built 100 kHz burst-mode laser. We also plan to develop multiplexed two-dimensional coherent anti-Stokes Raman spectroscopy (2D-CARS) thermometry and particle image velocimetry to provide simultaneous temperature and velocity field measurements in collaboration with Dr. Christopher Kliewer (Sandia). In the longer term, the thrust of this research program will transition to diagnostics development and fundamental experimental studies in several areas of emphasis for the CRF's BES program, including dynamics and reactivity at interfaces, ion and X-ray methods, and ultrafast laser spectroscopy and diagnostics.

References

[1] N. Swaminathan, R.W. Grout, Phys. Fluids, 18 (2006) 045102.
[2] P.E. Hamlington, A.Y. Poludnenko, E.S. Oran, Phys. Fluids, 23 (2011) 125111.
[3] S. Balachandar, J.K. Eaton, Annu. Rev. Fluid Mech., 42 (2010) 111-133.
[4] J.R. Fessler, J.D. Kulick, J.K. Eaton, Phys. Fluids, 6 (1994) 3742-3749.
[5] E.K. Longmire, J.K. Eaton, J. Fluid Mech., 236 (1992) 217-257.
[6] R. Monchaux, M. Bourgoin, A. Cartellier, Phys. Fluids, 22 (2010) 103304.
[7] T.C.W. Lau, G.J. Nathan, International Journal of Multiphase Flow, 88 (2017) 191-204.
[8] G. Evensen, Data assimilation: the ensemble Kalman filter, Springer Science & Business Media, 2009.
[9] E. Kalnay, Atmospheric modeling, data assimilation and predictability, Cambridge university press, 2003.
[10] R. Kistler, E. Kalnay, W. Collins, S. Saha, G. White, J. Woollen, M. Chelliah, W. Ebisuzaki, M. Kanamitsu, V. Kousky, Bulletin of the American Meteorological society, 82 (2001) 247-268.
[11] E. Ott, B.R. Hunt, I. Szunyogh, A.V. Zimin, E.J. Kostelich, M. Corazza, E. Kalnay, D.J. Patil, J.A. Yorke, Tellus A, 56 (2004) 415-428.

BES-supported publications (2016-present)

B. Coriton, J.H. Frank, "Experimental study of vorticity-strain rate interaction in turbulent partially premixed jet flames using tomographic particle image velocimetry," *Phys. Fluids*, **28**, 025109 (2016).

B. Coriton, J.H. Frank, A. Gomez, "Interaction of turbulent premixed flames with combustion products: Role of stoichiometry," *Combust. Fame,* **170**, 37-52 (2016).

B. Coriton, J. H. Frank, "Impact of heat release on strain rate field in turbulent premixed Bunsen flames," *Proc. Combust. Inst.*, *Proc. Combust. Inst.,* **36**, 1885-1892 (2017).

M. Kamal, B. Coriton, R. Zhou, J. H. Frank, S. Hochgreb, "Scalar dissipation rate and scales in swirling turbulent premixed flames," *Proc. Combust. Inst.*, **36**, 1957-1965 (2017).

B. Coriton, S.-K. Im, M. Gamba, J. H. Frank, "Flow field and scalar measurements in a series of turbulent partially-premixed dimethyl ether/air jet flames," *Combust. Flame,* **180** 40-52 (2017).

J. W. Labahn, H. Wu, B. Coriton, J. H. Frank, M. Ihme, "Data assimilation using high-speed measurements and LES to examine local extinction events in turbulent flames," *Proc. Combust. Inst.,* submitted.

B. Zhou, J. H. Frank, "Alignment of strain rate eigenvectors in turbulent premixed counterflow flames," *Combust. Flame,* submitted.

Computer-Aided Construction of Chemical Kinetic Models

William H. Green
Department of Chemical Engineering
Massachusetts Institute of Technology
Cambridge, MA 02139
whgreen@mit.edu

I. Program Scope

The combustion chemistry of even simple fuels can be extremely complex, involving hundreds or thousands of kinetically significant species. The most reasonable way to deal with this complexity is to use a computer not only to numerically solve the kinetic model, but also to construct the kinetic model in the first place. Because these large models contain so many numerical parameters (e.g. rate coefficients, thermochemistry) one never has sufficient data to uniquely determine them all experimentally. Instead one must work in "predictive" mode, using theoretical values for many of the numbers in the model, and as appropriate refining the most sensitive numbers through experiments. Predictive chemical kinetics is exactly what is needed for computer-aided design of combustion systems based on proposed alternative fuels, particularly for early assessment of the value and viability of proposed new fuels. It is also very helpful in other fuel chemistry problems, and in understanding emissions and environmental chemistry.

Our research effort is aimed at making accurate predictive chemical kinetics practical; this is a challenging goal which necessarily includes a range of science advances. Our research spans a wide range from quantum chemical calculations on individual molecules and elementary-step reactions, through the development of improved rate/thermo calculation procedures, the creation of algorithms and software for constructing and solving kinetic simulations, the invention of methods for model-reduction while maintaining error control, and finally comparisons with experiment. Many of the parameters in the models are derived from quantum chemistry, and the models are compared with experimental data measured in our lab or in collaboration with others.

II. Recent Results

A. Nitrogen (and Sulfur) Chemistry in Important Systems

We developed a computer method for rapidly predicting thermal (mostly free-radical) chemistry including nitrogen-containing molecules, and distributed it open-source as part of the Reaction Mechanism Generator (RMG) software suite. This was considerably more complicated than C,H,O chemistry because nitrogen has several different valencies, allowing a variety of different resonance forms and quite a rich set of possible functional groups and feasible types of chemical reactions. Some of these functional groups and reaction types have been well-studied in the literature; we filled in the gaps with quantum chemistry calculations.

As an initial demonstration we used the software to develop a detailed kinetic model for high temperature pyrolysis and oxidation of ethylamine, which was consistent with experimental data measured by Hanson's group at Stanford, for details see Ref.[9]. More recently we have been using this software to understand and quantitatively predict how NOx affects the rate of oxidation of hydrocarbons as a function of reaction conditions. At low temperatures in the dark NOx slows oxidation by destroying some alkylperoxyl radicals before they can cause chain branching, but much of the NOx is sequestered in forms which are inactive at low T,

such as HONO. As the temperature increases, the inhibition diminishes, and when the system enters the negative temperature coefficient region (where most RO_2 decomposes to HO_2 + alkene) NOx acts as a strong oxidation promoter in part through reactions involving HONO (which is reactive above 700 K). Our next step will be to use this new capability to understand why adding a very small quantity of a cetane improver such as 2-ethylhexylnitrate has such a large effect on the ignition delay under diesel-like reaction conditions.

We are currently using the same methods to add sulfur chemistry into RMG. Similar to nitrogen, sulfur exists in several valencies, and there are many gaps in the literature information on thermochemistry and reaction rates. As an initial test of our capabilities, we have built a detailed kinetic model for the low temperature oxidation of dimethylsulfide, an important process in the troposphere.

Our next goal is to understand the systems with rather high NOx and SOx concentrations that are common in oxy-combustion systems with high exhaust recycle to facilitate CO2 capture. One of the important unresolved problems preventing deployment of these efficient CO2 capture systems is high corrosion of the heat exchangers; our working hypothesis is that the NOx is catalyzing oxidation of SOx to sulfuric acid. With our new modeling capability we can analyze this chemistry in detail, to see if there is a way to modify the system to avoid the reaction conditions that form the corrosive acid.

B. Improved understanding of Fused-Ring Chemistry

We have recently developed a fuel-rich natural gas mechanism that is accurate in detail up to the second aromatic ring. We are now working hard to characterize the reactions of various substituted 1-, 2-, and 3-ring species, and have published some of the key mechanisms involving cyclopentadienyl radicals [8,10] This chemistry is sensitive to the thermochemistry of fused ring intermediates, so we have developed a more accurate way to rapidly compute the thermochemistry of those species [7] that are not estimated accurately using Benson-type techniques.

III. Ongoing Work and Future Plans

We continue to develop and test our ability to predict the kinetics of combustion and environmental systems including the common heteroatoms S and N. We will soon submit a paper presenting a detailed model for NOx formation in natural gas engines; curiously there are 4 distinct pathways which all contribute significantly to N fixation as well as the important reburn reactions which convert some of the NOx back to N_2.

We have done experimental work on several of the reaction pathways leading to formation of benzene and styrene using our laser flash photolysis photoionization mass spec apparatus. Those experiments reveal that the reactions which form benzene from acetylene are fast even at low temperature, limited only be the number of active radicals in the system. We also have observed products formed via an

unexpected aromatic-catalyzed H-atom transfer isomerization of phenylalkyl radicals, and confirmed the pathway with quantum chemistry calculations.

We have used machine-learning to develop an accurate estimator for thermochemistry, and also to estimate the uncertainty in each estimate. We then have the computer spawn quantum jobs for the most uncertain values, and use these to improve the estimator. We believe this type of machine active learning will find wide application in the future throughout chemical kinetics. Our vision for the future of computer-aided chemical kinetics is presented in Ref. [11].

We continue to work on improved methods for handling coupled hindered rotors, to more accurately compute the entropies and A factors of reactions for molecules containing several C-C or C-O single bonds, and hope to present those results in early 2019.

IV. Publications and submitted journal articles supported by DOE BES 2016-2018

1. Connie W. Gao, Joshua W. Allen, William H. Green, and Richard H. West, "Reaction Mechanism Generator: Automatic Construction of Chemical Kinetic Mechanisms", *Computer Physics Communications* **203**, 212-225 (2016). http://dx.doi.org/10.1016/j.cpc.2016.02.013

2. Rehab M.I. Elsamra, Amrit Jalan, Zachary J. Buras, Joshua E. Middaugh, and William H. Green, "Temperature and Pressure Dependent Kinetics of CH_2OO + CH_3COCH_3 and CH_2OO + CH_3CHO: Direct Measurements and Theoretical Analysis", *International Journal of Chemical Kinetics* **48**, 474-488 (2016). **https://doi.org/10.1002/kin.21007**

3. Enoch E. Dames and William H. Green, "The effect of alcohol and carbonyl functional groups on the competition between unimolecular decomposition and isomerization in C4 and C5 alkoxy radicals", *International Journal of Chemical Kinetics* **48**, 544-555 (2016). http://dx.doi.org/10.1002/kin.21015

4. Alon Grinberg Dana, Soumya Gudiyella, William H. Green, Santosh J. Shanbhogue, Dan Michaels, Nadim W. Chakroun, and Ahmed Ghoniem. "Automated Generation of Chemical Mechanisms for Predicting Extinction Strain Rates with Applications in Flame Stabilization and Combustion Instabilities", 55th AIAA Aerospace Sciences Meeting, AIAA SciTech Forum, (AIAA 2017-0835) http://dx.doi.org/10.2514/6.2017-0835

5. Kehang Han, William H. Green, and Richard H. West, "On-the-Fly Pruning for Rate-Based Reaction Mechanism Generation", *Computers and Chemical Engineering* **100**, 1-8 (2017). http://dx.doi.org:10.1016/j.compchemeng.2017.01.003

6. Colin M. Grambow, Adeel Jamal, Yi-Pei Li, William H. Green, Judit Zador, Yury V. Suleimanov, "Unexpected Unimolecular Reaction Pathways of a γ-Ketohydroperoxide from Combined Application of Automated Reaction Discovery Methods", *Journal of the American Chemical Society* **140**, 1035-1048 (2018). http://dx.doi.org/10.1021/jacs.7b11009

7. Kehang Han, Adeel Jamal, Colin M. Grambow, Zachary J. Buras, "An Extended Group Additivity Method for Polycyclic Thermochemistry Estimation", *International Journal of Chemical Kinetics* **50**, 294-303 (2018). **https://doi.org/10.1002/kin.21158**

8. Alan E. Long, Shamel S. Merchant, Aäron G. Vandeputte, Hans-Heinrich Carstensen, Alexander J. Vervust, Guy B. Marin, Kevin M. Van Geem, and William H. Green, "Pressure dependent kinetic analysis of pathways to naphthalene from cyclopentadienyl recombination", *Combustion & Flame* **187**, 247-256 (2018). https://doi.org/10.1016/j.combustflame.2017.09.008

9. Alon G. Dana, Beat Buesser, Shamel S. Merchant, and William H. Green, "Automated Reaction Mechanism Generation Including Heteroatoms: Nitrogen", *International Journal of Chemical Kinetics* **50**, 223-258 (2018). http://dx.doi.org/10.1002/kin.21154

10. Alexander J. Vervust, Marko R. Djokic, Shamel S. Merchant, Hans-Heinrich Carstensen, Alan E. Long, Guy B. Marin, William H. Green, and Kevin M. Van Geem, "Detailed experimental and modeling study of cyclopentadiene pyrolysis in the presence of ethene", *Energy & Fuels* **32**, 3290-3934 (2018). https://pubs.acs.org/doi/abs/10.1021/acs.energyfuels.7b03560

11. Murat Keceli,[1] Sarah Elliott,[2] Yi-Pei Li,[3] Matthew S. Johnson,[3] Carlo Cavallotti,[4] Yuri Georgievskii,[1] William H. Green,[3] Matteo Pelucchi,[4] Justin M. Wozniak,[5] Ahren W. Jasper,[1] Stephen J. Klippenstein[1], "Automated Computational Thermochemistry for Butane Oxidation: A Prelude to Predictive Automated Combustion Kinetics", *Proc. Combust. Inst.* (accepted).

Flame Chemistry and Diagnostics

Nils Hansen
Combustion Research Facility, Sandia National Laboratories, Livermore, CA 94551-0969
Email: nhansen@sandia.gov

SCOPE OF THE PROGRAM

In this program, we seek to understand the fundamental chemistry of combustion through a unique scheme of diagnostics development and experimental studies of laboratory-scale flames and reactors. Our goal is to provide reliable experimental data on the chemical composition of flames and reactors through state-of-the-art diagnostics. The experiments are designed to serve as benchmarks for the development and validation of detailed chemical kinetic models. In particular, we study the composition of laminar flames and of a jet-stirred reactor that is also operated near atmospheric pressure. We employ mass spectrometry and our experimental data in the form of species identification and quantification serve as stringent tests for the development and validation of any detailed chemical kinetic mechanisms. Over the past years, the overall objective of this program has been to fundamentally elucidate the chemistry of soot precursors and the formation of unwanted byproducts in incomplete combustion in flames fueled by hydrocarbons and oxygenates. Studying this complex combustion chemistry with an unprecedented level of detail requires determining the chemical structures and concentrations of species sampled from sooting or nearly-sooting model flames. Using the jet-stirred reactor we study the low-temperature oxidation chemistry of selected hydrocarbon and oxygenated fuels.

PROGRESS REPORT

Acetaldehyde Low-Temperature Oxidation in a Jet-Stirred Reactor: The routines developed previously for obtaining chemical insights into complex reaction networks from mass spectra obtained after sampling out of a jet-stirred reactor were used to explore the oxidation chemistry of acetaldehyde. The oxidation of acetaldehyde was studied at low-temperatures (528–946 K) in a jet-stirred reactor (JSR). This work described a detailed set of experimental results that capture the negative temperature coefficient (NTC) behavior in the low-temperature oxidation of acetaldehyde. To explain the observed NTC behavior, an updated mechanism was proposed, which well reproduces the concentration profiles of many observed peroxide intermediates. The kinetic analysis based on the updated mechanism revealed that the NTC behavior of acetaldehyde oxidation is caused by the competition between the O_2-addition to and the decomposition of the CH_3CO radical.

2D-Imaging of Sampling-Probe Perturbations in Laminar Premixed Flames using Kr X-ray Fluorescence: In a collaborative effort with the groups of Tranter and Kastengren (both Argonne), **t**he perturbation of the temperature field caused by a quartz sampling probe has been investigated in a fuel-rich low-pressure premixed ethylene/oxygen/argon/krypton flame using X-ray fluorescence. In these experiments, which were performed at the 7-BM beamline of the Advanced Photon Source (APS) at the Argonne National Laboratory, a continuous beam of hard X-rays at 15 keV was used to excite krypton atoms that were added in a concentration of 5 vol.-% to the unburnt gas mixture and the resulting krypton fluorescence at 12.65 keV was subsequently collected. The highly spatially resolved signal was converted into the local flame temperature to obtain temperature fields at various burner-probe separations as functions of the distance to the burner surface and the radial distance from the centerline.

Microwave Spectroscopic Detection of Flame-Sampled Combustion Intermediates: In collaboration with the groups of Kohse-Höinghaus (Bielefeld) and Grabow (Hannover), the suitability of microwave spectroscopy for the detection of flame-sampled intermediates has been tested. Microwave spectroscopy probes the rotational transitions of polar molecules in the gas phase and is a proven technique for the detection and identification of short-lived molecules produced from a variety of molecular sources. In this

explorative study, we demonstrated that two prerequisites can be met for microwave spectroscopy to become a quantitative tool for the analysis of high-temperature gas mixtures as found in combustion environments. Through the successful detection of combustion intermediates, we first showed that the rotational temperature of the targeted species can be sufficiently cooled to allow for a sensitive detection of low-lying rotational states after sampling from hot (~2200 K) flames. Second, we showed that signal intensity profiles can be assembled which, after correcting for the different flame temperatures at various sampling positions, agree well with mole fraction profiles obtained via flame-sampling molecular-beam mass spectrometry. Based on the described results, it is conceivable that rotational spectroscopy can contribute towards the unraveling of complex, high-temperature reaction networks.

OUTLOOK

Low-Temperature Oxidation in a Jet-Stirred Reactor: We will continue to explore the reaction network of low-temperature oxidation processes by using the above mentioned jet-stirred reactor with molecular-beam sampling capabilities. For this, mass spectrometry and microwave spectroscopy will be used as analytical tools. Our work on DME will be complemented with efforts to provide new insights into the oxidation of tetrahydrofuran, *n*- and *neo*-pentane. New information in the form of species identification and mole fraction profiles is critically needed to improve their respective combustion chemistry models. Preliminary mass spectra were recorded and the data reduction, *i.e.* species identification and quantification, is currently in progress. Special emphasis will be on the detection and quantification of the respective keto-hydroperoxides and other oxygenated elusive intermediates.

Experimental Studies on the Molecular-Growth Chemistry of Soot Precursors in Combustion Environments: PAH formation chemistry will be studied by analyzing the detailed chemical structures of laminar, premixed or opposed-flow flames using flame-sampling mass spectrometry. The data is expected to provide guidance and benchmarks needed to improve and test theoretical models describing soot-formation chemistry with predictive capabilities. Work on flames fueled by the C_5 fuels *n*-pentane, 1-pentene, and 2-methyl-2-butene is currently in progress. Based on earlier work that revealed fuel-structure dependence of benzene formation, we will study the fuel-structure influence on the aromatics formation beyond the first aromatic ring by using the isomeric allene and propyne as fuels. The importance of the $C_3H_3+C_6H_5$ and $C_3H_3+C_7H_7$ reactions on indene and naphthalene formation, will be tested.

New Concepts: New possibilities will be explored to generate new validation targets for the refinement of kinetic mechanisms through data research. For this effort, we want to shift the focus from individual flames towards the analysis of a compilation of flame data. The goal is the extraction of previously unexplored new chemical information from the large amounts of complex data. The idea is to translate flame data into new validation targets that are hidden in the given experimental uncertainties of the individual flames, but would become apparent in the ensemble of all flame data. Furthermore, we will be studying the formation of highly oxygenated species through ozone-assisted oxidation at low-temperatures.

PUBLICATIONS ACKNOWLEDGING BES SUPPORT 2016-PRESENT

1. *Experimental and modeling efforts towards a better understanding of acetaldehyde combustion*, T. Tao, S. Kang, W Sun, J. Wang, H. Liao, K. Moshammer, N. Hansen, C. K. Law, B. Yang, *Combust. Flame,* **2018,** *submitted*
2. *Investigation on the Low-Temperature Oxidation of* n-*Butanal in a Jet-Stirred Reactor,* H. Liao, T. Tao, W. Sun, N. Hansen, B. Chen, C. K. Law, B. Yang, *Proc. Combust. Inst.,* **2017,** *accepted for presentation*
3. *Insights into the Oxidation Kinetics of a Cetane Improver - 1,2-Dimethoxyethane (1,2-DME) with Experimental and Modeling Methods,* W. Sun, M. Lailliau, Z. Serinyel, G. Dayma, K. Moshammer, N. Hansen,B. Yang, P. Dagaut, *Proc. Combust. Inst.,* **2017,** *accepted for presentation*
4. *Knowledge Generation through Data Research: New Validation Targets for the Refinement of Kinetic Mechanisms,* N. Hansen, X. He, R. Griggs, K. Moshammer, *Proc. Combust. Inst.,* **2017,** *accepted for presentation*

5. *Investigation of Sampling-Probe Distorted Temperature Fields with X-Ray Fluorescence Spectroscopy*, N. Hansen, R. S. Tranter, J. B. Randazzo, J. P. A. Lockhart, A. L. Kastengren, *Proc. Combust. Inst.,* **2017,** *accepted for presentation*
6. *A High-Temperature Study of 2-Pentanone Oxidation: Experiment and Kinetic Modeling*, J. Pieper, C. Hemken, R. Büttgen, I. Graf, N. Hansen, A. Heufer, K. Kohse-Höinghaus, *Proc. Combust. Inst.,* **2017,** *accepted for presentation*
7. *Probing Fuel-Specific Reaction Intermediates from Laminar Premixed Flames fueled by two C_5 Ketones and Model Interpretations*, W. Sun, T. Tao, H. Liao, N. Hansen, B. Yang, *Proc. Combust. Inst.,* **2017,** *accepted for presentation*
8. *Detection, Identification, and Quantification of Keto-Hydroperoxides in Low-Temperature Oxidation*, N. Hansen, K. Moshammer, A. W. Jasper, *J. Phys. Chem. Lett.,* **2017,** *submitted* – invited Perspective
9. *Influences of the Molecular Fuel Structure on Combustion Reactions Towards Soot Precursors in Selected Alkane and Alkene Flames*, L. Ruwe, K. Moshammer, N. Hansen, and K. Kohse-Höinghaus, *Phys. Chem. Chem. Phys.,* **2018,** *in press*
10. *Exploring the negative temperature coefficient behavior of acetaldehyde based on detailed intermediate measurements in a jet stirred reactor*, T. Tao, W. Sun, N. Hansen, A. W. Jasper, K. Moshammer, B. Chen, Z. Wang, C. Huang, P. Dagaut, B. Yang, *Combust. Flame,* **2018,** 192, 120-129
11. *n-Heptane Cool Flame Chemistry: Unraveling Intermediate Species measured in a stirred reactor and motored engine*, Z.Wang, B. Chen, K. Moshammer, D. M. Popolan-Vaida, S. Sioud, V. S. Bhavani Shankar, D. Vuilleumier, T. Tao, L. Ruwe, E. Bräuer, N. Hansen, P. Dagaut, K. Kohse-Höinghaus, M. A. Raji, S. M. Sarathy, *Combust. Flame,* **2018,** 187, 199-216
12. *Unraveling the Structure and Chemical Mechanisms of Highly Oxygenated Intermediates in Oxidation of Organic Compounds*,Z. Wang, D. M. Popolan-Vaida, B. Chen, K. Moshammer, S. Mohamed, H. Wang, S. Sioud, M. A. Raji, K. Kohse-Höinghaus, N. Hansen, P. Dagaut, S. R. Leone, S. M. Sarathy, *Proc. Nat. Acad. Sci.*, **2017,** 114(50), 13102-13107
13. *Microwave Spectroscopic Detection of Flame-Sampled Combustion Intermediates*, N. Hansen, J. Wullenkord, D. A. Obenchain, K. Kohse-Höinghaus, J.-U. Grabow, *RSC Advances,* **2017,** 7(60), 37867-37872
14. *2D-Imaging of Sampling-Probe Perturbations in Laminar Premixed Flames using Kr X-ray Fluorescence*, N. Hansen, R. S. Tranter, K. Moshammer, J. B. Randazzo, J. P. A. Lockhart, P. G. Fugazzi, T. Tao, A. L. Kastengren, *Combust. Flame,* **2017,** 181, 214-224
15. *Exploring the High-Temperature Kinetics of Diethyl Carbonate (DEC) under Pyrolysis and Flame Conditions*, W. Sun, C. Huang, T. Tao, F. Zhang, W. Li, N. Hansen, B. Yang, *Combust. Flame,* **2017,** 181, 71-81
16. *Investigating Repetitive Reaction Pathways for the Formation of Polycyclic Aromatic Hydrocarbons in Combustion Processes*, N. Hansen, M. Schenk, K. Moshammer, K. Kohse-Höinghaus, *Combust. Flame,* **2017,** 180, 250-261
17. *Premixed Flame Chemistry of a Gasoline Primary Reference Fuel Surrogate*, H. Selim, S. Y. Mohamed, N. Hansen, S. M. Sarathy, *Combust. Flame,* **2017,** 179, 300-311
18. *The Influence of* iso*-Butanol Addition to the Chemistry of Premixed 1,3-Butadiene Flames*, M. Braun-Unkhoff, N. Hansen, T. Methling, K. Moshammer, B. Yang, *Proc. Combust. Inst.,* **2017,** 36(1), 1311-1319
19. *Investigation of the Chemical Structures of Laminar Premixed Flames Fueled by Acetaldehyde*, T. Tao, W. Sun, B. Yang, N. Hansen, K. Moshammer, C. K. Law, *Proc. Combust. Inst.,* **2017,** 36(1), 1287-1294
20. *Photoionization Mass Spectrometry and Modeling Study of a Low-Pressure Premixed Flame of Ethyl Pentanoate (Ethyl Valerate)*, D. A. Knyazkov, I. Gerasimov, N. Hansen, A. G. Shmakov, O. P. Korobeinichev, *Proc. Combust. Inst.,* **2017,** 36(1), 1185-1192
21. *Aromatic Ring Formation in Diffusive 1,3-Butadiene Flames*, K. Moshammer, L. Seidel, Y. Wang, H. Selim, S. M. Sarathy, F. Mauss, N. Hansen, *Proc. Combust. Inst.,* **2017,** 36(1), 947-955
22. *The Influence of Dimethoxy Methane (DMM)/Dimethyl Carbonate (DMC) Addition on Premixed Ethane/Oxygen/Argon Flame*, W. Sun, B. Yang, N. Hansen, K. Moshammer, *Proc. Combust. Inst.,* **2017,** 36(1), 449-457

23. *The Importance of Third O_2 Addition in 2-Methylhexane Auto-Oxidation*, Z. Wang, S. Y. Mohamed, L. Zhang, K. Moshammer, D. M. Popolan-Vaida, V. S. B. Shankar, A. Lucassen, L. Ruwe, N. Hansen, P. Dagaut, S. M. Sarathy, *Proc. Combust. Inst.,* **2017,** 36(1), 373-382
24. *Consumption and Hydrocarbon Growth Processes in a 2-Methyl-2-Butene Flame*, L. Ruwe, K. Moshammer, N. Hansen, K. Kohse-Höinghaus, *Combust. Flame,* **2017,** 175, 34-46
25. *Quantification of the Keto-hydroperoxide ($HOOCH_2OCHO$) and Other Elusive Intermediates in Low-Temperature Combustion of Dimethyl Ether*, K. Moshammer, A. W. Jasper, D. M. Popolan-Vaida, Z. Wang, V. S. B. Shankar, L. Ruwe, C. A. Taatjes, P. Dagaut, N. Hansen, *J. Phys. Chem. A,* **2016,** 120(40), 7890-7901
26. *Detailed Speciation and Reactivity Characterization of Fuel-Specific In-Cylinder Reforming Products and the Associated Impact on Engine Performance*, B. Wolk, I. Ekoto, W. F. Northrop, K. Moshammer, N. Hansen, *Fuel,* **2016,** 185, 348-361
27. *Additional Chain-Branching Pathways in the Low-Temperature Oxidation of Branched Alkanes*, Z. Wang, L. Zhang, K. Moshammer, D. M. Popolan-Vaida, V. S. B. Shankar, A. Lucassen, C. Hemken. C. A. Taatjes, S. R. Leone, K. Kohse-Höinghaus, N. Hansen, P. Dagaut, S. M. Sarathy, *Combust. Flame,* **2016,** 164(2), 386-396
28. *An Experimental and Kinetic Modeling Study on Dimethyl Carbonate (DMC) Pyrolysis and Combustion*, W. Sun, N. Hansen, C. K. Westbrook, F. Zhang, G. Wang, K. Moshammer, C. K. Law, B. Yang, *Combust. Flame,* **2016,** 164(2), 224-238

Theoretical Studies of Potential Energy Surfaces

Lawrence B. Harding
Chemical Sciences and Engineering Division
Argonne National Laboratory, Argonne, IL 60439
harding@anl.gov

Program Scope

The goal of this program is to calculate accurate potential energy surfaces for both reactive and non-reactive systems. Our approach is to use state-of-the-art electronic structure methods (CASPT2, MR-CI, CCSD(T), etc.) to characterize multi-dimensional potential energy surfaces. Depending on the nature of the problem, the calculations may focus on local regions of a potential surface or may cover the surface more globally. A second aspect of this program is the development of techniques to fit multi-dimensional potential surfaces to convenient, global, analytic functions suitable for use in dynamics calculations. A new part of this program is the use of diffusion Monte-Carlo calculations to obtain high accuracy, anharmonic zero point energies for molecules having multiple minima.

Recent Progress

Diffusion Monte-Carlo for High Accuracy Anharmonic Zero Point Energies

The accuracy of electronic structure calculations has now reached the point where a significant remaining source of error in calculated heats of formation is in the zero point energy. This year we have continued work on our program to address this issue using a combination of a novel potential energy surface fitting strategy and diffusion Monte-Carlo methods[1] to obtain high accuracy predictions of anharmonic, zero point energies for combustion related species. The first step in this process is to fit full dimensional, analytic potentials in the vicinity of the minima. The focus this year has been on species having complex torsional potentials involving two or more hindered rotors. A good example is ethylene glycol, having three strongly coupled hindered rotations. A two dimensional plot of this potential is shown in Figure 1. In this plot a total of seven minima can be seen. Structures for the three most stable minima are superimposed on the plot. The global minimum is a fairly tight structure, having a four-fold degeneracy, consisting of two enantiomeric pairs. One of these pairs is shown in the upper left and lower right of Figure 1. The stability of this structure is due to a combination of hydrogen bonding and the 'gauche' effect. Altogether there are over 20 minima for these three hindered rotors having an energy spread of 1300 cm^{-1} separated by barriers

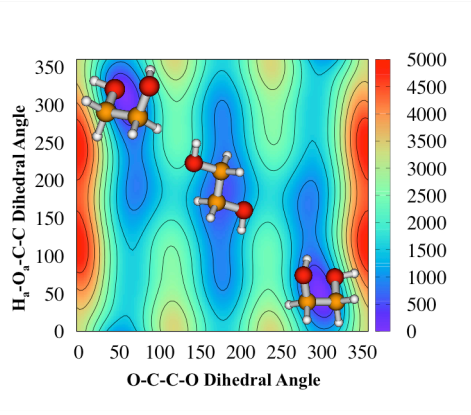

Figure 1. Two dimensional, contour plot of the torsional potential for ethylene glycol. The second HOCC dihedral angle is fixed at 180°. The energy scale on the right is in cm^{-1}.

ranging from less than 500 cm^{-1} to over 2000 cm^{-1}. Other similar molecules studied this year include ethanol, methandiol and dimethyl peroxide.

We now have a library of over 50, full dimensional, analytic, potential energy surfaces for molecules having from 3 to 11 atoms. In a collaboration begun this year with Ahren Jasper, we are now using these potential energy surfaces to estimate anharmonic corrections to rovibrational, partition functions via Monte Carlo phase space integrals. Non-fluxional molecules are generally found to have positive anharmonicity corrections of ~3% per mode at 2500 K. Anharmonicity corrections for fluxional molecules are larger and more variable, ranging from -7% to +9% per mode at 2500 K for those molecules studied thus far.

Photodissociation of Vinyl Cyanide

This year, in collaboration with Stephen Klippenstein, we completed a theoretical analysis of the photodissociation of vinyl cyanide in support of experiments being done by Kirill Prozument. In Figure 2 we show a schematic of the potential energy surface calculated at the CCSD(T)/CBS//B3LYP/6-311G** level of theory. The relative energies from the present theoretical treatment agree with those from Active Tables to within ±1 kcal/mol in all cases.

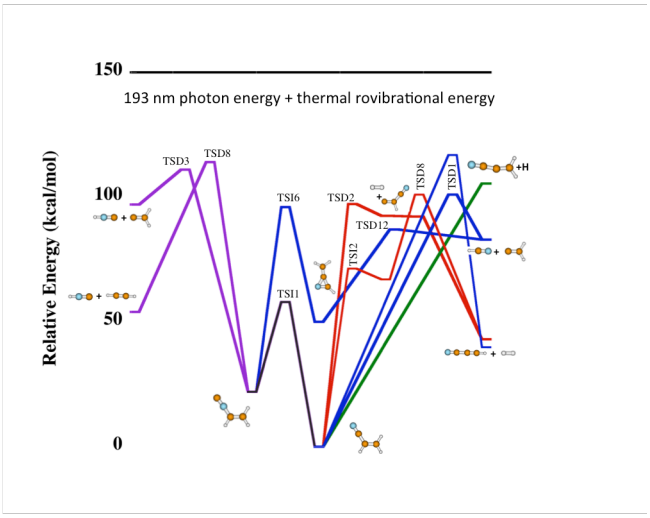

Figure 2. Energies of the minima and saddle points of the vinyl cyanide potential energy surface relevant to photodissociation.

At the energy of the photodissociation experiments, the dominant decomposition channel is predicted to be CH bond cleavage leading to the cyanovinyl radical (shown in green in Figure 2). The lowest energy decomposition channel leads to HCN plus vinylidene via a three step process: (i) isomerization to vinyl isocyanide; (ii) ring closure to a three membered ring intermediate; and (iii) dissociation to HCN plus vinylidene. Although this is the lowest energy channel, the tightness of the saddle point for ring closure causes this route to be unimportant at all but the lowest energies. The direct dissociation of vinyl cyanide to HCN plus vinylidene, although having a higher barrier, is actually the dominate mechanism for this product channel at the energy of the photodissociation experiments. At intermediate energies, (1,1) elimination of H_2 dominates leading to the formation of HCCCN via the isomerization of a transient carbene. The predicted branching ratio between HCN and HCCCN is in excellent agreement with that derived from experiment.

.

Competition between Isomerization and β-scission in Alkyl Radicals.

This year we have also started a project examining the competition between isomerization, via hydrogen migration, and β-scission in alkyl radicals. The calculations are being done at the CCSD(T)/CBS//B2PLYPD3/cc-pVTZ level. We are examining hydrogen migration pathways and both β-CH and β-CC bond cleavages in alkyl radicals containing two to five carbons. Preliminary results indicate that (1,2) and (1,3) hydrogen migrations will not effectively compete with β-scissions. However, at least at low temperatures, (1,4) and (1,5) hydrogen migrations will compete with β-scissions.

Future Plans

In a collaboration with A. Jasper, we plan to continue our studies of anharmonic, partition functions for fluxional molecules, extending our previous work to molecules having two or more hindered rotational degrees of freedom. We also plan to extend our previous study of the O_2 plus vinyl radical reaction in an attempt to identify the mechanism by which CH_3+CO_2 products are produced. One possibility under consideration involves a 'roaming' type mechanism. We are also planning to use Morokuma's global reaction route mapping strategy (GRRM)[2] to discover previously missed pathways.

Acknowledgement: This work was performed under the auspices of the Office of Basic Energy Sciences, Division of Chemical Sciences, Geosciences and Biosciences, U.S. Department of Energy, under Contract DE-AC02-06CH11357.

References:

(1) A. B. McCoy, Int. Rev. Phys. Chem. **25**, 77-107 (2006).
(2) S. Maeda, K. Ohno and K. Morokuma, Phys. Chem. Chem. Phys. **15**, 3683 (2013).

PUBLICATIONS (2015 - Present):

Resolving Some Paradoxes in the Thermal Decomposition Mechanism of Acetaldehyde
R. Sivaramakrishnan, J. V. Michael, L. B. Harding, S. J. Klippenstein
J. Phys. Chem. A **119**, 7724-7733 (2015)

Thermal Dissociation and Roaming Isomerization of Nitromethane: Experiment and Theory
C. Annesley, J. Randazzo, S. J. Klippenstein, L. B. Harding, A. W. Jasper, Y. Georgievski, B. Ruscic, R. S. Tranter, J. Phys. Chem. A **119**, 7872-7893 (2015)

Comment on "A Novel and Facile Decay Path of Criegee Intermediates by Intramolecular Insertion Reactions Via Roaming Transition States" [J. Chem. Phys. 142, 124312 (2015)]
L. B. Harding and S. J. Klippenstein, J. Chem. Phys. **143**, 167101-1 / 167101-2 (2015)

Accurate Anharmonic Zero Point Energies for some Combustion Related Species from Diffusion Monte Carlo
L. B. Harding, Y. Georgievskii, and S. J. Klippenstein, J. Phys. Chem. A **121**, 4334-4340 (2017)

Ab Initio Computations and Active Thermochemical Tables Hand in Hand: Heats of Formation of Core Combustion Species
J. J. Klippenstein, L. B. Harding and B. Ruscic, J. Phys. Chem. A **121**, 6580-6602 (2017)

Time-Resolved Kinetic Chirped-Pulse Roational Spectroscopy in a Room Temperature Flow Reactor
D. P. Zaleski, L. B. Harding, S. J. Klippenstein, B. Ruscic and K. Prozument J. Phys. Chem. Letts. **8**, 6180-6188 (2017)

Anharmonic Rovibrational Partition Functions for Fluxional Species at High Temperature via Monte Carol Phase Space Integrals
A. W. Jasper, Z. B. Gruey, L. B. Harding, Y. Georgievskii, S. J. Klippenstein and A. F. Wagner J. Phys. Chem. **122**, 1727-1740 (2018)

Nascent Energy Distribution of the Criegee Intermediate CH_2OO from Direct Dynamics Calculations of Primary Ozonide Dissociation
M. Pfeifle, Y.-T. Ma, A. W. Jasper, L. B. Harding, W. Hase, and S. J. Klippenstein
J. Chem. Phys. (accepted)

High Pressure Oxidation of Propane
H. Hasemi, J. M. Christensen, L. B. Harding, S. J. Klippenstein and P. Glarborg
Proc. Combust. Inst. (accepted)

Theory of Electronic Structure and Chemical Dynamics

Martin Head-Gordon, William H. Miller, Eric Neuscamman, David Prendergast
Chemical Sciences Division, Lawrence Berkeley National Laboratory and
Department of Chemistry, University of California, Berkeley, California 94720.
mhg@cchem.berkeley.edu, millerwh@berkeley.edu, eneuscamman@berkeley.edu, dgprendergast@lbl.gov

Scope of the Project: To expand knowledge of transient species such as radicals relevant to combustion chemistry and other areas including catalysis, new theoretical methods are needed for reliable computer-based prediction of their properties. The two main areas of relevant theory are electronic structure methods and techniques for chemical dynamics. Within electronic structure theory, focus centers on the development of new density functional theory methods and new wave function theories. Examples of current activity include the introduction of combinatorial design strategies for density functionals, and new quantum Monte Carlo approaches for excited states. In chemical dynamics, recent progress centers on the development of tractable semi-classical dynamics approaches that can address non-adiabatic processes. The focus is on turning semi-classical theory into a practical way of adding quantum effects to classical molecular dynamics simulations of large, complex molecular systems. Newly developed theoretical methods, as well as existing approaches, are employed to study prototype radical reactions, often in collaboration with experimental efforts in the related subtasks (see separate LBNL abstracts). These studies help to deepen understanding of the role of reactive intermediates in diverse areas of chemistry. They also sometimes reveal frontiers where new theoretical developments are needed in order to permit better calculations in the future.

Recent Progress

Due to length limitations, only a selection of projects can be summarized here.

High Accuracy Excited States and Novel Ansatzes. Neuscamman and co-workers have made substantial progress in both novel ansatz design and excited state methods. For excited states, we have developed a new quantum Monte Carlo methodology for the efficient evaluation and optimization of a rigorous excited state variational principle that allows all aspects of a wave function to be tailored for an individual excited state in much the same way as they have long been for ground states. In addition, the methodology can evaluate a rigorous measure of wave function error for ground and excited states alike and so can take a systematic approach to balancing descriptions of different states. These methods for variational excited state evaluations have been paired with a new variation-after-response ansatz that allows a wave function to fully relax itself within the presence of its own linear response, thus capturing important nonlinear effects that are absent in excited state descriptions such as configuration interaction singles and time-dependent density functional theory. Preliminary investigations have shown this approach to be effective in a number charge-transfer examples, where nonlinear orbital relaxations are especially important. In addition to excited state methods, we have also developed new wave function approaches to strongly correlated ground states. In one case, new QMC technology has also allowed for the development of a polynomial-cost, variational analogue to pairwise coupled cluster theory. In another case, we have now successfully realized wave function stenciling in real space QMC where it can work in conjunction with diffusion Monte Carlo. This method has already proven capable of accurately dissociating a double bond using a single, restricted Slater determinant, a major simplification compared to traditional multireference approaches.

Density functionals. Head-Gordon and co-workers have been seeking the limit of transferable accuracy that can be achieved with current forms for density functionals. To achieve high accuracy, non-local density-based corrections for long-range dispersion interactions are added, as well as the option of non-local range-separated hybrid (RSH) treatment of exact exchange. They introduced a novel "survival of the most transferable" (SOMT) procedure to achieve this goal. SOMT is a combinatorial design protocol that involves training a very large numbers of functionals using a fraction of the data, and then selecting the functional that performs best on the remaining data (with the fewest parameters). Recently, this approach has been used to create new density functionals, each

of which may be most accurate in its class for target problems in chemistry, as measured by performance on test data. The most recent, and most accurate one is a RSH meta-GGA including the VV10 van der Waals correction. On a statistical basis, this functional, ωB97M-V, provides substantially improved accuracy for thermochemistry, barrier heights, isomerization energies and non-covalent binding energies relative to existing functionals of the same class. Like all broadly applicable density functionals, it performs increasingly poorly for problems that exhibit strong correlation effects and/or sensitivity to self-interaction errors, where wavefunction methods are still advisable. Nonetheless, for most chemical problems, this functional, and its hybrid GGA cousin, ωB97X-V, and non-hybrid meta-GGA cousin, B97M-V, represent a very useful step forwards. Implementations of B97M-V for condensed matter codes have been recently completed. Across a database of almost 5000 trusted ab initio datapoints, 200 density functionals were assessed to establish these conclusions. Two other useful developments have been recently completed to improve the applicability of DFT. First, a comprehensive optimization of the D3 damping function for dispersion corrections leads to useful improvements in the accuracy of widely used functionals such as BLYP and revPBE0, and the recent meta and hydrid meta-GGAs, MS2 and MS2h. Second, a geometric counterpoise correction, termed DFT-C, has been developed to automatically reduce the effect of basis set superposition error (BSSE) on DFT calculations using the def2-SVPD basis, perhaps the smallest basis set capable of yielding reliable intermolecular interactions. Notably, DFT-C also corrects *intra*-molecular BSSE.

Semi-classical dynamics. It has been long established that semi-classical (SC) theory provides a very good description of essentially *all* quantum effects in molecular dynamics, and the outstanding challenge has been to what extent one can implement it efficiently enough to make it routinely useful. Recently, however, Miller and co-workers have been exploring how successful even simpler, *purely classical* MD approaches can be (with some judicious SC ideas incorporated), especially for the important case of *electronically non-adiabatic processes*, i.e., involving transitions between different electronic states. The two essential ingredients to the approach are, (a) how are the electronic degrees of freedom described within a classical mechanics framework (currently by the Meyer-Miller (MM) 'electronic oscillator' model), and (b) how one identifies specific electronic states (initially and finally) within a classical picture (where the 'symmetrical quasi-classical' (SQC) model is currently being used). In concert, these approaches have given remarkably good results for a series of standard "strong coupling" non-adiabatic problems, even describing 'quantum coherence' effects within a standard classical MD simulation. Recent developments of the SQC/MM approach have been (1) to show that it can treat very weak electronic coupling as well as it does strong coupling (by using a "triangular" modification of the 'window functions' of the SQC model), and (2) how off-diagonal elements of the electronic density matrix can be obtained within the same ensemble of trajectories that gives the diagonal elements (i.e., the populations). The most recent advance has been to show how the SQC/MM approach can be implemented in the adiabatic electronic representation in such a way that only the usual first-derivative coupling elements are required, and not the second-derivative coupling terms that are much more difficult to obtain; there is no approximation involved, the second-derivative coupling terms simply do not appear in the modified equations of motion that are introduced. This will greatly facilitate application of the SQC/MM approach using *ab initio* electronic structure calculations for the potential energy surfaces and (first-derivative) non-adiabatic coupling elements.

Future Plans:

(i) *High Accuracy Core Excitations:* Current efforts focus on extending our variational excited state work to core excitations, where the method's ability to capture secondary relaxations beyond the primary excitation will if anything be more relevant than in the charge transfer case. In this context, variation-after-response will be employed to deal with the large orbital relaxations that accompany a core excitation while, in contrast to delta SCF, maintaining a spin-pure structure for the excitation itself. Our accuracy balancing approach will be applied to the difficult problem of predicting peak positions in core spectra. All of these advantages will also be used together to prepare accurate nodal surfaces for use in core excitation diffusion Monte Carlo, thus expanding the remit of

this high-accuracy method into a crucial area of chemical spectroscopy. Finally, we will explore opportunities for extending our excited state variational methods into the time domain by exploiting similarities between fully variational quantum dynamics and variational principles for excited states.

(ii) *Density functionals:* To achieve improved accuracy, it is desirable to extend the very successful survival-of-the-most-transferable paradigm to the highest level (rung 5), from the recently completed meta-GGA (rung 3) and hybrid meta-GGA (rung 4) efforts. A rung 5 double hybrid functional of this type that includes PT2 correlation is being finalized and tested. Whilst more computationally demanding, this may be the most accurate possible within the SOMT paradigm. Additionally, a series of new tests of density functionals, designed to provide reliable benchmark data that involves energy differences that are distinct from the normal chemical tests, is under construction. Examples include dipole moments, polarizabilities, and measures of delocalization error. Such information can assess existing functionals and inform the design of future functionals.

(iii) *Inner shell excitations and spectra:* The addition of David Prendergast to the program will allow new innovations in this area that synergize with Neuscamman's Monte-Carlo based research. Activity will center on extensions of a flexible formalism for the description of many-body electronic structure relevant to inner-shell excitations and associated Golden-Rule expressions for measurable spectra, with particular attention to photoabsorption (in the linear regime). Initial results already exceed the accuracy of Bethe-Salpeter calculations for a fraction of the cost with the promise to enable exploration of larger system sizes due to favorable computational scaling with little need for additional software development. Synergizing with the DFT work discussed above, we will build on this foundation with exploration in two main areas: (a) use of hybrid functionals and (b) TDDFT approximations to higher excited states.

Recent Publications Citing DOE Support (2015-2018)

- Blunt, N. S.; Neuscamman, E., Charge-transfer Excited States: Seeking a Balanced and Efficient Wave Function Ansatz in Variational Monte Carlo. *J. Chem. Phys.* **2017**, 147 (19), 194101. DOI: 10.1063/1.4998197.
- Cotton, S. J. and W. H. Miller, "A Symmetrical Quasi-Classical Spin-Mapping Model for the Electronic Degrees of Freedom in Non-Adiabatic Processes", *J. Phys. Chem. A* **2015**, 119, 12138-12145 (2015).
- Cotton, S. J. and W. H. Miller, "The Symmetrical Quasi-Classical Model for Electronically Non-Adiabatic Processes Applied to Energy Transfer Dynamics in Site-Exciton Models of Light-Harvesting Complexes", *J. Chem. Theory Comput.* **2016**, 12, 983-991; doi: 10.1021/acs.jctc.5b01178
- Cotton, S.J. and W. H. Miller, "A New Symmetrical Quasi-Classical Model for Electronically Non-Adiabatic Processes: Application to the Case of Weak Non-Adiabatic Coupling", *J. Chem. Phys.* **2016,** 145, 144108.1-16; doi: 10.1063/1.4963914
- Cotton, S.J., R. Liang, and W. H. Miller, "On the Adiabatic Representation of Meyer-Miller Electronic-Nuclear Dynamics", *J. Chem. Phys.* **2017**, *147*, 064112; doi: 10.1063/1.4995301
- Goetz, B. V. D.; Neuscamman, E., Suppressing Ionic Terms with Number-Counting Jastrow Factors in Real Space. *J. Chem. Theory Comput.* **2017**, *13*, 2035-2042. DOI: 10.1021/acs.jctc.7b00158
- Goldey, M.B., B. Belzunces, and M. Head-Gordon, "Attenuated MP2 with a long-range dispersion correction for treating non-bonded interactions", *J. Chem. Theory Comput.* **2015**, 11, 4159−4168; DOI: 10.1021/acs.jctc.5b00509
- Lehtola, S., M. Head-Gordon, and H. Jónsson, "Complex orbitals, multiple local minima and symmetry breaking in Perdew-Zunger self-interaction corrected density-functional theory calculations", *J. Chem. Theory Comput.* **2016**, 12, 3195-3207 (2016); DOI: 10.1021/acs.jctc.6b00347
- Lehtola, S., J.A. Parkhill and M. Head-Gordon, "Cost-effective description of strong correlation: efficient implementations of the perfect quadruples and perfect hextuples models", *J. Chem. Phys.* **2016**, 145, 134110 (2016); doi: 10.1063/1.4964317
- Mardirossian, N. and M. Head-Gordon, "Mapping the genome of meta-generalized gradient approximation density functionals: The search for B97M-V", *J. Chem. Phys.* **2015**, 142, 074111; doi: 10.1063/1.4907719
- Mardirossian, N. and M. Head-Gordon, "ωB97M-V: A combinatorially-optimized, range-separated hybrid, meta-GGA density functional with VV10 nonlocal correlation", *J. Chem. Phys.* **2016**, 144, 214110 (2016); doi: 10.1063/1.4952647

- Mardirossian, N. and M. Head-Gordon, "How accurate are the Minnesota density functionals for thermochemistry, non-covalent interactions, isomerization energies and barrier heights of molecules containing main group elements?" *J. Chem. Theory Comput.* **2016**, 12, 4303–4325; DOI: 10.1021/acs.jctc.6b00637
- Mardirossian, N. and M. Head-Gordon, "Note: The performance of new density functionals for a recent blind test of non-covalent interactions", J. Chem. Phys. **2016**, 145, 186101; DOI: 10.1063/1.4967424
- Mardirossian, N.; Pestana, L. R.; Womack, J. C.; Skylaris, C.-K.; Head-Gordon, T.; Head-Gordon, M., Use of the rVV10 Nonlocal Correlation Functional in the B97M-V Density Functional: Defining B97M-rV and Related Functionals. *J. Phys. Chem. Lett.* **2017**, *8*, 35-40; doi: 10.1021/acs.jpclett.6b02527
- Miller, W.H. and S. J. Cotton, "Communication: Note on Detailed Balance in Symmetrical Quasi-Classical Models for Electronically Non-Adiabatic Dynamics", *J. Chem. Phys.* **2015**, 142, 131103.1-3; doi: 10.1063/1.4916945
- Miller, W.H. and S. J. Cotton, "Communication: Wigner Functions in Action-Angle Variables, Bohr-Sommerfeld Quantization, the Heisenberg Correspondence Principle, and a Symmetrical Quasi-Classical Approach to the Full Electronic Density Matrix", *J. Chem. Phys.* **2016**, 145, 081101.1-4; doi: 10.1063/1.4961551
- Miller, W.H. and S. J. Cotton, "Classical Molecular Dynamics Simulation of Electronically Non-Adiabatic Processes", *Faraday Discuss.* **2016**, 195, 9-30; doi: 10.1039/c6fd00181e
- Neuscamman, E. "Communication: Variation After Response in Quantum Monte Carlo" *J. Chem. Phys.* **2016**, 145, 081103, http://dx.doi.org/10.1063/1.4961686
- Pestana, L. R.; Mardirossian, N.; Head-Gordon, M.; Head-Gordon, T., "Ab initio molecular dynamics simulations of liquid water using high quality meta-GGA functionals." *Chem. Sci.* **2017**, *8*, 3554-3565; doi: 10.1039/c6sc04711d
- Robinson, P. J.; Pineda Flores, S. D.; Neuscamman, E., Excitation Variance Matching with Limited Configuration Interaction Expansions in Variational Monte Carlo. *J. Chem. Phys.* **2017**, 147 (16), 164114. DOI: 10.1063/1.5008743
- Sharada, S.M, D. Stück, E.J. Sundstrom, A.T. Bell, and M. Head-Gordon, "Wavefunction stability analysis without analytical electronic hessians: Application to orbital-optimized post-Hartree-Fock methods and VV10-containing density functionals," *Mol. Phys.* **2015**, 113, 1802-1808. DOI:10.1080/00268976.2015.1014442CH
- Small, D.W., E.J. Sundstrom, and M. Head-Gordon, "A simple way to test for collinearity in spin symmetry broken wave functions: Theory and application to Generalized Hartree-Fock", *J. Chem. Phys.* **2015**, 142, 094112 (9 pages). http://dx.doi.org/10.1063/1.4913740
- Small, D. W.; Head-Gordon, M., Coupled cluster valence bond theory for open-shell systems with application to very long range strong correlation in a polycarbene dimer. *J. Chem. Phys.* **2017**, *147*, 024107; doi: 10.1063/1.4991797
- Stein, T., B. Bandyopadhyay, T. Troy, Y. Fang, O. Kostko, M. Ahmed, and M. Head-Gordon, "Ab initio dynamics and photoionization mass spectrometry reveal ion-molecule pathways from ionized acetylene clusters to benzene cation", *Proc. Nat. Acad. Sci*. **2017**, *114*, E4125-E4133; doi: 10.1073/pnas.1616464114.
- Witte, J.; Mardirossian, N.; Neaton, J. B.; Head-Gordon, M., Assessing DFT-D3 Damping Functions Across Widely Used Density Functionals: Can We Do Better? *J. Chem. Theory Comput.* **2017**, *13*, 2043-2052; doi: 10.1021/acs.jctc.7b00176
- Witte, J.; Neaton, J. B.; Head-Gordon, M., Effective empirical corrections for basis set superposition error in the def2-SVPD basis: gCP and DFT-C. *J. Chem. Phys.* **2017**, *146*, 234105; doi: 10.1063/1.4986962
- Womack, J.C., N. Mardirossian, M. Head-Gordon, and C.-K. Skylaris, "Self-consistent implementation of meta-GGA functionals for the ONETEP linear-scaling electronic structure package", *J. Chem. Phys.* **2016**, 145, 204114; doi: 10.1063/1.4967960
- Zhao, L. and Neuscamman, E. "An efficient variational principle for the direct optimization of excited states" *J. Chem. Theory Comput.* **2016**, 12, 3436, DOI: 10.1021/acs.jctc.6b00508
- Zhao, L. and Neuscamman, E. "Equation of motion theory for excited states in variational Monte Carlo and the Jastrow antisymmetric geminal power in Hilbert space" *J. Chem. Theory Comput.* **2016**, 12, 3719, DOI: 10.1021/acs.jctc.6b00480
- Zhao, L. and Neuscamman, E. "Amplitude determinant coupled cluster with pairwise doubles" *J. Chem. Theory Comput.* **2016**, 12, 5841, DOI: 10.1021/acs.jctc.6b00812

Semiclassical Methods for Pressure Dependent Kinetics and Electronically Nonadiabatic Chemistry

Ahren W. Jasper
Chemical Sciences and Engineering Division
Argonne National Laboratory
ajasper@anl.gov

Program Scope

The accuracy of a priori theoretical chemistry calculations is improving thanks to ongoing increases in computational power, the ready availability of accurate electronic structure methods and codes, and advances in kinetics and dynamics methods development. One accuracy milestone for dynamics and kinetics may be termed the "semiclassical accuracy" limit, representing the accuracy of the best non-quantal methods. These methods can have errors as low as ~20%, rivaling those of experiment in some applications. The principal goal of this project is to develop and validate new theoretical methods for broadening the applicability and improving the accuracy of theoretical chemical kinetics and dynamics and to aid in the realization of semiclassical accuracy for applications throughout gas phase chemistry. The developments we are presently focused on are: (1) predicting pressure dependence in elementary reactions using detailed models of energy transfer informed by classical trajectories, (2) characterizing spin-forbidden kinetics using both multistate trajectory methods and statistical theories, and (3) predicting anharmonic vibrational properties for polyatomic molecules at high energies and temperatures via Monte Carlo phase space integration.

Recent Progress

With co-workers at Argonne and, specifically, using potentials developed by Harding and Georgievskii, Monte Carlo phase space integration (MCPSI) was used to compute full dimensional and fully anharmonic—but classical—rovibrational partition functions for 22 small- and medium-sized molecules and radicals. Several of the species featured multiple minima and low-frequency nonlocal motions, and efficiently sampling these systems was facilitated using curvilinear (stretch, bend, and torsion) coordinates. The curvilinear coordinate MCPSI method was demonstrated to be applicable to the treatment of fluxional species with complex rovibrational structures and as many as 21 fully coupled rovibrational degrees of freedom. Trends in the computed anharmonicity corrections were identified and discussed. For many systems and largely independent of chemical composition, average per-mode rovibrational anharmonicities at elevated temperatures were shown to vary consistently with the number of degrees of freedom and with temperature once rovibrational coupling and torsional anharmonicity were accounted for. Significant corrections were found for systems with complex vibrational structures, such as systems with multiple large-amplitude modes and/or multiple minima. This work involved contributions from Zak Gruey, an undergraduate from UC Davis, who visited as part of the Science Undergraduate Laboratory Internship (SULI) program.

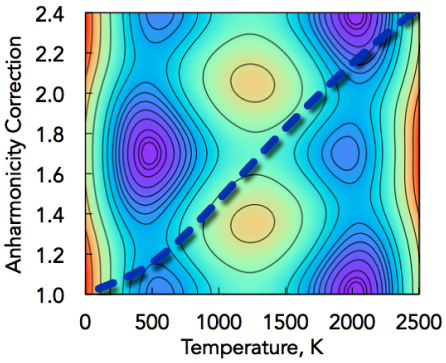

Fig. 1. Table of contents graphic for Ref. 6 showing the correction to the harmonic state count for NH_2OH overlaid over a contour plot of the PES as a function of the $–NH_2$ inversion and N–O torsion coordinates.

With Moshammer and Hansen (Sandia), photoionization cross sections were calculated for twelve species using a readily applicable approach based on the frozen-core Hartree-Fock approximation, as made available by Lucchese in his ePolyScat code. This approach was first validated against measured photoionization cross sections and found to have an average error of ~2x, which likely improves on the estimates commonly used to quantify species with unknown cross sections. Next, the ketohydroperoxide relevant to the low temperature oxidation of dimethyl ether was identified in a jet stirred reactor, and its mole fraction was quantified using the predicted cross section. This study demonstrated that theoretical cross sections can be useful for quantifying key intermediates, which in turn provide additional targets for testing chemical kinetic models.

With Klippenstein, Georgievskii (Argonne), and Mebel (FIU), the temperature- and pressure-dependent kinetics of several key steps in the HACA molecular growth mechanism were predicted. As part of this effort, the collision parameters (i.e., efficiencies, $\alpha = \langle \Delta E_d \rangle$, and effective Lennard-Jones rate parameters) required for predicting pressure dependence in the master equation were calculated using newly fitted potential energy surfaces for collisions involving small aromatic molecules and the colliders He, Ar, and N_2. Similar to our previous work on saturated hydrocarbons, we found that, for a given collider, the collision parameters depended most sensitively on the chemical composition of the hydrocarbon and were relatively insensitive to the chemical arrangement. Furthermore, parameterizations of the separable pairwise functional form for the interaction potential were found to be transferable to larger aromatics. The present strategies are therefore readily applicable to the study of larger PAHs.

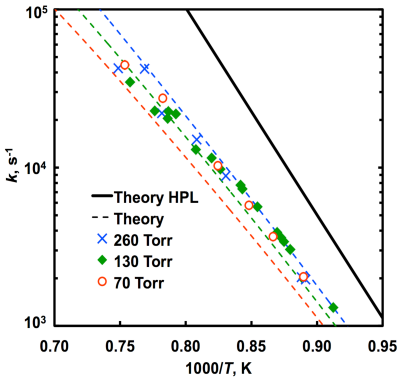

Fig. 2. Calculated and measured rate coefficients for the dissociation of 2-methyl-allyl

With Tranter (Argonne), the dissociation and the self-recombination of 2-methylallyl radicals were calculated using ab initio, transition state theory, classical trajectory, and master equation calculations. The predicted pressure- and temperature-dependent kinetics for both reactions were found to agree very well with the accompanying shock tube measurements, with, notably, no adjustments to the theory required (see Fig. 2). The observed quantitative agreement is likely somewhat fortuitous, as one might expect significant uncertainty in the partition function for the self-recombination adduct (2,5-dimethyl-1,5-hexadiene). Nonetheless, the comparisons provide yet another example of the good accuracy that can be achieved with fully a priori kinetics calculations, including trajectory-based predictions of pressure dependence.

As part of the AITSTME project (PI: Klippenstein), the spin-forbidden and spin-allowed product branching of $^3O + C_2H_4$ was calculated using a combination of quantum chemistry, master equation, classical trajectory, and nonadiabatic statistical theory calculations. This reaction has been widely studied, and it is known that product branching is largely controlled via the fate of the initial triplet adduct OC_2H_4, where intersystem crossing (ISC) to the singlet surface competes with spin-allowed bimolecular channels on the triplet surface. Here we used a Landau-Zener statistical calculation for the ISC rate (sometimes called "nonadiabatic transition state theory") alongside conventional TST to predict the temperature-dependent branching within a single master equation calculation. Product branching immediately following ISC was determined using short-time direct classical trajectories initiated at the crossing seam. Our predicted room temperature branching agreed well with available experimental results, as well as with a previous master equation study of Vereecken, Peeters, and co-workers, who used a more approximate treatment of ISC. The two master equation studies predict different product branching at elevated temperatures, however.

Future Work

We will continue the development and application of predictive models for pressure-dependent chemical kinetics. In ongoing work, collision rates and efficiencies are being generated for hundreds of species with as many as 16 non-hydrogen atoms in three bath gases (He, Ar, and N_2). New potential energy parameterizations were obtained to allow for the treatment of alcohols and peroxides, and previously developed parameterizations were used for hydrocarbons. Analytic formulas for Lennard–Jones collision parameters σ and ε were determined for each of these three classes of systems as a function of the number of non-hydrogen atoms. Collision efficiency parameters ($\alpha = \langle \Delta E_d \rangle$) are being calculated for the normal alkanes, alcohols, and peroxides using a newly developed automation strategy. Trends in α can be rationalized based on the number and type of internal rotors, thus allowing for the estimation of collision parameters for species not explicitly considered.

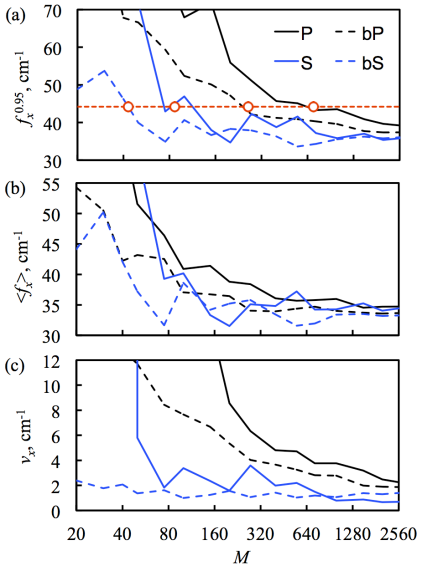

Fig. 3. (a) Convergence of the out of sample (prediction) error $f_x^{0.95}$ for a separable pairwise exp/6 fit of the CH_3OH + Ar interaction PES as a function of the number of sampled data M. The (b) mean prediction error $\langle f_x \rangle$ and the (c) variance in the fitting error v_x converge at different rates for the four sampling types: pseudorandom (P), Sobol quasirandom (S), and biased P and S (bP and bS).

An important limitation to rapidly generating accurate trajectory-based collision parameters is the difficulty in obtaining high-quality analytic representations of the intermolecular potential. We have been developing automated parameterization schemes for the intermolecular potential using both (1) class-based pairwise exp/6 (Buckingham) representations (describing, e.g., the interaction of Ar with all alcohols), and (2) system-specific permutationally-invariant polynomials representations. We are exploring with Davis (Argonne) efficiency and accuracy improvements related to the choice of sampling strategy and functional form optimization. In preliminary work, we quantified the efficiency four sampling strategies: pseudorandom (P), Sobol quasirandom (S), and biased versions of each (bP and bS). Figure 3 shows the convergence in the out of sample (prediction) error as a function of the number of sampled geometries/energies M for each sampling type. For this system, the biased Sobol scheme is 10x more efficient than the unbiased pseudorandom scheme that is most often used. The optimized scheme requires just ~4 ab initio data per parameter. These trends persist both for larger alcohols and in the higher dimensional fits required for larger bath gases.

The MCPSI method for calculating vibrational anharmonicity will continue to be applied and developed. We will focus on systems where the accuracy of existing vibrational anharmonicity approaches is not known, such as those involving constrained torsions and rings. We have implemented our curvilinear coordinate MCPSI approach “as scale” on Argonne’s petascale machine, Theta. There we have calculated converged semiclassical rovibrational state counts and partition functions for systems with two and three coupled torsions and as many as 30 rotational and vibrational modes. In addition to serving as benchmark results for simpler models, these results are being analyzed and a variety of physical insights about the nature of mode coupling at high temperature are being made. For example, kinetic couplings can become significant for floppy motions at high energies/temperatures, thus reducing the usefulness of separable valence (i.e., stretch, bend, torsion) descriptions of vibrational motions under these extreme conditions.

Publications supported by this project since 2016

1. Nascent energy distribution of the Criegee intermediate CH_2OO from direct dynamics calculations of primary ozonide dissociation. M. Pfeifle, Y.-T. Ma, A. W. Jasper, L. B. Harding, W. L. Hase, and S. J. Klippenstein, *J. Chem. Phys.*, accepted (2018).
2. Automated computational thermochemistry for butane oxidation: A prelude to predictive automated combustion kinetics. M. Keçeli, S. Elliott, Y.-P. Li, M. S. Johnson, C. Cavallotti, Y. Georgievskii, W. H. Green, M. Pelucchi, J. M. Wozniak, A. W. Jasper, and S. J. Klippenstein, *Proc. Combust. Inst.*, accepted (2018).
3. Toward accurate high temperature anharmonic partition functions. D. H. Bross, A. W. Jasper, B. Ruscic, and A. F. Wagner, *Proc. Combust. Inst.*, accepted (2018).
4. Theory and modeling of relevance to prompt-NO formation at high pressure. S. J. Klippenstein, M. Pfeifle, A. W. Jasper, and P. Glarborg, *Combust. Flame.*, accepted (2018).
5. Theoretical investigation of intersystem crossing in the cyanonitrene molecule. $^1NCN \rightarrow {}^3NCN$. M. Pfeifle, Y. Georgievskii, A. W. Jasper, and S. J. Klippenstein, *Chem. Phys.* 147, 084310 (2018).
6. Anharmonic rovibrational partition functions for fluxional species at high temperatures via Monte Carlo phase space integrals. A. W. Jasper, Z. B. Gruey, L. B. Harding, Y. Georgievskii, S. J. Klippenstein, and A. F. Wagner, *J. Phys. Chem. A*, 122, 1272–1740 (2018).
7. Exploring the negative temperature coefficient behavior of acetaldehyde based on detailed intermediate measurements in a jet stirred reactor. T. Tao, W. Sun, N. Hansen, A. W. Jasper, K. Moshammer, B. Chen, Z. Wang, C. Huang, P. Dagaut, and B. Yang, *Combust. Flame.*, 192, 120–129 (2018).
8. Theoretical study of the Ti-Cl bond cleavage reaction in $TiCl_4$. D. Nurkowski, A. W. Jasper, J. Akroyd, and M. Kraft, *Z. Phys. Chem.* 231, 1489–1506 (2017).
9. Recombination and dissociation of 2-methyl allyl radicals: Experiment and theory. R. S. Tranter, A. W. Jasper, J. B. Randazzo, J. P. A. Lockhart, and J. P. Porterfield, *Proc. Combust. Inst.* 36, 211–218 (2017).
10. Theoretical kinetics of O + C_2H_4. X. Li, A. W. Jasper, J. Zádor, J. A. Miller, and S. J. Klippenstein, *Proc. Combust. Inst.* 36, 219–227 (2017).
11. Temperature- and pressure-dependent rate coefficients for the HACA pathways from benzene to naphthalene. A. M. Mebel, Y. Georgievskii, A. W. Jasper, and S. J. Klippenstein, *Proc. Combust. Inst.* 36, 919–926 (2017).
12. Quantification of the keto-hydroperoxide ($HOOCH_2OCHO$) and other elusive intermediates during low-temperature oxidation of dimethyl ether. K. Moshammer, A. W. Jasper, D. M. Popolan-Vaida, Z. Wang, V. S. B. Shankar, L. Ruwe, C. A. Taatjes, P. Dagaut, and N. Hansen, *J. Phys. Chem. A* 120, 7890–7901 (2016).
13. Pressure dependent rate constants for PAH growth: formation of indene and its conversion to naphthalene. A. M. Mebel, Y. Georgievskii, A. W. Jasper, and S. J. Klippenstein, *Faraday Discuss. Chem. Soc.* 195, 637–670 (2016).
14. Low temperature kinetics of the first steps of water cluster formation. V. Roussel, M. Capron, J. Bourgalais, A. Benidar, A. W. Jasper, S. J. Klippenstein, L. Biennier, and S. D. Le Picard, *Phys. Rev. Lett.* 116, 113401 (2016).
15. Comment on "When rate constants are not enough." J. A. Miller, S. J. Klippenstein, S. H. Robertson, M. J. Pilling, R. Shannon, J. Zádor, A. W. Jasper, C. F. Goldsmith, and M. P. Burke, *J. Phys. Chem. A* 120, 306–312 (2016).

Probing the Reaction Dynamics of Hydrogen-Deficient Hydrocarbon Molecules and Radical Intermediates via Crossed Molecular Beams

Ralf I. Kaiser
Department of Chemistry, University of Hawai'i at Manoa, Honolulu, HI 96822
ralfk@hawaii.edu

1. Program Scope

The major goals of this project are to explore experimentally by exploiting molecular beams the fundamental reaction dynamics and underlying potential energy surfaces (PESs) of hydrocarbon molecules and their corresponding (resonantly free stabilized and aromatic) radical precursors, which are relevant to the formation and molecular growth of polycyclic aromatic hydrocarbons (PAHs). First, reactions are initiated in a crossed molecular beams machine under single collision conditions by crossing two supersonic reactant beams containing radicals and/or closed shell species under a well-defined collision energy and intersection angle. By recording angular-resolved time of flight (TOF) spectra, we obtain information on the reaction products, intermediates involved, branching ratios of competing reaction channels, reaction energetics, and on the underlying reaction mechanisms. Second, in collaboration with Dr. Musahid Ahmed (Advanced Light Source, Lawrence Berkeley Laboratory), reactions are carried out in a chemical reactor at well characterized pressure and temperature distributions with reaction products interrogated isomer selectively by tunable vacuum ultraviolet light (VUV) via photoionization (PI) coupled with a reflectron time of flight mass spectrometer (ReTOFMS). Merged with electronic structure calculations (Prof. Alexander M. Mebel, Florida International University), these data are of crucial importance to comprehend the detailed formation mechanisms of two key classes of molecules involved in mass-growth processes leading to carbonaceous nanostructures from the bottom up: resonantly stabilized free radicals (RSFRs) and polycyclic aromatic hydrocarbons (PAHs).

2. Recent Progress

2.1. Formation Mechanisms and Reaction Dynamics to PAHs Carrying Three Rings

Having elucidated the formation mechanisms and chemical dynamics leading to (hydrogenated and substituted) PAHs carrying two rings, i.e. naphthalene (two six membered rings; $C_{10}H_8$) [**P1,P2, P3, P9, P13, P16, P24]** and indene (one six and one five membered ring; C_9H_8) [**P1, P4, P7, P16],** we have started to expand our mechanistical studies to the formation of three-ring PAHs carrying three six membered rings phenanthrene ($C_{14}H_{10}$), dihydrophenanthrene ($C_{14}H_{12}$), and anthracene ($C_{14}H_{10}$) [**P17, P18, P23]** and two six membered plus one five membered ring acenaphthylene ($C_{12}H_8$) [**P6**]. These studies revealed that the HACA mechanism neither yields anthracene ($C_{14}H_{10}$) nor phenanthrene ($C_{14}H_{10}$) form naphthyl radicals ($C_{10}H_7$), but solely acenaphthylene ($C_{12}H_8$) (Fig. 3). However, Hydrogen Abstraction – aCetylene Addition mechanisms (HACA) starting from non-PAH radicals such as biphenylyl ($C_{12}H_9$) reacting with acetylene (C_2H_2) can synthesize via bay-closure phenanthrene ($C_{14}H_{10}$), but not the anthracene isomer ($C_{14}H_{10}$). On the other hand, the Hydrogen Abstraction – Vinylacetylene Addition mechanism (HAVA) starting from 1-/2- naphthyl radicals ($C_{10}H_7$) reacting with vinylacetylene (C_4H_4) can form via ring annulation phenanthrene ($C_{14}H_{10}$) and anthracene ($C_{14}H_{10}$) (Fig. 1).

2.2. Formation Mechanisms and Reaction Dynamics to PAHs Carrying Four Rings

We expanded our studies on the growth of PAHs to PAH systems carrying four six membered rings utilizing pyrene ($C_{16}H_{10}$) as a prototype. By exploring the reaction of the 4-phenanthrenyl radical ($[C_{14}H_9]^{\bullet}$) with acetylene (C_2H_2) under conditions prevalent in high temperature combustion systems, we provide testimony on a facile, isomer-selective formation of pyrene ($C_{16}H_{10}$). Along with the Hydrogen Abstraction – Vinylacetylene Addition (HAVA) mechanism, molecular mass growth processes from pyrene may lead through systematic ring expansions not only to more complex PAHs, but ultimately to two-dimensional graphene-type structures thus facilitating an understanding toward soot growth in combustion systems [**P23**] (Fig. 2). This research was carried out in collaboration with Dr. Ahmed (ALS) and Profs. Mebel (FIU; computations) and Fischer (UC Berkeley; synthesis of precursor).

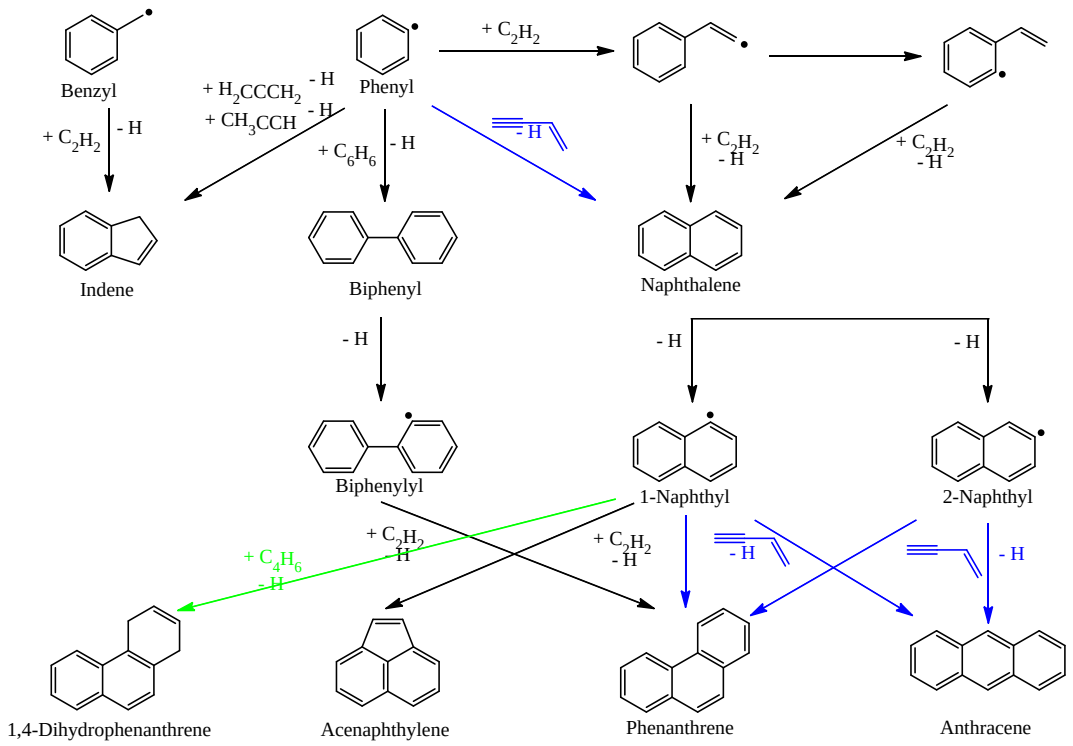

Fig. 1: Experimentally and computationally derived routes to PAHs via the hydrogen abstraction – acetylene addition (HACA) (black) and the barrier-less hydrogen abstraction – vinylacetylene addition (HAVA) reaction pathways (blue). Pathways involving barrierless reactions with 1,3-butadiene are color coded in green.

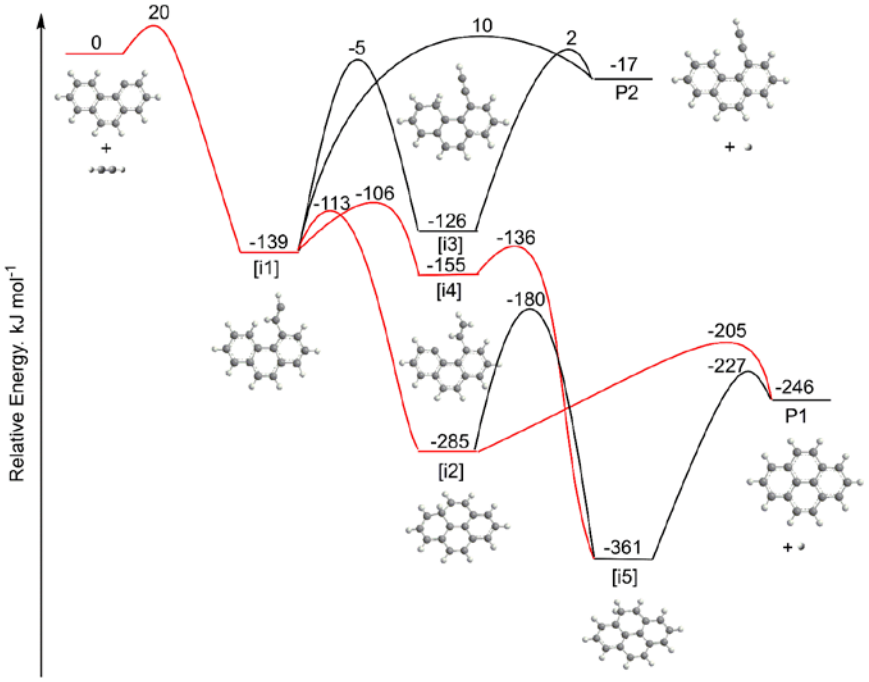

Fig. 2 (left): Potential energy surface (PES) for the 4-phenanthrenyl ($[C_{14}H_9]^{\bullet}$) reaction with acetylene (C_2H_2) calculated at the G3(MP2,CC)//B3LYP/6-311G(d,p) level of theory. The favorable pathways leading to pyrene are colored in red.

3. Future Plans

Having established synthetic pathways to PAHs carrying up to three rings (naphthalene, indene; phenanthrene, anthracene, acenaphthylene), we will expand our studies to the formation of more complex PAHs such as triphenylene and fluoranthene (four rings) along with corannulene (six rings) and coronene (seven rings) as building blocks to two and three dimensional carbon nanostructures. Further, our molecular beam studies plan unravelling the synthesis of the simplest representatives of key classes of PAHs: phenacenes, acenes, and helicenes. Electronic structure calculations are conducted by Prof. Mebel (Florida International University). Commercially unavailable precursors will be synthesized by Prof. Felix Fischer (UC Berkeley). This also helps to define the role and complementary nature of three reaction mechanisms in PAH growth: the Hydrogen Abstraction – aCetylene Addition mechanism (HACA), the Hydrogen Abstraction – Vinylacetylene Addition mechanism (HAVA), and the Phenyl Addition – dehydroCyclization pathway (PAC).

4. Acknowledgements

This work was supported by US Department of Energy (Basic Energy Sciences; DE-FG02-03-ER15411).

5. Publications Acknowledging DE-FG02-03ER15411 (3/2015 – now)

P1 R.I. Kaiser, D.S.N. Parker, A.M. Mebel, Reaction Dynamics in Astrochemistry: Low Temperature Pathways to Polycyclic Aromatic Hydrocarbons in the Interstellar Medium. Annu. Rev. Phys. Chem. 66, 43-67 (2015).

P2 T. Yang, L. Muzangwa, D.S.N. Parker, R. I. Kaiser, A.M. Mebel, Synthesis of 2- and 1-Methyl-1,4-Dihydronaphthalene Isomers via the Crossed Beam Reactions of Phenyl Radicals (C_6H_5) with Isoprene ($CH_2C(CH_3)CHCH_2$) and 1,3-Pentadiene ($CH_2CHCHCHCH_3$). Phys. Chem. Chem. Phys. 17, 530-540 (2015).

P3 L.G. Muzangwa, T. Yang, D.S.N. Parker, R.I. Kaiser, A.M. Mebel, A. Jamal, M. Ryazantsev, K. Morokuma, A Crossed Molecular Beam and Ab Initio Study on the Formation of 5- and 6-Methyl-1,4-Dihydronaphthalene ($C_{11}H_{12}$) via the Reaction of Meta-Tolyl (C_7H_7) with 1,3-Butadiene (C_4H_6). Phys. Chem. Chem. Phys. 17, 7699-7706 (2015).

P4 T. Yang, D.S.N. Parker, B. B. Dangi, R. I. Kaiser, A.M. Mebel, Formation of 5- and 6-Methyl-1H-Indene ($C_{10}H_{10}$) via the Reactions of the Para-Tolyl Radical ($C_6H_4CH_3$) with Allene (H_2CCCH_2) and Methylacetylene ($HCCCH_3$) under Single Collision Conditions. Phys. Chem. Chem. Phys. 17, 10510-10519 (2015).

P5 D.S.N. Parker, R.I. Kaiser, O. Kostko, T.P. Troy, M. Ahmed, A.M. Mebel, A.G.G.M. Tielens, On the Synthesis of (Iso)Quinoline and Its Role in the Formation of Nucleobases in the Interstellar Medium. Astrophys. J. 803, 53 (2015).

P6 D.S.N. Parker, R.I. Kaiser, B. Bandyopadhyay, O. Kostko, T.P. Troy, M. Ahmed, Unexpected Chemistry from the Reaction of Naphthyl plus Acetylene at Combustion-like Temperatures. Angew. Chemie Int. Ed. 54, 5421-5424 (2015).

P7 D.S.N. Parker, R.I. Kaiser, O. Kostko, M. Ahmed, Selective Formation of Indene through the Reaction of Benzyl Radicals with Acetylene Chem. Phys. Chem. 16, 2091-2093 (2015).

P8 D.S.N. Parker, R.I. Kaiser, T. P. Troy, O. Kostko, M. Ahmed, A.M. Mebel, Toward the Oxidation of the Phenyl Radical and Prevention of PAH Formation in Combustion Systems. J. Phys. Chem. A 119, 7145-7154 (2015).

P9 T. Yang, L. Muzangwa, R.I. Kaiser, A. Jamal, K. Morokuma, A Combined Crossed Molecular Beam and Theoretical Investigation of the Reaction of the Meta-Tolyl Radical with Vinylacetylene - Toward the Formation of Methylnaphthalenes. Phys. Chem. Chem. Phys. 17, 21564 - 21575 (2015).

P10 A.M. Mebel, R.I. Kaiser, Formation of Resonantly Stabilized Free Radicals via the Reactions of Atomic Carbon, Dicarbon, and Tricarbon with Unsaturated Hydrocarbons: Theory and Crossed Molecular Beams Experiments. Int. Rev. Phys. Chem. 34, 461-514 (2015).

P11 D.S.N. Parker, R.I. Kaiser, O. Kostko, T.P. Troy, M. Ahmed, B.-J. Sun, S.-H. Chen, A.H.H. Chang. On the Formation of Pyridine in the Interstellar Medium. Phys. Chem. Chem. Phys. 17, 32000 – 32008 (2015).

P12 D.S.N. Parker, T. Yang, B.B. Dangi, R.I. Kaiser, P. P. Bera, T.J. Lee, Low Temperature Formation of Nitrogen-Substituted Polycyclic Aromatic Hydrocarbons (NPAHs) - Barrierless Routes to Dihydro(iso)quinolines. Astrophys. J. 815, 115 (2015).

P13 T. Yang, T. P. Troy, B. Xu, O. Kostko, M. Ahmed, A.M. Mebel, R.I. Kaiser, Hydrogen-Abstraction/Acetylene-Addition Exposed. Angew. Chemie Int. Ed. 55, 14983-14987 (2016).

P14 A.M. Thomas, T. Yang, B.B. Dangi, R.I. Kaiser, G.-S. Kim, A.M. Mebel, Oxidation of the Para-Tolyl Radical by Molecular Oxygen Under Single-Collison Conditions: Formation of the Para-Toloxy Radical. J. Phys. Chem. Lett. 7, 5121-5127 (2016).

P15 D.S.N. Parker, R.I. Kaiser, On the Formation of Nitrogen-Substituted Polycyclic Aromatic Hydrocarbons (NPAHs) in Circumstellar and Interstellar Environments. Chem. Soc. Rev. 46, 452 - 463 (2017).

P16 A.M. Mebel, A. Landera, R.I. Kaiser, Formation Mechanisms of Naphthalene and Indene: From the Interstellar Medium to Combustion Flames. J. Phys. Chem. A 121, 901–926 (2017).

P17 T. Yang, R.I. Kaiser, T.P. Troy, B. Xu, O. Kostko, M. Ahmed, A.M. Mebel, M.V. Zagidullin, V.N. Azyazov, HACA's Heritage: A Free-Radical Pathway to Phenanthrene in Circumstellar Envelopes of Asymptotic Giant Branch Stars. Angew. Chemie Int. Ed. 56, 4515-4519 (2017).

P18 A.M. Thomas, M. Lucas, T. Yang, R.I. Kaiser, L. Fuentes, D. Belisario-Lara, A.M. Mebel, A Free Radical Pathway to Hydrogenated Phenanthrene in Molecular Clouds - Low Temperature Growth of Polycyclic Aromatic Hydrocarbons. Chem. Phys. Chem. 18, 1971-1976 (2017).

P19 M. Lucas, L. Zhao, A.M. Thomas, R. I. Kaiser, A.M. Mebel, Gas Phase Synthesis of the Elusive Cyclooctatetraenyl Radical (C_8H_7) Angewandte Chemie – International Edition 44, 13533-13897 (2017).

P20 L. Zhao, R.I. Kaiser, B. Xu, U. Ablikim, M. Ahmed, D. Joshi, G. Veber, F. Fischer, A.M. Mebel, On the Synthesis of Pyrene in Circumstellar Envelopes and Its Role in the Formation of 2D Nanostructures. Nature Astronomy doi:10.1038/s41550-018-0399-y (2018).

P21 A.M. Thomas, M. Lucas, L. Zhao, J. Liddiard, R.I. Kaiser, A.M. Mebel, A Combined Crossed Molecular Beams and Computational Study on the Observation of the Penta-1-yn-3,4-dienyl-1 (C_5H_3) Radical from Dissociating Triplet C_6H_6 Collision Complexes. Physical Chemistry Chemical Physics doi.org/10.1039/c8cp00357b (2018).

P22 M. Lucas, A.M. Thomas, R. I. Kaiser, A.M. Mebel, A Combined Experimental and Computational Investigation of the Elementary Reaction of Ground State Atomic Carbon (C; ^3P_j) with Pyridine (C_5H_5N; X^1A_1) via Ring Expansion and Ring Degradation Pathways. The Journal of Physical Chemistry A 10.1021/acs.jpca.8b00756 (2018).

P23 L. Zhao, R.I. Kaiser, B. Xu, U. Ablikim, M. Ahmed, M. Evseev, E.K. Bashkirov, V.N. Azyazov, A.M. Mebel, V. Vuitton, Low-Temperature Formation of Anthracene and Phenanthrene and Implications to the Synthesis of Polycyclic Aromatic Hydrocarbons in Titan's Atmosphere (submitted 2018).

P24 L. Zhao, R.I. Kaiser, B. Xu, U. Ablikim, M. Ahmed, A.M. Mebel, A VUV Photoionization Study on the Formation of the Simplest Polycyclic Aromatic Hydrocarbon: Naphthalene ($C_{10}H_8$) (submitted 2018).

Time-Resolved Nonlinear Optical Diagnostics

Christopher J. Kliewer (PI)
Combustion Research Facility, Sandia National Laboratories
P.O. Box 969, MS 9055
Livermore, CA 94551-0969
cjkliew@sandia.gov

Program Scope

This program focuses on the development of innovative laser-based techniques for measuring temperature and concentrations of important combustion species as well as the investigation of fundamental physical and chemical processes that directly affect quantitative application of these techniques. Our development efforts focus on crossed-beam approaches such as time-resolved nonlinear wave-mixing. A critical aspect of our research includes the study of fundamental spectroscopy, energy transfer, molecular dynamics, and photochemical processes. This aspect of the research is essential to the development of accurate models and quantitative application of techniques to the complex environments encountered in combustion systems. These investigations use custom-built tunable picosecond (ps) and commercial femtosecond lasers, which enable efficient nonlinear excitation, provide high temporal resolution for pump/probe studies of collisional processes, and are amenable to detailed physical models of laser-molecule interactions.

Recent Progress

Rotational Coherence Beating Observed from Molecular Oxygen: Coupling of Electronic and Nuclear Spin Angular Momentum. In recent years, our group has developed time-resolved methods in coherent Raman spectroscopy that take advantage of femtosecond coherence preparation pulses. Recent advances in this field have created a new set of nonlinear optical tools with greater detection efficiency, higher precision, and greater capability for multiplexing to detect several molecular species in a single apparatus. Further, using ultrafast laser sources and methods to perform coherent Raman measurements has proven to provide reduced sensitivity to various coherent and incoherent optical interferences that reduce the accuracy of data interpretation. However, the spectroscopic modeling of these new techniques has required the development of new time-domain calculations of the coherent Raman response, and the time-domain signal is then Fourier transformed to yield the frequency-resolved spectrum for a hybrid time- and frequency-resolved experiment such as encountered in femtosecond pump / picosecond probe CARS arrangements. For the most part, the assembly of these spectral models has been a straightforward process, as has been demonstrated for molecular N_2. This has allowed us to take advantage of the refinements made to the N_2 CARS codes over the past 30 years for nanosecond based approaches. In the case of the O_2 molecule, the adaptation was not quite as straightforward. Figure 1 displays a pure-rotational CARS spectrum of molecular O_2 at 1 atm pressure, room temperature, and a 550 picosecond delay. The contour of the spectrum does not resemble a smooth rotational-state Boltzmann distribution, as would be predicted by a direct adaptation of current O_2 CARS models used to fit nanosecond-pulse based CARS measurements. Instead the spectrum exhibits a frequency-dependent beating pattern. This rotational state dependent

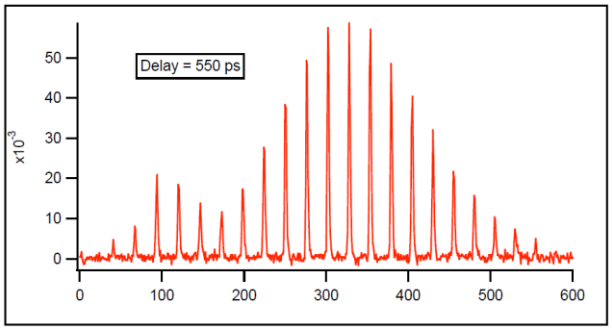

FIG. 1. Hybrid femtosecond/picosecond CARS spectrum of molecular O_2 at 760 Torr and 295 K. The probe delay is 550 picoseconds. The strange spectral contour is explained by rotational quantum state specific beating caused by the coupling of nuclear and electronic angular momentum. Every line is composed of a triplet of allowed transitions, $\Delta N = 2$, $\Delta J = 2$

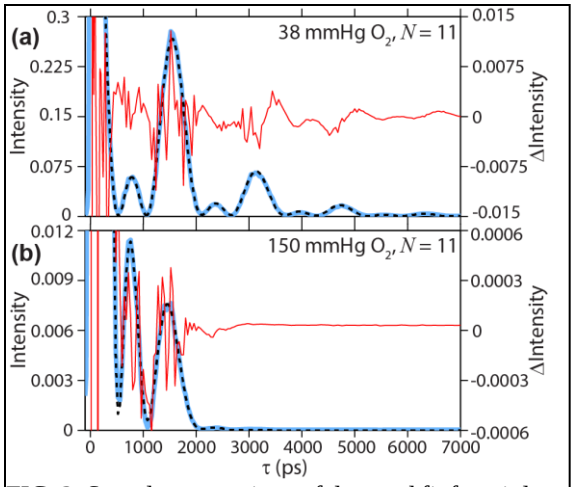

FIG. 2. Sample comparison of data and fit for triplet transition out of N = 11 for (a) 38 mmHg and (b) 150 mmHg O_2. (a,b) In each panel, the experimental time trace (blue line) and fit (black dashed line) are plotted against the Intensity axis, and the (experimental – fit) residual (red line) is plotted against the ΔIntensity axis..

beating arises from the electronic and nuclear characteristics of O_2. Given the unpaired electrons in the ground electronic state, the total molecular angular momentum, *J*, is given by $J = N + S,\ N + S - 1,\ \ldots |N - S|$, where S is the total spin angular momentum quantum number. Each state defined by the rotational quantum number, *N*, is a triplet with $J = N,\ N \pm 1$. The allowed transitions of $\Delta J = 0,\ 1,\ 2$ correspond to the following set of transitions out of each *N*: three close-lying ${}^{S}S$ ($\Delta J = 2$) lines, one ${}^{S}Q$ ($\Delta J = 0$) transition calculated to be quite weak,[A] and two ${}^{S}R$ ($\Delta J = 1$) transitions ~2 cm^{-1} from the ${}^{S}S$ lines first measured by Jammu and coworkers[B] with intensities decreasing rapidly with increasing *N*.[C] Thus, each transition observed in the frequency resolved spectrum of Figure 1 is composed of a triplet arising from the three strong and allowed $\Delta N = 2,\ \Delta J = 2$ transitions. The frequency splitting of the triplet is only ~0.02 cm^{-1} and depends on the rotational quantum number. We carried out a series of time-resolved O_2 pure-rotational CARS experiments at pressures from 30 Torr to 760 Torr monitoring the rotational state dependent coherence beating frequencies through via probe delay scans. This allowed us to measure the triplet splitting frequencies, and these have now been incorporated into a time-domain CARS fitting routine for molecular O_2. A sample fitting of the time-domain CARS intensity for O_2 N'=11 is shown in Figure 2. By incorporating the triplet ground state splitting of rotational transitions into the time-domain model, we are now able to accurately interpret the time-resolved CARS experiments.

Future Work

Single-laser-shot imaging of coherence lifetime: structured illumination 2D-CARS measurements. We have begun a collaboration with Lund University's Professor Joakim Bood, Per-Erik Bengtsson, and Elias Kristensson to develop a single laser shot coherence lifetime imaging experiment. Coherence lifetime imaging, similar to fluorescence lifetime imaging, provides a unique glimpse of spatially resolved energy transfer and dephasing in a sample. In combustion applications, this could yield

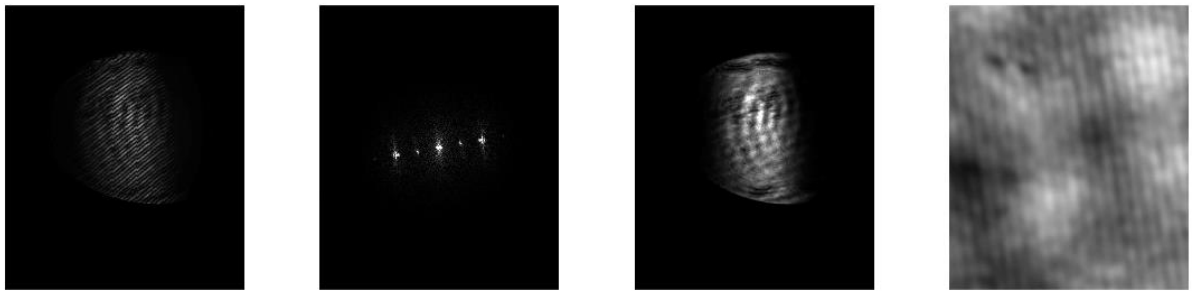

FIG. 3. Preliminary 2D-CARS data utilizing structured illumination. From Left to Right. The first panel shows a 2D-CARS signal from the J=1 to 3 transition of molecular H_2. The second panel is an image of the 2D spatial Fourier transform of the image. The clear frequencies appear because of the fringe interference of the +/- 1 orders isolated from the grating. The third image is the 2D-CARS image extracted from a single frequency in the 2D spatial Fourier transform corresponding to the desired probe beam. Finally, the last image on the right shows a close-up of the fringe pattern. The direction of the interference lines may be tuned for each of the four probe beams.

information on molecular species concentrations, mixing, and temperature without the need for a hyperspectral image deconvolution. We were able to achieve this deconvolution for N_2 systems at ambient pressure, but high-pressure situations with line-broadening or multi-species interactions would rule out such a setup. Further, applications for such a metric would exceed far beyond combustion. In the life sciences, cell imaging and biomedical research microscopy methods seek new contrast mechanisms to decipher one local chemical environment from another, coherence lifetime imaging with single-shot implementation would be a major break-through for this community. To accomplish this, we have designed an experimental approach that combines 2D-CARS (developed in our lab at Sandia) with the SLIPI, structured illumination, methods (developed at Lund University). In this approach, the two-beam CARS pump/Stokes pulse intersects the sample. The probe beam, however, is separated via beam-splitters into four separate beams. Each of these beams propagates through a time-of-flight optical delay stage and is then passed through a transmission grating. These gratings are designed to optimize the +/- 1 orders. The position of the grating is relay imaged to the experiment. In this way, each of the four probe beams gets imprinted with a fringe pattern at a controllable angle. The CARS beams are recombined into a single beam, and scattered from the sample. The resulting image contains four separate probe delays, with independent spatial frequencies, which can be extracted through spatial Fourier transform. An initial set of data is shown in Figure 3.

Molecular alignment and coherence: strong-field effects. We have recently observed unique changes to the H_2 time-domain coherent Raman signal as a function of the strength of a strong-field alignment pulse in the nanosecond regime. We plan to use a nanosecond laser with programmable pulse shape as the strong field. This laser is currently available in Rob Barlow's lab at Sandia. The benefit of this experiment is that a very well-defined field strength may be used to study the effects that a strong adiabatic laser field has on the nonadiabatic alignment of molecules. Instead of having a Gaussian time-profile, a flat-top time profile may be used. This allows for an electric field strength that is constant on the time scales of the femtosecond nonadiabatic molecular alignment probe, even with the standard timing jitter expected from nanosecond pulsed lasers. Fundamental questions we plan to answer involve: How do adiabatic and nonadiabatic molecular alignment processes interact with one another? How are ultrafast coherent scattering signals affected by some level of pre-alignment in the molecules?

High-pressure diagnostics development. We have recently completed the construction of an optical high pressure cell capable of up to 100 atm pressure and up to 1000 K temperature, and incorporated an active pulse-shaper into our femtosecond laser setup to correct for higher order chirp in the cell windows. Thus, we plan to continue development of high pressure nonlinear mixing strategies, and tailored probe arrangements for multiplex coherent imaging of temperature and species concentrations at high pressure. Nonlinear optical strategies benefit from the squared number density dependence at high pressure, but fast dephasing requires the use of tailored probe pulses. We plan to develop molecular phase mask pulse shaping for excitation of only the species of interest, while eliminating the broad signal from neighboring transitions of other species which are collisionally broadened.

Multiplexing 2D-CARS with particle imaging velocimetry (PIV). With the recent development of the first 2D-CARS measurements in our lab, our plan is to begin multiplexing the diagnostic with other techniques to gain access to joint statistics not previously attainable, such as the instantaneous thermal field and flow field obtained by combining 2D-CARS with PIV, respectively. Initial experiments will be conducted to determine if the particle scattering will interfere with the interpretation of the 2D-CARS signals, since the temperature is extracted by retrieving intensity spectra. However, since the signal is Raman shifted from the scattering frequency, it is expected that the PIV measurement will not interfere with the 2D-CARS assessment. Once this is determined, in collaboration with Dr. Jonathan Frank (CRF, Sandia), we will perform joint PIV and 2D-CARS in turbulent DME flames of current interest in Jonathan's lab. Planar CARS measurements before and after the addition of the PIV seeding particles at increasing densities will ensure the negligible effects of the seeding density on the combustion itself, or, at least, set

an upper limit on the seeding density before perturbations to the evaluated 2D-CARS temperatures are observed.

Direct measurement of N_2-Fuel and N_2-H_2O broadening coefficients. With the successful development of the time-domain technique for acquiring high-accuracy S-branch broadening coefficients, demonstrated thus far for the N_2-N_2 and N_2-H_2 collisional systems, we propose to continue the collaboration with Per-Erik Bengtsson of Lund University, Sweden, to tackle the relative paucity of broadening coefficient data in the literature for air-fuel collisional systems. Initial studies will focus on the collisional broadening of N_2 and O_2 when perturbed by DME, ethane, ethylene, propane, and propylene. Accurate broadening models must be developed for these collisional environments, especially at elevated pressures. We will alter our current time-domain CARS code to implement these new linewidth libraries and test the validity of the model in our newly constructed high-pressure, high-temperature cell.

References

A. Altmann, K.; Strey, G.; Hochenbleicher, J. G.; Brandmuller, J., Simulation of Intensity Contour in Raman Spectrum of Oxygen Regarding Spin Splitting. *Z. Naturforsch., Part A* **1972,** *A 27* (1), 56-64.

B. Jammu, K. S.; Stjohn, G. E.; Welsh, H. L., Pressure Broadening of Rotational Raman Lines of Some Simple Gases. *Can. J. Phys.* **1966,** *44* (4), 797-814.

C. Brown, K. W.; Rich, N. H.; Nibler, J. W., High-Resolution Rotational CARS Spectrum of Oxygen. *J. Mol. Spectrosc.* **1992,** *151* (2), 482-492.

Journal publications supported by this BES project (2016-2018)

1. M. Campbell, A. Bohlin, P. Schrader, R. Bambha, C. J. Kliewer, K. Johansson, and H. Michelsen, "Design and characterization of a linear Hencken-type burner," Rev. Sci. Instrum. **87**, 115114 (2016)

2. A. Bohlin, C. Jainski, B.D. Patterson, A. Dreizler, and C.J. Kliewer, "Multiparameter spatio-thermochemical probing of flame-wall interactions advanced with coherent Raman imaging," Proc. Combust. Inst. **36**, 4557-4564 (2017)

3. T.L. Courtney, A. Bohlin, B.D. Patterson, C.J. Kliewer, "Pure-Rotational H_2 Thermometry by Ultrabroadband Coherent Anti-Stokes Raman Spectroscopy," J. Chem. Phys. **146**, 224202 (2017)

4. A. Bohlin, B.D. Patterson, C.J. Kliewer, "Dispersive Fourier Transformation for Megahertz Detection of Coherent Raman Spectra," Optics Communications **402**, 115-118 (2017)

5. M. Campbell, P.E. Schrader, A.L. Catalano, K.O. Johansson, G.A. Bohlin, N.K. Richards-Henderson, C.J. Kliewer, H.A. Michelsen, "A Small Porous-Plug Burner for Studies of Combustion Chemistry and Soot Formation," Rev. Sci. Instrum. **88**, 125106 (2017)

6. T.L. Courtney, B.D. Patterson, C.J. Kliewer, "Rotational Coherence Beating in Molecular Oxygen: Coupling of Electronic and Nuclear Spin Angular Momentum," J. Chem. Phys. (2018) *submitted*

THEORETICAL CHEMICAL KINETICS

Stephen J. Klippenstein
Chemical Sciences and Engineering Division
Argonne National Laboratory
Argonne, IL, 60439
sjk@anl.gov

Program Scope

The focus of this program is the development and application of theoretical methods for exploring gas phase chemical kinetics. The research involves a combination of *ab initio* electronic structure calculations, variational transition state theory (TST), classical trajectory simulations, and master equation (ME) calculations. Detailed applications, including careful comparisons with experiment as feasible, are used to (i) develop a deeper understanding of the applicability of various foundational principles of gas phase chemical kinetics, (ii) motivate improvements in theoretical chemical kinetics methodologies, and (iii) enhance our understanding of various aspects of combustion, atmospheric, and interstellar chemistry. The specific reactions studied are generally motivated by global modeling efforts and state-of-the-art experimental observations.

Recent Progress

Toluene Oxidation: In collaboration with a team from Milan (Pelucchi, Cavallotti, Faravelli) we studied a number of reactions of relevance to the oxidation of toluene and explored their ramifications for global observables through an update to the POLIMI kinetic model. In particular, ab initio transition state theory analyses were performed for the H-abstractions from toluene by OH, HO_2, O, and O_2. Furthermore, our earlier study of the high-pressure limit for the benzyl + O_2 recombination was extended to include a detailed master equation based analysis of the pressure dependence of the rate and branching to various channels. Overall, the updated model is in reasonably good agreement with the experimental observations, aside from the O_2 + toluene rate constant, where almost an order of magnitude discrepancy remains. This discrepancy suggests that either the observations are plagued by the effect of impurities or some alternative channel besides abstraction dominates the O_2 + toluene kinetics.

Nitrogen Chemistry in Combustion: We contributed to a comprehensive review, led by Glarborg (DTU), summarizing the chemical processes that govern the formation and destruction of NO_x in combustion processes. The mechanisms for thermal and prompt-NO, for fuel-NO, and NO formation via NNH or N_2O were discussed, along with the chemistry of NO removal processes such as reburning and selective non-catalytic reduction of NO. The success of the overall model is a triumph of many years of elementary kinetics work carefully examining a wide variety of speculated reaction processes. As part of this review, we performed a number of new theoretical analyses.

Kinetics and Dynamics of Criegee Intermediates: We continued our work on Criegee intermediates (CI) with three further studies. In a collaboration led by Lester (UPenn) we studied the effect of selective deuteration on the role of tunneling in the decomposition of CH_3CHOO and CD_3CHOO to hydroxyl radicals. Remarkably, our prior model for the decay of the undeuterated CI accurately reproduced the new experimental observations for the deuterated species (after appropriate mass substitutions in the rovibrational analyses). In separate work,

again led by Lester, the utility of the combination of IR activated time-resolved pump-probe laser experiments and ab initio RRKM calculations was illustrated through a review of our recent results for the decomposition of $(CH_3)_2COO$. Finally, in collaboration with Hase (TexasTech) we provided a thorough anlaysis of the branching between prompt and thermal decay of the CH_2OO arising from ethlyene ozonolysis. The analysis implemented direct dynamical probes of the CH_2OO nascent energy distribution, high level electronic structure analyses, and a pair of master equation treatments. The analysis clearly indicates the importance of deviations in the nascent energy distributions from the statistical assumptions that have been employed in all previous studies.

High Accuracy Ab Initio Kinetics for Combustion: In collaboration with Harding and Ruscic, we developed high accuracy ab initio schemes for predicting the heats of formation of small molecules (< 35 electrons) and implemented them for a set of 348 combustion relevant species. These schemes were validated both theoretically, through analysis of the convergence of the underlying components, and through comparison with an extensive Active Thermochemical Tables (ATcT) database (for a set of 150 species). The estimated 2σ uncertainties of the three methods, ANL0, ANL0-F12, and ANL1, are in the range of ± 1.0-1.5 kJ/mol for single-reference and moderately multireference species, for which the contribution from higher order excitations are 5 kJ/mol or less.

Automated Combustion Thermochemistry and Kinetics: Large-scale automated implementation of high-level computational theoretical chemical kinetics offers the prospect for dramatically improving the fidelity of combustion chemical modeling. As a first step toward this goal, we have developed a procedure for automatically generating thermochemical data for all the species of relevance to the combustion of an arbitrary fuel. We have completed our first illustration of this concept with the generation of a full set of thermochemical data for an RMG generated mechanism for butane oxidation. The programmatic/developmental effort for this work is funded through the exascale computation project (DOE-ASCR), while specific applications are motivated by our DOE-BES efforts.

Future Directions

Our attempts to automate high-level theoretical thermochemical kinetics will facilitate large scale couplings with kinetic modeling efforts. As a first step, we are now exploring the feasibility of improving all aspects of classic mechanisms for species such as n-heptane. Such efforts are expected to more clearly point out shortcomings in such mechanisms, such as the neglect of direct non-thermal processes. These studies will thus serve as a motivation for more detailed studies of the chemical dynamics of combustion processes.

The process of reviewing current NO_x understanding pointed out the need for improved understanding of certain reactions. For example, the CH_3 + NCN reaction may contribute to prompt NO in rich flames. We intend to pursue theoretical studies of a number of such reactions.

We plan to extend our work on the kinetics of Creigee intermediates to larger systems, which are of greater interest to atmospheric chemists. In collaboration with Lester, we are in the process of studying the kinetics of methyl-vinyl ketone oxide kinetics. We also intend to apply our dynamics based prompt versus thermal CI analysis to larger systems and to incorporate a two-dimensional master equation based analysis. Finally, we are interested in exploring the role of roaming in OO fission from the vinylhydroperoxides.

We intend to continue collaborating with Jasper on the development of effective procedures for coupling trajectory simulations of energy transfer with the two-dimensional ME

in order to accurately predict the pressure dependence of chemical reaction kinetics.

We remain interested in developing formalisms for treating the kinetic effect of the instability of radicals that commonly arises in the 1000 - 2000 K temperature range.

DOE Supported Publications, 2016-Present

1. **Comment on "A Novel and Facile Decay Path of Criegee Intermediates by Intramolecular Insertion Reactions via Roaming Mechanisms",** L. B. Harding, S. J. Klippenstein, *J. Chem. Phys*. **143**, 167101 (2016).
2. **Dimethylamine Addition to Formaldehyde Catalyzed by a Single Water Molecule: A Facile Route for Carbinolamine Formation and Potential Promoter of Aerosol Growth,** M. K. Louie, J. S. Francisco, M. Verdicchio, S. J. Klippenstein, A. Sinha, *J. Phys. Chem. A* **120**, 1358-1368 (2016).
3. **Low Temperature Kinetics of the First Steps of Water Cluster Formation,** J. Bourgalais, V. Roussel, M. Capron, A. Benidar, S. J. Klippenstein, L. Biennier, S. D. Le Picard, *Phys. Rev. Lett.* **116***,* 113401 (2016).
4. **Communication: Real Time Observation of Unimolecular Decay of Criegee Intermediates to OH Radical Products,** Y. Fang, F. Liu, V. P. Barber, S. J. Klippenstein, A. B. McCoy, M. I. Lester**,** *J. Chem. Phys.* **144,** 061102 (2016).
5. **Pressure Dependent Low Temperature Kinetics for CN + CH_3CN: Competition Between Chemical Reaction and van der Waals Complex Formation,** C. Sleiman, S. Gonzalez Rubio, S. J. Klippenstein, D. Talbi, G. El Dib, A. Canosa, *Phys. Chem. Chem. Phys.* **18**, 15118-15132 (2016).
6. **Direct Observation of Unimolecular Decay of CH_3CH_2CHOO Criegee Intermediates to OH Radical Products,** Y. Fang, F. Liu, S. J. Klippenstein, M. I. Lester**,** *J. Chem. Phys*., **145**, 044312:1-9 (2016).
7. **Pressure Dependent Rate Constants for PAH Growth: Formation of Indene and its Conversion to Naphthalene,** A. M. Mebel, Y. Georgievskii, A. W. Jasper, S. J. Klippenstein**,** *Faraday Disc*. **195**, 637-670 (2016).
8. **Deep Tunneling in the Unimolecular Decay of CH_3CHOO Criegee Intermediates to OH Radical Products,** Y. Fang, F. Liu, V. P. Barber, S. J. Klippenstein, A. B. McCoy, M. I. Lester**,** *J. Chem. Phys*., **145***,* 234308 (2016).
9. **From Theoretical Reaction Dynamics to Chemical Modeling of Combustion,** S. J. Klippenstein*, Proc. Combust. Inst*., **36***,* 77-111 (2017).
10. **Recombination of Aromatic Radicals with Molecular Oxygen,** F. Zhang, A. Nicolle, L. Xing, S. J. Klippenstein**,** *Proc. Combust. Inst*. **36**, 169-177 (2017).
11. **Theoretical Kinetics of O + C_2H_4,** X. Li, A. W. Jasper, J. Zádor, J. A. Miller, S. J. Klippenstein**.** *Proc. Combust. Inst*. **36**, 219-227 (2017).
12. **Temperature- and Pressure-Dependent Rate Coefficients for the HACA Pathways from Benzene to Naphthalene,** A. M. Mebel, Y.Georgievskii, A. W. Jasper, S. J. Klippenstein**,** *Proc. Combust. Inst*. **36**, 919-926 (2017).
13. **First-Principles Chemical Kinetic Modeling of Methyl Trans-3-Hexenoate Epoxidation by HO_2,** S. Cagnina, A. Nicolle, T. de Bruin, Y. Georgievskii, S. J. Klippenstein, *J. Phys. Chem. A*, **121**, 1909-1915 (2017).
14. **Tunneling Effects in the Unimolecular Decay of $(CH_3)_2COO$ Criegee Intermediates to OH Radical Products,** Y. Fang, V. P. Barber, S. J. Klippenstein, A. B. McCoy, Marsha I. Lester, J. Chem. Phys., **146***,* 134307 (2017).

15. **Accurate Anharmonic Zero Point Energies for some Combustion Related Species from Diffusion Monte Carlo,** L. B. Harding, Y. Georgievskii, S. J. Klippenstein**,** J. Phys. Chem. A, **121***,* 4334-4340 (2017).
16. **Ephemeral Collision Complexes Mediate Chemically Termolecular Transformations that Affect System Chemistry,** M. P. Burke, S. J. Klippenstein**,** Nature Chem., **9***,* 1078-1082 (2017).
17. **Ab Initio Computations and Active Thermochemical Tables Hand in Hand: Heats of Formation of Core Combustion Species,** S. J. Klippenstein, L. B. Harding, B. Ruscic**,** J. Phys. Chem. A, **121,** 6580-6602 (2017).
18. **Theoretical Investigation of Intersystem Crossing in the Cyanonitrene Molecule, ^{1}NCN $\rightarrow$ ^{3}NCN,** M. Pfeifle, Y. Georgievskii, A. W. Jasper, S. J. Klippenstein**,** J. Chem. Phys., **147**, 084310 (2017).
19. **Theoretical Kinetics Analysis for H-atom Addition to 1,3-Butadiene and Related Reactions on the $\dot{C}_4H_7$ Potential Energy Surface,** Y. Li , S. J. Klippenstein, C.-W. Zhou, H. J. Curran**,** J. Phys. Chem. A, **121,** 7433-7445 (2017).
20. **Selective Deuteration Illuminates the Importance of Tunneling in the Unimolecular Decay of Criegee Intermediates to Hydroxyl Radical Products,** A. M. Green, V. P. Barber, Y. Fang, S. J. Klippenstein, M. I. Lester, Proc. Nat. Acad. Sci., **114**, 12372-12377 (2017).
21. **Dynamic Time-Resolved Chirped-Pulse Rotational Spectroscopy of Vinyl Cyanide Photoproducts in a Room Temperature Flow Reactor,** D. P. Zaleski, L. B. Harding, S. J. Klippenstein, B. Ruscic, K. Prozument**,** J. Phys. Chem. Lett., **8**, 6180-6188 (2017).
22. **Anharmonic Rovibrational Partition Functions for Fluxional Species at High Temperatures via Monte Carlo Phase Space Integrals,** A. W. Jasper, Z. B. Gruey, L. B. Harding, S. J. Klippenstein, A. F. Wagner, J. Phys. Chem. A., **122,** 1727-1740 (2018).
23. **Modeling Nitrogen Chemistry in Combustion,** P. Glarborg, B. Ruscic, J. A. Miller, S. J. Klippenstein, Prog. Energy Combust. Sci., **67***,* 31-68 (2018).
24. **H-Abstraction Reactions by OH, HO_2, O, O_2, and Benzyl Radical Addition to O_2 and Their Implications for Kinetic Modelling of Toluene Oxidation,** M. Pelucchi, C. Cavallotti, T. Faravelli, S. J. Klippenstein**,** Phys. Chem. Chem. Phys., *in press* (2018).
25. **Unimolecular Decay of Criegee Intermediates to OH Radical Products: Prompt and Thermal Decay Processes,** M. I. Lester, S. J. Klippenstein, Acc. Chem. Res., *in press* (2018).
26. **Small Ester Combustion Chemistry: Computational Kinetics and Experimental Study of Methyl Acetate and Ethyl Acetate,** A. Ahmed, W. J. Pitz, C. Cavallotti, M. Mehl, N. Lokachari, E. J. K. Nilsson, J.-Y. Wang, A. A. Konnov, S. W. Wagnon, B. Chen, Z. Wang, H. J. Curran, S. J. Klippenstein, W. J. Roberts, S. M. Sarathy, Proc. Combust. Inst., *accepted for presentation* (2018).
27. **Automated Computational Thermochemistry for Butane Oxidation: A Prelude to Predictive Automated Combustion Kinetics,** M. Keceli, S. Elliott, Y.-P. Li, M. S. Johnson, C. Cavallotti, Y. Georgievskii, W. H. Green, M. Pelucchi, J. M. Wozniak, A. W. Jasper, S. J. Klippenstein**,** Proc. Combust. Inst., *accepted for presentation* (2018).
28. **Nascent Energy Distribution of the Criegee Intermediate CH_2OO from Direct Dynamics Calculations of Primary Ozonide Dissociation,** M. Pfeifle, Y.-T. Ma, A. W. Jasper, L. B. Harding, W. L. Hase, S. J. Klippenstein, J. Chem. Phys., *in press* (2018).

ARGONNE-SANDIA CONSORTIUM ON HIGH-PRESSURE COMBUSTION CHEMISTRY

Stephen J. Klippenstein (PI), Raghu Sivaramakrishnan, Robert S. Tranter
Chemical Sciences and Engineering Division, Argonne National Laboratory, Argonne, IL, 60439
sjk@anl.gov
Leonid Sheps, Craig A. Taatjes (PI)
Combustion Research Facility, Mail Stop 9055, Sandia National Laboratories
Livermore, CA 94551-0969
cataatj@sandia.gov

Program Scope: The goal of this project is to explore the fundamental effects of high pressure on the chemical kinetics of combustion and to use that knowledge in the development of accurate models for combustion chemistry at the high pressures of current and future combustion devices. We design and implement novel experiments, theory, and modeling to probe high-pressure combustion kinetics from elementary reactions, to submechanisms, to flames. The work focuses on integrating modeling, experiment, and theory (MET) through feedback loops at all levels of chemical complexity. We are currently developing and testing the methodology for small alkanes, alcohols, and ethers as key prototype fuels. The consortium expands and enhances collaborations between Argonne's Chemical Dynamics in the Gas Phase Group and the Combustion Chemistry Group in Sandia's Combustion Research Facility.

Recent Progress:

Experimental method development: We continue to invest in the development of sensitive time-resolved experimental probes of reaction kinetics that enable direct high-pressure studies of chemical systems of interest to High Pressure Combustion Chemistry (HPCC). Our experimental facilities include a miniature high-repetition rate shock tube (HRRST) and two high-pressure flow reactors. These apparatuses cover a wide range of conditions (300 – 2500 K, 0.5 – 100 bar) and exploit complementary diagnostic methods: laser-induced fluorescence (LIF), electron impact mass spectrometry, and photoionization mass spectrometry (PIMS).

With the high-pressure photoionization mass spectrometry (HP-PIMS) apparatus completed in 2017, we turned to the optimization of experimental procedures, intended to position HP-PIMS as a robust "workhorse" method. We demonstrated Cl, Br, and F-atom initiated reactions using the photolysis of Cl_2, $(COCl)_2$, $CHBr_3$, and XeF_2. These radical precursors enable flexible design of experiments to accommodate different pressure and temperature regimes and a broad array of chemical systems.

Neopentane oxidation: We completed an experimental study of neopentane (2,2-dimethyl propane) oxidation at pressures ranging from 9 Torr to 2 bar as part of our ongoing studies on $C_3 - C_6$ alkanes, aimed at linking molecular structure with autoignition properties. Neopentane is a symmetric molecule, which constrains the available isomeric distribution of reactive intermediates and simplifies the interpretation of experimental results. In addition, ROO → HO_2 + alkene (a major channel in straight-chain and cyclic hydrocarbons) does not occur in neopentane because it has no secondary H atoms. As a result, we find that much of the reaction flux at low temperatures (< 800 K) proceeds via QOOH decomposition and QOOH + O_2 reactions, depending on the total pressure and the concentration of O_2. We identified the KHP species (3-hydroperoxy-2,2-dimethylpropanal) produced in neopentane oxidation and quantified several of its decomposition pathways. A high yield of Korcek decomposition to carbonyl + carboxylic acid (mainly methylpropanal + HCOOH) was measured. The radical product channels of KHP were also observed, ultimately forming acetone + CO + OH or methacrolein + HO_2 in a strongly oxidative atmosphere.

Tetrahydropyran and cyclohexane oxidation: We also extended our work on the reactivity of alkanes and ethers to 6-membered cyclic compounds cyclohexane and tetrahydropyran (THP). Together with Taatjes, Zádor, and Eskola (Helsinki) we performed an experimental and theoretical study of the HO_2 elimination pathways from ROO at P = 10 – 1500 Torr and T = 500 – 700 K. Both species undergo facile HO_2 elimination, but in THP a β-scission of the initial radical C–O bond starts to compete with O_2 addition at 700 K. This ring-opening pathway is a consequence of the ether functional group and ring-opening is ubiquitous in cyclic ether autoignition chemistry.

Butyl Oxidation: The reaction of O_2 with butyl radicals is a key early step in the oxidation of butane, which is a prototypical alkane fuel with combustion properties that mimic those of many larger alkanes. In collaboration with Eskola we performed a joint theory-experiment kinetic study of the 1- and 2-butyl + O_2 reactions. The laser photolysis PIMS experiments cover temperatures ranging from 200 to 500 K and pressures ranging from 0.3 to 6 Torr. The theoretical analysis employs a high-level ab initio variable reaction coordinate (VRC)-TST based master equation approach. The low temperature experimental observations validate the VRC-TST predictions for the capture rate, while the higher temperature measurements validate the underlying treatment of the pressure dependence, which allows for meaningful extrapolation to high pressure.

Dissociation of ethanol: Ethanol is a major constituent of many automotive gasolines and the high temperature and pressure chemistry of ethanol is of direct interest to the ASC-HPCC. Initial studies of the pyrolysis of ethanol were conducted at T2 of the Chemical Dynamics Beamline with the HRRST. The experiments span 31-48 bar and 1600 – 1800 K. Species identification based on mass, appearance energies of ions, and comparisons of the measured PI spectra with literature spectra indicated the presence of ethene, formaldehyde, ethane, ketene, acetylene, diacetylene, triacetylene, vinylacetylene, 2-butyne and acetaldehyde.

The three primary decomposition channels for ethanol are: $C_2H_4 + H_2O$ (1), $CH_3 + CH_2OH$ with further decomposition of CH_2OH to $CH_2O + H$ (2), and $C_2H_5 + OH$ with further decomposition of C_2H_5 to $C_2H_4 + H$ (3). Ethene and formaldehyde are the major products and appear immediately after the onset of reaction indicating they are primary products. Ethene comes predominantly from reaction 1 with a minor contribution from 3. H_2O, the co-product in reaction 1, was not observed because the maximum ionization energy used (12.0eV) was below the ionization threshold of water (12.6 eV). Formaldehyde acts as a marker for reaction 2. The experimental signal, Fig. 1, is in reasonable agreement with the literature appearance energy of 10.88eV, accounting for the photon energy bandwidth at T2. Reaction 2 also produces CH_3 radicals and these can recombine to give ethane, which also has m/z=30. The increase in signal above 11.5eV in Fig. 1 appears consistent with ethane.

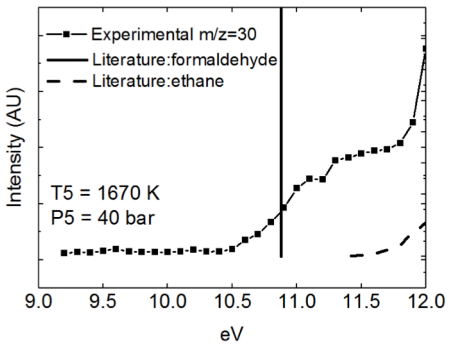

Figure 1: PI spectrum of m/z= 30 from HRRST experiments with 1%EtOH/Ar

The remaining species show good agreement with literature spectra. However, their time histories clearly identify them as secondary or later products. For instance, acetylene appears after ethene and probably results from H and OH attack on ethene. Similarly, acetylene is followed by the appearance of diacetylene and then triacetylene. Several, of the secondary species do not appear until after the reaction zone in the shock tube is quenched by rarefaction waves and represent radical species recombining to stable molecules. While not directly useful for understanding the pyrolysis of ethanol the long-time data provide a unique insight into the changes in composition that occur in the quench phase of shock tube experiment. They will be valuable for interpreting product distributions from single pulse and fast-valve sampling shock tube experiments.

Abstractions in OH + C_3H_8 and prompt dissociation of propyl radicals: Although OH abstraction reactions are one of the most important classes of reactions in combustion there have been only a limited number of direct measurements of channel specific rate constants at combustion relevant temperatures. We directly measured site-specific rate constants for abstraction of the secondary C-H bond in $OH + C_3H_8$ over the 921 - 1146 K temperature range [$k = (3.935 \pm 1.387) \times 10^{-11} \exp(-1681 \pm 362\ K/T)$ cm^3 $molecule^{-1}$ s^{-1}]. Atomic resonance absorption spectroscopy (ARAS) was used to monitor the formation of H-atoms from shock-heated mixtures of tert-butylhydroperoxide and C_3H_8 at high temperatures. Simulations for the experimental H-atom profiles are sensitive only to abstraction of the secondary C-H bond leading to unambiguous measurements of the rate constants.

Simulations of the lower temperature data (T <1000 K) indicate that the H-atom profiles are also influenced to a minor extent by the thermal dissociation of iso-propyl, $i\text{-}C_3H_7 \rightarrow H + C_3H_6$, at short time-scales. Since $i\text{-}C_3H_7$ is formed chemically activated from the abstraction process it may undergo prompt dissociation, which would explain the instantaneous H-atom rise at short time-scales. Consequently, direct dynamics calculations were performed to examine in greater detail the potential role of prompt dissociations of $i\text{-}C_3H_7$ and $n\text{-}C_3H_7$ in interpreting the lower temperature (< 1000 K) data from the present work. These simulations suggest that prompt dissociation of propyl radicals does not influence the present experimental observations. However, the dynamics calculations predict that there is indeed a significant amount of prompt dissociation; larger than the thermal prompt dissociation probabilities ($P_{diss} = 1 - f_{ne}$) at T > 1000 K. Consequently, including prompt propyl dissociation in kinetics models lead to ignition delays retarded by up to 11% in high temperature rich C_3H_8-air mixtures (Figure 2).

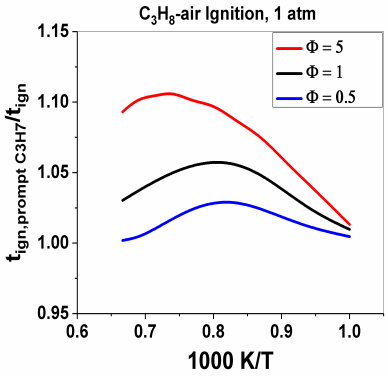

Figure 2: Ratio of predicted ignition delays, with and without propyl prompt dissociations

Core mechanism: We have developed a "core" combustion model for small molecules, i.e., C0 to C3 species. The model is heavily "theory-informed," with rate coefficients, thermochemistry, and transport properties all derived extensively from theoretical chemistry. The current version of this model includes 171 species and 1143 elementary reactions. It has not been tainted by tuning/optimization to global combustion observables (i.e., reactor species profiles, ignition delays, and laminar flame speeds). Instead, discrepancies between model predictions and experiment are used to drive further theory-based analyses to address potential shortcomings in the model. Simulations using our core combustion model are in good to excellent agreement with available autoignition delay and laminar flame speed data for blends of natural gas with and without H_2 enrichment. In collaboration with Chen (Sandia) the present core model was used to investigate natural gas flames at laminar engine-relevant thermochemical conditions where the ignition delay times are short due to very high ambient temperatures and pressures. At these conditions, it is not possible to measure or calculate well-defined values for the laminar flame speed, laminar flame thickness, and laminar flame time scale due to the explosive thermochemical state. Therefore corresponding reference values are numerically estimated (using the present core model) to investigate the enhancement of flame propagation, and the competition with autoignition that arises under nominally autoignitive conditions. It is shown that the nominally autoignitive conditions enhance flame propagation, which may be an ameliorating factor for the onset of engine knock.

Propane high pressure mechanism: In a collaboration led by Glarborg (DTU) we have investigated the oxidation properties of propane in a laminar flow reactor at a pressure of 100 bar and temperatures of 500-900 K. The rate constant for the important abstraction reaction $C_3H_8 + HO_2$ was calculated with ab initio transition state theory. A chemical kinetic model for high-pressure propane oxidation was established, with particular emphasis on the peroxide chemistry. Modeling predictions were in satisfactory agreement with the present experimental data as well as shock tube data (6-61 bar) and flame speeds (1-5 bar) from the literature.

NO_x formation at high pressures: An improved understanding of NO_x formation at high pressures would be of considerable utility to efforts to develop advanced combustion devices. In collaboration with Glarborg (DTU) and Jasper we have predicted the pressure dependence of some key reactions in the prompt NO mechanism ($CH + N_2$, H + NCN, and NCN + OH) and explored the role of pressure and prompt NO for premixed laminar flames at pressures ranging from 1 to 15 atm. Additional simulations at higher pressures, where experiments are not available, further explore the mechanistic changes at the pressures of relevance to applied combustion devices (e.g., 100 atm).

Future Directions:

Autoignition of hydrocarbon and oxygenated compounds: We will complete our ongoing studies of dimethyl ether (DME) and diethyl ether oxidation at pressures up to ~40 bar. This work will connect to related team efforts aimed at accurate modeling of DME combustion under the theory and modeling subtasks. We will also complete our investigation of cyclopentane autoignition in collaboration with Zádor. High- and low-pressure PIMS probing of cyclopentyl radical oxidation will be combined with calculated PES and chemical kinetics calculations, and results will be compared to our recent study of tetrahydrofuran, an analogous 5-membered cyclic ether.

Non-thermal kinetics: Prompt dissociation of oxygenated radicals is a general feature of many combustion systems and a topic of interest for HPCC. We will investigate the decomposition of 1- and 2-hydroxyethyl radicals, derived by H-abstraction from ethanol, which dissociate to vinyl alcohol or acetaldehyde + H and to ethene + OH, respectively. Similarly, we will study H-abstraction from methyl formate, where the possible radical products CH_3OCO and CH_2OCHO are predicted to decompose to $CH_3 + CO_2$ and $CH_2O + HCO$, respectively. The planning of these experiments benefits from preliminary simulations performed using our core mechanism. Tunable VUV PIMS probing will quantify the yields and measure the formation timescales for all stable products of these reactions, and these measurements will then benchmark kinetics calculations, which are already underway. Detailed comparisons will be made with theory-based models to provide definitive descriptions of the prompt dissociation process.

In related work we plan to continue our dynamical studies of small radical prompt dissociations. Ultimately, these dynamical studies will be used to guide the development of a statistical model to predict prompt dissociations of small radicals emanating from the bimolecular reactions of stable species with common hydrocarbon abstractors (H, O, and OH). Preliminary studies have also been initiated to probe the relevance of bimolecular reactions of HO_2* (hot HO_2 from $H + O_2$) with stable species (H_2, CH_4, and CH_3OH) and non-thermal reactions of hot stable species (CH_4*, H_2O*, C_2H_6*, CH_3OH*) with common hydrocarbon abstractors.

Thermal decomposition of Criegee intermediates: Criegee intermediates (CI) are known as key oxidants in the troposphere. The smallest CI, CH_2OO, was also predicted as an intermediate in DME combustion, although no experimental corroboration has yet been found. To assess the possible role of CI in ether combustion, we will probe the thermal decomposition of CH_2OO by transient UV spectroscopy (to determine total rate coefficients) and PIMS

(to measure product distributions). Although highly stable at room T, CH_2OO may dissociate quickly at elevated temperatures and pressures, and its products may be important to the modeling of DME combustion.

Core Mechanism: We will continue to compile our observations and predictions into a well-validated highly theory-informed nonempirical mechanism for C0-C3 hydrocarbons. We plan to publish a lengthy publication detailing this mechanism this summer. Also, in collaborative work with Curran (Galway), Turányi (ELTE), Pitsch (Aachen), and Faravelli (Milan) we are exploring the syngas mechanism in detail.

HRRST: We plan to continue pyrolytic studies of the core HPCC species at elevated temperatures and pressures. We have also started investigations of the recombination and decomposition of hydrocarbon radicals generated from nitrites in the autoigintion region at high pressures and will extend this to oxidation of the radicals. We are also developing methods to extract kinetic data for HRRST/PIMS experiments and a lab based PIMS source to complement the ALS experiments.

DOE-BES Supported Publications, 2016-Present

1. **Comment on "When Rate Constants are Not Enough" by John R. Barker, Michael Frenklach, and David R. Golden,** J. A. Miller, S. J. Klippenstein, S. H. Robertson, M. J. Pilling, R. Shannon, J. Zádor, A. W. Jasper, C. F. Goldsmith, M. P. Burke**,** *J. Phys. Chem. A* **120**, 306-312 (2016).
2. **Weakly Bound Free Radicals In Combustion: "Prompt" Dissociation of Formyl Radicals and Its Effect on Laminar Flame Speeds,** N. J. Labbe, R. Sivaramakrishnan, C. F. Goldsmith, Y. Georgievskii, J. A. Miller, S. J. Klippenstein**,** *J. Phys. Chem. Lett.* **7***,* 85-89 (2016).
3. **High Pressure Oxidation of Methane,** H. Hashemi, J. M. Christensen, S. Gersen, H. Levinsky, S. J. Klippenstein, P. Glarborg, *Combust. Flame*, **172***,* 349-364 (2016).
4. **Pressure-Dependent Competition among Reaction Pathways From First- and Second- O_2 Additions In The Low-Temperature Oxidation Of Tetrahydrofuran,** I. O. Antonov, J. Zádor, B. Rotavera, E. Papajak, D. L. Osborn, C. A. Taatjes, L. Sheps, *J. Phys. Chem. A*, **120**, 6582-6595 (2016).
5. **Resonance Stabilization Effects on Ketone Autoxidation: Isomer-Specific Cyclic Ether and Ketohydroperoxide Formation in the Low-Temperature (400–625 K) Oxidation of Diethyl Ketone,** A. M. Scheer, A. J. Eskola, D. L. Osborn, L. Sheps, C. A. Taatjes, *J. Phys. Chem. A*, **120**, 8625-8636 (2016).
6. **From Theoretical Reaction Dynamics to Chemical Modeling of Combustion,** S. J. Klippenstein, *Proc. Comb. Inst.* **36**, 219-227 (2017).
7. **Ramifications of Including Non-equilibrium Effects for HCO in Flame Chemistry,** N. J. Labbe, R. Sivaramakrishnan, C. F. Goldsmith, Y. Georgievskii, J. A. Miller, S. J. Klippenstein**,** *Proc. Comb. Inst*. **36**, 525-532 (2017).
8. **Influence of Oxygenation in Cyclic Hydrocarbons on Chain-Termination Reactions from R + O_2: Tetrahydropyran and Cyclohexane.** B. Rotavera, J. D. Savee, I. O. Antonov, R. L. Caravan, L. Sheps, D. L. Osborn, J. Zádor, and C. A. Taatjes. *Proc. Combust. Inst.*, **36**, 597-606 (2017).
9. **Direct Experimental Probing and Theoretical Analysis of the Reaction Between the Simplest Criegee Intermediate CH_2OO and Isoprene**, Z. C. J. Decker, K. Au, L. Vereecken, L. Sheps, *Phys. Chem. Chem. Phys.*, **19**, 8541-8551 (2017)
10. **Time-Resolved Measurements of Product Formation in the Low-Temperature (550 – 675 K) Oxidation of Neopentane: a Probe to Investigate Chain-Branching Mechanism**. A. J. Eskola, I. O. Antonov, L. Sheps, J. D. Savee, D. L. Osborn, and C. A. Taatjes. *Phys. Chem. Chem. Phys.*, **19**, 13731-13745 (2017)
11. **High Pressure Oxidation of Ethane,** H. Hashemi, J. G. Jacobsen, C. T. Rasmussen, J. M. Christensen, P. Glarborg, S. Gersen, M. van Essen, H. B. Levinsky, S. J. Klippenstein, *Combust. Flame*, **182**, 150-166 (2017).
12. **Modeling Nitrogen Chemistry in Combustion,** P. Glarborg, B. Ruscic, J. A. Miller, S. J. Klippenstein, *Prog. Energy Combust. Sci.,* **67**, 31-68 (2018).
13. **Theory and Modeling of Relevance to Prompt-NO Formation at High Pressure,** S. J. Klippenstein, M. Pfeifle, A. W. Jasper, P. Glarborg, *Combust. Flame*, in press (2018).
14. **Kinetics of 1-Butyl and 2-Butyl Radical Reactions with Molecular Oxygen: Experiment and Theory,** A. J. Eskola, T. T. Pekkanen, S. P. Joshi, R. S. Timonen, S. J. Klippenstein**,** *Proc. Combust. Inst*., **37**, accepted (2018).
15. **High-Pressure Oxidation of Propane,** H. Hashemi, J. M. Christensen, L. B. Harding, S. J. Klippenstein, P. Glarborg**,** *Proc. Combust. Inst*., **37**, accepted (2018).
16. **Direct Measurements of Channel Specific Rate Constants in OH + C_3H_8,** R. Sivaramakrishnan, C. F. Goldsmith, S. L. Peukert, J. V. Michael, *Proc. Combust. Inst.,* **37,** accepted, (2018).
17. **Reference Natural Gas Flames at Nominally Autoignitive Engine-Relevant Conditions,** A. Krisman, C. Mounaim-Rouselle, R. Sivaramakrishnan, J. A. Miller, J. H. Chen, *Proc. Combust. Inst.,* **37,** accepted, (2018).

Fundamental Molecular Spectroscopy and Chemical Dynamics

Stephen R. Leone and Daniel M. Neumark
Lawrence Berkeley National Laboratory and Departments of Chemistry and Physics, University of California, Berkeley, California 94720 (510) 643-5467 srl@berkeley.edu, 510-642-3502
dmneumark@berkeley.edu

Scope of the Project: Decades of research into reaction rates, branching fractions, dissociation dynamics, and energetics have vastly improved our fundamental understanding of chemical processes. Measurements of radical spectroscopy and excited state dynamics comprise key future goals of this effort, especially the development of new ways to probe excited state dynamics by Leone and Neumark. The Leone group has pioneered femtosecond time-resolved table-top x-ray spectroscopic probing of chemical reaction at sufficiently high photon energies to access the carbon K-edge. Ultrafast x-ray transient absorption spectroscopy based on this methodology investigates transition states and products. The Neumark program uses a suite of experimental methods aimed at the spectroscopy and photodissociation dynamics of reactive free radicals: slow electron velocity-map imaging of cryogenically cooled anions (cryo-SEVI), a high resolution variant of photoelectron spectroscopy, fast radical beam (FRBM) studies of radical photodissociation, in which a beam of radicals is generated by negative ion photodetachment, and molecular beam photodissociation of radicals (XBeam) carried out on species generated by flash pyrolysis of suitable precursors.

Recent Progress:

Femtosecond Soft X-ray Transient Absorption Experiments

A unique femtosecond soft x-ray transient absorption spectroscopy apparatus with x-ray probe energies up to 310 eV is used to characterize the electronic structure of transient intermediates of chemical reactions. The ultrafast photoinduced ring-opening reaction of 1,3-cyclohexadiene, a fundamental prototype of photochemical pericyclic reactions, is investigated. Following ultraviolet photoexcitation to the 1B excited state via a $\pi \rightarrow \pi^*$ transition at 266 nm, the key step in this reaction is the ultrafast relaxation through a transient 2A excited-state intermediate known as the pericyclic minimum, which leads to isomerization via non-adiabatic decay onto the ground state of the photoproduct. With the capability of femtosecond soft x-ray transient absorption spectroscopy near the carbon K-edge (284 eV), the electronic structure of this transient intermediate state is obtained.

Analogously, during the photoisomerization process of cycloheptatriene (CHT) where a hydrogen atom migrates between two neighboring carbon atoms, upon photoexcitation to the 1A" state with 266 nm, the molecule rapidly passes through two conical intersections, one involving a non-adiabatic transition to the 2A' state and the other leading to wave packet bifurcation, either back to the ground state CHT or to its hydrogen-shifted isomer. Transient features are captured at the conical intersections and computed to possibly involve a planarized geometry of CHT, a key intermediate in isomerization of the boat-like ground state.

The ultrafast excited state non-adiabatic dynamics of acetylacetone (pentane-2,4-dione) is directly probed up to 150 ps after excitation at 266 nm using time-resolved x-ray absorption spectroscopy near the carbon K-edge (284 eV). At this wavelength, the enolic tautomer of the molecule is excited to the S_2 ($^1\pi\pi^*$) electronic state from which it undergoes internal conversion to the lower-lying singlet states and intersystem crossing to the triplet states. In the experiment, rapid internal conversion leads to changes in the electronic structure within 2 ps after excitation, characterized by significant changes in the near-edge x-ray absorption fine-structure spectrum. Aided with density functional theory, the evolution of the core-to-valence resonances at the carbon K-edge directly establishes an ultrafast population of the T_1 state ($^3\pi\pi^*$) in acetylacetone via intersystem crossing from the S_2 state on a 1.5 ± 0.2 ps timescale.

Utilizing the well-known A band photodissociation of the C-I bond, iodine-containing molecules are used to investigate important radicals such as halomethyl ($\cdot CH_2Cl$, $\cdot CH_2Br$), allyl and *tert*-butyl radical, up to the carbon K edge x-ray regime. The broad band feature (150 eV-300 eV) of the soft x-ray probe allows interpretation of the radicals' electronic structures at multiple core-levels. As an example, CH_2ICl is photodissociated at 266 nm to form CH_2Cl and the signature of the CH_2Cl radical is captured at the carbon K edge as well as at the chlorine $L_{2,3}$ edges. By comparing transitions to the frontier orbitals in CH_2ICl and CH_2Cl, a shift of electron density during photodissociation is extracted revealing the stability through the differences with methyl radical in the orbital energy of the singly occupied carbon 2p orbital.

Free radical spectroscopy and dynamics

The spectroscopy and photodissociation dynamics of several peroxy radicals (RO_2) are investigated using slow photoelectron velocity-map imaging of cryogenically-cooled anions (cryo-SEVI) and with fast radical beam (FRBM) dissociation. In cryo-SEVI, mass-selected anions are stored in an rf ion trap at T=5 K and cooled by collisions with a low pressure buffer gas. Ions are then extracted and photodetached, and the resulting slow photoelectrons are selectively analysed with velocity-map imaging, yield photoelectron spectra with energy resolution as high as 1-2 cm^{-1} for complex species. The application of this method to the methoxide (CH_3O^-) and tert-butyl peroxide ($(CH_3)_3COO^-$) anions yields highly resolved vibrational structure of the corresponding radicals along with precise electron affinities.

Photodissociation dynamics of the methyl, ethyl, and t-butyl peroxy radicals are studied on the FRBM instrument. The radicals are generated by photodetachment of the corresponding peroxide anions and then photodissociated. Two and three-body channels are analysed via coincidence detection with a time-and position-sensitive detector. CH_3OO exhibits repulsive O loss resulting in the formation of $O(^1D)$ + CH_3O with high translational energy release. Minor two-body channels leading to OH + CH_2O and CH_3O + $O(^3P)$ formation are also detected. In addition, small amounts of H + $O(^3P)$ + CH_2O are observed and attributed to O loss followed by CH_3O dissociation. C_2H_5OO exhibits more complex dissociation dynamics, in which O loss and OH loss occur in roughly equivalent amounts with $O(^1D)$ formed as the dominant O atom electronic state via dissociation on a repulsive surface. Minor two-body channels leading to the formation of O_2 + C_2H_5 and HO_2 + C_2H_4 are also observed and attributed to a ground state dissociation pathway following internal conversion. Additionally, C_2H_5OO dissociation yields a three-body product channel, CH_3 + $O(^3P)$ + CH_2O, for which the proposed mechanism is repulsive O loss followed by dissociation of C_2H_5O over a barrier. These results differ significantly from *t*-BuOO, for which the major channel is found to be three-body fragmentation to form O, CH_3 and acetone (83%), with minor two-body fragmentation channels leading to the formation of O_2 + *tert*-butyl radical (10%) and HO_2 + isobutene (7%). The two-body channels proceed by internal conversion to the ground electronic state followed by statistical dissociation. For three-body dissociation, the translational energy distribution peaks closer to the maximal allowed translational energy and shows an anisotropic distribution in the plane of the dissociating fragments, implying rapid dissociation on an excited-state surface. The three radicals thus exhibit a complex mix of excited state dynamics vs. ground state dynamics, and two-body vs. three-body dissociation.

On the XBeam experiment, the photodissociation of jet-cooled cyclopentadienyl radicals, *c*-C_5H_5, at 248 nm is studied using photofragment translational spectroscopy. The radicals are generated by flash pyrolysis of anisole. Two dissociation channels are observed, H + C_5H_4 and C_3H_3 + C_2H_2. The C_5H_4 fragment is identified as ethynylallene by its ionization energy. The translational energy distribution determined for each channel suggests that both dissociation mechanisms occur via internal conversion to the ground electronic state followed by intramolecular vibrational redistribution and dissociation. The experimental branching ratio as well as RRKM calculations favor the formation of C_3H_3 + C_2H_2 over the H-atom loss channel. The RRKM calculations also support the observation of ethynylallene as the dominant C_5H_4 product isomer.

Future Plans:
The newly constructed UV-pump, soft x-ray-probe apparatus will be used to spectroscopically investigate fundamental hydrocarbon photochemical processes including radical formation, decomposition of carbonyl compounds, predissociation of aromatic systems and isomerization of heterocyclic rings. Electronic structures of transient species at conical intersections will be in particular interrogated to shed light on the nature of ultrafast dynamics in these photo-induced reactions. Additionally, coherent wave packet dynamics will be explored to detail the impact of vibrational wave packets on x-ray core-level absorption spectroscopy. Future efforts will involve improving the high-harmonic flux and stability to extend the soft x-ray probe to obtain energy-tunable pulses covering the nitrogen K-edge (410 eV) as well as the temporal resolution to achieve attosecond timescales.

Neumark will investigate the elastic, inelastic, and reactive scattering of atoms and reactive free radicals from flat liquid jets of water and other volatile solvents. The incorporation of flat jet technology into the XBeam molecular beam scattering instrument will build on the pioneering liquid scattering experiments carried out by Nathanson and co-workers. The proposed experiments will provide unprecedented insights into how the well-understood binary interactions that govern gas phase collision dynamics are modified when one of the scattering partners is a liquid. In addition, the flat jet geometry is suitable for carrying out transient absorption experiments in liquids at photon energies at or above the carbon K-edge, so mastering this technology will enable time-resolved x-ray experiments that will be of interest in the CPIMS and AMO programs in the DOE Basic Energy Sciences portfolio.

Recent Publications Citing DOE Support (2015-2018):

- E. N. Sullivan, B. Nichols, D. M. Neumark, *"Photodissociation dynamics of the simplest alkyl peroxy radicals, CH_3OO and C_2H_5OO, at 248 nm,"* J. Chem. Phys. *148*, 033409 (**2018**).
- B. Nichols, E. N. Sullivan, M. Ryazanov, C. M. Hong, D. M. Neumark, "*Investigation of the two- and three-fragment photodissociation of the tert-butyl peroxy radical at 248 nm*," J. Chem. Phys. 147, 134304 (**2017**).
- J. A. DeVine, M. L. Weichman, M. C. Babin, Daniel M. Neumark, "*Slow photoelectron velocity-map imaging of cold tert-butyl peroxide*," J. Chem. Phys. 147, 013915 (**2017**).
- M. L. Weichman, L. Cheng, J. B. Kim, J. F. Stanton, D. M. Neumark, "*Low-lying vibronic level structure of the ground state of the methoxy radical: Slow electron velocity-map imaging (SEVI) spectra and Koppel-Domcke-Cederbaum (KDC) vibronic Hamiltonian calculations*," J. Chem. Phys. 146, 224309 (**2017**).
- I. A. Ramphal, M. Shapero, C. Haibach-Morris, D. M. Neumark,"*Photodissociation dynamics of fulvenallene and the fulvenallenyl radical at 248 and 193 nm*," Phys. Chem. Chem. Phys. 19, 29305 (**2017**).
- A. Bhattacherjee, C. D. Pemmaraju, K. Schnorr, A. R. Attar, and S. R. Leone, *"Ultrafast intersystem crossing in acetylacetone via femtosecond x-ray transient absorption at the Carbon K-edge,"* J. Am. Chem. Soc. *139*, 16576 (**2017**).
- Z. Wang, D. M. Popolan-Vaida, B. Chen, K. Moshammer, S. Y. Mohamed, H. Wang, S. Sioud, M. A. Raji, K. Kohse-Höinghaus, N. Hansen, P. Dagaut, S. R. Leone, and S. M. Sarathy, *"Unraveling the structure and chemical mechanisms of highly oxygenated intermediates in oxidation of organic compounds,"* PNAS *114*, 13102 (**2017**)
- S. Chambreau, D. Popolan-Vaida, G. Vaghjiani, and S. R. Leone, *"Catalytic decomposition of hydroxylammonium nitrate ionic liquid: enhancement of NO formation,"* J. Phys. Chem. Lett. *8*, 2126 (**2017**).
- A. R. Attar, A. Bhattacherjee, C. D. Pemmaraju, Kirsten Schnorr, Kristina D. Closser, David Prendergast, and S. R. Leone, "*Femtosecond x-ray spectroscopy of an electrocyclic ring-opening reaction,"* Science *356*, 54 (**2017**).
- B. Nichols, E. N. Sullivan, M. Ryazanov, D. M. Neumark, *"Photodissociation Dynamics of the i-Methylvinoxy Radical at 308, 248, and 225 nm Using Fast Beam Photofragment Translational Spectroscopy"* J. Phys. Chem. A *121*, 579 (**2017**).

- J. A. DeVine, M. L. Weichman, S. J. Lyle, D. M. Neumark, *"High-resolution photoelectron imaging of cryogenically cooled α- and β-furanyl anions"* J. Mol. Spec. *332*, 16 (**2017**).
- A. D. Dutoi, S. R. Leone, *"Simulation of X-ray Transient Absorption for Following Vibrations in Coherently Ionized F2 Molecules,"* Chem. Phys. *482*, 249 (**2016**).
- S. D. Chambreau, C. J. Koh, D. M. Popolan-Vaida, C. J. Gallegos, J. B. Hooper, D. Bedrov, G. L. Vaghjiani, and S. R. Leone, *"Flow-Tube Investigations of Hypergolic Reactions of a Dicyanamide Ionic Liquid Via Tunable Vacuum Ultraviolet Aerosol Mass Spectrometry"*, J. Phys. Chem. A, *120*, 8011 (**2016**).
- A. W. Harrison, M. Ryazanov, E. N. Sullivan, D. M. Neumark, *"Photodissociation dynamics of the methyl perthiyl radical at 248 and 193 nm using fast-beam photofragment translational spectroscopy"* J. Chem. Phys. *145*, 024305 (**2016**).
- Z. Wang, L. Zhang, K. Moshammer, D. M Popolan-Vaida, V. S. Bhavani Shankar, A. Lucassen, C. Hemken, C. A Taatjes, S. R Leone, K. Kohse-Höinghaus, N. Hansen, P. Dagaut, S Mani Sarathy, *"Additional chain-branching pathways in the low-temperature oxidation of branched alkanes"*, Combustion and Flame, *164*, 386 (**2016**).
- N. C. Cole-Filipiak, M. Shapero, C. Haibach-Morris, and D. M. Neumark, *"Production and Photodissociation of the Methyl Perthiyl Radical"*, J. Phys. Chem. A, **120**, 4818 (**2016**).
- M. L. Weichman, J. A. DeVine, D. S. Levine, J. B. Kim, and D. M. Neumark, *"Isomer-specific vibronic structure of the 9-, 1-, and 2-anthracenyl radicals via slow photoelectron velocity-map imaging"* PNAS, *113*, 1698 (**2016**).
- A. Bhattacherjee, A. R. Attar, and S. R. Leone, "*Transition-state region in the A-band photodissociation of Allyl Iodide – A femtosecond extreme ultraviolet transient absorption study"*, J. Chem. Phys. *144*, 124311 **(2016)**.
- M. Shapero, N. C. Cole-Filipiak, C. Haibach-Morris, and D. M. Neumark, *"Benzyl Radical Photodissociation Dynamics at 248 nm"* J. Phys. Chem. A *119*, 12349 (**2015**).
- A. R. Attar, A. Bhattacherjee, and S. R. Leone, "*Direct observation of the Transition-State Region in the Photodissociation of CH_3I by Femtosecond Extreme Ultraviolet Transient Absorption Spectroscopy"*, J. Phys. Chem. Lett., 6, 5072 (**2015**).
- D. M. Popolan-Vaida, C.-L. Liu, T. Nah, K. R. Wilson, and S. R. Leone, *"Reaction of chlorine molecules with unsaturated submicron organic particles"*, Z. Phys. Chem. 229, 1521 (**2015**).
- K. Moshammer, A. W. Jasper, D. M. Popolan-Vaida, A. Lucassen, P. Diévart, H. Selim, A, J. Eskola, C. A. Taatjes, S. R. Leone, S. M. Sarathy, Y. Ju, P. Dagaut, K. Kohse-Höinghaus, and Nils Hansen, *"Detection and Identification of the Keto-Hydroperoxide ($HOOCH_2OCHO$) and Other Intermediates during Low-Temperature Oxidation of Dimethyl Ether"*, J. Phys. Chem. A, 119, 7361 (**2015**).
- M. L. Weichman, J. B. Kim and D. M. Neumark, *"Slow Photoelectron Velocity-Map Imaging Spectroscopy of the ortho-Hydroxyphenoxide Anion"*, J. Phys. Chem. A, **DOI:** 10.1021/acs.jpca.5b00768, **(2015)**.
- M. L. Weichman, J. B. Kim, J. A. DeVine, D. S. Levine and D. M. Neumark, *"Vibrational and Electronic Structure of the α- and β-naphthyl Radicals via Slow Photoelectron Velocity-Map Imaging"*, J. Am. Chem. Soc., *137*, 1420, **(2015)**.
- J. F. Lockyear, M. Fournier, I. R. Sims, J.-C. Guillemin, C. A. Taatjes, D. L. Osborn and S. R. Leone, "*Formation of fulvene in the reaction of C_2H with 1,3-butadiene*", Int. J. Mass. Spectrom. *378*, 232 (**2015)**.

SPECTROSCOPY AND DYNAMICS OF REACTION INTERMEDIATES IN COMBUSTION CHEMISTRY

Marsha I. Lester
Department of Chemistry
University of Pennsylvania
Philadelphia, PA 19104-6323
milester@sas.upenn.edu

I. Program Scope

This research program aims to characterize important, yet often elusive, reaction intermediates in combustion chemistry using novel spectroscopic and dynamical methods. Recent research has focused on carbonyl oxides of general form R_1R_2COO, known as Criegee intermediates, which are important intermediates in tropospheric hydrocarbon oxidation and some combustion reactions. Ongoing studies also aim to characterize hydroperoxyalkyl intermediates QOOH containing an alkyl radical center (Q) of importance in low temperature combustion of alkanes and autooxidation chemistry of hydrocarbons in the atmosphere.

II. Recent Progress

A. Unimolecular decay of carbonyl oxides to OH products

We have utilized a 1+1′ REMPI ionization scheme[1-3] for state-selective detection of OH $X^2\Pi$ radicals in velocity map imaging (VMI) studies. The initial VMI studies examined the angular and velocity distributions of OH products arising from unimolecular decay of vibrationally activated CH_3CHOO and $(CH_3)_2COO$ Criegee intermediates under collision free conditions.[4,5] The VMI studies reveal the release of excess energy to internal and translational degrees of freedom as a means of elucidating the dynamical pathway(s) to products. IR excitation in the CH stretch overtone region was used to access the transition state (TS) barrier region leading to OH products. The reaction pathway involves intramolecular 1,4 hydrogen atom transfer that results in isomerization to vinyl (or methylethenyl) hydroperoxide (VHP). This is followed by O-O bond cleavage to form OH + vinoxy (or 1-methyl vinoxy) products, although not via a simple barrierless O-O bond breaking process due to the presence of a submerged saddle point and associated product complex prior to dissociation. The VMI experiments on CH_3CHOO were complemented by quasi-classical trajectory (QCT) calculations from the TS to products.[4] Snapshots of the trajectories showed that the shallow minimum in the exit channel facilitates reorientation of the weakly interacting OH + vinoxy fragments at long range prior to dissociation.

The angular distributions of the OH products obtained using VMI are isotropic, indicating that CH_3CHOO and $(CH_3)_2COO$ undergo rotation prior to unimolecular decay.[4,5] This is consistent with the nanosecond timescales observed in recent direct time domain measurements as well as statistical RRKM evaluation of their microcanonical dissociation rates.[6] In both systems, the total kinetic energy release distributions derived from the 2D images are broad and unstructured, and account for ~20% of the energy released on average. The OH products are released with minimal excitation, indicating that most of available energy flows into internal excitation of the vinoxy (or 1-methyl vinoxy) products. For CH_3CHOO, the release of the excess energy to product internal and translational degrees of freedom differs considerably from a

statistical distribution, but is captured in QCT calculations initiated at critical configurations along the reaction pathway.[4] The best agreement comes from trajectories starting at a submerged saddle point in the exit channel. For $(CH_3)_2COO$, the release of excess energy to translation is well represented by a statistical distribution. In both systems, the OH $X^2\Pi$ (v=0) product rotational distributions differ from statistical models.

B. Pathway from Criegee intermediates to hydroxyacetone products

In collaboration with Taatjes and coworkers, we have also carried out experiments on hydroxyacetone ($CH_3C(O)CH_2OH$) formation using the multiplexed photoionization mass spectrometer at the Chemical Dynamics Beamline with tunable VUV radiation from the Advanced Light Source.[7] Hydroxyacetone was identified as a stable product from reactions of the $(CH_3)_2COO$ Criegee intermediate in a flow tube. In the experiment, the two isomers at m/z = 74 are distinguished by their different photoionization spectra and reaction times. Hydroxyacetone was observed as a persistent signal at m/z 74 at longer (≥ 5 ms) reaction times and higher photoionization energies starting at ca. 9.7 eV.

Complementary electronic structure calculations by Thompson suggested multiple reaction pathways for hydroxyacetone formation including unimolecular and self-reaction pathways.[7] Very recently, Kuwata et al.[8] reported calculations that provide a compelling explanation for the observation of hydroxyacetone. Their calculations reveal thermal unimolecular decay of $(CH_3)_2COO$ via H-atom transfer to VHP followed by (i) partial O-O bond fission, (ii) a roaming step involving reorientation of the OH fragment, and then (iii) OH addition to the double bond of the vinyl group to yield hydroxyacetone under collisional conditions. Alternatively, the O-O bond breaks to form OH + vinoxy products, as described above.

C. Photo-initiated dynamics involving multiple potentials for Criegee intermediates

Recently, we utilized velocity map imaging to demonstrate the prompt release of O ^1D products upon UV excitation of the CH_2OO Criegee intermediate in the long wavelength tail region (364 to 417 nm) of the $B^1A' - X^1A'$ spectrum.[9] The VMI images exhibit anisotropic distributions indicating that dissociation to H_2CO X^1A_1 + O ^1D products is rapid compared to the rotational period of CH_2OO and occurs on a picosecond or faster timescale. As a result, the broad oscillatory structure reported previously by several groups[10-12] in the long wavelength tail region of the UV absorption spectrum is attributed to short-lived resonances associated with the excited B^1A' state of CH_2OO, in accord with theoretical predictions.[13]

The total kinetic energy release distributions show that the available energy is nearly equally partitioned, on average, between product translational energy and internal excitation of the H_2CO co-fragments. The anisotropy and energy partitioning are unchanged with excitation wavelength, and consistent with previously reported experimental and theoretical findings of the CH_2OO B-X transition moment and dissociation energy to H_2CO X^1A_1 + O ^1D products.[14,15] Thus, the strong UV absorption spectrum[10-12,16] over the entire wavelength range (308 to 417 nm) arises from electronic excitation of CH_2OO from its ground X^1A' state to a single excited electronic state, namely the B^1A' state, which couples to repulsive singlet states and results in rapid O-O bond breakage and dissociation.

We have also examined the UV photo-induced dynamics of the less stable ($\Delta E \sim 3.6$ kcal mol^{-1}) and less abundant (≤ 30%) *anti*-conformer of CH_3CHOO.[17] The UV absorption spectrum of *anti*-CH_3CHOO has been shown to peak at 360 nm,[17] whereas that of *syn*-CH_3CHOO peaks at

320 nm and falls off considerably by 360 nm.[17, 18] We find significantly different partitioning of available energy into kinetic energy of the recoiling CH_3CHO $X^1A' + O\ ^1D$ products with 32% (on average) following excitation of *syn*-CH_3CHOO at 320 nm[19] as compared to 58% of the available energy for *anti*-CH_3CHOO at 400 nm. We utilize the distinctly different dissociation dynamics of the two conformers to separate the *syn*/*anti* contributions to the kinetic energy release distribution obtained at intermediate wavelengths (e.g. 370 nm) where both conformers are simultaneously excited. Our deconvolution based on dissociation dynamics agrees well with a prior study[17] that was based on the significantly faster reaction rate of *anti*-CH_3CHOO with water vapor to separate *syn*- and *anti*-CH_3CHOO contributions to the UV absorption spectrum.

Currently, we are examining the UV-vis spectrum and associated photodissociation dynamics of methyl vinyl ketone oxide (MVK-OO), which has extended π conjugation across the vinyl and carbonyl oxide functional groups. Laboratory synthesis of MVK-OO is achieved by reaction of a photolytically-generated, resonance-stabilized monoiodoalkene radical with O_2. Electronic excitation of MVK-OO on the strong $1^1\pi\pi^*$ and $2^1\pi\pi^*$ transitions is detected by depletion of the VUV photoionization signal at m/z = 86 and by observing the appearance of $O\ ^1D$ products using VMI.

III. Future Work

Future studies will examine photo-initiated dynamics involving multiple coupled potential energy surfaces for prototypical Criegee intermediates. In addition, we aim to stabilize prototypical carbon-centered alkyl hydroperoxy radicals (QOOH) at a critical intermediate point along the reaction pathway, and characterize the QOOH radicals and their oxygen adducts by infrared action spectroscopy. We plan to experimentally determine the transition state barrier from the QOOH intermediate to OH radical products through the threshold and energy-dependent rates of reaction.

IV. References

1. J. M. Beames, F. Liu, M. I. Lester and C. Murray, J. Chem. Phys. 134, 241102 (2011).
2. J. M. Beames, F. Liu, and M. I. Lester, Mol. Phys. 112, 897 (2014).
3. A. M. Green, F. Liu, and M. I. Lester, J. Chem. Phys.144, 184311 (2016).
4. N. M. Kidwell, H. Li, X. Wang, J. M. Bowman, and M. I. Lester, Nat. Chem. 8, 509-14 (2016).
5. H. Li, N. M. Kidwell, X. Wang, J. M. Bowman, and M. I. Lester, J. Chem. Phys. 145 104307 (2016).
6. Y. Fang, F. Liu, V. P. Barber, S. J. Klippenstein, A. B. McCoy, and M. I. Lester, J. Chem. Phys. 144, 061102 (2016).
7. C. A. Taatjes, F. Liu, B. Rotavera, M. Kumar, R. Caravan, D. L. Osborn, W. H. Thompson, and M. I. Lester, J. Phys. Chem. A 121, 16-23 (2017).
8. K. T. Kuwata, L. Luu, A. B. Weberg, K. Huang, A. J. Parsons, L. A. Peebles, N. B. Rackstraw, and M. J. Kim, J. Phys. Chem. A 122, 2485–2502 (2018).
9. M. F. Vansco, H. Li and M. I. Lester, J. Chem. Phys. 147, 013907 (2017).
10. L. Sheps, J. Phys. Chem. Lett. 4, 4201 (2013).
11. W.-L. Ting, Y.-H. Chen, W. Chao, M. C. Smith and J. J.-M. Lin, Phys. Chem. Chem. Phys. 16, 10438 (2014).
12. E. S. Foreman, K. M. Kapnas, Y. Jou, J. Kalinowski, D. Feng, R. B. Gerber and C. Murray, Phys. Chem. Chem. Phys. 17, 32539 (2015).

13. R. Dawes, B. Jiang and H. Guo, J. Am. Chem. Soc. 137, 50 (2015).
14. J. H. Lehman, H. Li, J. M. Beames and M. I. Lester, J. Chem. Phys. 139, 141103 (2013).
15. H. Li, Y. Fang, J. M. Beames and M. I. Lester, J. Chem. Phys. 142, 214312 (2015).
16. J. M. Beames, F. Liu, L. Lu, and M. I. Lester, J. Am. Chem. Soc. 134, 20045-48 (2012).
17. L. Sheps, A. M. Scully, and K. Au, *Phys. Chem. Chem. Phys.* **16,** 26701-06 (2014).
18. J. M. Beames, F. Liu, L. Lu, and M. I. Lester, *J. Chem. Phys.* **138,** 244307 (2013).
19. H. Li, Y. Fang, N. M. Kidwell, J. M. Beames, and M. I. Lester, *J. Phys. Chem. A* **119,** 8328-37 (2015).

V. Publications supported by this DOE project (2015-present)

1. M. F. Vansco, H. Li, and M. I. Lester, "Prompt release of O ^{1}D products upon UV excitation of CH_2OO Criegee intermediates", *J. Chem. Phys.* 147, 013907 (2017).
2. C. A. Taatjes, F. Liu, B. Rotavera, M. Kumar, R. Caravan, D. L. Osborn, W. H. Thompson, and M. I. Lester, "Hydroxyacetone production from C_3 Criegee intermediates", *J. Phys. Chem. A* 121, 16-23 (2017).
3. H. Li, N. M. Kidwell, X. Wang, J. M. Bowman, and M. I. Lester, "Velocity map imaging of OH radical products from IR activated $(CH_3)_2COO$ Criegee intermediates", *J. Chem. Phys.* 145 104307 (2016).
4. A. M. Green, F. Liu, and M. I. Lester, "UV + VUV double-resonance studies of autoionizing Rydberg states of the hydroxyl radical", *J. Chem. Phys.*144, 184311 (2016)**.**
5. N. M. Kidwell, H. Li, X. Wang, J. M. Bowman, and M. I. Lester, "Unimolecular dissociation dynamics of vibrationally activated CH_3CHOO Criegee intermediates to OH radical products", *Nat. Chem.* 8, 509-14 (2016).
6. H. Li, Y. Fang, N. M. Kidwell, J. M. Beames, and M. I. Lester, "UV photodissociation dynamics of the CH_3CHOO Criegee intermediate: Action spectroscopy and velocity map imaging of O-atom products", *J. Phys. Chem. A.* **119**, 8328-37 (2015).
7. H. Li, Y. Fang, J. M. Beames, and M. I. Lester, "Velocity map imaging of O-atom products from UV photodissociation of the CH_2OO Criegee intermediate", *J. Chem. Phys.* **142**, 214312 (2015).

Advanced Nonlinear Optical Methods for Quantitative Measurements in Flames

Robert P. Lucht
School of Mechanical Engineering, Purdue University
West Lafayette, IN 47907-2088
Lucht@purdue.edu

I. Program Scope

Nonlinear optical techniques such as laser-induced polarization spectroscopy (PS), resonant wave mixing (RWM), and ultrafast coherent anti-Stokes Raman scattering (CARS) are techniques that show great promise for sensitive measurements of transient gas-phase species, and diagnostic applications of these techniques are being pursued actively at laboratories throughout the world. The objective of this research program is to develop and test strategies for quantitative concentration and temperature measurements using nonlinear optical techniques in flames and plasmas. We have continued our fundamental theoretical and experimental investigations of these techniques. In recent years our theoretical and experimental efforts have been focused on investigating the potential of femtosecond (fs) laser systems for sensitive and accurate CARS measurements in gas-phase media. Our initial efforts have been focused on fs CARS, although the systems will be useful for a wide range of future diagnostic techniques involving two-photon transitions. In the last few years we have demonstrated the acquisition of single-shot temperature measurements at data rates of 5 kHz in highly turbulent, swirl-stabilized methane-air flames and now in pilot-stabilized jet flames with both gaseous and liquid fuels (these measurements are described in P1-P3, and P5-P8).

Last year we completed an extensive set of measurements in jet flames in collaboration with Prof. Assaad Masri's group at the University of Sydney. Visiting PhD student Albyn Lowe from the University of Sydney brought over the Sydney Needle Spray Burner (SYNSBURN$_{TM}$) experimental apparatus which was installed in our laboratory at Purdue University. Mr. Lowe and my PhD student Levi Thomas and postdoctoral research associate Dr. Aman Satija performed single-shot, 5 kHz fs CARS temperature measurements in jet flames stabilized on the SYNSBURN apparatus over a wide range of operating conditions. In particular, measurements were performed in jet flames in which liquid fuel was injected along the centerline using an injection tube placed different distances from the nozzle exit. We continue to analyze the data that were obtained during this experimental campaign; one paper has been accepted for presentation in the International Combustion Symposium and several others are in preparation for submission.

We are investigating the physics of both fs CARS and two-color PS by direct numerical integration (DNI) of the time-dependent density matrix equations for the resonant interaction. Significantly fewer restrictive assumptions are required using this DNI approach compared with the assumptions required to obtain analytical solutions. We are concentrating on the accurate simulation of two-photon processes, including Raman transitions, where numerous intermediate electronic levels contribute to the two-photon transition strength. Recent progress has been much more rapid in our modeling efforts after my PhD student Mingming Gu parallelized the time-dependent density matrix code with the assistance of my faculty colleague Prof. Carlo Scalo. The code was parallelized such that different computer nodes performed independent calculations for separate Q-branch transitions. The calculated electric field amplitude of the signal from each of these transitions was then added to give us the time-dependent CARS signal amplitude, and the spectrum was then calculated by Fourier transforming the time-dependent CARS signal amplitude. Using this parallelized computer code, we have investigated the in detail the effects of chirp in the pump and Stokes beams on the Raman excitation efficiency and on signal generation for chirped-probe-pulse (CPP) fs CARS.

We also began a theoretical analysis of Raman transitions, in particular pure rotational Raman transitions for the nitric oxide molecule. The theoretical approach is very similar to that employed to calculate two-photon absorption line strengths for nitric oxide described in paper P4. line strengths

were compared with the results of high-resolution two-photon-absorption laser-induced fluorescence measurements of nitric oxide. The theoretical results will be compared with pure rotational CARS measurements performed several years ago on this project.

II. Recent Progress

A. Pump and Stokes Chirp Effects for CPP Fs CARS

Fs CARS offers several major potential advantages compared with nanosecond (ns) CARS; i.e., CARS as usually performed with nanosecond pump and Stokes lasers. These potential advantages include an elimination of collisional effects in the signal generation and the capability of performing real-time temperature and species measurements at data rates of 1 kHz or greater as compared to 10-50 Hz for ns CARS. Our Coherent ultrafast laser system operates at 5 kHz with a fundamental pulse width of 55-60 fs and pulse energy of over 2 mJ.

After we parallelized our time-dependent density matrix code for fs CARS, we were able to speed up the calculations by a factor of almost 100 by parallelizing and rewriting the code using the Python programming language. This in turn has allowed us to extract much more physical insight from our computer calculations because we can perform parametric variation studies much faster. We are investigating the effects of chirp in the pump and Stokes beams on the Raman excitation efficiency and signal generation for CPP fs CARS. The key result of our study of pump and Stokes chirp effects is that as long as the sign and magnitudes of the chirp are nearly equal for the pump and Stokes beams, the Raman excitation efficiency decreases only slightly, even when the pulses are lengthened by a factor of two. This is a result that is very significant for projected future applications of the technique to high pressure systems, where the beams may have to propagate through thick windows which will induce significant chirp. We have been exploring the effects of inducing moderate chirp in the pump and Stokes beams in the laboratory by placing SF11 disks with thicknesses of 10, 20, or 30 mm in the beam paths as shown in Fig. 1. Our initial results indicate that inducing moderate levels of chirp appears to enhance the temperature accuracy and precision of the CPP fs CARS technique, as indicate by the single-shot temperature histogram shown in Fig. 2. For the histograms for flame conditions shown in Fig. 2, the average precision is 2.1% and the average absolute mean temperature accuracy is 1.1%.

B. Femtosecond CARS Temperature Measurements in the SYNSBURN Jet Flames

The single-shot, chirped-pulse-probe (CPP) fs CARS system used for temperature measurements in the SYNSBURN jet flames is shown in Fig. 2. The fundamental 800-nm beam was used for the pump and probe beams for the SYNSBURN measurements. The Stokes beam at 983 nm was generated by frequency doubling the idler output of the OPA. The resulting CARS signal was generated at a center wavelength of 675 nm. The jet flame is pilot stabilized and features a liquid fuel injector on the centerline in the inner tube. We investigated flames with liquid acetone and ethanol into surroundings main air jet stream. The fuel flow rate, the main air jet flow rate, and the distance of the liquid jet injection upstream of the jet nozzle exit plane were all parametrically varied. CPP fs CARS data were acquired along the axial centerline and radial scans were performed at selected axial locations for over thirty flames. We have now processed most of the data from our experimental campaign and are in the process of analyzing the results for insights into the structure of these turbulent jet spray flames.

Premixed methane/air jet flames and highly sooting, nonpremixed ethylene/nitrogen jet flames were also investigated. The CPP fs CARS measurements in the highly sooting flames were very encouraging despite issues with a broadband background from the soot emission. For 10 Hz ns CARS in sooting flames (see next section) we used a mechanical shutter to minimize the soot emission background, but this shutter could not be used for the 5 kHz CPP fs CARS. We plan to eliminate this background in future CPP fs CARS measurements using a Pockels cell and crossed polarizers.

C. Pure Rotational Raman in Nitric Oxide

We have performed pure rotational CARS measurements mixture of nitric oxide and nitrogen at room temperature. The simultaneous acquisition of pure rotational CARS spectra from known mixtures of these two species will enable us to determine with excellent accuracy the pure rotational Raman cross section for nitric oxide, given that the pure rotational Raman cross section of nitrogen is so well known. The theoretical analysis of the pure rotational Raman process in nitric oxide is based both on a density matrix analysis where the intermediate electronic levels of the molecule are taken into account and on a polarizability analysis where the intermediate levels are not explicitly included.

D. CARS Temperature Measurements in Sooting Ethylene Nitrogen Diffusion Flames

Temperature measurements were performed in sooting ethylene-air co-flow diffusion flames stabilized over a Yale burner. These measurements are intended to serve as benchmark data for comparison against previous and future computational work in these flames. The Yale burner also known as Smooke/Long burner is identified as the third target flame by the international sooting flame workshop. Measurements were performed using a dual-pump vibrational CARS system to obtain temperature measurements, without soot interference, with high spatial and temporal resolution. We were able to obtain excellent quality spectra in all parts of the flame including the highly sooting region and near the tip of the fuel nozzle where the nonresonant modulation of the CARS spectra is strong. Large discrepancies, in both peak temperature and temperature profiles, were observed between CARS temperature measurements and previously performed CFD calculations. A paper describing this work is in preparation for submission Combustion and Flame.

III. Future Work

We will continue to perform fs CARS experiments in our laboratory using the Coherent ultrafast laser system. Our studies of temperature measurements using CPP fs CARS will continue. We continue to investigate the effect of laser system parameters on the CPP fs CARS spectrum to improve the temperature accuracy of the technique. We will explore the potential for using CPP fs CARS for accurate concentration measurements for hydrocarbon species and other polyatomic molecules, very hard species to measure using ns CARS. We will make full use of the high-temperature, high-pressure gas cell that we have fabricated for fundamental studies of the effects of temperature and pressure on fs CARS measurements of temperature and species concentrations. We will explore further the effects of soot and droplets on the CPP fs CARS process.

Our theoretical studies of the physics of fs CARS will continue. The parallelization of our density matrix computer code will allow us to explore effects such as collisional narrowing that was simply not possible using the serial version of our code. The study of collisional narrowing requires communication between different computational nodes due to the transfer of coherence during rotational transfer collisions.

Our investigation of the physics of two-color PS for species such as NO will continue. We will explore collisional effects on the PS and 6WM processes in much more detail using a two-dye laser system that is just becoming operational. We will explore further the effects of buffer gas collisions on collision-induced resonances in single-photon, two-color PS of NO. We will continue to use the density matrix code to gain insight into the physics of the PS and 6WM processes; these codes will also be parallelized during next year so that we can incorporate Doppler broadening and velocity narrowing effects in model of two-color PS for atomic hydrogen.

IV. Refereed publications and submitted journal articles supported by this project 2016-2018

P1. C. N. Dennis, A. Satija, and R. P. Lucht, "High Dynamic Range Thermometry at 5 kHz in Hydrogen-Air Diffusion Flame using Chirped-Probe-Pulse Femtosecond Coherent Anti-Stokes Raman Scattering," *Journal of Raman Spectroscopy* **47**, 177-188 (2016). DOI: 10.1002/jrs.4773

P2. C. N. Dennis, C. D. Slabaugh, I. G. Boxx, W. Meier, and R. P. Lucht, "5 kHz Thermometry in a Swirl-Stabilized Gas Turbine Model Combustor using Chirped Probe Pulse Femtosecond CARS.

Part 1: Temporally Resolved Swirl-Flame Thermometry," *Combustion and Flame* **173**, 441-453 (2016). DOI: 10.1016/j.combustflame.2016.02.033

P3. C. D. Slabaugh, C. N. Dennis, I. G. Boxx, W. Meier, and R. P. Lucht, "5 kHz Thermometry in a Swirl-Stabilized Gas Turbine Model Combustor using Chirped Probe Pulse Femtosecond CARS. Part 2: Analysis of Swirl Flame Dynamics," *Combustion and Flame* **173**, 454-467 (2016). DOI: 10.1016/j.combustflame.2016.02.032

P4. W. D. Kulatilaka and R. P. Lucht, "Two-Photon-Absorption Line Strengths for Nitric Oxide: Comparison of Theory and Sub-Doppler, Laser-Induced Fluorescence Measurements," *Journal of Chemical Physics* **146**, 124311 (2017). DOI: 10.1063/1.4978921

P5. L. M. Thomas, A. Satija, and R. P. Lucht, "Technique Developments and Performance Analysis of Chirped-Probe-Pulse Femtosecond Coherent Anti-Stokes Raman Scattering Combustion Thermometry," *Applied Optics* **56**, 8797-8810 (2017). DOI: 10.1364/AO.56.008797

P6. D. Han, A. Satija, J. Kim, Y. Weng, J. P. Gore, R. P. Lucht, "Dual-Pump Vibrational CARS Measurements of Temperature and Species Concentrations in Turbulent Premixed Flames with CO_2 Addition," *Combustion and Flame* **181**, 239-250 (2017). DOI: 10.1016/j.combustflame.2017.03.027

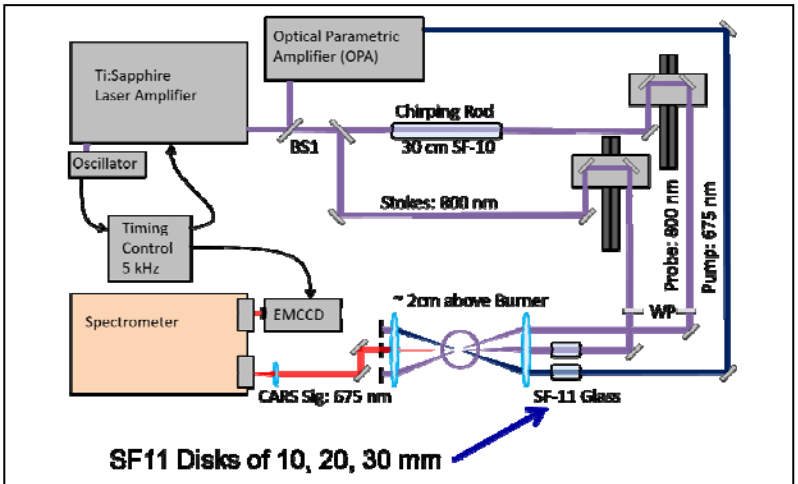

Figure 1. Schematic diagram of CPP fs CARS experiment for investigation of effects of moderate chirp in the pump and Stokes beams.

P7. A. Lowe, L. M. Thomas, A. Satija, R.P. Lucht, and A.R. Masri, "Chirped-Probe-Pulse Femtosecond CARS Thermometry in Turbulent Spray Flames," *Proceedings of the Combustion Institute*, submitted for publication, accepted for publication at the Symposium (2018).

P8. D. Han, J. Kim, A. Satija, J. P. Gore, and R. P. Lucht, "Experimental Study of CO_2 Diluted, Piloted, Turbulent CH_4/Air Premixed Flames using High-Repetition-Rate OH PLIF," *Combustion and Flame*, accepted for publication (2018).

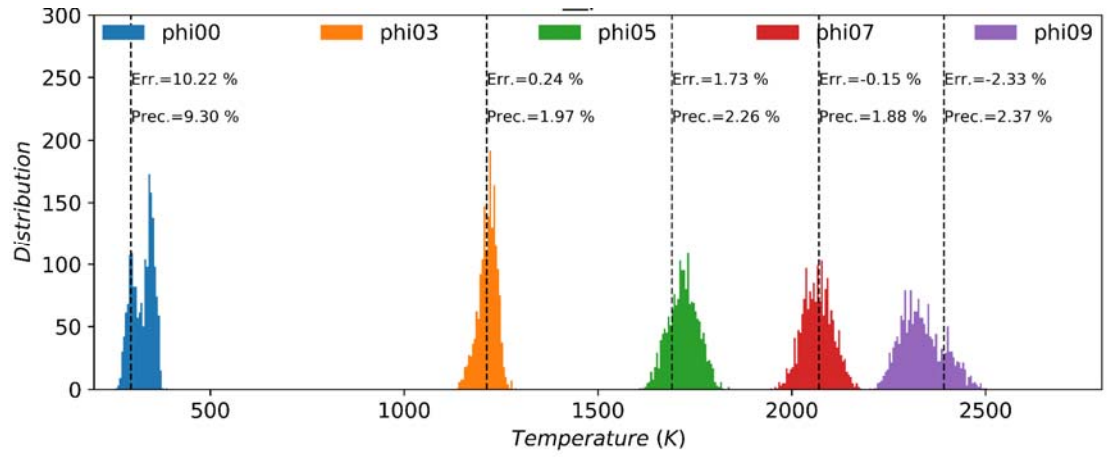

Figure 2. Histograms of single-shot CPP fs CARS temperature measurements in room air and in Hencken burner at equivalence ratios of 0.3, 0.5, 0.7, and 0.9. The single-shot spectra were fit using a single set of laser parameters obtained from spectra from the 0.7 equivalence ratio flame.

Particle Chemistry and Diagnostics Development

H. A. Michelsen
Sandia National Labs, MS 9055, P. O. Box 969, Livermore, CA 94551
hamiche@sandia.gov

I. Program Scope

The formation of solid carbonaceous particles at high temperatures is important in numerous natural environments, energy production and use technologies, and commercial applications. Such particles are formed in hot carbon plasmas,[1] by spray pyrolysis,[2] and during the detonation of explosives.[3-4] They are produced commercially for pigments, adsorbents, and composite materials.[2] They are generated in the outflow of carbon-rich stars and are one of the main components of interstellar dust.[5-6] The most ubiquitous and notorious of carbon particles formed under high-temperature conditions is soot, a product of incomplete combustion of hydrocarbon fuels. Despite its ubiquity and the enormous negative impact it has on human health and the environment,[7-8] the chemical pathway for soot formation is still unknown, and its surface chemistry following formation is poorly understood.[9]

The research program described here focuses on the development and use of diagnostics for carbonaceous particles in high-temperature, atmospheric, and other environments and the use of these diagnostics to study particle nucleation, growth, chemical and physical evolution, oxidation, and other chemical processing. The work involves *in situ* measurements of volume fraction, size, composition, and morphology of particles with fast time response and high sensitivity for studies of particle chemistry. Techniques are being developed for detection and characterization of particles from freshly nucleated particles that are <6 nm in diameter and composed of condensed large organic species to refractory particles resembling polycrystalline turbostratic graphite. Studies are targeted at developing an understanding at a fundamental level of particle-light interactions and carbonaceous-particle chemistry as a non-ideal material.

II. Recent Progress

Our work has focused on developing a detailed understanding of the chemical and physical mechanisms that influence the applicability of laser-based, X-ray, and mass spectrometric techniques for carbonaceous-particle detection and characterization under a wide range of conditions.

Assessing Mass Spectrometry for Identifying Large Hydrocarbon Precursors

Mass spectrometry is commonly used for measuring mixed hydrocarbon samples because it enables simultaneous or nearly simultaneous detection of multiple species. In addition to mass analysis, molecular-beam mass spectrometry studies using vacuum ultraviolet (VUV) radiation for photoionization have shown that identification of isomers of small gas-phase hydrocarbons can be accomplished using photoionization-efficiency (PIE) analysis, *i.e.*, analysis of the photon-energy dependence of a peak in a mass spectrum.[10-12] Unambiguous identification of larger isomers, *i.e.*, those containing five or more carbon and oxygen atoms, is challenging,[13] however, because (1) the possible number of isomers grows with the molecular size, (2) isomers of potential importance have small differences in heats of formation (the link between heat of formation and ionization-threshold energy (IE) has been explained and verified for alkanes, alkenes, and monosubstituted alkanes[14]), and (3) similar chemical structures lead to similar IEs and PIE curves.[12] Despite these challenges, PIE measurements have been used to separate isomers of larger species in chemically limited systems, *i.e.*, in systems with a limited number of possible isomers.

There are several key areas of investigation related to high-temperature carbonaceous particle formation that require measurement techniques capable of delivering chemical information on a molecular level. Carbonaceous-particle nucleation is poorly understood and is hypothesized to be initiated by large polycyclic aromatic hydrocarbons (PAHs),[9, 15] but the PAH size required for dimerization has not been established. It is not known if particle-precursor species are predominantly purely aromatic or if they have significant aliphatic content.

In aerosol mass spectrometry studies of precursor species containing more than 10 carbon atoms, the mass peak corresponding to signal from $C_{16}H_{10}$ isomers, is generally significant, as are other mass peaks whose masses have the structures of the most stable PAHs, *i.e.*, stabilomers. Explicit evidence suggesting the presence or absence of particular isomers is, however, lacking.

We have evaluated information provided by PIE measurements performed on samples collected from a premixed ethylene flame.[16] The results showed that quantitative isomer speciation is impossible, or nearly so. Nevertheless, we demonstrated that PIE analysis can provide insight into the chemistry of high-temperature carbonaceous-particle formation and can sometimes be used to partition precursor-species distributions into two classes of species, one class of species that contain several aromatics rings and another class of species that are purely aliphatic or contain only a few aromatic rings.[16-17]

We have used quantum chemistry to calculate the values of the adiabatic-ionization energy (AIE) of twenty-four $C_{16}H_{10}$ isomers. These calculations confirmed that the differences in AIEs between different isomers can be smaller than the average thermal energy at room temperature, even for a relatively small subset of isomers. We also showed that neither pyrene nor fluoranthene alone can account for the PIE signals from $C_{16}H_{10}$ isomers in the flame studied, even though a reasonable match for the flame-measured curves of $C_{16}H_{10}$ isomers can be found by considering a combination of pyrene and fluoranthene signals. We similarly demonstrated that coronene alone cannot account for the PIE signal from $C_{24}H_{12}$ isomers. We also showed that measurements that provide information about species volatility can be used with PIE analysis to facilitate characterization of precursor species.

Figure 1 presents aerosol mass spectra from samples extracted from a premixed ethylene flame at two heights above the burner (HABs) with and without a thermal denuder in the sampling line. Peaks of masses less than ~300 u are preferentially reduced by the thermal denuder, confirming that these masses are more volatile than the heavier masses but are sufficiently condensable to pass through vacuum adsorbed to stable particles when the sampling line is not heated.

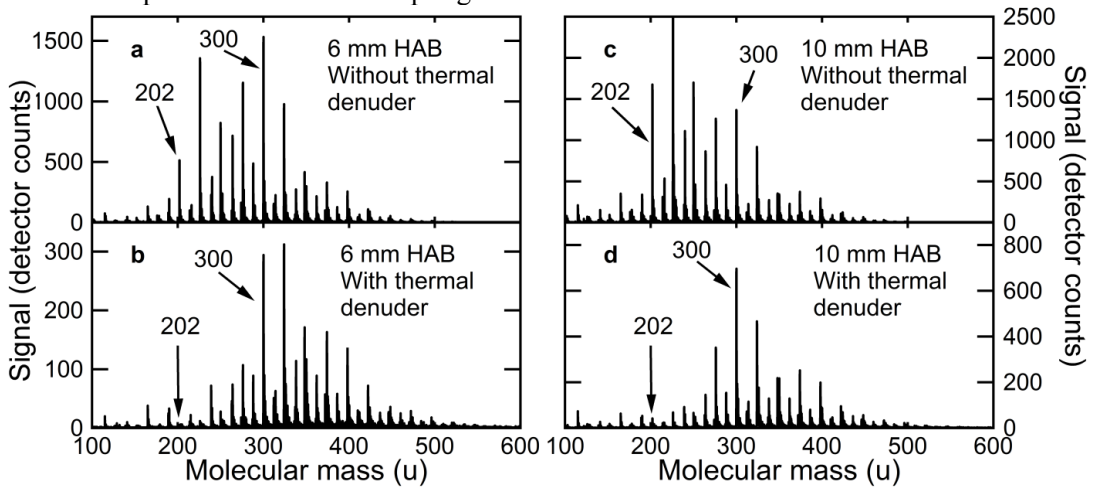

Figure 1. Aerosol mass spectra recorded in the premixed ethylene/oxygen/nitrogen flame: Mass spectra were recorded at 6 mm (a) without and (b) with a thermal denuder in front of the mass spectrometer and at 10 mm (c) with and (d) without the thermal denuder. Mass peaks at 202 ($C_{16}H_{10}$ isomers) and 300 u ($C_{24}H_{12}$ isomers) are indicated.

Figure 2 shows PIE curves recorded at a mass of 202 u at the two HABs corresponding to those in Fig. 1. The curves are nearly identical at these HABs. They are compared with PIE curves from two PAH isomers with a mass of 202 u, pyrene (Fig. 2a) and fluoranthene (Fig. 2b). Neither species reproduces the measured PIE curves from the flame samples, but a linear combination of curves from fluoranthene and pyrene is able to reproduce the flame-sample curves. If the samples are sent through a thermal denuder in the sampling line, the 200-u flame-PIE curves change but can still be fit with a linear combination of PIE curves from fluoranthene and pyrene, but the fit suggests less of a contribution from pyrene. Fluoranthene and pyrene are not the only isomers at this mass, and it is possible that other PAHs with similar ionization energies are involved. Because these PIE curves can be changed by including a thermal denuder that preferentially removes the more volatile isomers, these results demonstrate that the mass at 202 u is not attributable to a single isomer. The PIE curves from flames samples for a mass of 300 u are shown in Fig. 3, compared with a PIE curve for coronene. The comparison demonstrates that this mass in the flame samples is not entirely attributable to coronene. In this case, however, the thermal denuder has little effect on the flame PIE curves because, as demonstrated in Fig. 1, this mass is much less volatile and not strongly influenced by the thermal denuder.

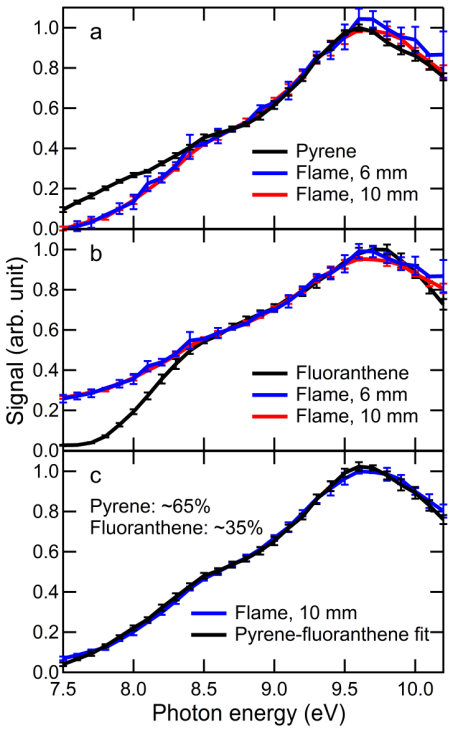

Figure 2. Comparison of flame PIE and known PAH-PIE curves for mass 202 u. Flame samples were extracted from a premixed ethylene/oxygen/nitrogen flame at HABs of 6 and 10 mm. (a) Comparison between the shapes of the pyrene-PIE curve and the flame-PIE curves of soot samples drawn from the flame. The flame-PIE curves were scaled and offset to fit the pyrene-PIE curve between 8.5 and 9.5 eV. (b) Same as in (a), but with the flame-PIE curves fit to the fluoranthene-PIE curve. (c) Comparison between the flame-PIE curve recorded from samples drawn at an HAB of 10 mm and the best fit of the PAH curves to the flame curve using a linear combination of the pyrene- and fluoranthene-PIE curves.

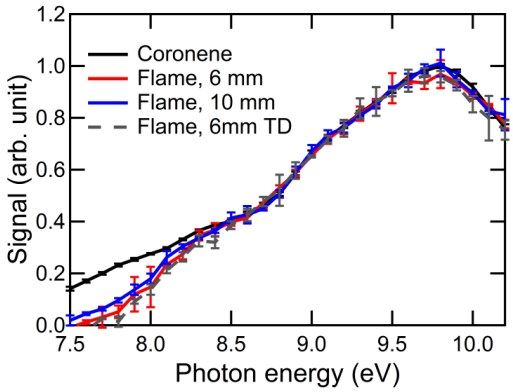

Figure 3. Comparison between the PIE curve of pure coronene and the flame-PIE curves at 300 u (samples extracted at HABs of 6 and 10 mm). A thermal denuder was in position during the recording of the dashed curve. The raw flame-PIE curves did not have zero signal levels at 7.5 eV, and the low curve values at low photon energies resulted from fits to the coronene-PIE curve (see text related to the fitting of the flame-PIE curves at 202 u to the pyrene-PIE curve for details). The error bars are 95% confidence intervals of the standard errors of the mean.

III. Future Work

Future work will refine and expand on the application of synchrotron- and free-electron-laser-based X-ray measurement techniques for studies of carbonaceous particle nucleation, growth, and surface chemistry. We will continue to develop laser-based diagnostics that can be used to probe particle size, morphology, and composition and apply these diagnostics to study particle formation and evolution.

IV. References

(1) Lida, Y.; Yeung, E. S. Optical Monitoring of Laser-Induced Plasma Derived from Graphite and Characterization of the Deposited Carbon Film. *Appl. Spectrosc.* **1994,** *48*, 945-950.

(2) Skrabalak, S. E. Ultrasound-Assisted Synthesis of Carbon Materials. *Phys. Chem. Chem. Phys.* **2009,** *11*, 4930-4942.

(3) Tarver, C. M. Condensed Matter Detonation: Theory and Practice. In *Shock Waves Science and Technology Library*, Zhang, F., Ed. Springer: Berlin, Heidelberg, **2012**, pp 339-372.

(4) Tarver, C. M. Theory and Modeling of Liquid Explosive Detonation. *J. Energ. Mater.* **2010,** *28*, 299-317.

(5) Allamandola, L. J.; Tielens, A. G. G. M.; Barker, J. R. Polycyclic Aromatic Hydrocarbons and the Unidentified Infrared Emission Bands-Auto Exhaust Along the Milky Way. *Astrophys. J.* **1985,** *290*, L25-L28.

(6) Tielens, A. G. G. M. In *Carbon Stardust: From Soot to Diamonds*, Carbon in the Galaxy, Tarter, J. C.; Chang, S.; DeFrees, D., Eds. NASA Conference Publication: **1990**; pp 59-111.

(7) Bond, T. C. et al., Bounding the Role of Black Carbon in the Climate System: A Scientific Assessment. *J. Geophys. Res.* **2013,** *118*, 5380-5552.
(8) WHO 7 Million Premature Deaths Annually Linked to Air Pollution. http://www.who.int/mediacentre/news/releases/2014/air-pollution/en/.
(9) Michelsen, H. A. Probing Soot Formation, Chemical and Physical Evolution, and Oxidation: A Review of *in Situ* Diagnostic Techniques and Needs. *Proc. Combust. Inst.* **2017,** *36*, 717-735.
(10) Taatjes, C. A.; Hansen, N.; McIlroy, A.; Miller, J. A.; Senosiain, J. P.; Klippenstein, S. J.; Qi, F.; Sheng, L.; Zhang, Y.; Cool, T. A. Enols Are Common Intermediates in Hydrocarbon Oxidation. *Science* **2005,** *308*, 1887-1889.
(11) Cool, T. A.; McIlroy, A.; Qi, F.; Westmoreland, P. R.; Poisson, L.; Peterka, D. S.; Ahmed, M. Photoionization Mass Spectrometer for Studies of Flame Chemistry with a Synchrotron Light Source. *Rev. Sci. Instrum.* **2005,** *76*, 094102.
(12) Hansen, N.; Cool, T. A.; Westmoreland, P. R.; Kohse-Höinghaus, K. Recent Contributions of Flame-Sampling Molecular-Beam Mass Spectrometry to a Fundamental Understanding of Combustion Chemistry. *Prog. Energy Combust. Sci.* **2009,** *35*, 168-191.
(13) Moshammer, K.; Lucassen, A.; Togbé, C.; Kohse-Höinghaus, K.; Hansen, N. Formation of Oxygenated and Hydrocarbon Intermediates in Premixed Combustion of 2-Methylfuran. *Z. Phys. Chem.* **2015,** *229*, 507-528.
(14) Cao, C. The Link between the Ionization Potential and Heat of Formation for Organic Homologous Compounds. *J. Phys. Org. Chem.* **2007,** *20*, 636-642.
(15) Wang, H. Formation of Nascent Soot and Other Condensed-Phase Materials in Flames. *Proc. Combust. Inst.* **2011,** *33*, 41-67.
(16) Johansson, K. O.; Zádor, J.; Elvati, P.; Campbell, M. F.; Schrader, P. E.; Richards-Henderson, N. K.; Wilson, K. R.; Violi, A.; Michelsen, H. A. Critical Assessment of Photoionization Efficiency Measurements for Characterization of Soot-Precursor Species. *J. Phys. Chem. A* **2017,** *121*, 4475-4485.
(17) Johansson, K. O.; Campbell, M. F.; Elvati, P.; Schrader, P. E.; Zádor, J.; Richards-Henderson, N. K.; Wilson, K. R.; Violi, A.; Michelsen, H. A. Photoionization Efficiencies of Five Polycyclic Aromatic Hydrocarbons. *J. Phys. Chem. A* **2017,** *121*, 4447-4454.

V. Publications and submitted journal articles supported by this project 2016-2018

1. M. F. Campbell, P. E. Schrader, A. L. Catalano, K. O. Johansson, G. A. Bohlin, N. K. Richards-Henderson, C. J. Kliewer, and H. A. Michelsen, "A small porous-plug burner for studies of combustion chemistry and soot formation", *Rev. Sci. Instrum.* **88**, 125106 (2017).
2. K. O. Johansson, F. El Gabaly, P. E. Schrader, M. F. Campbell, and H. A. Michelsen, "Evolution of maturity levels of particle surface and bulk during soot growth and oxidation in a flame", *Aerosol Sci. Technol.* **51**, 1333-1344 (2017).
3. K. O. Johansson, M. F. Campbell, P. Elvati, P. E. Schrader, J. Zádor, N. K. Richards-Henderson, K. R. Wilson, A. Violi, and H. A. Michelsen, "Photoionization efficiencies of five polycyclic aromatic hydrocarbons", *J. Phys. Chem. A* **121**, 4447-4454 (2017).
4. K. O. Johansson, J. Zádor, P. Elvati, M. F. Campbell, P. E. Schrader, N. K. Richards-Henderson, K. R. Wilson, A. Violi, and H. A. Michelsen, "Critical assessment of photoionization efficiency measurements for characterization of soot-precursor species", *J. Phys. Chem. A* **121**, 4475-4485 (2017).
5. H. A. Michelsen, "Probing soot formation, chemical and physical evolution, and oxidation: A review of *in situ* diagnostic techniques and needs", *Proc. Combust. Inst.* **36**, 717-735 (2017).
6. K. O. Johansson, T. Dillstrom, P. Elvati, M. F. Campbell, P. E. Schrader, D. M. Popolan-Vaida, N. K Richards-Henderson, K. R. Wilson, A. Violi, and H. A. Michelsen, "Radical-radical reactions, pyrene nucleation, and incipient soot formation in combustion", *Proc. Combust. Inst.* **36**, 799-806 (2017).
7. M. F. Campbell, A. Bohlin, P. E. Schrader, R. P. Bambha, C. J. Kliewer, K. O. Johansson, and H. A. Michelsen, "Design and characterization of a linear Hencken-type burner", *Rev. Sci. Instrum.* **87**, 115114 (2016).
8. K. O. Johansson, T. Dillstrom, M. F. Campbell, M. Monti, F. El Gabaly, P. E. Schrader, D. M. Popolan-Vaida, N. K Richards-Henderson, K. R. Wilson, A. Violi, and H. A. Michelsen, "Formation and emission of large furans and oxygenated hydrocarbons from flames", *Proc. Natl. Acad. Sci. USA* **113**, 8374-8379 (2016).

Reaction Dynamics in Polyatomic Molecular Systems

William H. Miller

Department of Chemistry, University of California, and
Chemical Sciences Division, Lawrence Berkeley National Laboratory
Berkeley, California 94720-1460
millerwh@berkeley.edu

I. Program Scope

The goal of this program is the development of theoretical methods and models for describing the dynamics of chemical reactions, with specific interest for application to polyatomic molecular systems of special interest and relevance. There is interest in developing the most rigorous possible theoretical approaches and also in more approximate treatments that are more readily applicable to complex systems.

II. Recent Progress

Effort in earlier years focused on developing *semiclassical* (SC) theory[1-3] into a practical way for adding quantum mechanical effects to classical molecular dynamics (MD) simulations, which are so ubiquitously applied to all types of dynamical processes in complex molecular systems, e.g., chemical reactions in clusters, nano-structures, molecules on or in solids, bio-molecular systems, etc. More recently, however, we have been exploring how successful even simpler, *purely classical* MD approaches can be (with some judicious SC ideas incorporated), especially for the important case of *electronically non-adiabatic processes*, i.e., those which involve transitions between different electronic states. The two essential ingredients to the approach, (a) how are the electronic degrees of freedom described within a classical mechanics framework, and (b) how one identifies specific electronic states (initially and finally) within a classical picture.

The Meyer-Miller (MM) classical vibronic Hamiltonian[4] maps the electronic degrees of freedom (DOF) of a coupled electronic-nuclear system onto a set of classical harmonic oscillators, each oscillator representing the occupation of the various electronic states. Since the electronic as well as the nuclear DOF are thus described classically, a standard classical MD simulation treats these DOF and their interaction dynamically consistently (albeit at the level of classical mechanics). (If all these DOF were treated quantum mechanically, the MM Hamiltonian becomes a representation of the exact QM *operator* and would thus provide the exact QM vibronic dynamics.) In a recent series of papers, a symmetrical quasi-classical (SQC) windowing methodology[5] has been described and applied to the MM Hamiltonian in order to "quantize" these electronic DOF both initially and finally[6]. It was found that this approach provides a very reasonable description of non-adiabatic dynamics exhibited in a suite of standard benchmark model problems for which exact quantum mechanical (QM) results are available for comparison. Among the examples were systems exhibiting strong quantum coherence effects and systems representative of condensed-phase non-adiabatic dynamics, including some which other simple approaches have difficulty in describing

correctly (e.g., the asymmetric spin-boson problem[6] and the inverted regime in electron transfer processes[7]).

It was also discussed in these recent papers how various aspects of the SQC/MM model are appealing from a theoretical perspective[8]: e.g., it has a straightforward theoretical justification, and by providing an equivalent treatment of the electronic and the nuclear DOF (i.e., via classical mechanics) it is able to describe "quantum" coherence and de-coherence without resorting to any "add on's" to the theory. The (classical) time evolution of the nuclear and electronic DOF is continuous at all times (as it is QM'ly), and it gives equivalent results whether implemented in adiabatic or diabatic representations. It was also emphasized that though the equations of motion that result from the MM Hamiltonian are "Ehrenfest" — in that the force on the nuclei at any time is the coherent average of that over all electronic states — the fact that zero point energy is included in the electronic oscillators means that there is an ensemble of trajectories for each initial state (rather than only one trajectory as in the "Ehrenfest method" itself), and the population of each final electronic state is determined by the fraction of that ensemble that end up in that state. I.e., each trajectory in this ensemble contributes to only one final electronic state. The approach thus does not suffer from the well-known "Ehrenfest disease" of having all final electronic states determined by one (average) nuclear trajectory. As a result, the SQC method of quantizing the electronic DOF initially and finally leads to detailed balance being described correctly[9]. From a practical perspective, the SQC/MM is attractive since it is trajectory-based and can be straightforwardly incorporated within the framework of a standard classical MD simulation. One has only to add one vibrational-like DOF for each electronic state, which are propagated along with the (perhaps very many) nuclear DOF via Hamilton's equations that result from the MM Hamiltonian.

Further developments and extensions of the SQC/MM approach have been (1) to show that it can treat very weak electronic coupling[10] as well as it does strong coupling (which most examples treated by us and others have been), and (2) how off-diagonal elements of the electronic density matrix[11] can be obtained within the same ensemble of trajectories that gives the diagonal elements (i.e., the populations).

The most recent important development has to do with the adiabatic representation of the MM vibronic Hamiltonian. As noted above, it is completely equivalent to its diabatic version but will usually be more convenient in applications that use *ab initio* electronic structure calculations to produce the adiabatic (Born-Oppenheimer) potential energy surfaces and the derivative couplings between them. The classical equations of motion (EOM) generated by Hamilton's equations from the adiabatic version of the MM Hamiltonian include both first- and second-derivative coupling terms, in complete analogy to this situation quantum mechanically (i.e., with the Schroedinger equation). Since the second-derivative terms are considerably more difficult to obtain than the first-derivative coupling, the former are usually neglected; this is an approximation that sometimes entails negligible error but not always. It has been shown[12], however, that by replacing the canonical momentum variable by the *kinematic momentum* and writing the classical equations of motion (EOM) in terms of it, only first derivative coupling terms are involved. They have not been neglected, they simply do not appear in these modified EOM, which are not of Hamiltonian form yet are completely

equivalent to the canonical EOM (i.e., Hamilton's equations) which *do* involve the second-derivative coupling terms. This means that SQC/MM calculations can be carried out in the adiabatic representation, without approximation, needing only the first-derivative couplings between the Born-Oppenheimer potential energy surfaces.

Figures 1 and 2 below show the time-dependent electronic transition probabilities obtained from SQC/MM calculations for a variety of versions of the spin-boson model, i.e., 2 electronic states coupled to a (large) number of nuclear degrees of freedom (modeled as harmonic oscillators with a distribution of frequencies and equilibrium positions). Various parameter regimes (and temperatures of the nuclear 'bath') are shown. The black and blue curves—which coincide to numerical accuracy in all cases—are with using the original diabatic representation and the adiabatic representation with the modified EOM (involving the kinematic momentum), respectively, verifying that the latter introduces no approximation to the SQC/MM results (which are, incidentally, in very good agreement with exact QM results for these systems). The red curves are the results of using the adiabatic representation with the canonical EOM (i.e., Hamilton's equations) and neglecting the second-derivative couplings. In Figure 1 one sees that little error is caused by making this approximation, while Figure 2 shows that in other cases the error can be enormous; see ref 12 for further discussion of these results and the specific parameters of the spin-boson model for each figure.

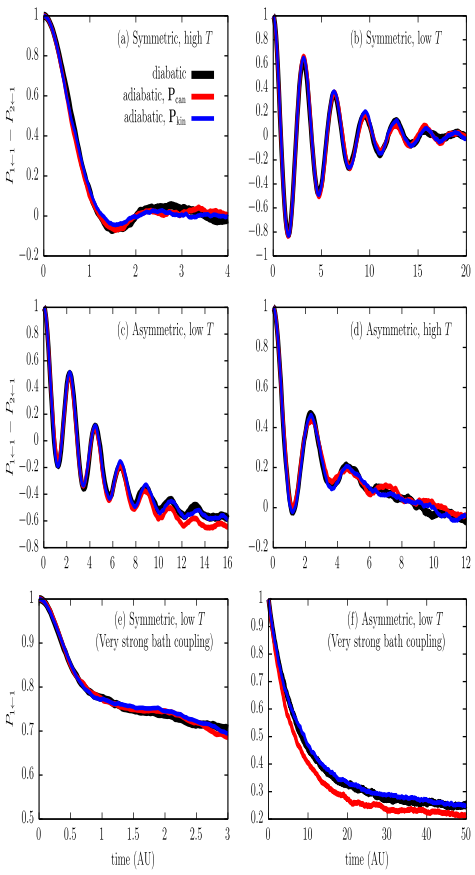

FIG. 1.

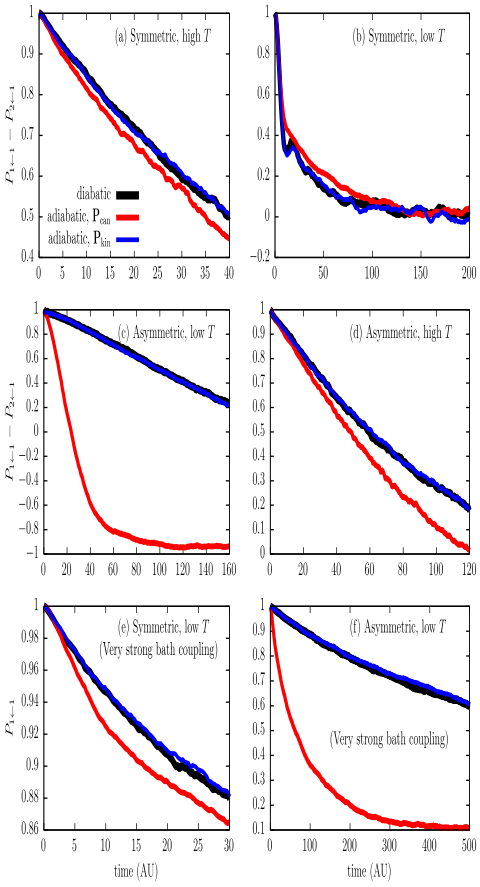

FIG. 2.

III. Future Plans

Since this quasi-classical model has proved quite reliable for describing electronically non-adiabatic dynamics in these simple model problems, work is in progress to extend its application to more general and complex non-adiabatic processes. A paper will soon be submitted, for example, applying the SQC/MM approach to ultrafast dynamics in a Frenkel site-exciton system involving 20 electronic states, with *ab initio* input for the potential energy surfaces.

References

1. For reviews, see W. H. Miller, Adv. Chem. Phys. **25**, 69-177 (1974); **30**, 77-136 (1975).
2. W. H. Miller, J. Chem. Phys. **53**, 1949-1959 (1970).
3. For reviews, see W. H. Miller, (a) J. Phys. Chem. A **105**, 2942-2955 (2001); (b) Proc. Natl. Acad. Sci. USA **102**, 6660-6664 (2005); (c) J. Chem. Phys. **125**, 132305.1-8 (2006).
4. H. D. Meyer and W. H. Miller, J. Chem. Phys. **71**, 2156-2169 (1979).
5. S. J. Cotton and W. H. Miller, J. Phys. Chem. A **117**, 7190-7194 (2013).
6. S. J. Cotton and W. H. Miller, J. Chem. Phys. **139**, 234112.1-9 (2013).
7. S. J. Cotton, K. Igumenshchev and W. H. Miller, J. Chem. Phys. **141**, 084104.1-14 (2014).
8. S. J. Cotton and W. H. Miller, J. Phys. Chem. A **119**, 12138-12145 (2015).
9. W. H. Miller and S. J. Cotton, J. Chem. Phys. **142**, 131103.1-3 (2015).
10. S. J. Cotton and W. H. Miller, J. Chem. Phys. **145**, 144108.1-16 (2016).
11. W. H. Miller and S. J. Cotton, J. Chem. Phys. **145**, 081101.1-4 (2016).
12. S. J. Cotton and W. H. Miller, J. Chem. Phys. **147**, 064112.1-10 (2017).

IV. 2015 - 2017 DOE Publications

1. W. H. Miller and S. J. Cotton, Communication: Note on Detailed Balance in Symmetrical Quasi-Classical Models for Electronically Non-Adiabatic Dynamics, J. Chem. Phys. **142**, 131103.1-3 (2015).
2. S. J. Cotton and W. H. Miller, A Symmetrical Quasi-Classical Spin-Mapping Model for the Electronic Degrees of Freedom in Non-Adiabatic Processes, J. Phys. Chem. A **119**, 12138-12145 (2015).
3. S. J. Cotton and W. H. Miller, The Symmetrical Quasi-Classical Model for Electronically Non-Adiabatic Processes Applied to Energy Transfer Dynamics in Site-Exciton Models of Light-Harvesting Complexes, J. Chem. Theory Comput. **12**, 983-991 (2016).
4. W. H. Miller and S. J. Cotton, Communication: Wigner Functions in Action-Angle Variables, Bohr-Sommerfeld Quantization, the Heisenberg Correspondence Principle, and a Symmetrical Quasi-Classical Approach to the Full Electronic Density Matrix, J. Chem. Phys. **145**, 081101.1-4 (2016).
5. S. J. Cotton and W. H. Miller, A New Symmetrical Quasi-Classical Model for Electronically Non-Adiabatic Processes: Application to the Case of Weak Non-Adiabatic Coupling, J. Chem. Phys. **145**, 144108.1-16 (2016).
6. W. H. Miller and S. J. Cotton, Classical Molecular Dynamics Simulation of Electronically Non-Adiabatic Processes, *Faraday Discuss.* **195**, 9-30 (2016).
7. S. J. Cotton and W. H. Miller, On the Adiabatic Representation of Meyer-Miller Electronic-Nuclear Dynamics, J. Chem. Phys. **147**, 064112.1-10 (2017).

Estimation and Analysis of Chemical Models

Habib N. Najm
Sandia National Laboratories
P.O. Box 969, MS 9051, Livermore, CA 94551
hnnajm@sandia.gov

I. Program Scope

The goal of this research program is to improve fundamental understanding of chemical models. The work involves: (1) Developing numerical methods for the efficient solution of chemical systems with elementary kinetics models, parallel codes for computing large scale chemical systems with detailed kinetics, and techniques for analysis of chemical system dynamics; (2) Developing numerical methods for uncertainty quantification (UQ) in chemical system computations; (3) Estimation of uncertain chemical model parameters; (4) Statistical methods for selection and validation of chemical models, based on experimental data; (5) UQ studies in computations of chemical systems; and (6) Computation and analysis of stochastic chemical systems. In the following, recent progress and future plans in these areas are discussed.

II. Recent Progress

A. Statistical Inference of Reaction Rate Coefficients

Development of the data-free inference (DFI) procedure, where Maximum Entropy (MaxEnt) and approximate Bayesian computation (ABC) methods are employed in the combustion chemical kinetic modeling context to enable Arrhenius parameter inference without direct access to data, has continued on multiple fronts. The algorithm has been extended to accommodate a variety of different statistics, which are typically reported in experiments designed to measure gas phase combustion reactions as, e.g. rate constants $k(T)$ values at different temperatures with attached error bars, Arrhenius parameters with error bars attached to both pre-exponential and activation energy, or to one and not the other, etc. When dealing with statistics in the form of $k(T)$ values the imposition of constraints on the data encompassing the entire experiment become decoupled, as these constraints are local to the particular temperature instances at which the experiment was performed, in which case we execute the algorithm in parallel across all temperatures, greatly accelerating the runtime of the data inference procedure. Given these different forms of reported statistics, we have investigated the quality of each of these types of reported statistics with respect to its sufficiency for enabling the reconstruction of representations of the missing data. We find that reporting statistics in the form of nominal (mean) $k(T)$ values and error bars (standard deviations), or as means and standard deviations on pre-exponentials and activation energies are both essentially sufficient for reconstructing consistent data. In fact it is only when information about the temperature variation of the uncertainty is lost, e.g. if the standard deviation of the activation energy is unreported, that the available information begins to become insufficient for recovering the missing correlations between Arrhenius parameters. As such we have found that the DFI procedure is quite robust to most forms of reported statistics available in the literature and can be applied immediately to the issue of missing or unreported data in the combustion literature.

The procedure has also been applied to a variety of additional reactions in the H_2-O_2 system, concentrating specifically on highly referenced experiments designed to measure critical chain reactions important to all hydrocarbon combustion processes such as: 1) H+O_2=OH+O, 2) H+H_2O=OH+H_2, 3) O+H_2=H+OH, and 4) O+H_2O=OH+OH. Particular attention has been given to reactions 1 & 2 as many combustion indicators such as homogeneous ignition delay times and laminar flame speeds are highly sensitive to the rates of these reactions, and also due to the practical experimental consideration that it is difficult to construct an experiment to measure reaction 1 without reaction 2 also being present to some degree, typically as a parasitic reaction consuming or producing H or OH atoms respectively when these are the typical target species whose concentration time history is being measured in the experiment. This reality is demonstrated in [B1] where consistent data is inferred using DFI for two separate experiments designed to measure reactions 1 & 2 respectively, and where the original data fitting performed by the experimentalists measuring reaction 1 used the result from experiment 2 to specify a nominal value of what they considered a parasitic reaction. Having generated ensembles of consistent data from both

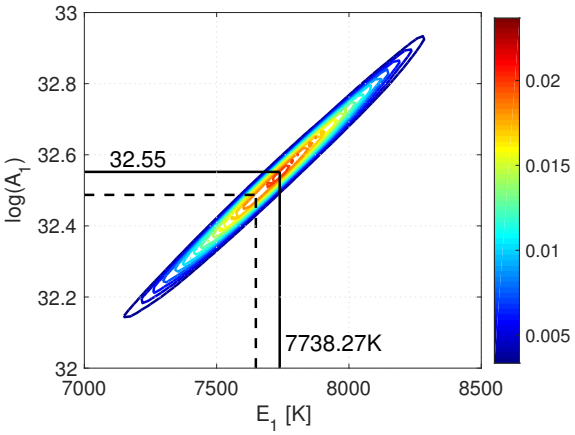

(a) Consensus marginal density of Arrhenius parameters for reaction 1 from combined learning. The maximum a posteriori estimates of the parameters are shown by the solid line, with the dashed line showing the results achieved using a separate learning approach.

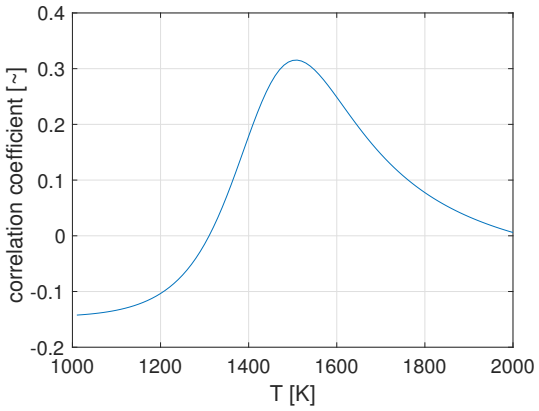

(b) Correlation coefficient between the rate constants of reactions 1 and 2 across the range of experiment temperatures.

Figure 1

experiments we refit both simultaneously in a combined learning setting (emulating the idea of the original experimentalists sharing their raw data before fitting model parameters), using Bayesian inference to construct a joint probability density on all the Arrhenius parameters across the two reactions. This joint probability density reveals the expected (but previously missing) strong correlation across the parameters within a reaction (see Fig. 1a) as well as the weaker, but still considerable, correlation between the parameters across reactions. This correlation (e.g. Fig. 1b) across reactions arises due to the fact that the data from both experiments (i.e. the concentration vs. time signals) is informative on reaction 2, which inexorably ties these two experiments together at the data level with subsequent consequences for resulting fitting efforts as we discovered. Furthermore, the most likely parameter estimates (maximum a posteriori estimates) of the parameters for both reactions are found to change when comparing a combined learning approach to a separate learning approach where we perform the fitting without combining the two datasets together, highlighting the bias introduced in the standard 'separate' fitting procedure where parasitic reactions are assigned nominal values by the experimentalists for fitting purposes. The reality that the data from a single experimental effort can inform the parameters of multiple reactions presents an interesting paradigm for learning, suggesting that redundant expensive experimental effort could have been avoided if the original data had been thoroughly analyzed in the first instance. Such analysis could be incorporated into an experimental design framework to determine what degree of further experimental expense is required to deliver a desired degree of uncertainty in the parameters.

This notion of bias introduction through the assumption of nominal values is also testable when operating in the data-centric framework presented by DFI. We extended the scope of the DFI procedure in [B1] with regards to the fitting of consistent data sets by recognizing that we are no longer tied to using the original fitting chemical mechanism employed by the experimentalists, and its accompanying assumptions, when they performed their data fitting. This original fitting mechanism choice is often an unavoidable source of bias, as almost every experimentalist whose data fitting context does not assume simple pseudo first-order kinetics (i.e. where the mechanism contains just a single reaction) typically use their own particular fitting mechanism with associated nominal parameter values of other reactions. We have extended our refitting of consistent hypothetical data sets to use arbitrary chemical mechanisms, whereby the original assumptions of the experimentalists (i.e. that only certain reactions are active in their experiment domain) can arise naturally if true. In particular for the H_2-O_2 system, we choose chemical mechanisms that are typically used in 'production' simulations such as direct numerical simulations (DNS) or large eddy simulations (LES) as our choice of fitting mechanism, with a view to establish a consistent data modeling strategy from the data fitting level right up to the predictive modeling level in order to avoid the introduction of bias.

Finally, the DFI procedure has been packaged into a generalized library suitable for application to missing data

problems where reported statistics and a known modeling framework can be specified to generate realizations of hypothetical missing data, and is being deployed in the Sandia Uncertainty Quantification Toolkit (UQTk).

B. Analysis and Reduction of Stochastic Chemical Systems

When the number of molecules of a chemical species within a volume of interest is small, $O(100)$, the accurate description of chemical processes requires the inclusion of stochastic effects. In this regime, chemical system dynamics are well represented using the chemical Langevin equation (CLE), a stochastic differential equation (SDE). In many systems of practical interest, the resulting CLE system is large and stiff, involving reaction rates spanning a wide range of time scales. While there are well-founded methods for dynamical analysis and reduction of ordinary differential equation systems, using computational singular perturbation (CSP) theory [1, 2], which have been used extensively for simplification of macroscale chemical system models, there is relatively little work done on analysis/reduction of SDEs by comparison.

In a previous report, we outlined our development and demonstration of a stochastic CSP (SCSP) method to address this challenge [B9]. The method involves an operator-split construction following similar CSP-based time integration for ODEs [3]. The method models the effect of fast time scales by projecting any initial condition toward the deterministic slow-manifold underlying the SDE, and forming the backbone of the basin of attraction for the stochastic motions. This is followed by explicit large time-step integration of the residual slow dynamics within the basin of attraction. This process is repeated for each time step. The net result is fast and stable explicit time integration of stiff SDEs. The method was outlined and demonstrated in [B9], using a model stiff SDE system, revealing significant computational savings.

In recent work, we extended the above SCSP time integration method to the full CLE. This pursuit resulted in significant additional complexity given the CLE noise term structure, and the multiplicity of Brownian motion source terms when dealing with multiple reactions. The resulting challenge required requisite algorithmic and code developments. We developed a general SCSP-CLE integration code, and applied it to a number of systems, including e.g. stochastic Michaelis-Menten kinetics. Preliminary results indicate that the approach works, providing requisite detection of exhausted modes, projection of the fast motions, and large time-step explicit time integration of slow dynamics in the attractive basin of the slow dynamics. While we have demonstrated the operation of the method, some challenges remain, having to do mainly with the eigensolution of the reaction term Jacobians. The current construction can lead, for some chemical systems, to defective Jacobian matrices, with consequent eigensolution challenges. This issue requires some reformulation, currently in progress, to avoid such matrices.

III. Future Plans

A. Random Walks on Manifolds

We rely on Bayesian inference methods for estimation of parameters in chemical models given experimental data. Similarly, we rely on Maximum Entropy (MaxEnt) inference for parameter estimation when given constraints, rather than actual data. In both cases, we rely on Markov Chain Monte Carlo (MCMC) methods for generating samples from the sought after posterior density on model parameters. MCMC can become a significant challenge when the region of large posterior measure is strongly concentrated on some lower-dimensional manifold in the given large-dimensional parameter space. Such manifolds arise naturally in the above outlined DFI context, where available information in the form of constraints inherently defines a manifold on which data samples must lie. They also arise in a general Bayesian inference procedure with actual data when the parameters are constrained, e.g. due to some necessary invariant in the system. For example, sampling to estimate a set of eigenvectors has to employ orthogonal samples by construction, in order to have any meaningul degree of computational efficiency. Similarly, given, say some analysis that identifies necessary manifolds where parameters to be inferred must lie, a sensible inference procedure ought to explore parameters that are, by construction, constrained to be on these manifolds. We find this situation quite often to be relevant. Hence, we plan to, going forward, explore the utilization of suitable methods for geodesic sampling on manifolds in the general context of constrained Bayesian inference for estimation of chemical model parameters. These methods rely on learning the geometry of the manifold, and, using the associated geodesic metric to provide effective random samples embedded in the manifold. We will explore this direction in both the Bayesian inference and MaxEnt contexts.

B. Stochastic Chemical Systems

In future work with stochastic chemical systems, we will enhance the robustness of the SCSP method by reformulating the construction so that we avoid defective Jacobian matrices. We are currently looking at alternate means of doing this. With this in place, we will be proceeding to empirical convergence studies and demonstrations of the effectiveness of the construction on a set of CLE models of varying degrees of difficulty. We will also explore means of providing useful Importance Index (II) results from the analysis of data bases of stochastic chemical system computations. The key utility of the II as commonly used in CSP analysis of ODE systems is the identification of cause and effect relationships within the coupled system dynamics, by identifying which reactions dominate the (slow/fast) time evolution of any given species. We expect to explore similar questions in the SDE context. This information will then be useful for eliminating unimportant reactions and species, providing simplified stochastic models that capture requisite observables with requested accuracy. Further, following recent developments, where we extended the CSP formulation from ODEs to differential algebraic equation (DAE) systems, we will explore the similar extension of SCSP from SDEs to SDAEs. These latter systems are expected to arise whenever algebraic constraints on chemical species concentrations are explicitly stated on top of the stated CLE equation system.

References

[1] S.H. Lam and D.A. Goussis. The CSP Method for Simplifying Kinetics. *International Journal of Chemical Kinetics*, 26:461–486, 1994.

[2] M. Valorani, F. Creta, F. Donato, H.N. Najm, and D.A. Goussis. Skeletal Mechanism Generation and Analysis for *n*-heptane with CSP. *Proc. Comb. Inst.*, 31:483–490, 2007.

[3] M. Valorani and D.A. Goussis. Explicit Time-Scale Splitting Algorithm For Stiff Problems: Auto-Ignition Of Gaseous-Mixtures Behind A Steady Shock. *J. Comput. Phys.*, 169:44–79, 2001.

BES-Supported Published/In-Press/Submitted Publications [2016-2018]

[B1] T. A. Casey and H.N. Najm. Estimating the joint distribution of rate parameters across multiple reactions in the absence of experimental data. *Proc. Combust. Inst.* in press.

[B2] L. Hakim, G. Lacaze, M. Khalil, H. Najm, and J. Oefelein. Modeling auto-ignition transients in reacting Diesel jets. *ASME J. Eng. Gas Turb. Power*, 138(11):112806–112806–8, 2016. Paper #: GTP-16-1054.

[B3] L. Hakim, G. Lacaze, M. Khalil, K. Sargsyan, H. Najm, and J. Oefelein. Probabilistic parameter estimation in a 2-step chemical kinetics model for n-dodecane jet autoignition. *Combustion Theory and Modeling*, 0(0):1–21, 2018.

[B4] M. Khalil, K. Chowdhary, C. Safta, K. Sargsyan, and H.N. Najm. Inference of reaction rate parameters based on summary statistics from experiments. *Proc. Comb. Inst.*, 36(1):699–708, 2017.

[B5] M. Khalil and H.N. Najm. Probabilistic Inference of Reaction Rate Parameters from Summary Statistics. *Combustion Theory and Modeling*. in press.

[B6] R. Malpica-Galassi, M. Valorani, H.N. Najm, C. Safta, M. Khalil, and P.P. Ciottoli. Chemical Model Reduction under Uncertainty. *Combustion and Flame*, 179:242–252, 2017.

[B7] C. Safta, M. Blaylock, J. Templeton, S. Domino, K. Sargsyan, and H. Najm. Uncertainty quantification in les of channel flow. *International Journal for Numerical Methods in Fluids*, 83:376–401, 2017.

[B8] K. Sargsyan, X. Huan, and H.N. Najm. Embedded model error representation for bayesian model calibration. *J. Comp. Phys.* submitted.

[B9] L. Wang, X. Han, Y. Cao, and H.N. Najm. Computational Singular Perturbation Analysis of Stochastic Chemical Systems with Stiffness. *J. Comput. Phys.*, 335:404–425, 2017.

Spectroscopy, Kinetics and Dynamics of Combustion Radicals
David. J. Nesbitt

Our research program involves experimental and theoretical study of transient chemical species relevant to fundamental combustion and atmospheric chemical processes. The work focuses on spectroscopy and unimolecular/bimolecular dynamics of highly reactive radical intermediates, combining i) high-resolution direct IR laser absorption methods with quantum shot noise limited detection, ii) high densities (10^{12}-10^{14} #/cm^3) of jet-cooled hydrocarbon radicals in slit supersonic discharge expansions, accompanied by iii) high-level *ab initio* potential surface and multidimensional quantum mechanics calculations. Key advantages of the slit discharge expansion techniques are i) generation of high concentrations of chemically reactive species yet ii) rapid subsequent cooling of these transient intermediates to $T_{rot} \approx 15$ K in a multipass geometry ideal for sub-Doppler laser absorption spectroscopy and quantum shot-noise limited detection sensitivity. Over the past year, our group has explored multiple jet-cooled transients via high-resolution IR laser spectroscopy, examples of which will be briefly discussed below.

A. Singlet Carbene Chemistry: Infrared Characterization of Jet-Cooled HCCl Diradical

The role of carbenes as kinetically important intermediates in a range of chemical processes has long been appreciated,[1,2] with motivations ranging from atmospheric chemistry to astrophysical modeling to understanding the coupling of electronic and vibrational degrees of freedom. Partially and fully halogenated methanes have extensive industrial applications, with deleterious contributions to ozone depletion and their usage restricted by international treaty. In the stratosphere, halomethanes are subject to photodissocation by solar ultraviolet (UV) radiation, generating halocarbenes and therefore playing a role in stratospheric chemistry and ozone depletion chemistry. Far beyond the terrestrial atmosphere, chlorohydrocarbon chemistry is believed to be relevant in interstellar molecular clouds.[3] It is therefore suspected that chlorocarbenes may prove to be a spectrally bright signature for more complex halo-organic chemistry and photochemistry in the interstellar medium. Theoretical interest in carbenes arises in part from its complex electronic configuration of two low-lying singlet states and one triplet state. This Renner-Teller interaction has been studied for multiple carbenes, in particular for methylene[4] and chlorocarbene.[5] For these species, the singlet-singlet electronic absorption bands are readily accessible with laser techniques, resulting in several laser-induced fluorescence (LIF) studies in the literature.[6-9] Remarkably, however, no high resolution infrared data has been available for gas phase HCCl in the ground electronic state.

Over the last year granting period, quantum shot noise limited infrared laser absorption methods have been used to explore the high-resolution rovibrational spectroscopy of jet cooled chlorocarbene (HCCl) diradical generated in a supersonic slit-jet discharge expansion, exploiting a Watson non-rigid asymmetric rotor Hamiltonian model to analyze the extensive, rotationally resolved absorption spectra on the C-H stretch ν_1 fundamental (see figure with sample Q branch).[10] Analysis of the near infrared data also reveals the additional presence of a bright combination band with one quantum of the H-C-Cl (ν_2) bend and two quanta of the (ν_3) C-Cl stretch. Rovibrational constants are obtained from least squares fits for each of the four excited vibrational states built

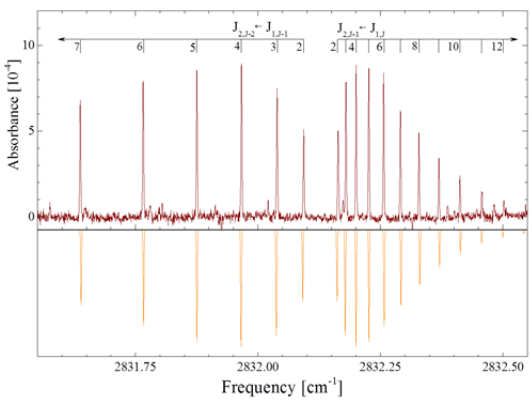

on the ν_1 fundamental and the (012) combination mode for each ^{35}Cl and ^{37}Cl atom isotopologue. IR transition intensity into these upper states arises from strong anharmonic mixing between the "bright" ν_1 C-H stretch and "dark" (012) H-C-Cl bend/C-Cl stretch combination modes, the deperturbation of which predicts a nearly equal mixture of the two zeroth order (100) and (012) harmonic states. Finally, ground state two-line combination differences are combined with previous laser-induced fluorescence results to predict rotational transitions for spectral searches into HCCl cosmochemistry in the interstellar medium.

B. Infrared Spectroscopy and *Ab Initio* Rovibrational Tunneling Dynamics of Benzyl Radical

The benzyl radical is a textbook example of resonantly stabilized, open shell organic species, with multiple "resonance structures" due to facile electron delocalization and rehybridization around the aromatic ring. Such resonant stabilization effects translate into an unusually low free energy, which in turn is responsible for making benzyl radical a relatively long-lived and therefore especially abundant transient intermediate in aromatic hydrocarbon chemistry. Systems of particular relevance are the combustion of fossil fuels, especially in the formation kinetics of polycyclic aromatic hydrocarbons (PAH) and, eventually, particulate soot.[11] Freshman chemistry teaches us that the unpaired radical center for benzyl can be localized on any of 3 locations: the CH_2 subunit (in two different Kekule structures) or on the one para- and two ortho- positions on the aromatic ring.[12] This leads to a total of five nearly equivalent structures describing the benzyl radical ground electronic state [13], whose additional uncertainty in the radical electron location results in resonance stabilization and imparts partial olefinic (sp^2) character to the nominally sp^3 hybridized toluyl CC bond. Such double bond character increases the barrier to internal rotation, thereby dramatically reducing the density of states for a given internal vibrational energy. This can therefore significantly impact the extent of intramolecular coupling of such hindered rotor states with other vibrational modes, and thus the time scale and/or high resolution spectral evidence for important unimolecular dynamics such as intramolecular vibrational redistribution (IVR).[14]

To help address these questions, we recently[15] obtained first gas phase high resolution spectra of highly reactive benzyl radicals generated by electron dissociative attachment to benzyl chloride doped in a neon-hydrogen-helium discharge and immediately cooled to T_{rot} = 15K in a high density, supersonic slit expansion environment. The sub-Doppler spectra are fit to an asymmetric-top rotational Hamiltonian, thereby yielding spectroscopic constants for the ground (v = 0) and CH stretch excited (ν_3, ν_4) vibrational levels of the ground electronic state. The rotational constants obtained for the ground state are in good agreement with previous laser induced fluorescence measurements (LIF), with vibrational band origins and in agreement with anharmonically corrected density functional theory calculations. To assist in detection of benzyl radical in the interstellar medium, we have also significantly improved the precision of the ground state rotational constants through combined analysis of the ground state IR and LIF combination differences. Of dynamical interest, there is no evidence in the sub-Doppler spectra for tunneling splittings due to internal rotation of the CH_2

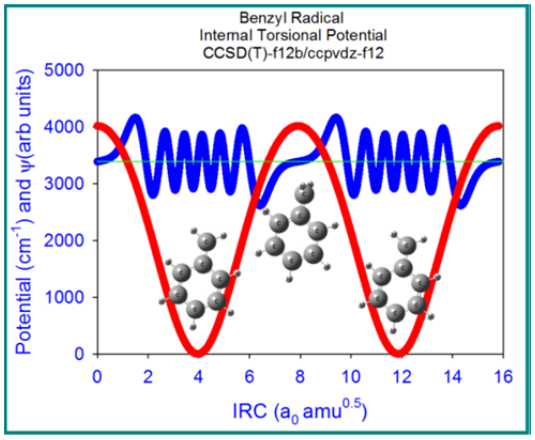

methylene subunit, which implies a significant rotational barrier consistent with partial double bond character in the CC bond. This is further confirmed with high level *ab initio* calculations at the CCSD(T)-f12b/ccpVdZ-f12 level, which predict a 11.45 kcal/mol zero-point energy corrected internal rotation barrier as indicated in the figure.

C. Infrared spectroscopy of Criegee intermediate precursors: CH_2 stretch vibrations and "charge-sloshing" dynamics in jet cooled CH_2I radical

Halogen substituted methyl species play significant roles in a range of atmospheric processes, ranging from alkene chemistry[16,17] to ozone depletion[18]. These species are also crucial in important technical applications, such as semiconductor device manufacturing[19], fire suppression and refrigeration.[20,21] The CH_2I radical has gained much recent attention as an important player in fundamental atmospheric and tropospheric chemistry, in particular, as an efficient precursor for formation of "Criegee intermediates" such as CH_2OO radical. The important class of transient radicals was first proposed in 1947 as an important collision complex in reactions between ozone and unsaturated hydrocarbons[22], but direct observation of these molecules was not reported until 2008.[23] In 2012 Welz et al. [24] provided evidence that they had generated the simplest Criegee intermediate using the following bimolecular displacement reaction: $CH_2I + O_2 \rightarrow CH_2OO + I$ and $CH_2O + IO$ with the CH_2I radical initially produced by UV photodissociation of CH_2I_2. These reactions are believed to represent important atmospheric pathways for producing highly reactive species that initiate catalytic ozone depletion, influence olefinic concentrations, and produce cyclic hydrocarbon compounds. Such iodine chemistry is particularly important in the marine boundary-layer environment, where methylene iodide (CH_2I_2) is generated by marine organisms, enters the atmosphere, and is quickly photodissociated by ultraviolet solar radiation into $CH_2I + I$. To date, however, there have been no reports of high resolution infrared spectroscopy for the CH_2I radical in the gas phase.

In this past year, the combination of a pulsed supersonic slit-discharge source and single-mode difference frequency direct absorption infrared spectroscopy have permitted first high resolution infrared study[25] of the iodomethyl (CH_2I) radical, with the CH_2I radical species generated in a slit jet Ne/He discharge and cooled to 16 K in the supersonic expansion. Dual beam detection and collisional collimation in the slit expansion yield sub-Doppler linewidths (60 MHz), an absolute frequency calibration of 16 MHz, and absorbance sensitivities within a factor of two of the shot-noise limit. Fully rovibrationally resolved direct absorption spectra of the CH_2 symmetric stretch mode (ν_2) are obtained and fitted to a Watson asymmetric top Hamiltonian with electron spin-rotation coupling, providing precision rotational constants and spin-rotation tensor elements for the vibrationally-excited state. Analysis of the asymmetric top rotational constants confirms a vibrationally averaged planar geometry in both the ground- and first-excited vibrational levels. Sub-Doppler resolution permits additional nuclear spin hyperfine structure to be observed, with splittings in excellent agreement with microwave measurements on the ground state. Spectroscopic data on CH_2I facilitate systematic comparison with previous studies of halogen-substituted methyl radicals, with the periodic trends

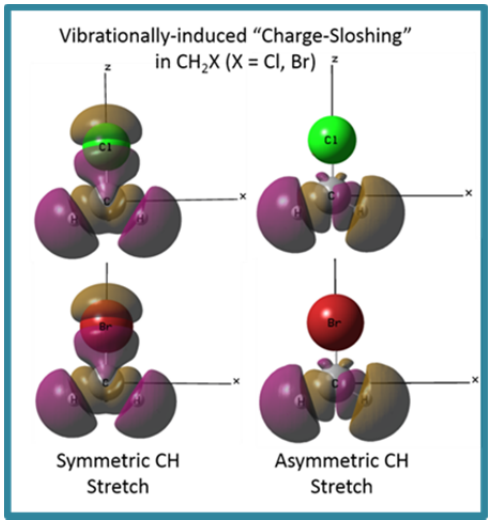

strongly correlated with electronegativity of the halogen atom. Interestingly, we do not observe any asymmetric CH_2 stretch transitions, despite S/N ≈ 25:1 on strongest lines in the corresponding symmetric CH_2 stretch manifold. This dramatic reversal of the more typical 3:1 antisymmetric/symmetric CH_2 stretch intensity ratio signals a vibrational transition moment poorly described by simple "bond-dipole" models. Instead, the data suggest this anomalous intensity ratio as arising from "charge sloshing" dynamics in the highly polar carbon-halogen bond, as supported by ab initio electron differential density plots and reminiscent of observations in other halomethyl radicals and protonated cluster ions.

[1] W. V. E. Doering, R. G. Buttery, R. G. Laughlin, and N. Chaudhuri, J. Am. Chem. Soc. **78** (13), 3224 (1956).
[2] D. B. Richardson, M. C. Simmons, and I. Dvoretzky, J. Am. Chem. Soc. **82** (18), 5001 (1960).
[3] G. A. Blake, V. G. Anicich, and W. T. Huntress, Astrophys. J. **300** (1), 415 (1986).
[4] G. Herzberg and J. W. C. Johns, Proc. Roy. Soc. London **295** (1441), 107 (1966).
[5] A. J. Merer and D. N. Travis, Can. J. Phys. **44** (3), 525 (1966).
[6] H. Petek, D. J. Nesbitt, D. C. Darwin, and C. B. Moore, J. Chem. Phys. **86** (3), 1172 (1987).
[7] W. H. Green, I. C. Chen, H. Bitto, D. R. Guyer, and C. B. Moore, J. Molec. Spectrosc. **138** (2), 614 (1989).
[8] B. C. Chang, M. Wu, G. E. Hall, and T. J. Sears, J. Chem. Phys. **101** (11), 9236 (1994).
[9] M. Kakimoto, S. Saito, and E. Hirota, J. Molec. Spectrosc. **97** (1), 194 (1983).
[10] A. Kortyna and D. J. Nesbitt, J. Chem. Phys. (to be submitted) (2018).
[11] A. Alexiou and A. Williams, Comb. Flame **104** (1-2), 51 (1996).
[12] R. T. Morrison and R. N. Boyd, *Organic Chemistry*. (Allyn and Bacon, Inc., Boston, 1979).
[13] L. Pauling and G. W. Wheland, J. Chem. Phys. **1** (6), 362 (1933).
[14] D. J. Nesbitt and R. W. Field, J. Phys. Chem. **100** (31), 12735 (1996).
[15] A. Kortyna, A. J. Samin, T. A. Miller, and D. J. Nesbitt, Phys. Chem. Chem. Phys. **19**, 29812 (2017).
[16] A. Saiz-Lopez, J. M. C. Plane, A. R. Baker, L. J. Carpenter, R. von Glasow, J. C. G. Martin, G. McFiggans, and R. W. Saunders, Chem. Rev. **112** (3), 1773 (2012).
[17] E. S. Foreman and C. Murray, J. Phys. Chem. A **119** (34), 8981 (2015).
[18] J. G. Calvert and S. E. Lindberg, Atmos. Env. **38** (30), 5087 (2004).
[19] *Handbook of Advanced Plasma Processing Techniques*. (Springer Verlag, Berlin, 2000).
[20] R. E. Tapscott, R. S. Sheinson, V. Babushok, M. R. Nyden, and R. G. Gann, in *NIST Technical Notes* (2001).
[21] J. Z. Su and A. K. Kim, Fire Tech. **38** (1), 7 (2002).
[22] R. Criegee and G. Wenner, Ann. Chem. Liebig **564** (1), 9 (1949).
[23] C. A. Taatjes, G. Meloni, T. M. Selby, A. J. Trevitt, D. L. Osborn, C. J. Percival, and D. E. Shallcross, J. Am. Chem. Soc. **130** (36), 11883 (2008).
[24] O. Welz, J. D. Savee, D. L. Osborn, S. S. Vasu, C. J. Percival, D. E. Shallcross, and C. A. Taatjes, Science **335** (6065), 204 (2012).
[25] A. Kortyna, D. M. B. Lesko, and D. J. Nesbitt, J. Chem. Phys. (submitted) (2018).

KINETICS, DYNAMICS, AND SPECTROSCOPY OF GAS PHASE CHEMISTRY

David L. Osborn
Combustion Research Facility, Mail Stop 9055, Sandia National Laboratories
Livermore, CA 94551-0969
dlosbor@sandia.gov

PROGRAM SCOPE

The goal of this program is to elucidate mechanisms of elementary chemical reactions through the use of multiplexed spectroscopy and mass spectrometry. We have developed a technique known as time-resolved multiplexed photoionization mass spectrometry (MPIMS), which is used to sensitively and selectively probe chemical reactions and reaction intermediates. This work is in collaboration with Sandia chemists Craig Taatjes, Leonid Sheps, and Judit Zádor, and a large group of scientists from other institutions in the US and abroad. The Sandia-designed MPIMS instrument utilizes tunable vacuum ultraviolet light from the Advanced Light Source (ALS) synchrotron at Lawrence Berkeley National Laboratory (LBNL) for sensitive, isomer-specific ionization of reactant and product molecules sampled from chemical reactions.

As a complementary approach, we also use Fourier transform spectroscopy (FTS), in both its continuous scanning and step-scan variants, to probe multiple species in chemical reactions. We have begun a new push to move photoelectron photoion coincidence spectroscopy past its roots in thermochemistry and ultrafast dynamics. Our innovations promise to make PEPICO a powerful tool for time-resolved probing of gas phase chemical reactions with superior performance in many areas compared to MPIMS.

RECENT PROGRESS

Isomer-resolved mass spectrometry

The multiplexed chemical kinetics photoionization mass spectrometer operates both at Sandia National Laboratories (using various discharge lamps to create vacuum ultraviolet radiation), and at the Chemical Dynamics Beamline of the ALS. The chemical reactor is based on the Gutman design, which allows the study of photodissociation and bimolecular reactions at pressures of 1 – 40 Torr and temperatures of 250 – 1000 K.

During the past 3-year period, we have applied this apparatus to a broad array of chemical problems. In addition to the work discussed below, we have studied reactions of Criegee intermediates with organic acids and NO_2, the reaction of OH radicals with CH_3OO and its relevance to tropospheric methanol, and the oxidation chemistry of cyclohexene and ethyl butyrate.

Photo-tautomerization of acetaldehyde to vinyl alcohol: a major source of formic acid over the open oceans

In previous work we have shown that excitation of the $S_1 \leftarrow S_0$ transition of acetaldehyde (CH_3CHO) causes photo-tautomerization to its less stable enol isomer vinyl alcohol (VA, $H_2C{=}CHOH$). Because of our longstanding interest in the fundamentals of isomerization dynamics, we have explored how photo-tautomerization depends on pressure and potential energy, measuring its yield in a bath gas of N_2 at up to 1 atm pressure, from λ = 300 – 330 nm. The observed pressure and wavelength dependence of VA yield is a sensitive probe of coupling between singlet and triplet electronic states, and collisional energy transfer dynamics. In addition to the fundamental photochemical knowledge gained, the observation that photo-tautomerization is relevant at atmospheric pressure raises the question of the fate of VA in Earth's atmosphere. Da

Silva and co-workers[1] predict, based on ab initio master equation calculations, that the OH + VA reaction creates formic acid, a critical molecule whose globally averaged concentration is 2 -3 times higher than predicted by atmospheric models. In collaboration with Dwayne Heard and Lisa Whalley of the University of Leeds, and Dylan Millet of the University of Minnesota, we have create a box model using detailed chemistry, and a global model using reduced chemistry to explore the potential impact of the formic acid created via this process. The results show that the addition of this chemistry provides a 7% increase to the global formic acid budget: significant, but not nearly enough to explain the discrepancies between observations and models of formic acid in the troposphere. However, to our surprise, the global model predicts that the VA generated by photo-tautomerization forms more than 50% of the formic acid over the open oceans. This previously unknown sink of acetaldehyde means that the sources of acetaldehyde over the open oceans must be substantially larger than current models suggest.

The absolute photoionization cross section of the OH radical

The hydroxyl (OH) radical has been extensively studied due to its importance in atmospheric and combustion[2] oxidation, and its presence in the interstellar medium.[3] As a second-row hydride, OH has served as an important benchmark for fundamental studies of electronic spectroscopy and structure. Photoionization of OH ($X\ ^2\Pi$) in the threshold region removes an electron from the valence ($2p\pi$) molecular orbital to form the ground electronic state of OH^+ ($X\ ^3\Sigma^-$), with a precisely known ionization energy of 13.0170 ± 0.0002 eV.[4] Both Dehmer and Cutler have reported high-resolution relative photoionization spectra,[5-6] but the absolute photoionization cross section has never been reported experimentally. Because of the increasing use of VUV photoionization for fundamental chemical reaction studies, we have used the $O(^1D) + H_2O$ reaction to generate OH radicals and, using a chemical kinetic model, determined their absolute concentration. Our theoretical colleagues Gozem and Krylov have used a new equation-of-motion coupled cluster Dyson orbital approach with a Coulomb wave description of the photoelectron wave function to predict the OH PI cross section. The agreement with our experiments is excellent. This approach is a relatively inexpensive method for computing photoionization cross sections, and if validated against experiment would be a major advance to predict PI cross sections of radicals and other reactive intermediates that are hard to characterize experimentally.

Radical thermometers and the photoelectron spectrum of the CH_3OO radical

The methyl peroxy radical is a key radical in both combustion and atmospheric chemistry. As a test of our new prototype Photoelectron Photoion Coincidence Spectrometer (PEPICO) that we built and tested at the Swiss Light Source Synchrotron, we have obtained the first photoelectron spectrum of the methyl peroxy radical. This project is a collaboration with Balint Sztaray (University of the Pacific), Andras Bodi (Paul Scherrer Institute), and Kent Ervin (University of Nevada, Reno). The radicals are created from photolysis of molecular chlorine in the presence of methane, which generates the methyl radical (CH_3). It reacts with excess O_2 at a pressure of 1.1 mbar to form the CH_3OO radical. There are several important results from this study. First, the predicted photoelectron spectrum via the Franck-Condon method treats the CH_3-OO torsional motion as a hindered rotor. This treatment is required because although the neutral and the ground state triplet cation have potential minimum in the staggered configuration, the low-lying singlet state cation has its minimum in the eclipsed configuration. Both states were used to extract our best estimate of the adiabatic ionization energy AIE(CH_3OO) = 10.265 ± 0.025 eV, with a triplet-singlet splitting of 0.15 eV.

Because we measure both electrons and cations in coincidence, in addition to the photoelectron spectrum we can also measure the onset of covalent bond breaking in the cation as the ionizing radiation energy is increased. The breakdown curve, which plots the decrease of parent ions and the increase in daughter ions as a function of photon energy, has good signal to noise: a quality that is unusual for ionization of open-shell neutral molecules. By modeling the breakdown diagram using an RRKM statistical model, we have measured a new heat of formation $\Delta_f H^{\circ}_{0K}$ (CH_3OO) = 22.06 ± 0.97 kJ mol^{-1}, reducing the uncertainty of the previously determined value by a factor of five. Finally, the comparison of the simulated to the experimental breakdown curve allows us to extract a CH_3OO temperature of 330 ± 30 K. This method demonstrates a "radical thermometer" that will be useful in future studies that generate reactive intermediates. There have been heated arguments in the past regarding whether radicals, produced for chemical kinetics studies by photodissociation, completely thermalize before they react. Our new PEPICO approach to measure radical temperatures will be useful both in the cases where one needs to ensure a thermally equilibrated radical temperature, and in cases where one wishes to study reactions of hot radicals.

Future Plans

Building on the advances we designed and tested in the prototype PEPICO spectrometer described above, in the next review period we will design and build the new CRF-PEPICO spectrometer for operation at Sandia and the Advanced Light Source. It will enable better molecular fingerprints to help resolve chemical reaction mechanisms that are beyond our capabilities at present. Among chemistry goals, we will pursue the investigation of how non-thermal reactant internal energy distributions affect chemical reaction mechanisms and outcomes. We will also attempt to synthesize precursors for several additional hydroperoxyalkyl isomers (QOOH), whose fundamental reactivity is still not sufficiently understood both in a fundamental and practical sense.

BES-sponsored publications, 2016 – present

1) Vacuum ultraviolet photoionization cross section of the hydroxyl radical, L. G. Dodson, J. D. Savee, S. Gozem, L. Shen, A. I. Krylov, C. A. Taatjes, D. L. Osborn, and M. Okumura, J. Chem. Phys. *submitted*.
2) Reactive removal of tropospheric carboxylic acids by Criegee Intermediates, R. Chhantyal-Pun, B. Rotavera, M. R. McGillen, M. A. H. Khan, A. J. Eskola, R. L. Caravan, L. Blacker, D. P. Tew, D. L. Osborn, C. J. Percival, C. A. Taatjes, D. E. Shallcross, and A. J. Orr-Ewing, Proc. Nat. Acad. Sci. *submitted*.
3) Photo-tautomerization of acetaldehyde as a photochemical source of formic acid in the troposphere, M. Shaw, B. Sztaray, L. K. Whalley, D. Heard, D. B. Millet, M. J. T. Jordan, D. L. Osborn, and S. H. Kable, Nat. Comm. *accepted*.
4) The reaction of OH with CH_3OO is not a major source of atmospheric methanol, R. L. Caravan, M. A. H. Khan, J. Zador, L. Sheps, I. O. Antonov, B. Rotavera, K. Ramasesha, K. Au, M. Chem, D. Roesch, D. L. Osborn, C. Fittschen, C. Schoemaecker, M. Duncianu, A. Grira, S. Dusanter, A. Tomas, C. J. Percival, D. E. Shallcross, and C. A. Taatjes, Nat. Chem *submitted*.
5) QOOH-mediated reactions in cyclohexene oxidation, A. L. Koritzke, J. C. Davis, R. L. Caravan, M. G. Christianson, D. L. Osborn, C. A. Taatjes, and B. Rotavera, Proc. Combust. Inst. *accepted*
6) Study of the low temperature chlorine atom initiated oxidation of methyl and ethyl butyrate using synchrotron photoionization TOF-mass spectrometry, J. Czekner, C. A. Taatjes, D. L. Osborn, and G. Meloni, Phys. Chem. Chem. Phys. **20**, 5785 (2018).
7) Radical Thermometers, Thermochemistry, and Photoelectron Spectra: A Photoelectron Photoion Coincidence Spectroscopy Study of the Methyl Peroxy Radical, K. Voronova, K. M. Ervin, K. G. Torma, P. Hemberger, A. Bodi, T. Gerber, D. L. Osborn, and B. Sztaray, J. Phys. Chem. Lett. **9**, 534 (2018).
8) Products of Criegee intermediate reactions with NO_2: experimental measurements and tropospheric implications, R. L. Caravan, M. A. H. Khan, B. Rotavera, E. Papajak, I. O. Antonov, M. W. Chen, K. Au,

W. Chao, D. L. Osborn, J.J.M. Lin, C. J. Percival, D. E. Shallcross, and C. A. Taatjes, Faraday Discussions **200**, 313 (2017).

9) The reaction of Criegee intermediate CH_2OO with water dimer: primary products and atmospheric impact, L. Sheps, B. Rotavera, A. J. Eskola, D. L. Osborn, C. A. Taatjes, K. Au, D. E. Shallcross, M. A. H. Khan, and C. J. Percival, Phys. Chem. Chem. Phys. **19**, 21970 (2017).
10) Time-resolved measurements of product formation in the low-temperature (550 – 675 K) oxidation of neopentane: a probe to investigate chain-branching mechansim, A. J. Eskola, I. O. Antonov, L. Sheps, J. D. Savee, D. L. Osborn, and C. A. Taatjes, Phys. Chem. Chem. Phys. **21**, 13731 (2017).
11) CRF-PEPICO: Double velocity map imaging photoelectron photoion coincidence spectroscopy for reaction kinetics studies, B. Sztaray, K. Voronova, K. G. Torma, K. J. Covert, A. Bodi, P. Hemberger, T. Gerber, and D. L. Osborn, J. Chem. Phys. **147**, 013944 (2017).
12) Infrared spectra of gas-phase 1- and 2-propenol isomers, M. F. Shaw, D. L. Osborn, M. J. T. Jordan, and S. H. Kable, J. Phys. Chem. A **121**, 3679 (2017).
13) Reactions of atomic carbon with butene isomers: implications for molecular growth in carbon-rich environments, J. Bourgalais, M. Spencer, D. L. Osborn, F. Goulay, S. D. Le Picard, J. Phys. Chem. A **120**, 9138 (2016).
14) Direct measurements of unimolecular and bimolecular reaction kinetics of the Criegee intermediate $(CH_3)_2COO$, R. Chhantyal-Pun, O. Welz, J. D. Savee, A. J. Eskola, E. P. F. Lee, L. Blacker, H. Hill, M. Ashcroft, M. A. Khan, G. Lloyd-Jones, L. Evans, B. Rotavera, H. Huang, D. L. Osborn, D. Mok, J. M. Dyke, D. E. Shallcross, C. Percival, A. J. Orr-Ewing, and C. A. Taatjes, J. Phys. Chem. A **121**, 4 (2017).
15) Hydroxyacetone production from C_3 Criegee intermediates, C. A. Taatjes, F. Liu, B. Rotavera, M. Kumar, R. L. Caravan, D. L. Osborn, W. H. Thompson, M. I. Lester, J. Phys. Chem. A **121**, 16 (2017).
16) Resonance stabilization effects on ketone autoxidationn: isomer-specific cyclic ether and ketohydroperoxide formation in the low-temperature (400 – 625 K) oxidation of diethyl ketone, A. M. Scheer, A. J. Eskola, D. L. Osborn, L. Sheps, C. A. Taatjes, J. Phys. Chem. A **120**, 8625 (2016)
17) Laser-driven hydrothermal process studied with excimer laser pulses, R. Mariella Jr., A. Rubenchik, E. Fong, M. Norton, W. Hollingsworth, J. Clarkson, H. Johnsen, and D. L. Osborn, J. Appl. Phys. **122**, 075104 (2017).
18) Reaction mechanisms on multiwell potential energy surfaces in combustion (and atmospheric) chemistry, D. L. Osborn, Ann. Rev. Phys. Chem. **68**, 233 (2017).
19) Breaking through the false coincidence barrier in electron-ion coincidence experiments, D. L. Osborn, C. C. Hayden, P. Hemberger, A. Bodi, K. Voronova, and B. Sztaray, J. Chem. Phys. **145**, 164202 (2016).
20) Pressure-dependent competition among reaction pathways from first- and second-O_2 additions in the low-temperature oxidation of tetrahydrofuran, I. O. Antonov, J. Zador, B. Rotavera, E. Papajak, D. L. Osborn, C. A. Taatjes, and L. Sheps, J. Phys. Chem. A **120**, 6582 (2016).
21) Influence of oxygenation in cyclic hydrocarbons on chain-termination reactions from R + O_2: tetrahydropyran and cyclohexane, B. Rotavera, J. D. Savee, I. O. Antonov, R. L. Caravan, L. Sheps, D. L. Osborn, J. Zador, and C. A. Taatjes, Proc. Combust. Inst. **36**, 597 (2017).
22) Formation and stability of gas-phase o-benzoquinone from oxidation of ortho-hydroxyphenyl: a combined neutral and distonic radical study, M. B. Prendergast, B. B. Kirk, J. D. Savee, D. L. Osborn, C. A. Taatjes, K. S. Masters, S. J. Blanksby, G. da Silva, A. J. Trevitt, Phys. Chem. Chem. Phys. **18**, 4320 (2016).
23) Low temperature chlorine-initiated oxidation of small-chain methyl esters: quantification of chain-terminating HO_2-elimination channels, G. Muller, A. Scheer, D. L. Osborn, C. A. Taatjes, and G. Meloni, J. Phys. Chem. A 120, 1677 (2016).

References Cited

1. So, S.; Wille, U.; da Silva, G., Atmospheric Chemistry of Enols: A Theoretical Study of the Vinyl Alcohol + OH + O-2 Reaction Mechanism. *Environ. Sci. Technol.* **2014,** *48* (12), 6694-6701.
2. Miller, J. A.; Pilling, M. J.; Troe, J., Unravelling Combustion Mechanisms Through a Quantitative Understanding of Elementary Reactions. *Proc. Combust. Inst.* **2005,** *30* (1), 43-88.
3. Weinreb, S.; Barrett, A. H.; Meeks, M. L.; Henry, J. C., Radio Observations of OH in the Interstellar Medium. *Nature* **1963,** *200* (4909), 829-831.
4. Wiedmann, R. T.; Tonkyn, R. G.; White, M. G.; Wang, K.; McKoy, V., Rotationally Resolved Threshold Photoelectron Spectra of OH and OD. *J. Chem. Phys.* **1992,** *97* (2), 768-772.
5. Dehmer, P. M., Photoionization of OH in the Region 750–950 Å. *Chem. Phys. Lett.* **1984,** *110* (1), 79-84.
6. Cutler, J. N.; He, Z. X.; Samson, J. A. R., Relative Photoionization Cross Section Study of OH and OD from 68 nm to 95 nm. *J. Phys. B: At. Mol. Opt. Phys.* **1995,** *28* (21), 4577.

Chemical Kinetic Modeling of Combustion Chemistry

William J. Pitz, Charles K. Westbrook
Lawrence Livermore National Laboratory, Livermore, CA 94550
pitz1@llnl.gov

1. Program Scope

We develop chemical kinetic reaction models to describe the combustion of hydrocarbons and other related fuels, including bio-derived fuels. These models are validated through comparisons between simulations and experimental results in carefully controlled laboratory-scale facilities including shock tubes, stirred reactors, and rapid compression machines. After validation, these models are then used to understand more complex combustion phenomena in practical engines and other combustion systems. We identify particularly sensitive parts of these models and provide that information to other DOE/BES researchers who can use theory and new experiments to refine the kinetic models. We try to anticipate kinetic modeling needs of the DOE combustion community, so other researchers can have accurate models to assist in their own research projects. Our kinetic models are freely available at https://combustion.llnl.gov/ and provide a valuable service to the combustion community.

2. Recent Progress

Our work has focused on developing and improving the chemical kinetic models of transportation fuels. These kinetic models use fuel-component surrogate mixtures to represent the properties of complex gasoline and diesel fuels. We also develop kinetic models for new bio-derived fuels with properties that are attractive for blending into gasoline and diesel fuels.

A. Development and validation of new kinetic models for bio-derived fuels

We have developed chemical kinetic models for two new types of fuels that could be derived from biomass and provide attractive ignition and flame-speed properties for blending into gasoline. These are cyclopentanone and methyl- & ethyl- acetates. In the case of methyl- and ethyl- acetates, a chemical kinetic model to describe their pyrolysis and oxidation was assembled. For the H-abstraction reactions from methyl acetate, most of the reaction rates were previously measured or computed fundamentally in the literature. However, for ethyl acetate, only H-atom abstractions by H and HO_2 were available. We collaborated with Cavallotti and Klippenstein who used new tools they developed at ANL to calculate OH and HO_2 reaction rates with methyl- and ethyl-acetate. One tool is EStokTP, a new code for automatically implementing *ab initio* TST analyses from a simple specification of reactants and methods. Other reaction rate constants for methyl and ethyl acetate were mostly available from fundamental measurements or *ab initio* calculations in the literature, including molecular decompositions of the fuel, H atom abstraction rates for the fuel, and fuel radical decomposition rates. To validate and improve the model, we also collaborated with Curran's group at NUIG who performed shock tube experiments to obtain ignition delay times, Sarathy's group at KAUST who performed jet-stirred reactor experiments to obtain intermediate species concentrations, and Konnov's group at Lund University who conducted

laminar flame speed measurements. The validated and improved chemical kinetic model for the two selected acetates shows generally good agreement with the experimental data.

A detailed chemical kinetic model for cyclopentanone was also developed and validated. The development of the model was facilitated by previous fundamental, experimental, and theoretical studies of cyclopentanone. Sheer et al. at SNL investigated cyclopentanone in a flow reactor at the Advanced Light Source and identified the main low temperature reaction paths. Fundamental rate constant calculations were available in the literature on the unimolecular decomposition of cyclopentanone and its H-atom abstraction reactions by the most relevant radicals. Fundamentally obtained rate constants for the low temperature reaction of cyclopentanone radicals were not available in the literature and we collaborated with Green's group at MIT concerning these reaction rates. Calculations were performed at MIT on the HO_2 elimination rate constant from fuel peroxy radicals which was considered a critical pathway by Sheer et al. Further calculations by MIT of the low temperature reactions of cyclopentanone are planned. To validate the chemical kinetic model for ignition delay at high-pressure conditions in internal combustion engine, experiments were performed in a shock tube and a rapid compression machine by Curran's group at NUIG. To provide further validation of the evolution of intermediate species, laser absorption experiments in a shock tube were performed by Vasu's group at University of Central Florida (UCF). The validated kinetic model simulates well the ignition of cyclopentanone for the shock tube and RCM data measured at NUIG. It also simulates the CO species histories measured in the UCF shock tube at high pressures, but some improvement is needed at atmospheric pressure.

Both the alkyl-acetates and cyclopentanone kinetic models were incorporated into to the LLNL gasoline surrogate model so that the complex behavior of these biofuel components could be predicted when they are blended into gasoline fuels. Prediction of their blending behavior was enabled by fundamentally-determined rate constants from experiments and from *ab initio* calculations.

B. New reaction rate-constant rules for alkanes

Reaction rate-constant rules for different types of reaction classes allow the development of chemical kinetic models for a multitude of fuels without having to measure or calculate rate constants for each specific case. Reaction rate rules also ensure consistency in rate constant expressions for each reaction class (e.g. H-atom abstraction, etc.). This approach has been used successfully for the last ~ 20 years in kinetic models. We are developing new reaction rate-constant expression rules based on fundamentally-determined rate constants for use in kinetic models of n-alkanes and iso-alkanes to allow more accurate description of their ignition and oxidation behavior. The goal is to use these new rules to simulate accurately the behavior of a whole series of alkanes from ~C5 to ~C16. We have been focusing particularly on reaction rate rules for low temperature chemistry that controls the autoignition of alkanes. In developing these rules for low temperature chemistry, we collaborated with Curran's group at NUIG. We examined *ab initio* rate constants computed by three university teams, Green's group at MIT, Dean's group at Colorado School of Mines and Miyoshi at University Tokyo. These groups were chosen because

they all computed *ab initio* low temperature rate constants for large alkanes. Although these research groups have carried out systematic calculations of the reaction rates in low temperature chemistry, our collaborative work found that solely relying on rate constants from a single source to specify the reaction rate rules of all the reaction classes did not necessarily lead to satisfactory predictions. Instead, better performance of kinetic models was often achieved by relying on multiple sources of rate constants to specify the reaction rate rules[1]. For example in our current work, the rate constant rules for the $R + O_2 = RO_2$ reaction class was chosen from Miyoshi and for the RO_2 = alkene + HO_2 molecular elimination reaction class was chosen from Villano et al. (Dean's group). We have now developed preliminary reaction rate rules for n-alkanes and iso-alkanes that are able to more accurately simulate their autoignition and oxidation behavior over a wider range of conditions than previously possible.

C. Evolution of kinetic reaction mechanisms

Westbrook has recently written a paper with LLNL co-authors on the co-evolution of kinetic reaction mechanisms and application of these models to simulate practical, real engines. This paper was recently published as a perspective in a themed collection on "Kinetics in the Real World " in PCCP. The paper tracks the historical progress from early kinetic models for small molecules to later kinetic models for larger molecules that can be applied to much more complex problems. The paper notes recent emergence of very large multi-fuel surrogate kinetic mechanisms that has allowed many different fuel types to be addressed in real engine applications. To illustrate this point, simulations from the LLNL multi-fuel kinetics surrogate model are reported that simulate relatively accurately the ignition behavior of many single component fuels and fuel blends in terms of the standard fuel-octane properties of MON and RON.

3. Future Plans

In the future, we plan to continue our development of chemical kinetic models for bio-derived fuels that have attractive properties for blending into gasoline and diesel fuel components. We also will continue our work on the development of accurate reaction-rate rules for the low temperature chemistry of alkanes by examining the heptane isomers. We will work toward extending our reaction-rate rule development to include alkenes, cyclic alkanes and their derivatives.

Acknowledgements

This work was performed under the auspices of the U.S. Department of Energy by Lawrence Livermore National Laboratory under Contract DE-AC52-07NA27344.

References

1. J. Bugler, K. P. Somers, E. J. Silke and H. J. Curran, "Revisiting the Kinetics and Thermodynamics of the Low-Temperature Oxidation Pathways of Alkanes: A Case Study of the Three Pentane Isomers," J. Phys. Chem. A 119, 7510-7527 (2015.

Published papers in 2016 to 2018

1. Westbrook, C. K., Mehl, M., Pitz, W. J., Kukkadapu, G., Wagnon, S. and Zhang, K., "Multi-Fuel Surrogate Chemical Kinetic Mechanisms for Real World Applications," Physical Chemistry Chemical Physics (2018). http://dx.doi.org/10.1039/C7CP07901J
2. K. Zhang, N. Lokachari, E. Ninnemann, S. Khanniche, W. H. Green, H. J. Curran, S. Vasu, S. Kim and W. J. Pitz, "An experimental, theoretical, and modeling study of the ignition behavior of cyclopentanone," 37th Inter. Symp. Combustion, accepted (2018).
3. A. Ahmed, W. J. Pitz, C. Cavallotti, M. Mehl, N. Lokachari, E. J. K. Nilsson, J.-Y. Wang, A. A. Konnov, S. W. Wagnon, B. Chen, Z. Wang, H. J. Curran, S. J. Klippenstein, W. L. Roberts and S. M. Sarathy, "Small Ester Combustion Chemistry: Computational Kinetics and Experimental Study of Methyl Acetate and Ethyl Acetate," 37th Inter. Symp. Combustion, accepted (2018).
4. S. W. Wagnon, S. Thion, E. J. K. Nilsson, M. Mehl, Z. Serinyel, K. Zhang, P. Dagaut, A. A. Konnov, G. Dayma and W. J. Pitz, "Experimental and modeling studies of a biofuel surrogate compound: laminar burning velocities and jet-stirred reactor measurements of anisole," Combust. Flame 189, 325-336 (2018).
5. G. Kukkadapu, D. Kang, S. W. Wagnon, K. Zhang, M. Mehl, M. M. Palaciosc, H. Wang, S. S. Goldsborough, C. K. Westbrook and W. J. Pitz, "Kinetic modeling study of surrogate components for gasoline, jet and diesel fuels: C7-C11 methylated aromatics," Proc. Combust. Inst., accepted (2018).
6. Westbrook, C. K., Sjöberg, M. and Cernansky, N. P., "New Chemical Kinetic Method of Determining RON and MON Values for Single Component and Multicomponent Mixtures of Engine Fuels," Combust. Flame (2018), In press.
7. Westbrook, C. K., Mehl, M., Pitz, W. J. and Sjöberg, M., "Chemical Kinetics of Octane Sensitivity in a Spark-Ignition Engine," Combustion and Flame 175 (2017) 2-15.
8. Fridlyand, A., Johnson, M. S., Goldsborough, S. S., West, R. H., McNenly, M. J., Mehl, M. and Pitz, W. J., "The Role of Correlations in Uncertainty Quantification of Transportation Relevant Fuel Models," Combustion and Flame (2017).
9. Zhang, Y., Somers, K. P., Mehl, M., Pitz, W. J., Cracknell, R. F. and Curran, H. J., "Probing the Antagonistic Effect of Toluene as a Component in Surrogate Fuel Models at Low Temperatures and High Pressures. A Case Study of Toluene/Dimethyl Ether Mixtures," Proceedings of the Combustion Institute 36 (1) (2017) 413–421.
10. Sun, W., Wang, G., Li, S., Zhang, R., Yang, B., Yang, J., Li, Y., Westbrook, C. K. and Law, C. K., "Speciation and the Laminar Burning Velocities of Poly(Oxymethylene) Dimethyl Ether 3 ($POMDME_3$) Flames: An Experimental and Modeling Study," Proceedings of the Combustion Institute 36 (1) (2017) 1269-1278.
11. Al Rashidi, M. J. A., Thion, S., Togbé, C., Dayma, G., Mehl, M., Dagaut, P., Pitz, W. J., Zádor, J. and Sarathy, S. M., "Elucidating Reactivity Regimes in Cyclopentane Oxidation: Jet Stirred Reactor Experiments, Computational Chemistry, and Kinetic Modeling," Proceedings of The Combustion Institute Volume 36, Issue 1, 2017, Pages 469–477.
12. Atef, N., Kukkadapu, G., Mohamed, S. Y., Rashidi, M. A., Banyon, C., Mehl, M., Heufer, K. A., Nasir, E. F., Alfazazi, A., Das, A. K., Westbrook, C. K., Pitz, W. J., Lu, T., Farooq, A., Sung, C.-J., Curran, H. J. and Sarathy, S. M., "A Comprehensive Iso-Octane Combustion Model with Improved Thermochemistry and Chemical Kinetics," Combustion and Flame 178 (2017) 111-134.
13. Zhou, C.-W., Simmie, J. M., Pitz, W. J. and Curran, H. J., "Towards the Development of a Fundamentally-Based Chemical Model for Cyclopentanone: High Pressure Limit Rate Constants for H-Atom Abstraction and Fuel Radical Decomposition," Journal of Physical Chemistry A 120 (36) (2016) 7037-7044.
14. Sun, W., Yang, B., Hansen, N., Westbrook, C. K., Zhang, F., Wang, G., Moshammer, K. and Law, C. K., "An Experimental and Kinetic Modeling Study on Dimethyl Carbonate (DMC) Pyrolysis and Combustion," Combustion and Flame 164 (2016) 224–238.

INVESTIGATION OF NON-PREMIXED TURBULENT COMBUSTION

Grant: DE-FG02-90ER14128

Stephen B. Pope & Perrine Pepiot
Sibley School of Mechanical & Aerospace Engineering
Cornell University, Ithaca, NY 14853
s.b.pope@cornell.edu, pp427@cornell.edu

1 Scope of the Research Program

The underlying theme of this work is the development of computational approaches which allow our detailed knowledge of the chemical kinetics of combustion to be applied to the modeling and simulation of combustion devices. The principal modeling approaches used are large-eddy simulation (LES) to describe the flow and turbulence, and particle-based probability density function (PDF) methods to treat the turbulence-chemistry interactions. Research is currently focused on the validation and optimization of a pre-partitioned adaptive chemistry (PPAC) approach for use in LES-PDF simulations, in which individual particles evolve according to an adaptively chosen reduced set of kinetic equations tailored for their specific compositions. The main objective is to significantly reduce both the time and memory required for a computation with a given kinetic mechanism, and enable affordable computations with significantly more detailed chemistry descriptions. A related objective is the adequate consideration of the chemistry associated with pollutant formation from complex fuel combustion, especially soot precursors formation.

2 Recent Progress - An Adaptive Methodology to Implement Detailed Chemistry in LES/PDF

Development of a combined PPAC-RCCE-ISAT methodology for efficient implementation of combustion chemistry for particle PDF methods. A key focus during this period has been enhancing the initially proposed PPAC framework [3] by combining it with a storage retrieval technique (ISAT) and a dimension reduction method (RCCE) which leads to the twin benefits of avoiding redundant direct integrations and drastically reducing the number of variables that need to retained at runtime during the computation.

- PPAC-ISAT: The performance of ISAT is known to degrade significantly when the number of species exceeds 50. Consequently, invoking ISAT on reduced model, as is done in PPAC-ISAT, is highly desirable instead of calling ISAT directly on a large detailed mechanism. Additionally, PPAC-ISAT leads to ISAT sampling a smaller portion of the accessed region of composition space. This leads to an increased retrieve fraction (seen to be 8-10% higher in our tests) and smaller query time for the individual tables. We found that the overall incurred error in the adaptive simulation is controlled according to the specified error tolerance (10^{-4}). For an incurred error of approximately 10^{-4} in temperature, the query time for PPAC-ISAT is 50% of the query time observed when ISAT is called using the detailed mechanism.
- PPAC-RCCE: A distinguishing feature of the PPAC framework is that it leads to a reduction in both CPU time and storage requirements as opposed to on-the-fly approaches that leads

to CPU savings only. The savings in storage requirements are significantly enhanced by combining PPAC with RCCE. We found that the combined PPAC-RCCE method reduces the number of active variables to approximately 50% of those needed by PPAC while maintaining approximately the same incurred error.

- PPAC-RCCE-ISAT: It is important note that though the PPAC-RCCE coupling leads to significant reduction in storage requirements, the CPU time is approximately the same as PPAC, since the integration is performed with the same reduced models utilized in PPAC. A combined PPAC-RCCE-ISAT methodology leads to significantly enhanced savings in both CPU time (by retrieving from an ISAT table whenever possible) and storage requirement (by carrying only represented species and elements needed for RCCE) compared to initially proposed PPAC implementation.

Adequacy of PaSR-derived sampling database for turbulent flames. The starting point for the PPAC methodology is the creation of a database in the preprocessing stage which approximates the accessed region of the composition space in the adaptive simulation. We are exploring the possibility of generating this database using PaSR with parameters designed to emulate the adaptive turbulent combustion simulation. To gauge the adequacy of a PaSR-derived database to approximate the accessed region of composition space in turbulent flames, we are utilizing compositions obtained from DNS of a temporal jet flame [1] and from DNS of a lifted ethylene flame [2]. The compositions obtained from these DNS databases are compared to compositions collected from PaSR runs with parameters chosen to emulate the DNS configurations. The comparison between compositions obtained from different sets in high dimensional composition space is performed by using ISAT. Specifically, we build an ISAT table using compositions for each set of compositions. This is followed by examining the fraction of compositions that can be retrieved in the second set using the ISAT table built on the first set and vice-a-versa. This approach reveals the commonality as well differences in the two sets of compositions, from which guidelines are being constructed in order to better condition the PPAC approach (Fig. 1).

3 Future Plans

The work in the near future will focus on the development of an error-controlled PPAC methodology for efficient implementation of combustion chemistry. We note that the originally proposed PPAC method lacks error-checking and control. This implies that the accuracy at runtime can be guaranteed if and only if the database used for generating reduced models is exactly similar to the compositions encountered at runtime. This restricts the broader applicability of the method and consequently there is an important need to integrate an error-control into the existing PPAC framework. The development of such an improved algorithm will be the main focus of our research in the upcoming reporting period. A key insight towards attaining full error control is to note that the collection of reduced models derived in the preprocessing stage of PPAC are certain to be valid (in accordance with the specified error tolerance) on the region of the composition space accessed by the database used to create them. Additionally, we note that, a computationally inexpensive method for gauging whether an encountered composition is within the accessed region of an existing database has already been developed using ISAT. Hence, a simple extension to make the original implementation of PPAC error controlled, is to add an initial check before the reaction step to ensure the composition encountered is one where one of the reduced models is valid. If the check

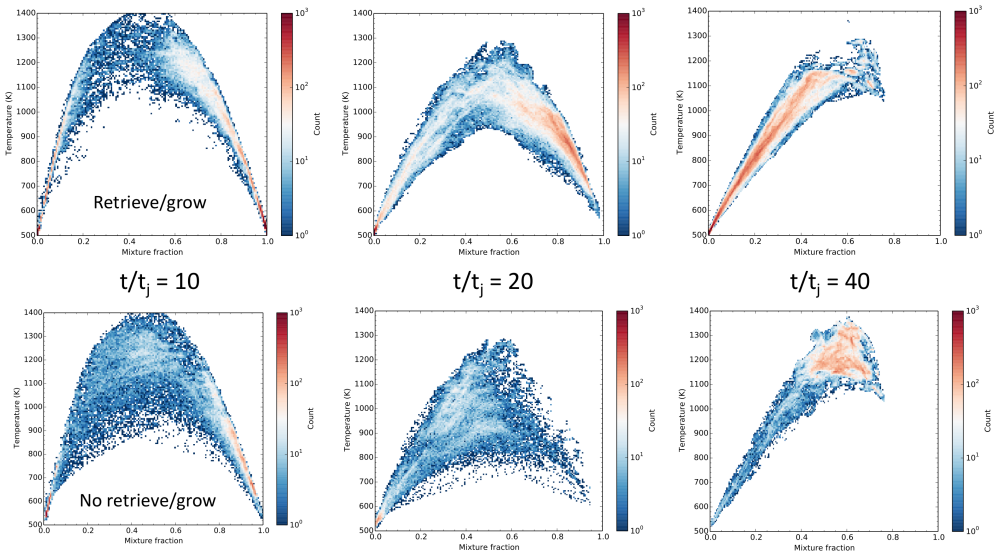

Figure 1: Visualization in temperature-mixture fraction space of retrieved/non-retrieved compositions between low Re DNS data from Hawkes *al.* and a typical sample database built for PPAC using simple 0D and 1D flame configurations. This illustrates that the later configurations may not be fully sufficient to derive a comprehensive set of reduced model for the PPAC strategy.

is successful, the adaptive simulation proceeds as usual in PPAC; however, if the check fails then the integration is performed using the detailed mechanism. It is important to appreciate that the aforementioned method is still reliant on the composition database used in the preprocessing stage to be representative of the compositions encountered in the adaptive simulation. If this is not the case, then majority of the compositions will be integrated using the detailed mechanism thereby negating any advantages of using PPAC.

A more advanced approach entails transitioning from the previous approach to the conventional PPAC algorithm with the preprocessing stage being performed at runtime with compositions collected from the adaptive simulation itself before the transition. This step can be repeated if the updated database is seen to be inadequate (quantified in terms of the number of compositions that need to be resolved using the detailed mechanism) in the subsequent adaptive simulation. This proposed method essentially removes the dependence of PPAC performance on the initial database used for creating the initial set of reduced models. If the initial database accurately mimics the compositions encountered at runtime the transition does not need to invoked; alternatively, if this is not the case the transition ensures one gains the advantage of using PPAC.

4 Publications from DOE Research 2015-2018

1. Jaravel, T., Riber, E., Cuenot, B., Pepiot, P. (2018) "Large Eddy Simulation of the Sandia flame D using reduced mechanism for accurate pollutant prediction", Combust. Flame 188,180 – 198.

2. R.R. Tirunagari, S.B. Pope (2016) "Characterization of extinction/re-ignition events in turbulent premixed counterflow flames using strain-rate analysis", Proc. Combust. Inst., accepted.

3. R.R. Tirunagari, S.B. Pope (2016) "An Investigation of Turbulent Premixed Counterflow

Flames using Large-Eddy Simulations and Probability Density Function Methods", Combust. Flame 166, 229–242.

4. R.R. Tirunagari, M.W.A. Pettit, A.M. Kempf, S.B. Pope (2015) "A Simple Approach for Specifying Velocity Inflow Boundary Conditions in Simulations of Turbulent Opposed-Jet Flows", Flow, Turb. Combust., submitted for publication.
5. R.R. Tirunagari, S.B. Pope (2015) "LES/PDF for Premixed Combustion in the DNS Limit", Combust. Th. Model., submitted for publication.
6. Y. Liang, S. B. Pope, and P. Pepiot (2015) "An adaptive methodology for the efficient implementation of combustion chemistry in particle PDF methods", Combust. Flame 162, 3236–3253.
7. M. Mehta, R. O. Fox, and P. Pepiot. (2015) "Reduced chemical kinetics for the modeling of TiO_2 nanoparticle synthesis in flame reactors", Ind. Eng. Chem. Res. 54, 5407–5415.
8. K. Narayanaswamy, P. Pitsch, and P. Pepiot (2015) "A chemical mechanism for low to high temperature oxidation of methylcyclohexane as a component of transportation fuel surrogates", Combust. Flame, 162, 1193–1213.

References

[1] E. Hawkes, R. Sankaran, J. C. Sutherland, J. H. Chen, *Proc. Comb. Inst.* (2007) 31, 1633 – 1640.

[2] C. S. Yoo, E. S. Richardson, R. Sankaran, J. H. Chen, *Proc. Comb. Inst.* (2011) 33, 1619 – 1627.

[3] Y. Liang, S. B. Pope, P. Pepiot, *Comb. Flame* (2015) 162, 3236 – 3253.

OPTICAL PROBES OF ATOMIC AND MOLECULAR DECAY PROCESSES

S.T. Pratt
Building 200, B-125
Argonne National Laboratory
9700 South Cass Avenue
Argonne, Illinois 60439
E-mail: stpratt@anl.gov

PROGRAM SCOPE

The study of molecular photoabsorption, photoionization, and photodissociation dynamics can provide considerable insight into how energy and angular momentum flow among the electronic, vibrational, and rotational degrees of freedom in isolated, highly energized molecules. This project is focused on these dynamics in small molecules, with the goal of determining the mechanisms of these decay processes and their product branching distributions. In addition to intramolecular dynamics, a second aspect of this work involves the determination of absolute photoabsorption and photoionization cross sections, as well as the general principles that determine them. The experimental approach uses both laboratory-based laser techniques for single- and multiphoton excititation of valence-shell processes, and facilities-based vacuum-ultraviolet (VUV) and x-ray techniques for the excitation of both valence-shell and inner-shell processes. The detection methods include mass spectrometry, photoion- and photoelectron-imaging, high-resolution photoelectron spectroscopy, photoelectron-photoion coincidence techniques, and VUV Fourier-transform absorption spectroscopy. Currently, photoelectron imaging is also being used to study circular dichroism in photoelectron angular distributions as a means to characterize chiral molecules. Finally, experiments enabled by new vuv and x-ray free electron laser sources are being explored.

RECENT PROGRESS

Over the past year, new experiments have been performed both in the laboratory at Argonne and at the SOLEIL synchrotron facility. I have also spent time analyzing results from previous experiments and preparing them for publication. The work at Argonne has focused on double-resonance studies of the photoionization of molecular nitrogen, N_2, while the work at SOLEIL has focused on the study of small reactive species and radicals, with a particular focus on C_4H_5. I have also been involved in a number of collaborations focusing on the photoionization dynamics of small molecules.

Photoionization of C_4H_5 and other small radicals

In collaboration with J. C. Loison (ISM, Bordeaux), I have produced C_4H_5 radicals from 1- and 2-butyne by using a fluorine abstraction reaction at the SOLEIL synchrotron. This approach has allowed detailed photoelectron-photoion coincidence studies of the valence shell photoionization of C_4H_5 radicals. Most of the work focused on the CH_3CCCH_2 radical produced by hydrogen abstraction from 2-butyne. In particular, we have recorded a high-resolution photoionization spectrum that shows considerable structure resulting from electronic autoionization of Rydberg series converging to excited electronic states of the corresponding radical cation. We have also recorded photoelectron images at the energies of a number of these autoionizing resonances, and the corresponding photoelectron energy spectra and angular distributions should provide insight into the nature of these resonances. The data also allow the extraction of a threshold photoelectron spectrum of C_4H_5 with high signal-to-noise ratio, from the first ionization threshold near 8 eV up to 11.5 eV. This energy range is sufficient to reveal two electronically excited states of the cation for the first time. At higher F-atom concentrations, both C_4H_4 and C_4H_3 species can be observed, and threshold photoelectron spectra have been obtained for these as well. These spectra show evidence for more than one isomer of the C_4H_4 and C_4H_3, and the analysis of these data is underway. While there have been previous studies of the photoionization of C_4H_3, C_4H_4, and C_4H_5 [(see, for example, N. Hansen et al., J. Phys. Chem. A 110, 3670 (2006)], the present data provide a more complete perspective on these species.

Kinetic studies using the fluorine-abstraction flow-tube apparatus were also used to determine the absolute photoionization cross section of the CH_3CCCH_2 radical at a fixed photon energy, which can be

used to put the full spectrum on an absolute scale. During a second beamtime, the fluorine-abstraction approach was agin used to record photoionization spectra, threshold photoelectron spectra, and absolute photoionization cross sections of HNC, CH_3, C_2H_5, $C_6H_5CH_2$, and C_3H_3. Studies of a series of additional molecules were also attempted (including HCN, HCCCN, and HCCCCH), but under these conditions, the addition of F to the triple bond was much more efficient that H abstraction. Studies with the C_3H_3 radical were also performed to investigate the kinetics of the production of C_6H_6 ring compounds.

Photoabsorption and Photoionization of Molecular Nitrogen

Although N_2 is the most abundant molecule in earth's atmosphere, many substantial features in its near-threshold photoabsorption and photoionization spectra are only tentatively assigned. The principal reason for this is that this energy region includes not only Rydberg series converging to vibrational levels of the X $^2\Sigma_g^+$, A $^2\Pi_u$, and B $^2\Sigma_u^+$ states of the ion, but also high vibrational levels of the b' $^1\Sigma_u^+$ valence state. Strong interactions amongst these states lead to seemingly erratic behavior in the regularity of the Rydberg series. Furthermore, many of the autoionizing states are sufficiently broad that rotational structure cannot be resolved at even the lowest sample temperatures. In the past year, we have focused on the analysis of the photoelectron angular distribution of rotationally resolved resonances the region of two intense features between 126100 cm^{-1} and 126500 cm^{-1}. We developed a simple model based on earlier work on H_2 by Raoult et al. [J. Chim. Physique **77**, 599-604 (1980)] that provided reasonably good agreement with experiment not only for vibrationally autoionizing Rydberg states, but also for electronically autoionizing Rydberg and valence states. The success of the model provided insight into the nature of both the autoionizing resonances and the corresponding ionization continuum.

As discussed last year, new double resonance experiments are now being performed at Argonne on the photoionization spectrum of N_2 just above the ionization threshold to help interpret the spectrum. In these experiments, the a" (X $^2\Sigma_g^+$)3sσ_g, v' = 0 state is pumped via a two-photon transition, and a second tunable laser drives the transition from there into the region of interest. The overall process involves three photons, so the same parity levels are accessed as in a single-photon transition from the ground state of N_2. Using this approach, we have observed transitions from the a" $^1\Sigma_g^+$ state to Rydberg series converging to the X $^2\Sigma_g^+$, A $^2\Pi_u$, and B $^2\Sigma_u^+$ states of the ion, as well as to the b' $^1\Sigma_u^+$ valence state. One of the interesting features of these data is that most of these transitions involve two-electron transitions from the dominant a" $^1\Sigma_g^+$ state configuration. These transitions are very similar to "shake-up" transition observed in x-ray spectra, but can be studied with significantly higher resolution in the present scheme.

Even with rotational labelling in the a" $^1\Sigma_g^+$ state, the complexity of the multistate interactions responsible for these features makes it difficult to analyze the observed double-resonance spectra. We are making progress on this analysis, which will be aided by multichannel quantum defect theory calculations by Christian Jungen (Orsay). Taking a step back, however, we have also applied this double-resonance approach to a number of additional features in the near-threshold photoionization spectrum. For example, the first two members of the "new Ogawa series" give rise to intense, unresolved features at ~128910 cm^{-1} and 130720 cm^{-1}, respectively. These features have previously been assigned as transitions to the v' = 0 and 1 levels of a Rydberg state with an A $^2\Pi_u$ core, and the band contour suggests the upper level had overall Σ symmetry. Although the individual rotational lines are broad, by pumping sufficiently high J levels in the a" $^1\Sigma_g^+$, v = 0 state, we can resolve the rotational structure in the upper state and show definitively that it is indeed a $^1\Sigma_g^+$ level. In this case, the only likely assignment is to the (A $^2\Pi_u$)4dπ $^1\Sigma_u^+$ Rydberg state. We have also recorded photoelectron images for rotationally resolved autoionizing levels of this state, and we are currently analyzing the photoelectron angular distributions using the same approach as in our earlier single-photon studies. By working our way through the simpler resonances in this fashion, we ultimately hope to provide a comprehensive and convincing analysis of the spectrum in the region both above and below the first ionization threshold.

Inner-shell and inner-valence processes in methyl iodide

Methyl iodide has always been a prototypical system for the study of photodissociation dynamics, and it is becoming one for time-resolved studies using free electron lasers. The latter studies involve inner-shell excitation of the molecules, and the high intensities often lead to the formation of multiple electron holes

and high charge states. These excited systems decay through a complex chain of Auger (autoionization) and fluorescence processes, and unravelling these decay processes is challenging. Unfortunately, detailed information on many relevant Auger processes of inner-shell and and inner-valence excited methyl iodide are not available. I have been collaborating with David Holland (STFC) and a graduate student, Ruaridh Forbes (University College London) to record the relevant data at the SOLEIL synchrotron, and to interpret these data in a manner that will be useful for ongoing and future experiments using free-electron lasers. The new data include information about excitation of the 3d and 4d subshells of the iodine atom, as well as the 1s shell of the carbon atom, and are currently being prepared for publication.

Infrared-VUV studies of vibrational autoionization in CH_3SH
I collaborated with Professor Y. P. Lee (Taiwan) on the interpretation of infrared-VUV double-resonance studies of CH_3SH. This double-resonance approach allowed the enhanced excitation of selected vibrationally autoionizing states of CH_3SH, and provided information on the mode selectivity of the autoionization and competing decay processes.

FUTURE PLANS
In the coming year, I will continue to work on the analysis of the photoionization data on molecular nitrogen recorded at Argonne. This is a long-term effort that will result in multiple publications. I will also work to complete the analysis of the new coincidence data on C_4H_5, C_4H_4, and C_4H_3, and work up the data on the series of radical photoionization cross sections from my most recent beamtime at SOLEIL. In my laboratory work at Argonne, I will work to complete my double-resonance studies on N_2. I will also continue to explore the possibility of using photoelectron circular dichroism to study the radicals produced by the photodissociation of chiral molecules.

I currently have two sets of beamtime at SOLEIL scheduled for July of this year. In the first, I will work on the Fourier-transform vacuum ultraviolet (VUV) spectrometer to record comprehensive high-resolution absorption measurements and oscillator strengths in both the bound and continuum regions of the spectrum of nitric oxide. Owing to the work of Ernst Miescher and his students, NO the Rydberg states of NO are among the best understood of any molecule. Nevertheless, comprehensive measurements of the oscillator strengths are still missing. These quantities will not only provide a more stringent test of our understanding of the highly excited states of this molecule, but also provide important information for modelling of interstellar chemistry. In the second beamtime, I will use photoelectron-photoion coincidence experiments to study vibrational, electronic, and spin-orbit autoionization in HBr. This work will complement our recent study of rotationally resolved autoionization in N_2, with the added possibility of determining the rotational distributions in the photoion. This work is expected to provide a much improved understanding of these three autoionization processes and the interactions among them.

I have been invited to participate on an experiment on molecular nitrogen at the FERMI free-electron laser (FEL) in December by Professor Kiyoshi Ueda (Tohoku University). This facility produces intense, ultrafast coherent photon pulses in the VUV region that also have transform-limited bandwidths. In these experiments, we will use the FEL to excite electronic wavepackets composed of two or more Rydberg and valence states of N_2, and probe them with either a near-infrared ultrafast pulse or a second vuv pulse. We hope to observe both angular and radial electronic wavepackets, and to monitor their time dependence by photoelectron imaging or Ramsey interference experiments. This effort will make use of the knowledge we have obtained through my experiments on N_2 at Argonne and at SOLEIL. I have also applied for additional beamtime at the FERMI FEL with David Holland, Katharine Reid, and Henrik Stapelfeldt (Aarhus University). This proposal focuses on photoelectron angular distributions from electronically autoionizing states in fixed-in-space N_2 molecules that are prepared by using impulsive alignment with an ultrafast near-infrared laser.

I will continue to collaborate with Christian Jungen (Orsay) on the theoretical analysis of the vacuum ultraviolet photoabsorption and photoionization spectra of molecular nitrogen. This work will make use of new double-resonance spectra from my laboratory as well as new high-resolution photoabsorption spectra for the Fourier-transform spectrometer at the SOLEIL synchrotron. The ultimate long-term goal of

this work will be to provide a comprehensive assignment of the spectrum of molecular nitrogen up to the B $^2\Sigma_u^+$ threshold of the N_2^+ ion. Because N_2 is a workhorse system in ultrafast studies of molecules, this effort is expected to have a broad impact in molecular physics and chemistry.

ACKNOWLEDGEMENTS
This work was performed in collaboration with my postdoc, Ananya Sen. Work on oriented NO was performed in collaboration with K. L. Reid (Nottingham). Work at Soleil was performed in collaboration with S. Boyé-Péronne and B. Gans (Institut des Sciences Moléculaires d'Orsay), J. C. Loison (University of Bordeaux), D. M. P. Holland (STFC, Daresbury), U. Jacovella (ETH-Zürich), E. F. McCormack (Bryn Mawr College), and N. de Oliveira (Soleil). Theoretical work on N_2 was performed in collaboration with Ch. Jungen (Laboratoire Aime Cotton). This work was supported by the U.S. Department of Energy, Office of Science, Office of Basic Energy Sciences, Division of Chemical Sciences, Geosciences, and Biological Sciences under contract No. DE-AC02-06CH11357.

DOE-SPONSORED PUBLICATIONS SINCE 2016

1. N. Saquet, D.M.P. Holland, S.T. Pratt, D. Cubaynes, X. Tang, G. A. Garcia, L. Nahon, and K.L. Reid
EFFECT OF ELECTRONIC ANGULAR MOMENTUM EXCHANGE ON PHOTOELECTRON ANISOTROPY FOLLOWING THE TWO-COLOUR IONIZATION OF KRYPTON ATOMS
Phys. Rev. A 93, 033419 (11 pages) (2016).

2. A. Pićon, C. S. Lehmann, C. Bostedt, A. Rudenko, A. Marinelli, T. Osipov, D. Rolles, N. Berrah, C. Bomme, M. Bucher, G. Doumy, B. Erk, K. R. Ferguson, T. Gorkhover, P. J. Ho, E. P. Kanter, B. Krässig, J. Krzywinski, A. A. Lutman, A. M. March, D. Moonshiram, D. Ray, L. Young, S. T. Pratt, and S. H. Southworth
HETERO-SITE-SPECIFIC ULTRAFAST INTRAMOLECULAR DYNAMICS
Nat. Commun. **7**, 11652 (6 pages) (2016).

3. C. S. Lehmann, A. Pićon, C. Bostedt, A. Rudenko, A. Marinelli, D. Moonshiram, T. Osipov, D. Rolles, N. Berrah, C. Bomme, M. Bucher, G. Doumy, B. Erk, K. R. Ferguson, T. Gorkhover, P. J. Ho, E. P. Kanter, B. Krässig, J. Krzywinski, A. A. Lutman, A. M. March, D. Ray, L. Young, S. T. Pratt, and S. H. Southworth
ULTRAFAST X-RAY-INDUCED NUCLEAR DYNAMICS IN DIATOMIC MOLECULES USING FEMTOSECOND X-RAY-PUMP - X-RAY-PROBE SPECTROSCOPY
Phys. Rev. A 94, 013426 (7 pages) (2016).

4. A. Sen, S. T. Pratt, and K. L. Reid
CIRCULAR DICHROISM IN PHOTOELECTRON IMAGES FROM ALIGNED NITRIC OXIDE MOLECULES
J. Chem. Phys. **147**, 013927 (2017).

5. A. M. Chartrand, E. F. McCormack, U. Jacovella, D. M. P. Holland, Bérenger Gans, Xiaofeng Tang, G. A. Garcia, L. Nahon, and S. T. Pratt
PHOTOELECTRON ANGULAR DISTRIBUTIONS FROM ROTATIONALLY RESOLVED AUTOIONIZING STATES OF N_2
J. Chem. Phys. **147**, 224303 (2017).

6. Min Xie, Zhitao Shen, S. T. Pratt, and Yuan-Pern Lee
VIBRATIONAL AUTOIONIZATION OF STATE-SELECTIVE JET-COOLED METHANETHIOL (CH_3SH) INVESTIGATED WITH INFRARED + VACUUM-ULTRAVIOLET PHOTOIONIZATION
Phys. Chem. Chem. Phys. **19**, 29153-29161 (2017).

Reaction Mechanisms Studied with Chirped-Pulse Rotational Spectroscopy

Kirill Prozument
Argonne National Laboratory
Chemical Sciences and Engineering Division
Argonne, IL 60439
prozument@anl.gov

1. Scope of the Program

The goal of the Program is to gain detailed understanding of the dynamical processes that govern chemical reactivity. Oftentimes, the rates predicted for even simple reactions are in disagreement with experimental observations. The discrepancy may arise because such effects as roaming dynamics, tunneling reaction mechanism, lack of thermal equilibration of reaction intermediates and others are often neglected in kinetics models. We investigate the pyrolysis and photolysis reactions that help us reveal these mechanisms. We aim at generalizing our findings to broad classes of reactions. The experimental approach in this Program is based on chirped-pulse Fourier transform millimeter-wave (CP-FTmmW) spectroscopy. The reaction products are detected non-destructively, with quantum state specificity and time resolution. Because CP-FTmmW spectroscopy is also quantitative, branching ratios are measured and compared with theoretical models. The versatility of the CP-FTmmW technique is sufficient for its application to a wide range of experiments in reaction dynamics and kinetics in the gas phase. The program is currently focused of two experimental directions: i) investigation of pyrolysis chemistry in the micro-tubular reactor at 1000–1800 K, and ii) *in situ* time-resolved chirped-pulse spectroscopy of photoproducts at room temperature. A key part of the Program is development of the Artificial Intelligence (AI) methods for automation of spectroscopic assignment. The need for that component is pressing as vast amounts of potentially useful spectroscopic data are generated in broadband rotational experiments, but rarely are fully analyzed. The goal of the AI thrust is that vast amounts of *spectroscopic* data becomes the *chemical* information, ready for reaction mechanisms discovery.

2. Recent Progress

1) Pyrolysis of Methyl Nitrite

Using the recently constructed CW pyrolysis/CP-FTmmW apparatus, we started investigation of complex chemical network of reactions initiated by thermal decomposition of methyl nitrite (CH_3ONO). Our preliminary results are encouraging. We observe eleven reaction products and developing the kinetic model to aid our understanding of the underlying reaction mechanisms.

2) TReK-CP Spectroscopy of Vinyl Cyanide Photoproducts

We have investigated the 193 nm photodissociation of vinyl cyanide (CH_2CHCN) using the Time-Resolved Kinetic Chirped-Pulse spectroscopy, a technique that was recently developed in the PI's

laboratory.[a)] In the present TReK-CP study, the CH_2CHCN precursor is flowing through a room temperature tubular reactor. The photolysis laser and the mm-wave beam of the spectrometer propagate collinearly within the reactor for maximum overlap. The chemistry is initiated by photodissociation of vinyl cyanide, and HCN, HNC, and HCCCN photoproducts are observed by the CP-FTmmW spectrometer *in situ* and in real time.

In collaboration with Lawrence Harding, Stephen Klippenstein, and Branko Ruscic, we have developed a model to explain formation of HCCCN that is consistent with our observations, and significantly improves the established understanding of this molecular system in the literature. In Figure 1, the vibrational population distributions (VPDs) of HCCCN are plotted as a function of time elapsed since the photolysis event. Although the UV photolysis products are usually formed with considerable amount of excess vibrational energy, the observations in Fig. 1 suggest the opposite: vibrationally cold photoproducts are thermalizing up to the ambient room temperature of the reactor.

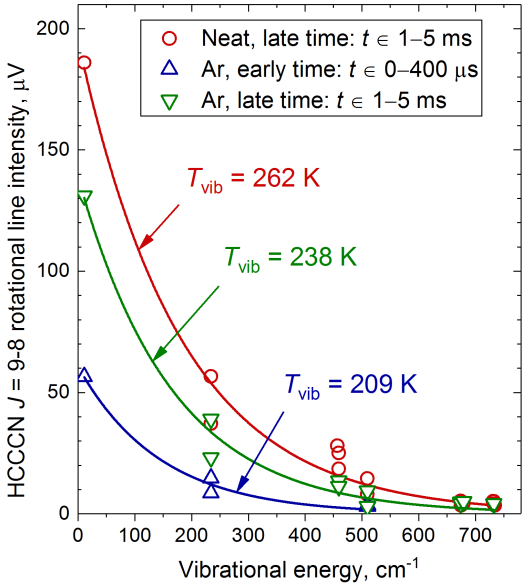

Figure 1. The VPDs of HCCCN photoproducts as a function of time. Acquired in a sync-HDR mode of BrightSpec W-band spectrometer. The data is approximated by the Boltzmann distribution and the vibrational temperatures are shown.

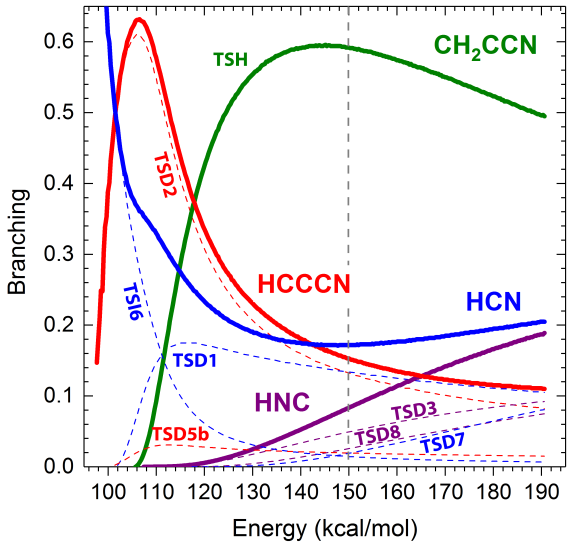

Figure 2. Calculated branchings for dissociation of CH_2CHCN via various transition states. Calculations are for a range of excitation energies; the vertical dashed line corresponds to the energy of one laser photon at 193 nm.

The potential energy surface was calculated, and three $CH_2CHCN \rightarrow HCCCN$ pathways were identified. Two of them are direct H_2 loss (TSD2, TSD5b in Fig. 2) with expected excess energy deposited in the products, and one – consecutive loss of two H-atoms via the TSH transition state:

$$CH_2CHCN \rightarrow CH_2CCN + H \rightarrow HCCCN + 2H$$

Analysis of the experimental VPDs and branching ratios in light of ab initio calculations of PES, reaction enthalpies from Active Thermochemical Tables, and CH_2CHCN dissociation rate calculations suggest that a large fraction of HCCCN is forming via the tunneling reaction mechanism in $CH_2CCN \rightarrow HCCCN + H$ decomposition on the ~ 1 ms time-scale.

3) Assignment of Rotational Spectra using Artificial Neural Networks

The potential of machine learning based on artificial neural networks (ANNs) in numerous areas of human activity has now been demonstrated. These areas include speech and image recognition, translation, surveillance, and even playing the game of Go. In the last several years, machine learning was instrumental in physical sciences, applied to a remarkably diverse cohort of problems.

Our rationale in approaching the high resolution broadband rotational spectroscopy with the AI tools is twofold. First, a typical chirped-pulse rotational spectrum contains ~10^4 resolution elements and reaches ~10^4 in dynamic range. Transitions form patterns and, sometimes, patterns of broken patterns! An ANN is extremely well-positioned to train on such patterns. Second, the amounts of useful spectroscopic data in these experiments rapidly increases and an effective automation approach is needed to match the data throughput of chirped-pulse spectroscopy.

In order to train an ANN, we create training sets that are comprised of the molecular Hamiltonian parameters (A, B, C constants, distortion, electric quadrupole constant, etc.) amended by the molecular type label (linear, symmetric top, asymmetric top) and the corresponding spectrum that we simulate. The constants do no need to belong to any existing molecule; however, physical constraints must be put on the parameter space (e.g. $A > B > C$, $D_J \geq 0$). Once trained, the ANN may be used to recognize the type of molecule and to deduce the constants.

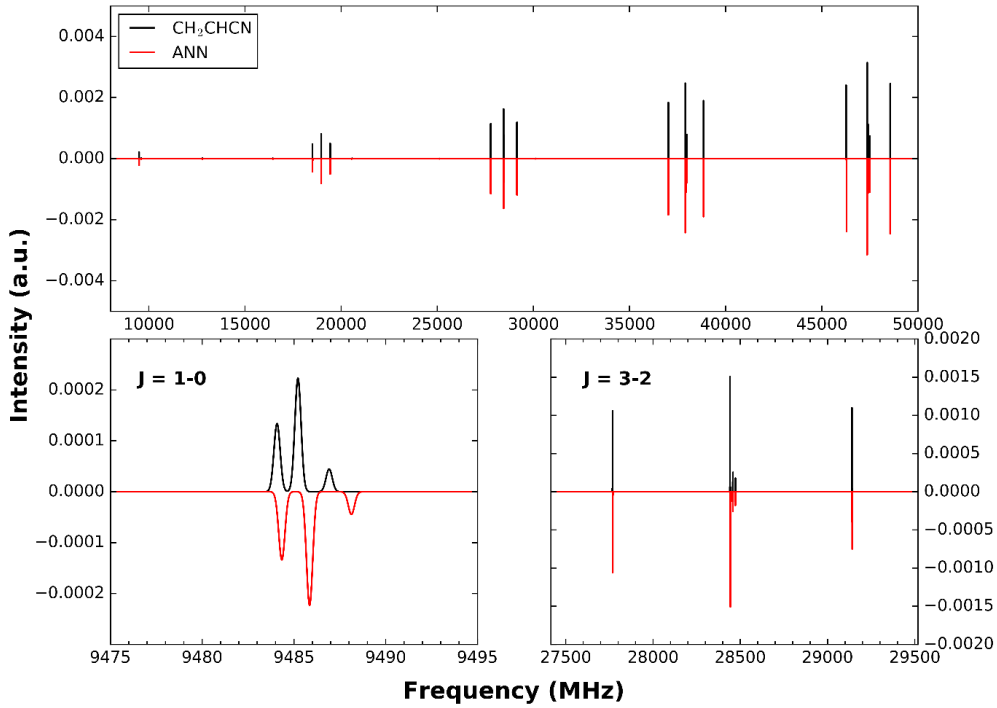

Figure 3. A comparison of simulations of CH_2CHCN from experimentally known constants (black) and constants fitted by the ANN (red). The FWHM = 400 kHz and T_{rot} = 2 K. The ANN does not fit the A rotational constant for a-type spectra, and A was set to the experimental value for creating the simulation.

We demonstrate how the ANN performs on a-type transitions of CH_2CHCN. The spectrum of vinyl cyanide is actually a hybrid ($\mu_a \approx 3.8$ D and $\mu_b \approx 0.9$ D). Since the ANN has not yet been trained on hybrid spectra, only the a-type transitions were included in the peak pick. Vinyl cyanide also displays hyperfine structure. The ANN fit is shown in Fig. 3, with T_{rot} = 2 K, and the agreement

is quite good. $(B + C)_{\mathrm{ANN}}$ = 9485.4448 MHz and $(B + C)_{\mathrm{exp}}$ = 9485.0410 MHz. $(B - C)_{\mathrm{ANN}}$ = 456.3159 MHz and $(B - C)_{\mathrm{exp}}$ = 457.3847 MHz.

With the ANNs, the time required to assign a spectrum and to derive the Hamiltonian parameters is *independent* of the number of those parameters *n* and the number of lines in the spectrum. With any *n* that we tested, it takes about 50 μs to assign a spectrum. In contrast, the existing combinatorial methods scale with some high power of *n* as the parameters are added. Even when only *A*, *B*, *C* are fitted, assignment by a combinatorial method requires seconds to hours depending on the level of spectral congestion.

3. Future Plans

In collaboration with Raghu Sivaramakrishnan we plan to develop a kinetic model to describe the apparently complex chemistry of methyl nitrite that we are observing in a heated micro-tubular reactor. Experimentally, the pyrolysis of isotopically labeled precursor will be investigated. We will also collaborate with the group of Robert Kee to couple the computations of gas flow dynamics with chemical kinetics models and with experimental branching ratios. The chemical model will be solved consistently across the temperature, pressure and velocity distributions within the reactor for reliable theoretical branching ratios.

The TReK-CP experiments with the 260 – 290 GHz spectrometer are planned. Observation of the cyanovinyl radical (CH_2CCN) and its kinetics following the photolysis of CH_2CHCN will aid in understanding of this system. Isotope labeling experiments are planned as well. We also plan to initiate H-atom abstraction reactions by CN radicals. The interest is two-fold. Firstly, comparison of the HCN kinetics in the abstraction and CH_2CHCN photodissociation reactions will be instructive. Secondly, we are interested in studying the consecutive chemistry of the remaining radical.

The AI research direction of the Program will be actively pursued. We are going to approach the task of assigning a real spectrum. The issues with separating the noise and spurious frequencies will be addressed.

DOE-Sponsored Publications Since 2017

a) Zaleski, D. P.; Harding, L. B.; Klippenstein, S. J.; Ruscic, B.; Prozument, K. Time-Resolved Kinetic Chirped-Pulse Rotational Spectroscopy in a Room-Temperature Flow Reactor. *J. Phys. Chem. Lett.* **2017**, *8*, 6180-6188.

b) Zaleski, D. P.; Prozument, K. Pseudo-Equilibrium Geometry of HNO Determined by an E-Band CP-FTmmW Spectrometer. *Chem. Phys. Lett.* **2017**, *680*, 101-108.

c) Zaleski, D. P.; Duan, C.; Carvajal, M.; Kleiner, I.; Prozument, K. The Broadband Rotational Spectrum of Fully Deuterated Acetaldehyde (CD_3CDO) in a CW Supersonic Expansion. *J. Mol. Spectrosc.* **2017**, *342*, 17-24.

Towards Novel Ultrafast Spectroscopic Probes of Non-Adiabatic Dynamics

Krupa Ramasesha
Combustion Research Facility, Mail Stop 9055
Sandia National Laboratories
Livermore, CA 94551
kramase@sandia.gov

I. Program Scope

This program aims to apply ultrafast spectroscopy to follow fundamental gas-phase molecular dynamics. The proposed work will develop molecular structure-specific probes to follow coupled electronic and nuclear motion on femtosecond to picosecond timescales in gas-phase small molecules. The coupling of electronic and nuclear degrees of freedom, representing a breakdown of the Born-Oppenheimer approximation, gives rise to complex pathways of non-radiative energy dissipation in electronically excited molecules, which often involve participation of several electronic states. Identifying the motions that couple electronic states, the timescales and dynamics of excited state population relaxation, and the role of the coupled vibrational modes of a molecule in guiding energy flow are crucial to our understanding of non-equilibrium dynamics, and will form the mainstay of this program.

II. Recent Progress

Over the last year, a state-of-the art ultrafast laboratory space has been planned and designed. The design of the lab space includes an environment-controlled enclosure that will eventually house a high power ultrafast laser system capable of carrier-envelope phase stabilization and two travelling-wave optical parametric amplifiers (TOPAS) for nonlinear frequency conversion. The laboratory will be able to support experiments using soft X-rays, infrared and THz pulses that are sensitive to laboratory conditions. The enclosure promises temperature and humidity stability and will be equipped with a HEPA air filtration system.

In parallel, we are building a supercontinuum infrared generation set-up pumped by an existing ultrafast Ti:Sapphire laser system that generates 4 mJ/pulse, 45 fs pulses at 1 kHz for studying non-adiabatic dynamics and vibrational dynamics in acetyl acetone. The set-up includes a series of nonlinear crystals to collinearly generate doubled and tripled frequencies of the fundamental 800 nm output of the Ti:Sapphire amplifier. A Type I BBO crystal cut at 29.2° doubles the 800 nm output of the Ti:Sapphire amplifier to 400 nm, and a Type I BBO crystal cut at 44.26° sums the 400 nm and residual 800 nm to generate 267 nm. Between the doubling and tripling crystals, we have placed a BBO crystal cut at 66° to compensate for temporal walk-off between the 800 nm and 400 nm pulses prior to tripling. Additionally, a dual-waveplate is inserted between the doubling and tripling crystals to rotate the 800 nm polarization onto the polarization of the 400 nm pulses. These pulses are focused in air using a $f = 50$ mm broadband concave dielectric mirror coated for high reflectivity at all three wavelengths. Such laser-driven plasma has been shown to generate linearly polarized <100 fs infrared pulses with bandwidth spanning the entire mid-IR region of the spectrum[1,2]. We are in the process of building a nitrogen gas purging contraption for continually refreshing the gas in the plasma, which we expect to provide enhanced pulse-to-pulse stability and increase in infrared output energy, while cutting down on toxic gas production such as O_3 and NO_x that are also known to damage the coatings on optics. We are also currently in the process of characterizing the spatial, spectral and temporal profiles of the plasma-generated supercontinuum pulses.

III. Future Work

In the following year, renovation of the ultrafast laboratory space at the Combustion Research Facility will begin, guided by the design we have developed over the last year.

We will, in the meantime, continue to push forward with developing supercontinuum infrared spectroscopy as a means for probing excited state structural dynamics in polyatomic molecules. We will

characterize the spectral content and the temporal duration of the supercontinuum pulses, and use these pulses to probe high-frequency molecular vibrations in polyatomic molecules as reporters of large-scale structural deformations following electronic excitation. These pulses will be used in a pump-probe transient absorption scheme, where a UV pulse will serve as the pump for electronic excitation and the supercontinuum infrared pulses will serve as the probe of molecular vibrations. The pump and probe beams will be spatially overlapped in a gas cell containing the molecule of interest, and the transmitted infrared pulses will be dispersed on a liquid nitrogen cooled HgCdTe array detector and recorded as a function of pump-probe time delay. The first platform for applying this technique will be in studying non-adiabatic dynamics in acetyl acetone. The presence of a strong intramolecular hydrogen bonding in acetyl acetone between O-H and C=O moieties allows the O-H and C=O stretch frequencies to be used as reporters of backbone deformations of the molecule that modify the strength of this interaction. It has been shown theoretically that relaxation of electronically excited AcAc from S_2 ($\pi\pi^*$) involves significant changes to the backbone structure as it traverses through conical intersections, accessing lower-lying singlet and triplet states[5,6]; hence, probing the evolution of high frequency vibrations in the molecule can effectively constrain possible structures as a function of time. O-H and C=O stretching vibrations are particularly advantageous since their vibrational frequencies are highly sensitive to their local bonding environment and their infrared cross-sections are relatively high. The O-H stretching vibration in particular is spectrally isolated from the fingerprint region and its frequency has been theoretically predicted to change by more than 100 cm^{-1} between ground state and triplet excited state structures of malonaldehyde[7], an analog of acetyl acetone, making it a valuable reporter of structural dynamics. Supercontinuum infrared pulses will allow single-shot detection of all infrared active vibrations in the mid-IR, making this a powerful source for probing structural and vibrational dynamics.

IV. References

1. Ramasesha, K., De Marco, L., Mandal, A. & Tokmakoff, A. Water vibrations have strongly mixed intra- and intermolecular character. *Nat. Chem.* **5,** 935–940 (2013).
2. Petersen, P. B. & Tokmakoff, A. Source for ultrafast continuum infrared and terahertz radiation. *Opt. Lett.* **35,** 1962–4 (2010).
3. Attar, A. R. *et al.* Femtosecond x-ray spectroscopy of an electrocyclic ring-opening reaction. *Science (80-.).* **356,** 54 (2017).
4. Pertot, Y. *et al.* Time-resolved x-ray absorption spectroscopy with a water window high-harmonic source. *Science (80-.).* **355,** 264 (2017).
5. Coe, J. D. & Martínez, T. J. Ab initio molecular dynamics of excited-state intramolecular proton transfer around a three-state conical intersection in malonaldehyde. *J. Phys. Chem. A* **110,** 618–630 (2006).
6. Upadhyaya, H. P., Kumar, A. & Naik, P. D. Photodissociation dynamics of enolic acetylacetone at 266, 248, and 193 nm: Mechanism and nascent state product distribution of OH. *J. Chem. Phys.* **118,** 2590 (2003).
7. Barone, V. & Adamo, C. Proton transfer in the ground and lowest excited states of malonaldehyde: A comparative density functional and post-Hartree-Fock study. *J. Chem. Phys.* **105,** 11007 (1996).

Photoinitiated Reactions of Radicals and Diradicals in Molecular Beams

Hanna Reisler
Department of Chemistry, University of Southern California
Los Angeles, CA 90089-0482
reisler@usc.edu

Program Scope

Open shell species such as radicals, diradicals and molecules in excited electronic states are central to reactive processes in combustion and environmental chemistry. Our program is concerned with photo-initiated reactions of radicals, carbenes, and other open shell species. The goal is to investigate the detailed dissociation dynamics of species in which multiple pathways participate, including molecular rearrangements, and compare them to high-level calculations. Studies include unimolecular reactions on the ground state as well as photodissociation dynamics on excited Rydberg and valence states that involve multiple potential energy surfaces.

Recent Progress

We have made progress on two topics: The photophysics and photochemistry of hydroxycarbenes, and the jet-cooled photodissociation of pyruvic acid. These topics are related because alpha-keto aliphatic hydroxylic acids such as pyruvic acid are known sources of hydroxycarbenes, at least upon pyrolysis. Manuscripts are in preparation on each of these topics, and below I present brief summaries.

Excited electronic states of hydroxycarbenes

Hydroxycarbenes, the high-energy tautomers of aldehydes, are reactive and difficult to isolate and stuy in molecular beams. Schreiner and coworkers isolated and spectroscopically probed HCOH (hydroxycarbene, HC) and CH_3COH (methylhydroxycarbene, MHC) in an argon matrix[1,2]. In our group we produced them in the UV photodissociation of the CH_2OH and CH_3CHOH radicals. The IR vibrational spectra of HC and MHC were reported in the Ar matrix [1,2] and in He droplets [3], as well as the UV absorption spectra to their first excited state, S_1. [1,2] Theoretical calculations of the ground and S_1 state geometries and energies agreed with observations. [1,2] Koziol et al. computed IR [4] and photoelectron [5] spectra of *cis*- and *trans*-HC. While much is known about the ground state potential energy surface and reactivity of HCOH, much less is known about the excited states of these hydroxycarbenes. We carried out calculations of excited state energies and oscillator strengths for the *cis*- and *trans* isomers of HC and MHC focusing on Rydberg states. We find that above the S_1 state and below the ionization threshold, HC and MHC have only Rydberg states. These states can be used for REMPI detection of hydroxycarbenes. The presence of an additional methyl group in MHC alters the charge distribution and excitation and ionization energies in predictable ways, mainly due to hyperconjugation effects.

We obtained the ground state equilibrium geometries of the neutral and cationic forms of the hydroxycarbenes by optimization at the MP2/aug-cc-pVTZ level using Q-Chem. We used the EOM-EE-CCSD method to calculate vertical and adiabatic excitation energies and oscillator strengths, and EOM-IP-CCSD to compute ionization energies (IEs). The aug-cc-pVTZ basis set was employed for all single point energy calculations and IEs. The results of the electronic structure calculations are summarized in Table 1, which includes also the corresponding quantum defects calculated by the Rydberg formula.

To aid in the understanding of the nature of the Rydberg states and their electron-core interactions, we computed Natural Transition Orbitals (NTOs), which are shown in Figure 1. Qualitative understanding of

the nature of the excited states, oscillator strengths, and the direction of the transition dipole moment is gained from the shapes of the orbitals involved in the transition and their symmetries.

Table 1: Ionization energies, vertical and adiabatic excitation energies of Rydberg states, oscillator strengths and quantum defects for excited states of HC and MHC.

	State	E_{vert} (eV)	E_{adiab} (eV)	Oscillator Strength	Quantum defect (δ)
	HC				
trans-HC	$2^1A'(3s)$	5.67	4.87	0.010	1.141
	$3^1A'(3px)$	6.65	5.96	0.036	0.856
	$4^1A'(3py)$	7.51	6.88	0.089	0.454
	$2^1A''(3pz)$	7.54	6.86	0.026	0.436
	$1^2A'(IE)$	9.61	8.94		
cis-HC	$2^1A'(3s)$	5.34	4.76	0.025	1.219
	$3^1A'(3px)$	6.77	6.01	0.065	0.818
	$4^1A'(3py)$	7.65	6.93	0.057	0.378
	$2^1A''(3pz)$	7.54	6.81	0.013	0.448
	$1^2A'(IE)$	9.63	8.91		
	MHC				
trans-MHC	$2^1A'(3s)$	5.47	4.59	0.007	1.017
	$3^1A'(3px)$	6.37	5.65	0.023	0.694
	$2^1A''(3pz)$	6.72	5.99	0.047	0.518
	$4^1A'(3py)$	6.79	6.11	0.137	0.478
	$1^2A'(IE)$	8.93	8.21		
cis-MHC	$2^1A'(3s)$	5.59	4.80	0.085	1.002
	$3^1A'(3px)$	6.42	5.62	0.073	0.703
	$2^1A''(3pz)$	6.74	6.03	0.051	0.546
	$4^1A'(3py)$	6.75	6.08	0.130	0.540
	$1^2A'(IE)$	9.00	8.24		

A clear distinction between Rydberg and valence orbitals is obtained from the sizes of the NTOs. The HOMO and first excited valence orbital are almost similar in size (1.2-1.3 Å radius). The radius of the Rydberg orbitals is much larger and ranges from 2.6 to 4.1 Å. The orbitals are rather similar for the *cis* and *tran* isomers, and therefore we show only the orbitals of the *trans* isomer in Figure 1. The Rydberg orbital of the 3s state, the lowest in the series, is not as spherically symmetric as expected due to stronger interactions with the core, which also reduce the size of this orbital compared to the 3p orbitals. The $3p_x$ orbital is also deformed due to interactions with the ion core along the X-axis, which lies in the C-O-H direction. The $3p_y$ orbital has the largest size in both HC and MHC, and also the smallest quantum defect. Clearly, the quantum defect manifests itself in the shape and size of the Rydberg orbitals.

Based on the data of Table 1, several REMPI schemes should be feasible for detection of these carbenes, whose cations are known to be fairly stable. For HC a (2+1) REMPI scheme via the $3p_y$ state, which has the largest oscillator strength, should be feasible with 330 – 360 nm excitation. Two color schemes are also possible with several different combinations. Similar schemes can be devised for MHC, with excitation at about 360- 410 nm.

Photodissociation of jet-cooled pyruvic acid

Pyruvic acid is important in environmental chemistry because it absorbs solar radiation and is known to dissociate. It is also a possible source of MHC for molecular beam studies. However, its photoinitiated decomposition mechanism at room temperature and in collisional environments is still unsettled [6]. For

example, upon UV irradiation at relatively low inert gas pressures, CO_2 is identified as the main product, but its yield decreases sharptly with increasing pressure. The mechanism of the pressure dependence remains unexplained. In addition, there is very little known about the photophysics and photochemistry of pyruvic acid in the cold environment of molecular beams. We obtained preliminary results on the jet-cooled spectrosopcy of pyruvic acid, and the production of H-fragments by an efficient two-photon absorption via the S_1 state terminating in a fast dissociative state.

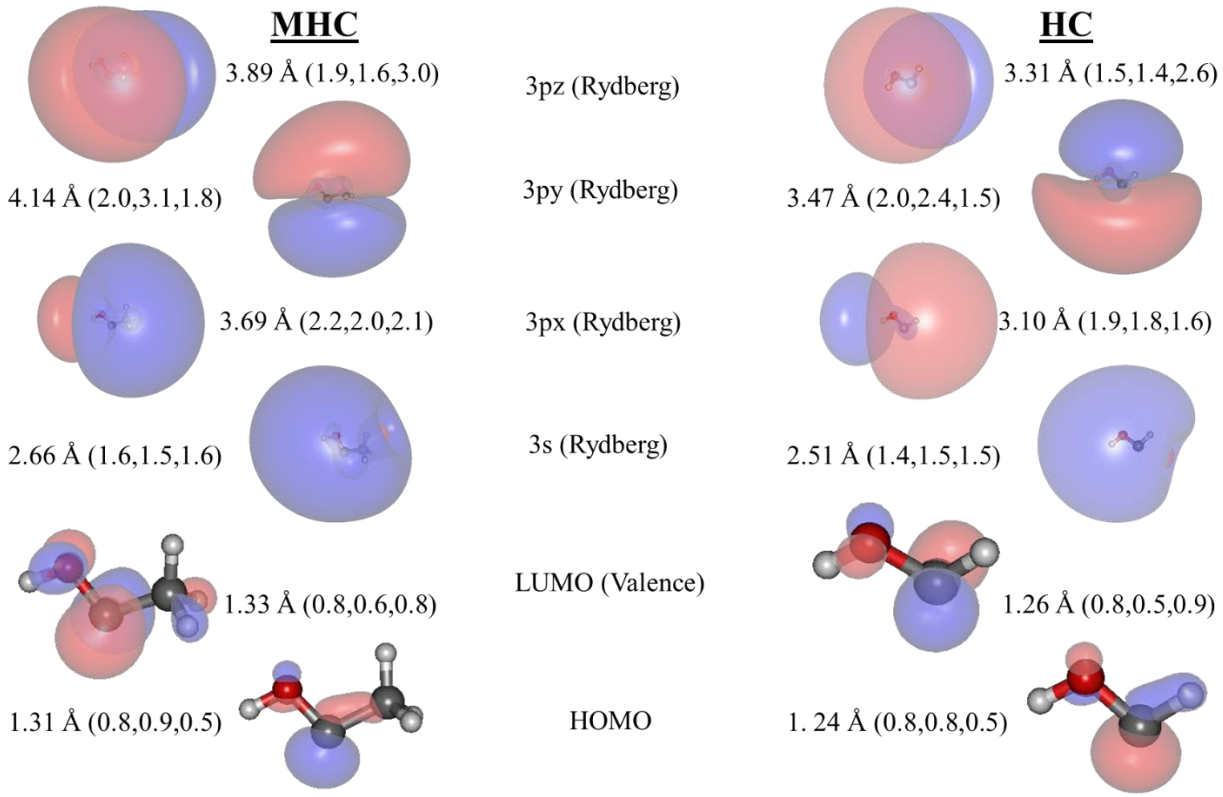

Figure 1: Natural Transition Orbitals of *trans*-MHC (left) and *trans*- HC (right), describing valence and Rydberg orbitals.

The first absorption band of pyruvic acid ($S_1 \leftarrow S_0$) lies at 310-380 nm at 298 K and shows only broad and unresolved features. Upon $S_1 \leftarrow S_0$ excitation in molecular beams seeded in He or Ar, however, the spectrum sharpens and becomes much better resolved. While we could not observe the absorption spectrum directly, we detected fairly strong H-fragment signals by using 1+1' (VUV + UV) REMPI. The fluence dependence of the excitation laser radiation shows that the H fragmens are produced by a two-photon transition via S_1. The H-atom photofragment yield spectrum obtained while scanning the excitation laser across the $S_1 \leftarrow S_0$ transition matches well the broad spectral features observed in the 298 K absorption spectrum. The spectral peaks in the molecular beam, however, are much narrower (about 4 cm^{-1}) and well resolved, indicating a fairly long lifetime of the S_1 state. Thus, absorption of another photon from the S_1 state is quite facile. Time-sliced velocity map images of the H-photofragments obtained at several wavelengths near the absorption onset and also near the absorption maximum show broad and bimodal kinetic energy release (KER) extending up to about 28,000 cm^{-1}. The high KER confirms the two-photon absorption mechanism via S_1.

To check the feasiblity of two-photon transition via S_1, we carried out electronic structure calculations of the excited state transition of pyruvic acid using EOM-EE-CCSD/6-311(2+)G**. The vertical excitation energy to S_1 is at 3.7 eV (338 nm), in good agreement with the observed 298 K absorption maximum. The vertical transitions to S_2 and S_3 lie at 5.7 eV and 7.0 eV, respectively, and one or both of them can be reached from the S_1 state. Both have significant oscillator strengths for excitation from the S_1 state.

The lowest energy peak in the H-photofragment yield spectrum appears at 26,710 cm^{-1} (374.4 nm, 3.3 eV), in good agreement with the 298 K absorption spectrum. It is most likely the origin band. Although we have not yet completed the assignment of the spectrum, the peaks observed near the band origin appear to involve torsional motions of either CH_3 or around the central C-C bond, which are expected to give rise to vibrational progressions. It is intriguing that we observe similar photofragment yield spectra when monitoring mass 41 (CH_3CO) and mass 45 (HOCO), which are other likely products of the two-photon dissociation processes. Our attempt to detect CO_2 by 3+1 REMPI were unsuccessful.

Future work

The work on the photodissociation of pyruvic acid and the characterization of hydroxycarbenes will continue. We are particularly excited about the collaboration we initiated with David Osborn on pyruvic acid. The experiments are carried out at the Advanced Light Source and exploit his mass spectrometer system. One of my graduate students already had a productive visit, during which large amount of data were collected following the 351 nm photodissociation of pyruvic acid, and several products were identified by tunable ionization energy. These results are now being analyzed and the work will continue, along with our work on the spectroscopy and two-photon dissociation of pyruvic acid. Studies of the production and photochemistry of hydroxycarbenes will continue as well.

References

1. Schreiner, P. R.; Reisenauer, H. P.; Pickard, F. C.; Simmonett, A. C.; Allen, W. D.; Matyus, E.; Csaszar, A. G., *Nature* **2008,** *453* (7197), 906-909.
2. Schreiner, P. R.; Reisenauer, H. P.; Ley, D.; Gerbig, D.; Wu, C.-H.; Allen, W. D., *Science* **2011,** *332* (6035), 1300-1303.
3. Leavitt, C. M.; Moradi, C. P.; Stanton, J. F.; Douberly, G. E., *J. Chem. Phys.* 2014, *140* (17), 171102.
4. Koziol, L.; Wang, Y. M.; Braams, B. J.; Bowman, J. M.; Krylov, A. I., *J. Chem. Phys.* **2008,** *128* (20), 204310.
5. Koziol, L.; Mozhayskiy, V.A; Braams, B.J.; Bowman J.M., Krylov, A.I., *J. Phys. Chem. A* **2009,** *113,* 7802–7809.
6. Reed Harris, A.E.: Doussin, J.-F.; Carpenter, B.K. ,Vaida, V., J. Phys. Chem. A **2016,** 120, 10123−10133.

Publications 2014-2017

1. C.P. Rodrigo, S. Sutradhar, and H. Reisler, "Imaging studies of excited and dissociative states of hydroxymethylene produced in the photodissociation of the hydroxymethyl radical", J. Phys. Chem. A (Yarkonly Festschrift), 118(51), 11916-11925 (2014).
2. S. Sutradhar, B.R. Samanta, A.K. Samanta, and H. Reisler, "Temperature dependence of the photo-dissociation of CO_2 from high vibrational levels: 205-230 nm imaging studies of $CO(X^1\Sigma^+)$ and $O(^3P, ^1D)$ products", J. Chem. Phys. 147, 013916 (2017).

Active Thermochemical Tables

Branko Ruscic
Chemical Sciences and Engineering Division, Argonne National Laboratory,
9700 South Cass Avenue, Argonne, IL 60439
ruscic@anl.gov

Program Scope

The *spiritus movens* of this program is the need to provide the scientific community with accurate and reliable thermochemical information on chemical species that are relevant in energy-generating chemical processes or play prominent roles in subsequent environmental chemistry. Detailed knowledge of thermodynamic parameters for a broad array of stable and ephemeral chemical species is pivotal to chemistry and essential in many industries. In particular, the availability of accurate, reliable, and internally consistent thermochemical values is a *conditio sine qua non* in kinetics, reaction dynamics, formulation of plausible reaction mechanisms, and construction of predictive models of complex chemical environments. In addition, the availability of accurate thermochemical values has historically been the prime driver for steady advancements of increasingly sophisticated electronic structure theories.

The focus of this program is on bringing substantial innovations to the thermochemical field through development of new methodologies, and utilizing them to systematically improve both the quality and quantity of available thermochemical data relevant to energy–producing processes. In order to achieve the stated goals, this program has developed a novel approach that is centered on analyzing and optimally utilizing the information content of *all available* thermochemically relevant determinations. The aim is not only to dynamically produce the best currently possible thermochemical parameters for the targeted chemical species, but also to allow efficient updates with new knowledge, properly propagating its consequences through all affected chemical species, as well as to provide critical tests of new experimental or theoretical data, and to generate pointers to new determinations that are most likely to efficiently improve the overall thermochemical knowledge base. In order to provide a broad perspective of this area of science, the effort of this program is synergistically coordinated with related experimental and theoretical efforts within the Chemical Dynamics Group at Argonne.

Recent Progress

Over the past year we have continued the development of Active Thermochemical Tables (ATcT). ATcT are a new paradigm for developing accurate and reliable thermochemical values for stable and reactive chemical species. Thermochemical determinations (reaction enthalpies, equilibrium constants, bond dissociation energies, etc.) by definition simultaneously involve several chemical species, and thus define the enthalpy of formation of one target chemical species only *relative* to other species. As a consequence, enthalpies of formation generally do not correspond to directly measured quantities; rather, they are indirectly defined via complex manifolds of thermochemical dependencies. Historically, extracting the enthalpies of formation from intertwined (and frequently inconsistent) dependencies was an intractable proposition, resulting in the adoption of a simplified *sequential* approach of inferring the enthalpies of formation one at the time (A begets B, B begets C, etc.), delivering static sets of enthalpies of formation that contain hidden progenitor-progeny relationships and cannot be updated with new knowledge without introducing inconsistencies. The success of ATcT is rooted in treating the intertwined determinations as a network of simultaneous dependences that is amenable to mathematical and statistical manipulation, converting the originally intractable problem to an information-rich environment that produces a quantum leap in the quality and reliability of the resulting thermochemistry. The Thermochemical Network (TN) corresponds to a system of qualified constrains that must be simultaneously satisfied in order to produce enthalpies of formation that correctly reflect the epistemic content of the TN, providing that the uncertainties of the determinations present in the TN are realistic. Because of the unavoidable presence of determinations with 'optimistic' uncertainties (a.k.a. erroneous determinations), ATcT first performs an iterative statistical analysis, which isolates them and brings the TN to self-consistency. Once self-consistency is achieved, ATcT proceeds to solve the TN simultaneously for all included species.

We are currently working on ver. 1.122p of the ATcT TN, which contains >1700 species, intertwined by ~22,500 active determinations (as well as several thousand additional determinations that have been rendered inactive during various analyses and TN improvements). Originally, version 1.122 of the TN (containing ~1200 species) was created in an effort to produce the best possible thermochemistry for essential combustion-related species that are related to three prototypical fuels: methane, ethane, and methanol, considering various sequential bond dissociations and involving all possible CH_n, n = 4 - 0, C_2H_n, n = 6 - 0, COH_n, n = 4 - 0, and OH_n, n = 2 - 0 species. Ver. 1.122 of the TN was subsequently expanded during various projects, creating a number of increasingly expanded subversions (ver. 1.122a through 1.122p). Subversions 1.122a and 1.122b were created to generate the best currently available isomerization energy of HCN ↔ HNC (both species being important in NO_x chemistry during combustion and in the atmosphere, as well as being of considerable astrophysical interest).

Subversion 1.122b was also used in the development of the latest addition to state-of-the-art electronic structure approaches: the ANL0, ANL0-F12 and ANL1 computational protocols, which were developed in collaboration with S. J. Klippenstein and L. B. Harding. The ANL approaches are - in their spirit - not dissimilar to existing state-of-the-art Weizmann, HEAT, Feller-Peterson-Dixon, or Focal Point protocols, though they were custom-tailored to achieve wide applicability to combustion-related species containing C, H, N, and O. The protocols are based on CCSD(T) computations extrapolated to complete-basis-set limit, with corrections for higher-order excitations, anharmonic zero-point energy, core–valence, relativistic, and diagonal Born–Oppenheimer effects, ultimately producing enthalpies of formation with uncertainties (95% confidence intervals) of the order of ±1.0-1.5 kJ/mol for single-reference and moderately multireference species with up to 34 electrons, for which higher order excitations are < 5 kJ/mol. The introductory paper reports ~150 ATcT enthalpies of formation and ~350 newly computed enthalpies of formation (at 0 K) of essential combustion-related species; the latter providing an excellent motivation for further expansion of the ATcT TN, which is a currently ongoing project.

In collaboration with P. Glarborg (DTU), J. A. Miller and S. J. Klippenstein (ANL), the same version of ATcT TN was exploited to provide consistent thermochemistry (in the form of NASA polynomials) of species related to modeling nitrogen chemistry in combustion, which resulted in a comprehensive study that summarized decades of dedicated research in the area of formation and destruction of NO_x, drawing on recent advances in the knowledge of thermochemistry and reaction rates from theoretical work. The study examined different mechanisms for formation and consumption of NO_x, evaluated key reaction steps, and validated the predictive capabilities of various subsets of the model against experimental data.

Additional expansion of ATcT TN (ver. 1.122d), was performed in support of a collaborative study (L. Cheng, Johns Hopkins U., J. Gauss, U. Mainz, P. B. Armentrout, U. Utah, J. F. Stanton, U. Florida) that combined experiment and theory and produced benchmark scalar-relativistic coupled-cluster calculations for dissociation energies of 20 diatomic molecules containing 3d transition metals. ATcT TN was subsequently significantly expanded (ver. 1.122e) to incorporate biofuel-related species (methyl formate, methylacetate, and a number of related radicals) in support of a large collaborative project involving the groups of J. F. Stanton and G. B. Ellison. The study reported experimental and theoretical results on the thermal decomposition of methyl acetate and methyl butanoate in a flash-pyrolysis microreactor. ATcT TN ver. 1.112g and 1.122h were generated during a collaborative project with the group of C.-Y. Ng (U. C. Davis), which was centered on the determination of the appearance energy of methylium (CH_3^+) from methane with unprecedented accuracy (14.32271 ± 0.00013 eV), using a novel photoionization technique based on VUV laser pulsed field ionization photoion detection scheme. The study has also shown that the appearance of the 'step' in VUV pulsed-field photoelectron studies indeed corresponds to the 0 K photodissociative ionization threshold, and experimentally demonstrated the correctness of the previously proposed underlying mechanism that proceeds via dissociation of high Rydberg states followed by field ionization of the fragments. The determined CH_3^+/CH_4 fragmentation onset, in conjunction with the ATcT approach (one of the roles of which was to settle residual ambiguities with respect to the correct adiabatic ionization energy of methyl radical, and arbitrate between two competing highly accurate measurements, ultimately leading to 9.84054 ± 0.00025 eV), led to the most accurate value thus far for the bond dissociation energy of methane, producing $D_0(H\text{-}CH_3)$ = 432.463 ± 0.027 kJ/mol.

Versions of ATcT TN 1.122n and 1.122o were used in a study involving the ionization energy of H_2O_2, performed in a collaborative effort involving members of the recently established ATcT Task Force One (ATcT TF1, J. F. Stanton and T. L. Nguyen, U. Florida, J. H. Baraban, Ben-Gurion U., P. B. Changala, JILA, G. B. Ellison, U. Colorado, and B.R. and D. H. Bross, ANL). The study involved an analysis involving state-of-the-art quantum chemistry (HEAT) results, spectral simulations taking advantage of multidimensional Franck-Condon calculations, combined with careful reassessment of prior experimental results, and used within a multi-step exercise of the ATcT approach to establish a refined adiabatic ionization energy for H_2O_2, rectifying recent claims of a possible lower ionization energy arising from synchrotron-based determinations. This study was highlighted on the journal cover page.

Several subversions, culminating in the current version 1.122p, were used in revising the enthalpy of formation of N_2H_4. Earlier on (ver. 1.118), the ATcT value was based entirely on calorimetry of the liquid phase and the vaporization enthalpy; however, it was apparent that the experiments are inconsistent with high-level computational results (such as W4), which prompted us to reanalyze more carefully the TN surrounding this species and add additional mid-level computations. Alas, while the analyses kept confirming the inconsistency, the formal uncertainty of experimental results was so tight that they stubbornly maintained supremacy, and only if their uncertainties were arbitrarily relaxed, the results for gas-phase N_2H_4 showed some drift toward the theoretical results (ver. 1.120). The problem was eventually solved in favor of theory, but only after incorporating extremely accurate computations (collaboration with D. Feller), which finally provided sufficient cumulative statistical weight to theory.

We have a number of other national and international collaborations, not discussed above, two of which nevertheless deserve a special mention, because they are related to two new ATcT Task Forces (K. Peterson, WSU, and R. Dawes, MST). It goes without saying that we also have a number of past and ongoing internal collaborations (D. H. Bross, A. F. Wagner, S. J. Klippenstein, L. B. Harding, A. W. Jasper, R. Sivaramakrishnan, K. Prozument, R. S. Tranter, M. Davis).

Future Plans

Future plans of this program pivot around further development and expansion of the Active Thermochemical Tables approach, continuing to provide accurate thermochemistry, and driving targeted thermochemically-relevant theoretical and experimental investigations of radicals and transient species that are intimately related to combustion and post-combustion atmospheric processes. A significant part of the effort will be focused on continued 'finalization' and dissemination of the resulting ATcT thermochemistry, typically involving groups of related chemical species. One important component of this process, focused on their enthalpies of formation, consists of testing and analyzing the TN dependencies, using tools such as the variance/covariance decomposition approach and analyses of the influence of relevant determinations via the hat-matrix, followed by improving the connectivity within the TN and adding new high-quality results (either virtual, i.e. computational, or actual, i.e. experimental) to coerce the resulting thermochemistry toward stable, 'release quality' values. This iterative process unavoidably results in an expansion of the TN with new related chemical species, which is an added benefit. Another equally important component focuses on enhancing the accuracy of their partition functions, typically by upgrading RRHO partition functions with NRRAO partition functions, which is a currently ongoing effort. Future plans invariably incorporate a continuation of the current effort of expanding our web site (ATcT.anl.gov) that displays the ATcT thermochemistry together with ever increasing amounts of pertinent metadata. The web site is generated automatically, maintains rigorous archival capability, and provides data that is helpful to a wide community of users (10000+ unique visitors per month). Pertinent metadata that we will continue generating aims to adequately document the provenance of each thermochemical value, entailing a variance decomposition analysis for each of the chemical species. Finally, another long-term component of future progress consists of enhancing the underlying ATcT software, making it more efficient as well as user-friendly.

This work is supported by the U.S. Department of Energy, Office of Basic Energy Sciences, Division of Chemical Sciences, Geosciences, and Biosciences, under Contract No. DE–AC02–06CH11357.

Publications resulting from DOE sponsored research (2015 – present)

- *Modeling Nitrogen Chemistry in Combustion*, P. Glarborg, J. A. Miller, B. Ruscic, and S. J. Klippenstein, *Progress Energy Combust. Sci.* **67**, 31-68 (2018), DOI: 10.1016/j.pecs.2018.01.002
- *Time-Resolved Kinetic Chirped-Pulse Rotational Spectroscopy in a Room-Temperature Flow Reactor*, D. P. Zaleski, L. B. Harding, S. J. Klippenstein, B. Ruscic, and K. Prozument, *J. Phys. Chem. Lett.* **8**, 6180-6188 (2017), DOI: 10.1021/acs.jpclett.7b02864
- *Post-Transition State Dynamics and Product Energy Partitioning Following Thermal Excitation of the F···HCH$_2$CN Transition State: Disagreement with Experiment*, S. Pratihar, X. Ma, J. Xie, R. Scott, E. Gao, B. Ruscic, A. J. A. Aquino, D. W Setser, and W. L. Hase, *J. Chem. Phys.* **147**, 144301/1-15, DOI: 10.1063/1.4985894
- *Active Thermochemical Tables: The Adiabatic Ionization Energy of Hydrogen Peroxide*, P. B. Changala, T. L. Nguyen, J. H. Baraban, G. B. Ellison, J. F. Stanton, D. H. Bross, and B. Ruscic, *J. Phys. Chem. A* **121**, 8799-8806 (2017), DOI: 10.1021/acs.jpca.7b06221 (*highlighted on the journal cover, see https://pubs.acs.org/toc/jpcafh/121/46#*)
- *Ab initio Computations and Active Thermochemical Tables Hand in Hand: Heats of Formation of Core Combustion Species*, S. J. Klippenstein, L. B. Harding, and B. Ruscic, *J. Phys. Chem. A* **121**, 6580–6602 (2017), DOI: 10.1021/acs.jpca.7b05945
- *Enthalpy of Formation of N$_2$H$_4$ (Hydrazine) Revisited*. D. Feller, D. H. Bross, and B. Ruscic, *J. Phys. Chem. A* **121**, 6187-6198 (2017), DOI: 10.1021/acs.jpca.7b06017
- *Thermal Decomposition of Potential Ester Biofuels, Part I: Methyl Acetate and Methyl Butanoate*, J. P. Porterfield, D. H. Bross, B. Ruscic, J. H. Thorpe, T. L. Nguyen, J. H. Baraban, J. F. Stanton, J. W. Daily, and G. B. Ellison, *J. Chem. Phys. A* **121**, 4658-4677 (2017), DOI: 10.1021/acs.jpca.7b02639 (*Veronica Vaida Festschrift*)
- *An Experimental and Theoretical Study of the Thermal Decomposition of C$_4$H$_6$ Isomers*, J. P. A. Lockhart, C. F. Goldsmith, J. B. Randazzo, B. Ruscic, and R. S. Tranter, *J. Phys. Chem. A* **121**, 3827-3850 (2017), DOI: 10.1021/acs.jpca.7b01186
- *A Vacuum Ultraviolet laser Pulsed Field Ionization-Photoion Study of Methane (CH$_4$): Determination of the Appearance Energy of Methylium From Methane with Unprecedented Precision and the Resulting Impact on the Bond Dissociation Energies of CH$_4$ and CH$_4^+$*, Y.-C. Chang, B. Xiong, D. H. Bross, B. Ruscic, and C. Y. Ng, *Phys. Chem. Chem. Phys.* **19**, 9592-9605 (2017), DOI: 10.1039/c6cp08200a *(part of 2017 PCCP Hot Articles collection)*
- *Bond Dissociation Energies for Diatomic Molecules Containing 3d Transition Metals: Benchmark Scalar-Relativistic Coupled-Cluster Calculations for Twenty Molecules*, L. Cheng, J. Gauss, B. Ruscic, P. Armentrout, and J. Stanton, *J. Chem. Theory Comput.* **13**, 1044-1056 (2017), DOI: 10.1021/acs.jctc.6b00970
- *Active Thermochemical Tables (ATcT) Enthalpies of Formation Based on version 1.122 of the Thermochemical Network*, B. Ruscic and D. H. Bross, Argonne National Laboratory, Argonne, Ill. (2016), (including provenances, correlated species, and most influential determinations) http://atct.anl.gov/Thermochemical%20Data/version%201.122/
- *Active Thermochemical Tables (ATcT) Enthalpies of Formation Based on version 1.118 of the Thermochemical Network (with a New Search Functionality Based on the ATcT Species Dictionary)*, B. Ruscic, Argonne National Laboratory, Argonne, Ill. (2016), http://atct.anl.gov/Thermochemical%20Data/version%201.118/
- *Extension of Active Thermochemical Tables (ATcT) Values ver. 1.118 with Provenances of the Enthalpies of Formation Based on Variance Decomposition Analysis and References*, B. Ruscic and D. H. Bross, Argonne National Laboratory, Argonne, Ill. (2016), http://atct.anl.gov/Thermochemical%20Data/version%201.118/index.php
- *On the HCN – HNC Energy Difference*, T. L. Nguyen, J. H. Baraban, B. Ruscic, and J. F. Stanton, *J. Phys. Chem. A* **119**, 10929–10934 (2015), DOI: 10.1021/acs.jpca.5b08406
- *Thermal Dissociation and Roaming Isomerization of Nitromethane: Experiment and Theory*, C. J. Annesley, J. B. Randazzo, S. J. Klippenstein, L. B. Harding, A. W. Jasper, Y. Georgievski, B. Ruscic, and R. S. Tranter, *J. Phys. Chem. A* **119**, 7872-7893 (2015), DOI: 10.1021/acs.jpca.5b01563
- *Active Thermochemical Tables: Sequential Bond Dissociation Enthalpies of Methane, Ethane, and Methanol and the Related Thermochemistry*, B. Ruscic, *J. Phys. Chem. A* **119**, 7810-7837 (2015), DOI: 10.1021/acs.jpca.5b01346
- *IUPAC Technical Report: Standard Electrode Potentials Involving Radicals in Aqueous Solution: Inorganic Radicals*, D. A. Armstrong, R. E. Huie, W. H. Koppenol, S. V. Lymar, G. Merényi, P. Neta, B. Ruscic, D. M. Stanbury, S. Steenken, and P. Wardman, *Pure Appl. Chem.* **87**, 1139-1150 (2015), DOI: 10.1515/pac-2014-0502
- *High-Temperature Chemistry of HCl and Cl$_2$*, M. Pelucchi, A. Frassoldati, T. Faravelli, B. Ruscic, and P. Glarborg, *Combust. Flame* **162**, 2693-2704 (2015), DOI: 10.1016/j.combustflame.2015.04.002

Theoretical Studies of Potential Energy Surfaces and Computational Methods

Ron Shepard
Chemical Sciences and Engineering Division,
Argonne National Laboratory, Argonne, IL 60439
[email: shepard@tcg.anl.gov]

Program Scope: This project involves the development, implementation, and application of theoretical methods for the calculation and characterization of potential energy surfaces (PES) involving molecular species that occur in hydrocarbon combustion, atmospheric chemistry, and gas phase dynamics. These potential energy surfaces require an accurate and balanced treatment of reactants, intermediates, and products. This difficult challenge is met with general multiconfiguration self-consistent field (MCSCF) and multireference single- and double-excitation configuration interaction (MR-SDCI) methods. In contrast to the more common single-reference electronic structure methods, this approach is capable of describing accurately molecular systems that are highly distorted away from their equilibrium geometries, including reactant, fragment, and transition-state geometries, and of describing regions of the potential surface that are associated with electronic wave functions of widely varying nature. The MCSCF reference wave functions are designed to be sufficiently flexible to describe qualitatively the changes in the electronic structure over the broad range of molecular geometries of interest. The necessary mixing of ionic, covalent, and Rydberg contributions, along with the appropriate treatment of the different electron-spin components (e.g. closed shell, high-spin open-shell, low-spin open-shell, radical, diradical, etc.) of the wave functions are treated correctly at this level. Further treatment of electron correlation effects is included using large-scale multireference CI wave functions, particularly including the single and double excitations relative to the MCSCF reference space. The recent focus has included the development and application of the Graphically Contracted Function (GCF) method.

Recent Progress: ELECTRONIC STRUCTURE CODE MAINTENANCE, DEVELOPMENT, AND APPLICATIONS: A major component of this project is the development and maintenance of the COLUMBUS Program System. The COLUMBUS Program System computes MCSCF and MR-SDCI wave functions, MR-ACPF (averaged coupled-pair functional) energies, MR-AQCC (averaged quadratic coupled cluster) energies, spin-orbit CI energies, analytic energy gradients, and nonadiabatic coupling. Geometry optimizations to equilibrium and saddle-point structures can be done automatically for both ground and excited electronic states. The COLUMBUS Program System is maintained and developed collaboratively with several researchers including Russell M. Pitzer (Ohio State University), Thomas Mueller (Jülich Supercomputer Center, Germany), and Hans Lischka (Tianjin University, China, University of Vienna, Austria, and Texas Tech University). The nonadiabatic coupling and geometry optimization for conical intersections is done in collaboration with David R. Yarkony (Johns Hopkins University). The distributed development effort and software coordination uses an svn repository of source code. The parallel sections of the code are

This work was performed under the auspices of the Office of Basic Energy Sciences, Division of Chemical Sciences, Geosciences, and Biosciences, U.S. Department of Energy, under contract number DE-AC02-06CH11357.

based on the single-program multiple-data (SPMD) programming model with explicit message passing using the portable MPI library, and the portable Global Array Library (distributed from PNNL) is used for data distribution. The COLUMBUS codes incorporate several of the newer language features of F90 and later in order to facilitate future development and maintenance efforts. Development versions of the single-facet and multifacet GCF methods are included within the COLUMBUS repository.

GRAPHICALLY CONTRACTED FUNCTION METHOD: We have developed a novel expansion basis for electronic wave functions [see *J. Chem. Phys.* **141**, 064105 (2014) and references therein]. In this approach, the wave function is written as a linear combination of *graphically contracted functions* (GCF), and each GCF in turn is formally equivalent to a linear combination of configuration state functions (CSFs) that comprise an underlying full-CI linear expansion space of dimension N_{CSF}. The CSF coefficients that define the GCFs are nonlinear functions of a smaller number of essential variables $N_{\varphi} \ll N_{CSF}$. The initial implementation of the GCF method relied on the nonlinear basis dimension N_{GCF} to extend the wave function flexibility and to converge molecular properties toward the full-CI limit. We have now implemented an alternative, and potentially more efficient, approach to enhance the wave function flexibility that consists of allowing multiple partially contracted wave functions to be associated with each Shavitt graph node within each GCF. The initial approach is now called the single-facet GCF (SFGCF) method, and this new approach is called the multifacet GCF (MFGCF) method. All of the properties and algorithms previously developed for the SFGCF method are being implemented within the MFGCF code: state-averaging, Hamiltonian matrix construction, one- and two-particle reduced density matrix (RDM) construction, Slater determinant overlaps, graph density computation and display, and spin-density matrix computation. MFGCF expansions with facet counts in the range $f_{MAX} \approx 4$ to 10 have been shown to approach the full-CI PES to within chemical accuracy (1 kcal/mole or better). The GCF method is formulated in terms of spin eigenfunctions using the Graphical Unitary Group Approach (GUGA) of Shavitt, and consequently it does not suffer from spin contamination or spin instability. This is an important feature for the study of radicals and excited states that occur in hydrocarbon combustion, atmospheric chemistry, and gas phase dynamics. The GCF method scales much better with orbital basis function dimension and with the number of electrons than traditional high-level electronic structure methods. No intrinsic restrictions are imposed on the orbital occupations, and in particular there are no artificial excitation-level or occupation restrictions with respect to a reference function or reference space; in this sense, the method is more correctly characterized as a multiconfigurational method rather than a multireference method. Because the wave function is a linear combination of GCF basis functions rather than a single expansion term, this allows the method to be used for both ground and excited electronic states, the increased wave function flexibility leads to higher accuracy, and this expansion form facilitates the computation of transition moments, nonadiabatic coupling, and other properties that at present can only be computed reliably with multireference and multiconfigurational approaches.

An important feature of the GCF method is the recursive computation of transition reduced density matrices (RDM). In our current GCF implementation, these RDM matrix elements are computed according to the following nested loop structure. The indices *p, q, r*, and *s* correspond to the *n* orbital levels of the Shavitt graph used to define the GCF.

DO $p = 1, n$
    Compute D_{pp}, d_{pppp}.
    DO $q = (p+1), n$
        Compute D_{pq}, $d_{ppqq,}$ d_{pqpq}.
        DO $r = (q+1), n$
            Compute d_{ppqr}, d_{pqpr}, $d_{prqq,}$ $d_{pqqr,}$, $d_{pqrr,}$ d_{prqr}.
            DO $s = (r+1), n$
                Compute d_{pqrs}, d_{prqs}, d_{psqr}.
            ENDDO s
        ENDDO r
    ENDDO q
ENDDO p

Because of index symmetry, this results in the full set of distinct RDM matrix elements. In the case of $H_{PQ}=\langle P|\hat{H}|Q\rangle = Tr(\mathbf{hD}) + \frac{1}{2}Tr(\mathbf{gd})$ computation, these RDM elements are combined immediately with the 1- and 2-electron Hamiltonian integrals as they are computed, eliminating the need to store the full set of RDM elements. If these integrals are stored in the order that they are needed and accessed accordingly, then random access to the full integral list is obviated; this simplifies the overall storage requirements and I/O to external storage, it maximizes usage of local cache memory, and in a parallel environment it simplifies and reduces the overall communications requirements when these arrays are stored in a distributed fashion across the nodes.

The integral set (h_{pp}, h_{pq}, g_{pppp},…g_{psqr}) is sorted (reordered) after the MO transformation step into this final order. This requires an overall address to be determined from the orbital level indices p, q, r, and s. In our current implementation, this is achieved using an intermediate 2-D graphical structure, denoted G(0:n,0:m) where m is the number of orbital indices in the integral subset (1 through 4 in the above loop structure). G(0,0) is the root of the directed graph and G(n,m) is the head. The final indexing is achieved with a two step algorithm. In the first step, arc weights are assigned to the vertical arcs of the graph beginning with the graph head and proceeding to the graph tail and to the nodes of the graph. The arc weights are chosen to make the upper walk indices distinct and contiguous, and the node weights correspond to the total number of upper walks at each node.

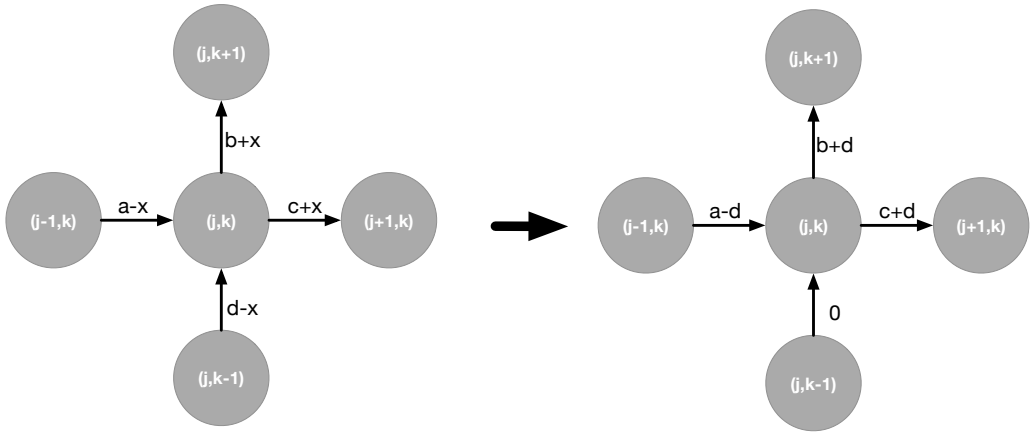

The second step of the algorithm consists of uniform shifts of the arcs associated with each node, the result of which is to reset the downward arc of each node to zero while

maintaining the same walk offset for each walk passing through that node. This is denoted schematically above for a single node G(j,k) and its four connecting arcs. The initial arc weights are denoted (a,b,c,d). These weights may be shifted by the value x as indicated in the figure on the left, and the sum of the arc weights passing through G(j,k) will remain unchanged. If the offset x is chosen to be d, the initial downward arc weight at this step, then the new arc weights are indicated in the figure on the right, and that new arc weight has the value zero. As the arc weights are reset, from the tail of the graph toward the head, moving upwards and to the right, the final result will be that all of the final vertical arc weights will have values of zero, and only the final horizontal arc weights will be nonzero. The vertical arc weights with all zero values need not be stored, the nonzero values may be stored simply a an array for subsequent use, and the intermediate graphical structure can thereafter be discarded. The arc weight summation is then represented as, for example for a 4-index element,

$$\sigma(p,q,r,s) = \alpha(p,1) + \alpha(q,2) + \alpha(r,3) + \alpha(s,4).$$

The implementation of this addressing scheme in the GCF procedure also uses point group symmetry. The above two-step algorithm may be extended in a straightforward way to account for this change. This results in a compact and efficient algorithm to compute contiguous addresses for integrals that are symmetry blocked, and it applies to totally symmetric and nontotally symmetric quantities. This leads to a very general and efficient indexing scheme that can be applied to various array and tensor quantities that arise in quantum chemistry and that involve arbitrary numbers of orbital indices. In addition to Hamiltonian and RDM arrays, other examples include Slater determinant coefficients in string-based approaches, T_1, T_2, T_3, T_4, etc. coupled-cluster coefficients, gradients, Hessian matrices, and other covariant derivative quantities, and other generalized contractions that arise as intermediate quantities in various computational procedures and molecular property evaluations. This procedure is implemented within a single module in the GCF code, and it is designed to internally set up the graphical representation for an arbitrary number of orbital indices, proceed through the two-step algorithm, and then finally return just the addressing array of interest.

Publications:

"The Representation and Parametrization of Orthogonal Matrices," R. Shepard, S. R. Brozell, and G. Gidofalvi. *J. Phys. Chem. A* **119**, 7924-7939 (2015).

"Shavitt Memorial Festschrift Collection," *Theor. Chem. Acc.* (2016). ISSN: 2194-8666, ISSN 2194-8674 (electronic). Edited by R. Shepard, T. H. Dunning, Jr., and R. M. Pitzer.

"Recent Developments with the Graphically Contracted Function Electronic Structure Method," R. Shepard, Gergely Gidofalvi, and Scott R. Brozell, *8th Molecular Quantum Mechanics, Celebration of the Swedish School Abstracts*, 56 (2016).

"Recent Developments with the Graphically Contracted Function Electronic Structure Method," R. Shepard, Scott R. Brozell, and Gergely Gidofalvi, ISTCP IX Abstracts (2016).

"Recent Developments with the Multifacet Graphically Contracted Function Electronic Structure Method," R. Shepard, Scott Brozell, Gergely Gidofalvi, *Abstracts of Papers of the American Chemical Society* **253**, 212-COMP (2017).

Mechanisms and Models for Simulating Gas Phase Chemical Reactivity

Raghu Sivaramakrishnan
Chemical Dynamics Group, Chemical Sciences & Engineering Division
Argonne National Laboratory, Argonne, IL 60439
raghu@anl.gov

I. Program Scope

Mechanisms describing the chemical reactivity of small gas phase species can be complex involving a myriad of unimolecular and bimolecular elementary steps. The primary scope of this program is to develop and validate detailed chemical kinetics mechanisms and models for use in predictive simulations of high temperature gas phase reactivity.

The kinetics models will be developed on the basis of a consistent framework incorporating theoretical predictions, experimental measurements, and evaluations of elementary reaction rate coefficients including feedback loops between them. The detailed models will subsequently be used for simulations of data from reactors, shock-tubes, rapid compression machines, and flames, the aim being the validation of the mechanistic aspects of these models over wide ranges of temperatures and pressures.

II. Recent Progress

A. Simulating Pyrolysis Chemistry in Micro-Tubular Reactors

The Chen nozzle was originally developed[1,2] as a facile, inexpensive, robust, and "clean" source for the generation of highly reactive intermediates (radicals, biradicals, and carbenes). These reactive species are produced at high temperatures under very short contact times in miniature Silicon Carbide (SiC) micro-tubular reactors. In recent years, this Chen nozzle radical source has been used to interrogate complex high temperature dissociation processes in biomass surrogates,[3,4] and PAH/soot precursor formation.[5] There has been an emphasis on using these microreactors to make high temperature kinetics measurements. This has prompted computational fluid dynamics[6] and experimental[7] studies of the complex flow fields within these microreactors.

In collaboration with R. J. Kee and collaborators (Colorado School of Mines) and K. Prozument we have developed a boundary-layer model[8] to describe the complex flow fields within the micro-tubular reactor. The present model shows that the flow can produce significant radial and axial variations in both the thermodynamics conditions and species concentrations. Thus, plug-flow models may not be appropriate. Results show that using He as a carrier gas produces much more plug-like flow than is the case with Ar as the carrier gas. The model represents a computationally efficient approach to modeling detailed kinetics and has been applied in this work to describe the thermal decomposition kinetics of CH_3CHO.[9]

This boundary layer model will also be applied to explain micro-tubular studies by Prozument on H + CH_3CHO and H + CH_3COCH_3. These studies have been initiated to probe the role of poorly characterized addition-elimination channels in these bimolecular reactions. The temperature profiles from the boundary-layer model reaffirm our prior supposition that some of the pyrolytic chemistry occurs at temperatures (800-1200 K) much lower than the wall temperatures where stable radicals can persist and undergo numerous bimolecular reactions. Preliminary simulations using a kinetics model indicate that H + Reactant addition-elimination reactions and radical-radical addition-eliminations influence the measurements. In particular, our simulations indicate that observations of $^{13}CH_2O$ in 0.1% $^{13}CH_3{}^{13}CHO$, 0.1% CH_3ONO (H-atom source) experiments in the micro-tubular reactor is due to $H^{13}CO + H^{13}CO \rightarrow {}^{13}CH_2O + {}^{13}CO$ at low temperatures (1000 K). At higher temperatures (>1200K), $H + {}^{13}CH_3{}^{13}CHO \rightarrow {}^{13}CH_3 + {}^{13}CH_2O$ is the dominant source for $^{13}CH_2O$. A kinetics model has also been assembled to explain the H + CH_3COCH_3 experiments. The role of radical-molecule and radical-radical addition-elimination reactions will be probed using the detailed kinetics in conjunction with the boundary-layer model. Experimental studies on alkylnitrites and hydroperoxides will also be interpreted with this approach.

B. Probing Variational Effects in the Thermal Decompositions of Hydroxyalkyl Radicals

Hydroxyalkyl radicals are often the dominant intermediates formed by H-atom abstractions from alcohols. These radicals are stable and have bond energies large enough that they persist even in high temperature flame-environments.[10] Recent studies on the thermal decomposition of the simplest hydroxyalkyl radical, CH_2OH, reveals that variational effects impact the predicted kinetics for the C-H β-bond scission reaction. These variational effects predominantly stem from the substantial changes (> factor of 3) in the O-H torsional frequency (with changes in the O-H bond length) in the transition state for the $CH_2OH \rightarrow H + CH_2O$ (β-bond scission) reaction. As a result of including this effect, the dominant decomposition pathway at high temperatures (>1000K) is predicted to be a well-skipping process ($CH_2OH \rightarrow CH_3O \rightarrow H + CH_2O$), in agreement with shock tube experiments[11] on the deuterated analogs of CH_2OH (CH_2OD and CD_2OH). These theoretical predictions and experimental data confound recent theoretical analyses that conclude that β-bond scission is the dominant mechanism for the decomposition of CH_2OH to eventual end products, $H + CH_2O$.

Larger hydroxyalkyl radicals such as CH_3CHOH and $CH_3C(OH)CH_3$ are the dominant radicals produced from hydrogen abstractions in ethanol and iso-propanol. Prior theoretical studies,[12,13] without consideration of variational effects have concluded that the lowest energy pathways for the decomposition of these two radicals through O-H bond β-scission, ($CH_3CHOH \rightarrow H + CH_3CHO$ and $CH_3C(OH)CH_3 \rightarrow H + CH_3COCH_3$) were kinetically dominant even under combustion (>1000 K) conditions. In light of our recent observations[11] for CH_2OH decomposition, the impact of including variational effects are assessed for the decompositions of these two larger hydroxyalkyl radicals. The kinetics implications of these variational analyses on the dissociations these hydroxyalkyl radicals will be assessed through master-equation calculations in collaboration with S. J. Klippenstein.

C. High Accuracy Thermochemical Kinetics for $H + CH_3$ (+M) ⇄ CH_4 (+M)

Due to its paramount role as a chain-terminating process, the chemical kinetics of $H + CH_3$ (+M) ⇄ CH_4 (+M) has received substantial attention[14] from the atmospheric and combustion chemistry communities. With the exception of the inferred high-pressure limiting rate constants, $k_{rec,\infty}$, from a shock tube study[15] of $D + CH_3$, direct measurements of the title reaction in the recombination direction are limited to low temperatures[16] (<600 K). On the other hand, direct shock tube measurements[17-19] of the rate constants in the dissociation direction, k_{diss}, span a higher temperature range 1500 - 4500 K, primarily due to the strong C-H bond in CH_4. Reconciling the thermally disparate experimental database on k_{rec} and k_{diss} requires accurate equilibrium constants for the title reaction that span an extended range of temperatures.

In a CH_4 dissociation study, Sutherland et al.[19] have utilized equilibrium constants (K_{eq}) calculated earlier by Ruscic[20-22] to obtain Troe fits to the relevant experimental data[16-19] on k_{rec} and k_{diss}. These K_{eq} values (300-4500 K) relied on thermochemical parameters for the CH_3 radical that were calculated using the usual rigid-rotor harmonic-oscillator (RRHO) approximation. Similarly, the IUPAC evaluation[23] for the thermochemistry of CH_3, which provides NASA polynomials that are widely used in combustion for simulations over extended T-ranges, also uses the same RRHO approximation. However, a theoretical study[24] of the CH_3 radical concluded that for this species the RRHO approximation is inadequate at high temperatures relevant to flame chemistry. In collaboration with Ruscic, accurate equilibrium constants were determined for the title reaction using the ATcT approach.[25-28] These accurate equilibrium constants were used along with results from a two-dimensional master equation approach[29] (in collaboration with Jasper and Klippenstein) and literature experiments on k_{rec} and k_{diss} to obtain an accurate representation for the kinetics of $H + CH_3$ (+M) ⇄ CH_4 (+M). With experimental studies limited to rare gases (He, Ar, and Kr), theory also offers predictive results for bath gases (N_2, H_2O, and CO_2) relevant to practical simulations. The impact of using an updated fit from this work for the title reaction is assessed through simulations of laminar flame speeds. Simulations of 1-10 atm CH_4-air flames (T_u = 298 K) were performed using two popular combustion models, USC-Mech[30] and Aramco Mech.[31] Replacing k(T,P) and CH_3 thermo with the present recommendations in either of these models[30,31] leads to a noticeable changes in flame speed predictions.

D. Thermal Decompositions of Xylyl Radicals

In collaboration with J.V. Michael, S.J. Klippenstein, and C. Cavallotti (Politechnico Milano), we have initiated a joint experiment-theory study of o-xylylbromide dissociation as a source for o-xylyl radicals and the subsequent dissociation kinetics of o-xylyl. The high sensitivity H-atom ARAS detection technique was used to obtain quantitative measurements of the H-atom yields and rate constants for *o*-xylyl decomposition (1267 K $\leq T \leq$ 1597 K; P ~ 0.3-1.0 atm). The results from these studies and comparisons to earlier studies are discussed in terms of two processes; *o*-xylyl → H + *o*-xylylene and *o*-xylyl → non-H-atom channel. The experimental data have been subsequently compared with the results of a computational investigation performed in collaboration. The full PES is composed of 20 wells connected by 37 transition states. Master equation simulations were performed to determine channel specific rate constants for the decomposition of *o*-, *m*-, and *p*-xylyl for a wide range of temperatures and pressures. The simulations predict that the main products of decomposition are *o*-xylylene + H, *p*-xylylene + H, styrene + H, phenyl + C_2H_4 and fulvenallene + CH_3, with H channels accounting for about 80% of the decomposition products. It was also found that *ortho-meta-para* isomerization is a fast process, with a rate that is competitive with that of decomposition. The theoretical analysis also helped clarify the decomposition kinetics of the *o*-xylylbromide precursor. A publication describing these joint experiment/theory studies is nearing submission.

E. Future work

There are high-level theoretical studies on the thermal dissociations of the smaller C_2 and C_3 radicals. However, such studies are lacking for the larger C_4 and C_5 radicals. In collaboration with Klippenstein we plan to characterize the thermal decompositions of these larger alkyl radicals. In collaboration with Tranter and co-workers we have initiated experimental and modeling studies on the unimolecular and bimolecular reactions of the four C_4H_9 isomers. The modeling studies will be informed by theoretical studies on C_4H_9 + C_4H_9 and radicals (H, CH_3) + C_4H_9 kinetics. In collaboration with Klippenstein and Nils Hansen (CRF-Sandia), we propose to simulate the formation of intermediates in fuel-rich flames of small alkenes/alkynes. A particular focus is on the formation and destruction of larger aromatics, and PAH's to further our understanding of soot precursor chemistry.

III. Acknowledgements

This work was supported by the U.S. Department of Energy, Office of Science, Office of Basic Energy Sciences, Division of Chemical Sciences, Geosciences, and Biosciences under Contract No. DE-AC02-06CH11357.

IV. References

1. D. Kohn, H. Clauberg, P. Chen, Rev. Sci. Instrum. 63 (1992), 4003.
2. J. Blush, H. Clauberg, D. Kohn, D. Minsek, X. Zhang, P. Chen, Acc. Chem. Res. 25 (1992) 385–392.
3. K. Urness, Q. Guan, A. Golan, J. Daily, M. Nimlos, J. Stanton, M. Ahmed, G. Ellison, J. Chem. Phys. 139 (2013) 124305.
4. K. Urness, Q. Guan, T. Troy, M. Ahmed, J. Daily, G. Ellison, J. Simmie, J. Phys. Chem. A 119 (2015) 9962.
5. D. Parker, R. Kaiser, B. Bandyopadhyay, O. Kostko, T. Troy, M. Ahmed, Angew. Chem. Int. Ed. 54 (2015) 5421.
6. Q. Guan, K. Urness, T. Ormand, D. E. David, G. Ellison, J. Daily, Intl. Rev. Phys. Chem. 33 (2014) 447.
7. R. Tranter, A. Kastengren, J. Porterfield, J. Randazzo, J. Lockhart, J. Baraban, G. Ellison, Proc. Combust. Inst. 36 (2017) 4603.
8. P. Weddle, C. Karakaya, H. Zhu, R. Sivaramakrishnan, K. Prozument, R. Kee, In Press, Int. J. Chem. Kin. (2018).
9. R. Sivaramakrishnan, J. V. Michael, L. B. Harding, S. J. Klippenstein, J. Phys. Chem. A 119 (2015) 7724.
10. N.J. Labbe, R. Sivaramakrishnan, S.J. Klippenstein, Proc. Combust. Inst. 35 (2015) 447.
11. N.J. Labbe, S.L. Peukert, L. Ye, R. Sivaramakrishnan, S.J. Klippenstein, J.V. Michael, "OH + CH_3OH Experiments and Theory Probe Mechanistic Aspects of CH_2OH Decomposition", In Preparation, J. Phys. Chem. A.
12. J.P. Senosiain, S.J. Klippenstein, J.A. Miller, J. Phys. Chem. A 110 (2006) 6960-6970.
13. J. Zador, A.W. Jasper, J.A. Miller, Phys. Chem. Chem. Phys. 11 (2009) 11040-11053.

14. D.L. Baulch, C.T. Bowman, C.J. Cobos, R.A. Cox, Th. Just, J.A. Kerr, M.J. Pilling, D. Stocker, J. Troe, W. Tsang, R.W. Walker, J. Warnatz, J. Phys. Chem. Ref. Data 34 (2005) 757-1397.
15. M.-C. Su, J.V. Michael, Proc. Combust. Inst. 29 (2002) 1219-1227
16. M. Brouard, M.T. Macpherson, M.J. Pilling, J. Phys. Chem. 93 (1989) 4047.
17. J.H. Kiefer, S.S. Kumaran, J. Phys. Chem. 97 (1993) 414-420.
18. (a) D.F. Davidson, M.D. Di Rosa, A.Y. Chang, R.K. Hanson, C.T. Bowman, Symp. Int. on Combust. 24 (1992) 589-596. (b) D.F. Davidson, R.K. Hanson, C.T. Bowman, Int. J. Chem. Kin. 27 (1995) 305-308. (c) S.K. Wang, D.F. Davidson, R.K. Hanson, J. Phys. Chem. A 120 (2016) 5427-5434.
19. J.W. Sutherland, M. –C. Su, J.V. Michael, Int. J. Chem. Kin. 33 (2001) 669-684.
20. B. Ruscic Private communication (Sept. 2000) to the authors of Ref. 15.
21. (a) B. Ruscic, M. Litorja, R.L. Asher, J. Phys. Chem. A 103 (1999) 8625 - 8633 (b) G. Herzberg, J. Mol. Spectrosc. 33 (1970) 147-168.
22. M.W. Chase, Jr., C.A. Davies, J.R. Downey, Jr., D.J. Frurip, R.A. McDonald, A.N. Syverud, J. Phys. Chem. Ref. Data 14 (1985) (Suppl. 1) 1-926.
23. B. Ruscic, J.E. Boggs, A. Burcat, A.G. Csaszar, J. Demaison, R. Janoschek, J.M.L. Martin, M.L. Morton, M.J. Rossi, J.F. Stanton, P.G. Szalay, P.R. Westmoreland, F. Zabel, T. Berces, J. Phys. Chem. Ref. Data 34 (2005) 573.
24. D.M. Medvedev, L.B. Harding, S.K. Gray, Mol. Phys. 104 (2006) 104, 73.
25. B. Ruscic, R.E. Pinzon, M.L. Morton, G. von Laszewski, S. Bittner, S.G. Nijsure, K.A. Amin, M. Minkoff, A.F. Wagner, J. Phys. Chem. A 108 (2004) 9979-9997.
26. B. Ruscic, R.E. Pinzon, G. von Laszewski, D. Kodeboyina, A. Burcat, D. Leahy, D. Montoya, A.F. Wagner, J. Phys. Conf. Ser. 16 (2005) 561-570.
27. B. Ruscic, R.E. Pinzon, M.L. Morton, N.K. Srinivasan, M.-C. Su, J.W. Sutherland, J.V. Michael, J. Phys. Chem. A 110 (2006) 110, 6592-6600.
28. B. Ruscic, D. Feller, K.A. Peterson, Theor. Chem. Acc. 133 (2014) 1415.
29. A.W. Jasper, K.M. Pelzer, J.A. Miller, E. Kamarchik, L.B. Harding, S.J. Klippenstein, Science 346 (2014) 1212.
30. H. Wang, X. You, A.V. Joshi, S.G. Davis, A. Laskin, F. Egolfopoulos, C.K. Law, USC Mech Version II. High-Temperature Combustion Reaction Model of H2/CO/C1-C4 Compounds. http://ignis.usc.edu/USC_Mech_11.htm
31. W.K. Metcalfe, S.M. Burke, S.S. Ahmed, H.J. Curran, Int. J. Chem. Kin. 45 (2013) 638-675.

V. Journal articles supported by this project 2015-2018

1. N. J. Labbe, R. Sivaramakrishnan, S. J. Klippenstein, "The Role of Radical + Fuel-Radical Well-Skipping Reactions in Ethanol and Methylformate Low-pressure Flames", Proc. Combust. Inst. **35** (2015) 447-455.
2. R. Sivaramakrishnan, J. V. Michael, L. B. Harding and S. J. Klippenstein, "Resolving some paradoxes in the thermal decomposition mechanism of CH_3CHO", J. Phys. Chem. A **119** (2015) 7724-7733.
3. M. J. Davis, W. Liu, R. Sivaramakrishnan, "Global Sensitivity Analysis with Small Sample Sizes: Ordinary Least Squares Approach, J. Phys. Chem. A **121** (2017) 553-570.
4. P. J. Weddle, C. Karakaya, H. Zhu, R. Sivaramakrishnan, K. Prozument, R. J. Kee, "Boundary-layer Model to Predict Chemically Reacting Flow within Heated, High-Speed, Micro-tubular Reactors" In Press, Int. J. Chem. Kin. (2018).
5. N. J. Labbe, A. W. Jasper, S. J. Klippenstein, J. A. Miller, R. Sivaramakrishnan, B. Ruscic, "From Anharmonic Partition Functions to Flame Chemistry: High Accuracy Thermochemical Kinetics for H + CH_3 (+M) ⇄ CH_4 (+M)", In Preparation, J. Phys. Chem. A (2018).
6. G. Magnotti, Z. Wang, W. Liu, R. Sivaramakrishnan, S. Som, M. J. Davis, "Sparsity Facilitates Chemical Reaction Selection for Engine Simulations", In Preparation, J. Phys. Chem. A (2018).
7. D. Polino, R. Sivaramakrishnan, S. J. Klippenstein, J. V. Michael, C. Cavallotti "Experimental and theoretical studies on the thermal decomposition of xylyl radicals", In Preparation, J. Phys. Chem. A (2018).
8. S. L. Peukert, R. Sivaramakrishnan, S. J. Klippenstein, J. V. Michael, "Shock tube and theoretical kinetics studies on the thermal decomposition of iso-propanol and it's reaction with D-atoms", In Preparation, J. Phys. Chem. A (2018).

Quantum Chemistry of Radicals and Reactive Intermediates

John F. Stanton
Quantum Theory Project
Departments of Chemistry and Physics
University of Florida
Gainesville, FL 32611
johnstanton@ufl.edu

Scope of Research

My research group works in the area of theoretical chemical physics, especially on the properties and chemistry of organic radicals and other reactive intermediates. This research follows a number of paths, including first-principles calculation of bond energies and other thermochemical information (as well as development of methodology needed for such calculations), methods for the simulation and analysis of molecular spectra (especially those relevant to experiments that can be used to glean thermochemical information), the development of *ab initio* quantum chemical methods needed for the accurate treatment of fundamental aspects of electronic structure and potential energy surfaces, and computational kinetics including semiclassical transition state theory and master equation modeling of chemical reactions.

Summary of Selected Recent Accomplishments

• We have recently completed our work on fourth-order vibrational perturbation theory, using the Watson Hamiltonian in the rectilinear normal representation, and the harmonic oscillator, rigid-rotor treatment as zeroth order. The second-order variant of this approach – widely known a VPT2 and used ubiquitously in computational chemistry – is well-known to provide quite good vibrational energy levels for rigid systems, a feature that can be easily rationalized since VPT2 is exact for the Morse potential. Less widely appreciates is that VPT2 is also the basis for the common treatments of rotation-vibration interaction that facilitate studies done with microwave spectroscopy and also provide key information for the extraction of "equilibrium" molecular geometries (those corresponding to minima on the potential energy surface). VPT4 based on the Watson Hamiltonian had not been worked out analytically before, due to the vast complexity in the equations and, perhaps, that VPT2 is sufficiently good that the extra effort was not warranted.

Nonetheless, our work with semiclassical transition state theory[1], in which the standard vibrational term level expressions[2] are extended to the case of a transition state, which is not a bound system, has motivated the extension of VPT to fourth-order. Recently, we have carried out detailed checks on our equations, and are certain that things are now correct. Initial results of this work were published with collaborators from Europe and the Schaefer group at Georgia[3], and the paper documenting our efforts is near the submission stage. Numbers for the water molecule indicate that VPT4 offers a small, but unambiguous improvement for the fundamental levels and also is able to account semi-quantitatively for the (weak) Darling-Dennison resonance involving the

[1] W.H. Miller *Trans. Farad. Soc.* 62, 40 (1977).
[2] Taylor series expansion of the vibrational energies in terms of $(n + \frac{1}{2})$.
[3] W.J. Morgan *et al. J. Phys. Chem. A* 14, 1333 (2018).

two-quantum stretching levels $2\nu_1$ and $2\nu_3$ (to which the VPT2 level of theory is "blind"). Work involving application of VPT4-SCTST to a one-dimensional problem was published two years ago, and is promising; we are currently aiming to apply it for a true multidimensional reactive potential energy surface.

• In collaboration with the Miller group at Ohio State[4], we have made a detailed investigation of the standard spectroscopic interpretation of the Jahn-Teller effect. It is standard procedure to make assignments in electronic spectra of Jahn-Teller systems (epitomized by the methoxy and cyclopentadienyl radicals so vital to combustion) and then fit the (necessarily incomplete) set of assigned levels to those corresponding to a (necessarily simplified) vibronic Hamiltonian. Although the number of levels usually assigned does not permit the fitting of elaborate, high-order Hamiltonians, it is not unusual to obtain quite good fits with "quadratic" Jahn-Teller Hamiltonians, even those that ignore a few members of the full parameter set. When this occurs, as it does – for example – in a recent work on the strongly distorted Jahn-Teller $\tilde{A}^2E''$ state of the notorious nitrate radical, it is generally believed that these parameters are robust in the sense that they are the "true" values that can be related to properties of the potential energy surface. For the A state of NO_3, however, there are very large differences between the "experimental" parameters from the level-fitting procedure and those obtained from high-level coupled-cluster calculations. Using a model system in which all levels are known, and fitting subsets of the entire spectrum of levels, we found that the fitted parameters of a truncated Jahn-Teller Hamiltonian are often in quite poor agreement with the exact values[5], even though the quality of the fits is satisfactory. Accordingly, it appears that the idea that well-fit Jahn-Teller spectra obtained experimentally provide an appropriate test for the ability of *ab initio* methods to model the Jahn-Teller effect is incorrect. Further work in exploring this area is ongoing.

•We have worked in a somewhat new area of spectroscopy – that based on the interaction of low-energy positrons with polyatomic molecules – which probes the vibrational energy level structure in a way quite different from traditional single-photon absorption and emission spectroscopy. In collaboration with the experimental group of C.M. Surko (UCSD) and G.F. Gribakin, a theorist at Queens Univ. Belfast, we have applied vibrational perturbation theory (involving both energy levels and – most important here – transition moments coupling various levels) and a serviceable theory for simulation of these spectra[6]. Going beyond the harmonic approximation, which had not previously been done, makes a dramatic improvement in terms of the correspondence of simulated and observed positron annihilation spectra, and we have developed a general framework for doing these calculations and streamlining the process.

• In addition, with Ruscic, we have worked on several projects associated with the Active Thermochemical Tables (ATcT) paradigm that has had a major impact on the quality and precision of thermochemical data. Principal amongst these is that we have revised the adiabatic ionization energy of hydrogen peroxide, which was recently measured by photoelectron spectroscopy and found to be roughly 0.05 eV higher than previously thought. Using a combination of very high-level coupled-cluster theory and multidimensional anharmonic Franck-Condon simulations, we were able to firmly show that the experimental spectrum had been misassigned; the updated value, based both on our purely theoretical work and a rigorous statistical analysis using the mechanism of ATcT, shows that the original values of this quantity were much closer to the truth than that from the recent photoelectron study.

• Additional information about our DOE-supported research can be found in the publications listed at the end of this document.

[4]H.K. Tran, J.F. Stanton and T.A. Miller *J. Mol. Spectr.* 343, 102 (2018).

[5]The levels that are fit correspond precisely to a *quartic* Hamiltonian.

[6]G.F. Gribakin *et al. Phys. Rev. A.* 96, 062709 (2017).

Students and Postdoctoral Supported:
T.L. Nguyen (postdoc)
C.A. Lopez (student)
J.T. Thorpe (student)

References from 3/2017-3/2018 acknowledging DE-FG02-07ER15884

G.F. Gribakin, J.F. Stanton, J. Danielson, M.R.Natisin and C.R. Surko Mode Coupling and Multiquantum Vibrational Excitation in Feshbach-Resonant Positron Annihilation in Molecules Phys. Rev. A 96, 062709 (2017).

B.B. Dangi, Y. Tang, R.I. Kaiser, K.-H. Chao, B.-J. Sun, A.H.H. Chang, T.L. Nguyen and J.F. Stanton Nonadiabiatic Dynamics in the Formation of the Elusive Disilavinylidene Molecule (H_2SiSi) Angew. Chim. 56, 1264 (2017).

H.K. Tran, J.F. Stanton and T.A. Miller "Quantifying the Effects of High-Order Coupling Terms on Fits Using a Second-Order Jahn-Teller Hamiltonian" J. Mol. Spectr. 343, 102 (2018).

P.B. Changala, T.L. Nguyen, J.H. Baraban, J.F. Stanton and B. Ruscic Active Thermochemical Tables: The Ionization Potential of Hydrogen Peroxide, J. Phys. Chem. A 121, 8799 (2017).

T.L. Nguyen and J.F.. Stanton High-Level Theoretical Study of the Reaction between Hydroxyl and Ammonia: Accurate Rate Constants from 200 to 2500 K J. Chem. Phys. 147, 152704 (2017).

J.P. Porterfield, D.H. Bross, B. Ruscic, J.H. Thorpe, T.L. Nguyen, J.H. Baraban, J.F. Stanton, J.W. Daily and G.B. Ellison Thermal Decomposition of Potential Ester Biofuels. Part I: Methyl Acetate and Methyl Butanoate J. Phys. Chem. A. 121, 4658 (2017).

M.L. Weichman, L. Cheng, J.B. Kim, J.F. Stanton and D.M. Neumark Low-lying Vibronic Level Structure of the Ground State of the Methoxy Radical: Slow-Electron Velocity Map Imaging (SEVI) and Koeppel-Domcke-Cederbaum (KDC) Vibronic Hamiltonian Calculations J. Chem. Phys. 146, 224309 (2017).

W.J. Morgan, D.A. Matthews, M. Ringholm, J. Agarwal, J.Z. Gong, K. Ruud, W.D. Allen, J.F. Stanton and H.F. Schaefer *J. Chem. Theo. Comp.* 14, 1333 (2018).

Universal and State-Resolved Imaging Studies of Chemical Dynamics

Arthur G. Suits
Department of Chemistry, University of Missouri, Columbia MO 65211
suitsa@missouri.edu

I. Program Scope

The focus of this program is on combining universal ion imaging probes providing global insight, with high-resolution state-resolved probes providing quantum mechanical detail, to develop a molecular-level understanding of chemical phenomena. Particular emphasis is placed upon elementary reactions important in understanding and predicting combustion chemistry. This research is conducted using state-of-the-art molecular beam machines, photodissociation, reactive scattering, and vacuum ultraviolet lasers in conjunction with ion imaging technqiues. A major focus of our effort remains crossed-beam reactive scattering of polyatomic molecules, with new directions introduced below. We recently moved our effort from Wayne State University to the University of Missouri, and the new grant at Missouri began in January last year.

II. Recent Progress

<u>O (^{3}P) + alkylamines</u>

A central component of our current DOE research is investigation of polyatomic reaction dynamics using crossed-beams with DC slice imaging. We have developed an intense O(^{3}P) beam source as mentioned in last year's abstract and have applied it to a range of systems as described in the following.

Recently we investigated the mechanism of the elementary reactions of O (^{3}P) radical with amines, dimethylamine (DMA) and trimethylamine (TMA). We have characterized the translational energy release and angular distributions of the reactions using crossed beam scattering combined with universal DC slice imaging. *Ab initio* calculations on the energies and structures along the reaction pathways were also performed to gain insight to the underlying dynamics. Combining these experimental and theoretical studies suggests that ISC from triplet to singlet potential energy surfaces plays an important role in the bimolecular reaction dynamics for O(^{3}P) reaction with amines, although through a perhaps unanticipated mechanism.

The electronic ground state atomic oxygen, O (^{3}P), was generated from the photolysis of SO_2 by 193 nm radiation. Amines (DMA or TMA) seeded in helium were crossed with the O (^{3}P) beam at 90° under single-collision conditions. The scattered products from the bimolecular reaction were ionized at the interaction region by an F_2 excimer laser (157 nm, 7.9 eV). The ions were then accelerated onto a position-sensitive detector that is gated to select a specific *m/z* ratio. The sliced and centroided images were accumulated, reflecting the product velocity-flux contour maps with the speed and angular information for the reaction.

For the bimolecular reaction of O (^{3}P) with TMA at a collision energy of E_{coll} = 8.0 kcal/mol, we detected only one product channel *m/z* 58 under our experimental conditions. This mass channel represents $(CH_3)_2NCH_2$ radical formed with hydroxyl radical (OH) co-fragment after TMA is attacked by the O (^{3}P) atom. The translational energy release distributions of both sideways and backscattered components peak at low energy, ~10% of the collision energy, while the angular distribution is flat, consistent with the isotropic image observed. These experimental

results clearly indicate an indirect reaction mechanism. Evidence of an indirect reaction has long been suggested in kinetics studies as well.

The reaction of O (^{3}P) with DMA was also explored at collision energy of 7.8 kcal mol^{-1}. A single product at *m/z* 44 was detected under our experimental conditions. This indicates an H abstraction pathway producing C_2H_6N radical in this reaction. There are two isomers for the C_2H_6N radical, CH_3NHCH_2 arising from H abstraction at the methyl site, and $N(CH_3)_2$ produced by abstraction at nitrogen. Based on the ionization energy, and confirmed with D substitution, we identify the product we detect as CH_3NHCH_2. Similar low translational energy release and isotropic angular distributions were also obtained here, confirming again that the complex-elimination mechanism plays an important role in bimolecular reactions of O (^{3}P) with amines to produce OH. The complex-elimination mechanism observed here agrees well with the previous cross-jet reactor study and kinetics measurements performed years ago for these reactions.

The crucial underlying question is the pathway for OH elimination from the complex. A careful search along the triplet and singlet potential energy surfaces (PESs) was performed by *ab initio* calculations at the CBS-QB3 level of theory. For the triplet PESs of the O (^{3}P) + TMA reaction, we could not locate any transition state (TS) for the direct H abstraction pathway to generate OH and $(CH_3)_2NCH_2$ products that we probed experimentally. This suggests that the direct reaction is barrierless. Interestingly, we find a roaming-type TS that has one low imaginary frequency (200 cm^{-1}) indicating a flat PES in this region, and two very low bound frequencies (40 and 50 cm^{-1}) corresponding to motions of the O atom relative to the TMA fragment. This roaming-type TS connects two shallow van der Waals complex wells, O…$N(CH_3)_3$ and $(CH_3)_2NCH_2$...OH in the reaction pathway. However, based on the fact of the observed long-lived complex formation and relatively high collision energy E_{coll} = 8.0 kcal mol^{-1} in the experiment, this shallow well is not likely a key aspect of the dynamics. We then searched through the singlet PESs since the coupling between singlet and triplet PESs inducing ISC is ubiquitous in chemistry and it is widely observed in O (^{3}P) reactions with unsaturated hydrocarbons such as C_2H_4 and CH_2CCH_2. We find one transition state (TS) separating two very deep complex wells ($ON(CH_3)_3$ and $(CH_3)_2NCH_2OH$) on the reaction pathway to form the probed products. However, this TS has a very high barrier energy, 45 kcal mol^{-1} above the O(^{3}P) + TMA reactant asymptotic limit. Therefore, the only plausible pathway for the reaction is that the O (^{3}P) radical attacks TMA to initiate direct H abstraction from the methyl group. Then, due to the long-range dipole-dipole interaction and the high dimensionality of the system, OH and $(CH_3)_2NCH_2$ radicals do not part immediately but undergo multiple collisions. At the long-range in the exit channel, where both triplet and singlet PESs have similar energy, the system crosses from the triplet to singlet surface and then falls into the very deep hydroxylamine well, forming $(CH_3)_2NCH_2OH$ 100 kcal mol^{-1} lower in energy than the reactants. The system will stay in the $(CH_3)_2NCH_2OH$ well for a time much longer than its rotational period of the complex, then eliminate OH radical. In this case, the reaction mechanism features ISC *leading to* long-lived complex formation rather than being caused by it. Although we believe this is the first demonstration of ISC occurring in the exit channel, we suspect it is not limited to this case.

<u>O (^{3}P) + alcohols</u>

We have recently begun a systematic study of O (^{3}P) reaction with alcohols, first using our 157nm single-photon probe for slice imaging detection. As we have shown in the past, this gives us some rough selectivity, in that with the probe laser unfocused, we exclusively detect species whose ionization energies are at or below the 7.9 eV photon energy. With the probe laser focused, we are

often able to detect product radicals with higher ionization energies by 1+1 ionization through Rydberg states. For O (^{3}P) reaction with n-propanol and isopropanol probed with an unfocused laser, abstraction at the primary methyl sites or the hydroxyl hydrogen would not yield products we can detect. It is also clear that these are less likely abstraction sites based on the much lower reaction exoergicity. In our initial studies, we have used an unfocused probe laser and examined H abstraction in these two alcohols. We show results for reaction of isopropanol at two collision energies in Figure 1. Although there is significant photochemical background in the forward direction, we are able to subtract this successfully. For both collision energies, the scattering is predominantly backward suggesting direct rebound dynamics. However, as the collision energy is increased, we see an additional forward scattering contribution. Less than 50% of the collision energy appears in translation, deviating significantly from the expected Heavy-Light-Heavy kinematic trend. Further investigation of related systems and a broader range of collision energies is now underway.

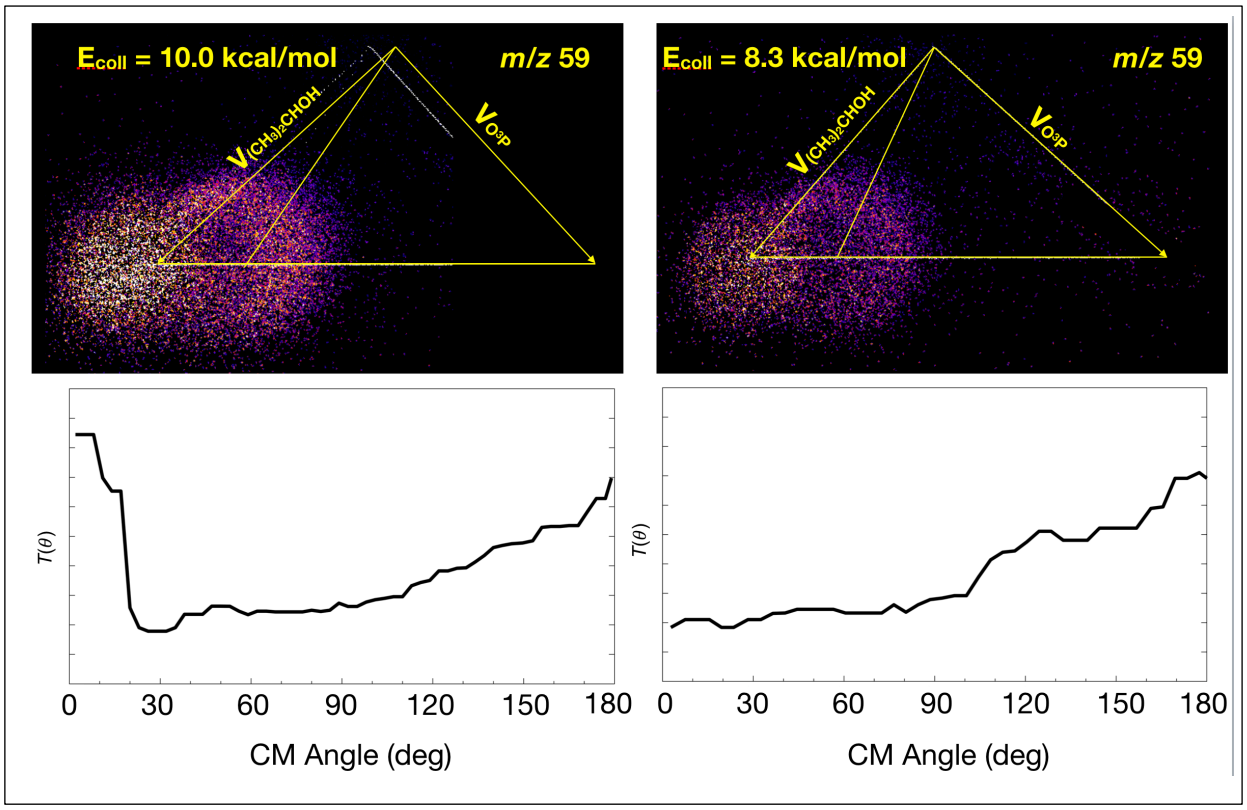

Figure 1. (Top) Crossed-beam DC slice imaging of $(CH_3)_2COH$ radical from O(^{3}P) reaction with isopropanol at indicated collision energy. (Bottom) Center of mass angular distribution for the reaction. Forward direction corresponds to the alcohol beam.

III. Future Directions

We have recently begun adapting a new detection technique developed by our collaborators in Wayne State University led by Dr. Wen Li. This powerful detection scheme uses the standard 2D imaging detector (Microchannel plate / phosphor screen) in conjunction with a high-speed

digitizer. This combination allows the user to record both the position of the ion strike in the standard imaging way, but also the arrival time of the ion at high resolution. This is achieved simply by exploiting the inherent pulse-height distribution on the detector that is manifested both in the spot intensity in the camera and the intensity of the digitizer signal, which may be correlated in software. There are two major advantages over the standard imaging method when using this approach. Firstly, by time stamping the arrival of ions, one is able to build a full 3D distribution of the ion cloud and thus able to slice the image with higher resolution (as this is limited by the digitizer speed rather than the decay time of the phosphor) and in orientations other than parallel to the plane of the detector. We plan to employ this method with femtosecond photodissociation and strong-field ionization to achieve very general time-resolved, multimass detection of photoproducts.

IV. DOE Publications 2014-present

B. Joalland, Shi, Y., Patel, N., Van Camp, R., & Suits, A., "Dynamics of Cl+ Propane, Butanes Revisited: A Crossed Beam Slice Imaging Study." *Phys. Chem. Chem. Phys.* (2014) DOI: 10.1039/C3CP51785C.

B. Joalland, Y. Shi, A. G. Suits and A. M. Mebel, "Roaming dynamics in radical addition/elimination reactions," *Nature Comm.* (2014) DOI: 10.1038/ncomms5064

B. Joalland, Y. Shi, A. D. Estillore, A. Kamasah, A. M. Mebel, A. G. Suits, "Dynamics of chlorine atom reactions with hydrocarbons: Insights from imaging the radical product in crossed beams," *J. Phys. Chem. A* (2014) doi:10.1021/jp504804n (Feature Article).

F. Cudry, J. M. Oldham, S. Lingenfelter, and A. G. Suits. "Strong-Field Ionization of Flash Pyrolysis Reaction Products." *J. Phys. Chem. A* (2015) **119**, 460-467. DOI: 10.1021/jp510552a.

Y. Shi, A. Kamasah, B. Joalland, and A. G. Suits. "Crossed-Beam DC Slice Imaging of Fluorine Atom Reactions with Linear Alkanes." *J. Chem. Phys.* (2015) **142**, 184309.

Shi, Y. Kamasah, A., Suits, A. G., ""H Abstraction Channels in the Crossed-Beam Reaction of F + 1-Propanol, 1-Butene and 1-Hexene by DC Slice Imaging" *J. Phys. Chem. A,* 120.45 (2016): 8933-8940. DOI: 10.1021/acs.jpca.6b08408.

Elementary Reaction Kinetics of Combustion Species

Craig A. Taatjes and Leonid Sheps
Combustion Research Facility, Mail Stop 9055, Sandia National Laboratories, Livermore, CA 94551-0969
cataatj@sandia.gov

SCOPE OF THE PROGRAM

This program aims to develop new methods for studying chemical kinetics and to apply these methods to the investigation of fundamental chemistry relevant to hydrocarbon oxidation and combustion science. One central goal is to perform accurate measurements of the rates at which important free radicals react with each other and with stable molecules. Another goal is to characterize complex reactions that occur via multiple potential wells by investigating the formation of products. These investigations employ simultaneous time-resolved detection of multiple species in well-characterized photolytically-initiated reaction systems where multiple consecutive and competing reactions may occur. Detailed characterization of these reactions under accessible experimental conditions increases the confidence with which these and similar reactions can be predicted for energy mission applications. This research often requires the development and use of new detection methods for precise and accurate kinetics measurements. Absorption-based techniques and mass-spectrometric methods have been emphasized, because many key intermediates are not amenable to fluorescence detection.

An important part of our strategy, especially for complex reaction systems, is using experimental data to test and refine detailed calculations (working in close cooperation with Stephen Klippenstein and Ahren Jasper at Argonne and Judit Zádor at Sandia), where the theory enables rigorous interpretation of experimental results and guides new measurements that will probe key aspects of potential energy surfaces. Moreover, we have increasingly aimed at producing elusive and scientifically important species that are intermediates in oxidation systems (e.g., Criegee intermediates, hydroperoxyalkyl radicals) and characterizing their reactivity through direct probing of their elementary reaction kinetics. We coordinate with Nils Hansen to link individual reaction studies to his controlled measurements of more complex reaction systems.

RECENT PROGRESS

We continue to apply frequency-modulation and direct absorption spectroscopy to measurements of OH and HO_2 product formation in reactions of hydrocarbon and oxygenated hydrocarbon radicals with O_2. These experiments are often coordinated with measurements of other products using the multiplexed photoionization mass spectrometric reactor at the Advanced Light Source (ALS), with David Osborn (see his abstract). We have also continued to expand our understanding of the chemistry of carbonyl oxides (Criegee intermediates), closed-shell singlet species that are nevertheless reactive with stable molecules. Their unusual electronic structure may make their reactivity a probe of multiple-state interactions.[1]

Following "universal" chain carriers in oxidation submechanisms. The key general radical chain carriers, OH and HO_2, are possible universal reporters on low-

temperature oxidation. We have followed the time behavior of both radicals during pulsed-photolytic Cl-initiated oxidation of cyclohexane and its oxygenated analog tetrahydropyran. Both radicals were measured with time-resolved infrared absorption in a temperature-controlled Herriott multipass cell in the temperature range of 500-750 K at 20 Torr. The experiments show two distinct timescales for radical formation in the oxidation of both fuels. In both systems, the faster timescale is strongly related to the "well-skipping" ($R + O_2 \rightarrow$ alkene + HO_2 or cyclic ether + OH) pathway and has a weak temperature dependence. In cyclohexane oxidation, the timescale of the slower HO_2 formation reflects the sequential $R + O_2 \rightarrow ROO \rightarrow$ alkene + HO_2 pathway and has a steep dependence on temperature, but the slower HO_2 formation in tetrahydropyran oxidation is surprisingly temperature insensitive. Differences in HO_2 and OH formation between tetrahydropyran and cyclohexane oxidation arise from ring-opening pathways in the tetrahydropyranyl + O_2 system that compete with the typical $R + O_2$ reaction scheme. This comparison of two similar fuels demonstrates the consequences of differing chemical mechanisms on OH and HO_2 formation and shows they can be highlighted by analysis of the eigenvalues of a system of simplified kinetic equations for the alkylperoxy-centered $R + O_2$ reaction pathways. Such analysis may prove useful for general complex oxidation systems.

Products in low-temperature oxidation of butanone. Previous work in our program has demonstrated the importance of vinoxylic resonance stabilization[2] and isomerization[3] in the initial radicals from ketone oxidation. The low temperature oxidation of two isotopologues of butanone were studied via multiplexed photoionization mass spectrometry at 500 and 700 K, and the products of the initial reaction steps were followed to determine the reactive pathways for R and QOOH isomers. We quantified branching ratios for ethene, diacetyl and the sum of (1-oxiranyl-2-ethanone + tetrahydrofuran-3-one) relative to the concentration of the HO_2 co-product methyl vinyl ketone (MVK). At 500 K, MVK produced from chain-inhibiting pathways is found to be the dominant reaction product. At 700 K, ethene, acetaldehyde and formaldehyde yields are in excess of MVK, as a result of enhanced C–C β-scission pathways of R and QOOH radicals before reaction yielding MVK.

Products of OH Reactions with Alkylperoxy Radicals. The reaction of OH with CH_3OO has recently been measured to be fast,[4] with a rate coefficient of $1\text{-}2 \times 10^{-10}$ cm^3 s^{-1}. However, the products of this reaction, which can have relevance in many hydrocarbon oxidation environments, are uncertain, because of the difficulty of characterizing radical-radical reactions experimentally and because the OH + CH_3OO reaction involves both singlet and triplet states. Theory[5] has found ~45% of reaction products are obtained via intersystem crossing in a weakly bound complex between incipient radical products CH_3O and HO_2. The branching to the closed shell products CH_3OH and O_2 (singlet or triplet) has been the source of some speculation. We have used synchrotron photoionization mass spectrometry to monitor a reacting system in which OH and CH_3OO are both generated by laser photolytically initiated reactions, and have quantified the ratio of formaldehyde (generated by subsequent reaction of the CH_3O radical) to methanol. A methanol branching fraction of (9 ± 5) % was derived from a series of six measurements of the CH_3OO + OH reaction at 30 Torr total pressure, and (6 ± 2) % from a separate measurement of CH_3OO + OD at 740 Torr, using a new high-pressure kinetic photoionization mass spectrometry machine developed under the Argonne-Sandia Consortium on High-Pressure Combustion

Chemistry. Our methanol product branching fraction strongly supports the theory of Müller *et al.*[5] who calculated a branching fraction of 7% to CH_3OH, but dramatically reduces their factor-of-3.5 uncertainty bounds.

Reactions of Carbonyl Oxides. Our product measurements for Criegee intermediate reactions have highlighted the important role of singlet association products. Accordingly, the reaction of the smallest carbonyl oxide, CH_2OO, with water monomer or dimer should form mainly hydroxymethyl hydroperoxide (HMHP). However, a recent extensive study by Wennberg and co-workers[6] had suggested that the reaction $CH_2OO + (H_2O)_2$ directly produces formic acid with a yield of 54%. Using time-resolved measurements of reaction kinetics by UV absorption and product analysis by photoionization mass spectrometry, we showed that the primary products of this reaction are formaldehyde and hydroxymethyl hydroperoxide (HMHP), with direct HCOOH yields of less than 10%.

FUTURE DIRECTIONS

We will continue our collaboration with David Osborn, using photoionization mass spectrometry machines at the Advanced Light Source, and explore effects of unsaturation and oxygenation on low-temperature oxidation chemistry in coordination with Judit Zádor, Ahren Jasper, and Stephen Klippenstein. Measurements of elementary oxidation reactions of representative hydrocarbon and substituted hydrocarbon molecules will continue, with a goal of reaching an understanding of the complex interactions that govern the product formation in these reactions.

References

1. Miliordos, E.; Xantheas, S. S., The Origin of the Reactivity of the Criegee Intermediate: Implications for Atmospheric Particle Growth. *Angew. Chem. Int. Ed.* **2016,** *55*, 1015 –1019.
2. Scheer, A. M.; Eskola, A. J.; Osborn, D. L.; Sheps, L.; Taatjes, C. A., Resonance Stabilization Effects on Ketone Autoxidation: Isomer-Specific Cyclic Ether and Ketohydroperoxide Formation in the Low-Temperature (400-625 K) Oxidation of Diethyl Ketone. *Journal of Physical Chemistry A* **2016,** *120*, 8625-8636.
3. Scheer, A. M.; Welz, O.; Sasaki, D. Y.; Osborn, D. L.; Taatjes, C. A., Facile Rearrangement of 3-Oxoalkyl Radicals is Evident in Low-Temperature Gas-Phase Oxidation of Ketones. *J. Am. Chem. Soc.* **2013,** *135*, 14256-14265.
4. Assaf, E.; Song, B.; Tomas, A.; Schoemaecker, C.; Fittschen, C., Rate Constant of the Reaction between CH_3O_2 Radicals and OH Radicals Revisited. *J. Phys. Chem. A* **2016,** *120*, 8923-8932.
5. Müller, J.-F.; Liu, Z.; Nguyen, V. S.; Stavrakou, T.; Harvey, J. N.; Peeters, J., The reaction of methyl peroxy and hydroxyl radicals as a major source of atmospheric methanol. *Nature Commun.* **2016,** *7*, 13213.
6. Nguyen, T. B.; Tyndall, G. S.; Crounse, J. D.; Teng, A. P.; Bates, K. H.; Schwantes, R. H.; Coggon, M. M.; Zhang, L.; Feiner, P.; Milller, D. O.; Skog, K. M.; Rivera-Rios, J. C.; Dorris, M.; Olson, K. F.; Koss, A.; Wild, R. J.; Brown, S. S.; Goldstein, A. H.; de Gouw, J. A.; Brune, W. H.; Keutsch, F. N.; Seinfeld, J. H.; Wennberg, P. O., Atmospheric fates of Criegee intermediates in the ozonolysis of isoprene. *Phys. Chem. Chem. Phys.* **2016,** *18*, 10241-10254.

Submitted and Accepted Publications with BES support, 2016 –

a. Rebecca L. Caravan, M. Anwar H. Khan, Judit Zádor, Leonid Sheps, Ivan O. Antonov, Brandon Rotavera, Krupa Ramasesha, Kendrew Au, Ming-Wei Chen, Daniel Rösch, David L. Osborn, Christa Fittschen, Coralie Schoemaecker, Marius Duncianu, Asma Grira, Sebastien Dusanter, Alexandre Tomas, Carl J. Percival, Dudley E. Shallcross and Craig A. Taatjes, "The reaction of OH with CH_3OO is not a major source of atmospheric methanol," submitted (2018).
b. Rabi Chhantyal-Pun, Brandon Rotavera, Max R. McGillen, M. Anwar H. Khan, Arkke J. Eskola, Rebecca L. Caravan, Lucy Blacker, David P. Tew, David L. Osborn, Carl J. Percival, Craig A. Taatjes, Dudley E. Shallcross, Andrew J. Orr-Ewing, "Reactive Removal of Tropospheric Carboxylic Acids by Criegee Intermediates," submitted (2018).
c. Leah G. Dodson, John D. Savee, Samer Gozem, Linhan Shen, Anna I. Krylov, Craig A. Taatjes, David L. Osborn, Mitchio Okumura, "Vacuum Ultraviolet Photoionization Cross Section of the Hydroxyl Radical," in revision (2018)
d. M. Anwar H. Khan, Kyle Lyons, Rabi Chhantyal-Pun, Max R. McGillen, Rebecca L. Caravan, Craig A. Taatjes, Andrew J. Orr-Ewing, Carl J. Percival, Dudley E. Shallcross, "Investigating the tropospheric chemistry of acetic acid using the global 3-D chemistry 1 transport model, STOCHEM-CRI," in revision (2018).

e. Alanna L. Koritzke, Jacob C. Davis, Rebecca L. Caravan, Matthew G. Christianson, David L. Osborn, Craig A. Taatjes and Brandon Rotavera, "QOOH-Mediated Reactions in Cyclohexene Oxidation," *Proc. Combust. Inst.*, accepted (2018).

f. M. A. H. Khan, C. J. Percival, R. Caravan, C. A. Taatjes and D. E. Shallcross, "Criegee Intermediates and their impacts on the troposphere," *Environ. Sci.: Processes Impacts* **20**, 437-453 (2018).

g. Ming-Wei Chen, Brandon Rotavera, Wen Chao, Judit Zádor, Craig A. Taatjes, Direct Measurement of OH and HO_2 Formation in R + O_2 Reactions of Cyclohexane and Tetrahydropyran, *Phys. Chem. Chem. Phys.* doi:10.1039/C7CP08164B (2018).

h. Joseph Czekner, Craig A. Taatjes, David L. Osborn, and Giovanni Meloni, "Study of Low Temperature Chlorine Atom Initiated Oxidation of Methyl and Ethyl Butyrate Using Synchrotron Photoionization TOF-Mass Spectrometry," *Phys. Chem. Chem. Phys.* **20**, 5785-5794 (2018).

i. Thomas J. Bannan, A. Murray Booth, Michael Le Breton, Asan Bacak, Jennifer B. A. Muller, Kimberley E. Leather, M. Anwar H. Khan, James D. Lee, Rachel E. Dunmore, James R. Hopkins, Zoë L. Fleming, Leonid Sheps, Craig A. Taatjes, Dudley E. Shallcross, Carl J. Percival, "Seasonality of Formic Acid (HCOOH) in London during the ClearfLo Campaign," *J. Geophys. Res. Atmos.* **122**, 12,488-12,498 (2017).

j. Leonid Sheps, Brandon Rotavera, Arkke Eskola, David L. Osborn, Craig A. Taatjes, Kendrew Au, Dudley. E. Shallcross, M. Anwar H. Khan, and Carl J. Percival, "The reaction of Criegee intermediate CH_2OO with water dimer: primary products and atmospheric impact," *Phys. Chem. Chem. Phys.* **19**, 21970-21979 (2017).

k. Arkke J. Eskola, Ivan O. Antonov, Leonid Sheps, John D. Savee, David L. Osborn, and Craig A. Taatjes, "Time-resolved measurements of product formation in the low-temperature (550 – 675 K) oxidation of neopentane: a probe to investigate chain-branching mechanism," *Phys. Chem. Chem. Phys.* **19**, 13731-13745 (2017).

l. Craig A. Taatjes, "Criegee Intermediates: What Direct Production and Detection Can Teach Us about Reactions of Carbonyl Oxides," *Annu. Rev. Phys. Chem.* **68**, 183-207, doi:10.1146/annurev-physchem-052516-050739 (2017).

m. Rebecca L. Caravan, M. Anwar H. Khan, Brandon Rotavera, Ewa Papajak, Ivan O. Antonov, Ming-Wei Chen, Kendrew Au, Wen Chao, David L. Osborn, Jim Jr-Min Lin, Carl J. Percival, Dudley E. Shallcross, Craig A. Taatjes, "Products of Criegee Intermediate Reactions with NO_2: Experimental Measurements and Tropospheric Implications," *Faraday Discuss.* **200**, 313-330, doi:10.1039/C7FD00007C (2017).

n. Craig A. Taatjes, Fang Liu, Brandon Rotavera, Manoj Kumar, Rebecca Caravan, David L. Osborn, Ward H. Thompson, and Marsha I. Lester, "Hydroxyacetone Production from C_3 Criegee Intermediates," *J. Phys. Chem. A* **121**, 16–23, (2017).

o. Rabi Chhantyal-Pun, Oliver Welz, John D. Savee, Arkke J. Eskola, Edmond P. F. Lee, Lucy Blacker, Henry R. Hill, Matilda Ashcroft, M. Anwar H. Khan, Guy C. Lloyd-Jones, Louise Evans, Brandon Rotavera, Haifeng Huang, David L. Osborn, Daniel K. W. Mok, John M. Dyke, Dudley E. Shallcross, Carl J. Percival, Andrew J. Orr-Ewing, and Craig A. Taatjes "Direct measurements of unimolecular and bimolecular reaction kinetics of the Criegee intermediate $(CH_3)_2COO$," *J. Phys. Chem. A* **121**, 4–15 (2017)

p. Adam M. Scheer, Arkke J. Eskola, David L. Osborn, Leonid Sheps, Craig A. Taatjes, "Resonance Stabilization Effects on Ketone Autoxidation: Isomer-Specific Cyclic Ether and Ketohydroperoxide Formation in the Low-Temperature (400 – 625 K) Oxidation of Diethyl Ketone," *J. Phys. Chem. A* **120**, 8625–8636 (2016).

q. Kai Moshammer, Ahren W. Jasper, Denisia M. Popolan-Vaida, Zhandong Wang, Vijai Shankar Bhavani Shankar, Lena Ruwe, Craig A. Taatjes, Philippe Dagaut, and Nils Hansen, "Quantification of the Keto-hydroperoxide ($HOOCH_2OCHO$) and Other Elusive Intermediates during Low-Temperature Oxidation of Dimethyl Ether," *J. Phys. Chem. A* **120**, 7890–7901 (2016).

r. Ivan O. Antonov, Judit Zádor, Brandon Rotavera, Ewa Papajak, David L. Osborn, Craig A. Taatjes, and Leonid Sheps, "Pressure-Dependent Competition among Reaction Pathways from First- and Second-O_2 Additions in the Low-Temperature Oxidation of Tetrahydrofuran," *J. Phys. Chem. A*, **120**, 6582–6595 (2016).

s. Zhandong Wang, Lidong Zhang, Kai Moshammer, Denisia M. Popolan-Vaida, Vijai Shankar Bhavani Shankar, Arnas Lucassen, Christian Hemken, Craig A. Taatjes, Stephen R. Leone, Katharina Kohse-Hoeinghaus, Nils Hansen, Philippe Dagaut, and S. Mani Sarathy, "Additional chain-branching pathways in the low-temperature oxidation of branched alkanes," *Combust. Flame* **164**, 386-396 (2016).

t. Matthew B. Prendergast, Benjamin B. Kirk, John D. Savee, David L. Osborn, Craig A. Taatjes, Kye-Simeon Masters, Stephen J. Blanksby, Gabriel da Silva, and Adam J. Trevitt, "Formation and stability of gas-phase o-benzoquinone from oxidation of ortho-hydroxyphenyl: a combined neutral and distonic radical study," *Phys. Chem. Chem. Phys.* **18**, 4320-4332 (2016).

u. Giel Muller, Adam Scheer, David L. Osborn, Craig A. Taatjes, and Giovanni Meloni, "Low Temperature Chlorine-Initiated Oxidation of Small-Chain Methyl Esters: Quantification of Chain-Terminating HO_2-Elimination Channels," *J. Phys. Chem. A* **120**, 1677-1690 (2016).

Elementary Reactions of PAH Formation

Robert S. Tranter
Chemical Sciences and Engineering Division, Argonne National Laboratory
Argonne, Il-60439
tranter@anl.gov

I. Program Scope

This program is focused on the experimental determination of kinetic and mechanistic parameters of elementary reactions, in particular those involved in the formation and destruction of the building blocks for aromatic species. The program also encompasses dissociation of novel fuels such as ethers and cyclic species and their dissociation products that are representative of oxygenated intermediates in combustion mechanisms. Thermal sources of radicals are investigated and characterized for use in more complex reaction systems where secondary chemistry can be significant. Recently, the scope has been increased to include thermally initiated roaming reactions. The approach involves a diaphragmless shock tube (DFST) equipped with laser schlieren densitometry (LS) and a time-of-flight mass spectrometer (TOF-MS). The combination of these techniques accesses a wide range of reaction temperatures and pressures. Finally, X-ray diagnostics are exploited to study flows in hostile environments to obtain a better understanding of how to accurately interpret information from some common experimental devices.

II. Recent Progress

A. Cyclic species: Pyrolysis of 2-methyl furan

Cyclic hydrocarbons are important in a broad range of high temperature chemical systems. Even apparently simple molecules such as cycloalkanes present significant challenges to accurate determination of the thermal decomposition mechanism and measurements of rate coefficients. If heteroatoms are introduced into the ring, then the potential reaction pathways multiply with concomitant challenges. The rich gas phase chemistry of heterocycles is illustrated in Figs 1 and 2 from a recent experimental and theoretical study on the pyrolysis of 2-methyl furan (2-MF) with Goldsmith (Brown). Reactions R2-R5 represent complex multistep processes that are initiated by formation of carbenes through intramolecular H and CH_3 shifts. Isomerization of the carbenes is facile and eventually leads to the products. R1 is a simple bond scission reaction that eliminates an H-atom from the methyl side group.

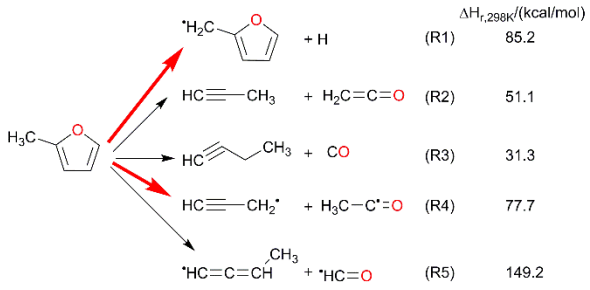

Figure 1. Reaction scheme for the initial multi-channel dissociation of 2-methyl furan. R2 – R5 result from complex pathways involving carbene intermediates.

The pyrolysis of 2-methyl furan was studied by DFST/LS (T=1600-2300K, P=60-240 Torr). The measured density gradient profiles were simulated with a chemical kinetic model containing reactions of 2-MF and sub models for CH_3, C_4H_6 and C_3H_3 chemistry from prior DFST/LS studies. Of the five potential dissociation paths for 2-MF the LS experiments were very sensitive to R1 and R4, somewhat sensitive to R3, but R2 and R5 are of near negligible importance. LS experiments are sensitive to enthalpy of reaction (ΔH_r), Fig. 1, and rate of reaction. The theoretical portion of this work yielded branching fractions for R1-R5 that are shown in Fig. 2. The low flux through R2 and R5 is consistent with the lack of sensitivity to these paths despite significant ΔH_r. R3 is predicted to consume around 25% of 2-MF.

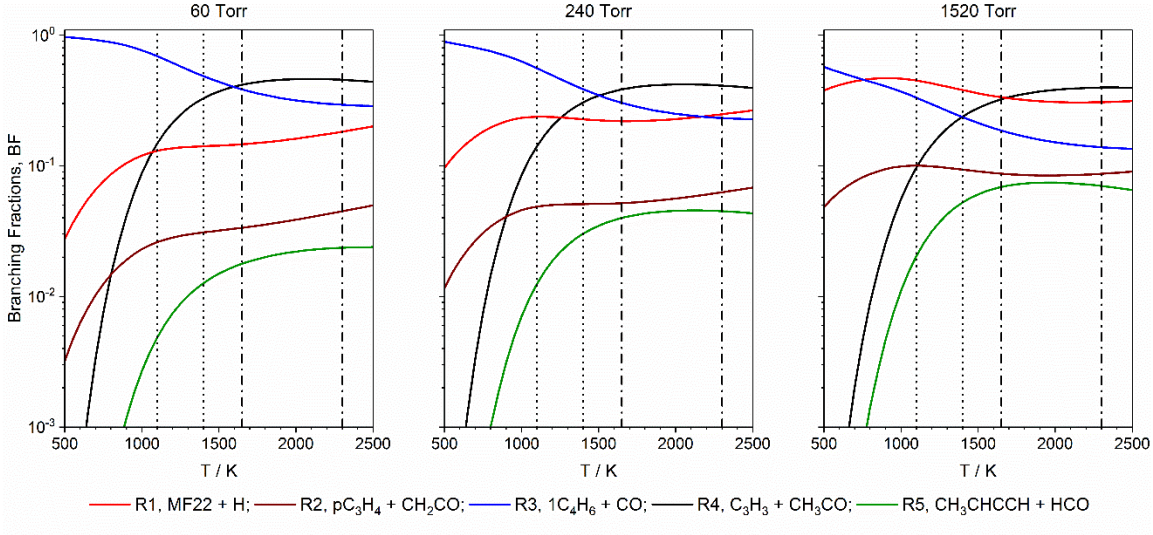

Figure 2: Calculated branching ratios for the 5 most significant reactions in the dissociation of 2-MF dilute in krypton. Dotted vertical lines mark the temperature range of the single pulse shock tube experiments (1520 Torr) by Lifshitz et al.[2] Vertical dash lines denote the range of the current experiments (60 and 240 Torr).

However, the relatively small ΔH_r in comparison to the other channels means that it contributes little to the observed LS signal. R3 is nonetheless a major channel, and has to be accurately accounted for in simulating 2-MF pyrolysis; particularly as the product 1-butyne readily dissociates to C_3H_3 and CH_3 radicals for T > 1600 K. R4 is predicted to be dominant over the complete range of LS experiments. The products of R4 are propargyl and acetyl radicals, the later immediately dissociates to CH_3+ CO. The master equation model also predicts that R1 is a minor channel at low pressures but becomes increasingly important as pressure increases.

The LS results are in broad agreement with a prior theoretical study by Somers et al.[1] A key finding of this work is that R1, elimination of H from the side group, is significantly more important over the complete experimental range than predicted by Sommers et al. and indicated in Fig. 2. In fact R1 accounts for 30-40% consumption of 2-MF even at P=60 Torr. The study also resolves some significant differences between the theoretical work of Sommers et al. and a single pulse shock study by Lifshtiz et al.[2] In particular several C_4H_6 isomers were identified by Lifshitz et al. and 1,3-butadiene was the dominant isomer. Lifhitz et al. postulated mechanisms for direct formation of these species from 2-MF involving carbene intermediates. However, Sommers et al. and the current theory, predicted that 1-butyne is the sole C_4H_6 product from 2MF. In principle, the various C_4H_6 species can isomerize and this would result in a distribution of isomers. However, our recent study of C_4H_6 isomers showed that at the conditions of the current work and Lifhitz's study that 1-butyne will dissociate to CH_3 + C_3H_3 and not isomerize to other C_4H_6 species. Consequently, it is concluded that the distribution of C_4H_6 isomers observed by Lifshitz et al. is due to addition of CH_3 + C_3H_3 probably in the cooling wave of the single pulse experiments.

A solid model has been developed for the initial dissociation of 2-MF that describes a broad set of experiments. However, there remain some challenges to developing a model that accurately extrapolates beyond the current work. These mainly lie in the development of a sufficiently high level theoretical models for the complex dissociation and a more thorough treatment of the collision energy transfer than was used in the present work. These aspects are the focus of ongoing work.

B. Alkyl radicals: low temperature creation, self-reaction and dissociation

#	Rxn	$\Delta H_{r,298K}$
1	$R\text{-}CH_2\text{-}O\text{-}NO = R\text{-}CH_2\text{-}O + NO$	41.9±0.6
2	$R\text{-}CH_2O = R + CH_2O$	11.3±0.3
3	$R = CH_3$ + alkene	23.3
4	R = H + alkene	34.4±1.7
5	R + R = RR	-86.8±1.6
6	$R + R = R_{-H} + RH$	-66.0±2.7
7	R + H = RH	-100.0±1.3
8	$R + H = R_{-H} + H_2$	-69.9±1.7
9	$R + CH_3 = RCH_3$	-89.3
10	$CH_3 + CH_3 = C_2H_6$	-90.0

Table 1: Generic mechanism for decomposition of alkyl nitrites. $\Delta H_{r,298K}$ are averaged from R=C_2H_5, n-C_3H_7 and i-C_3H_7.

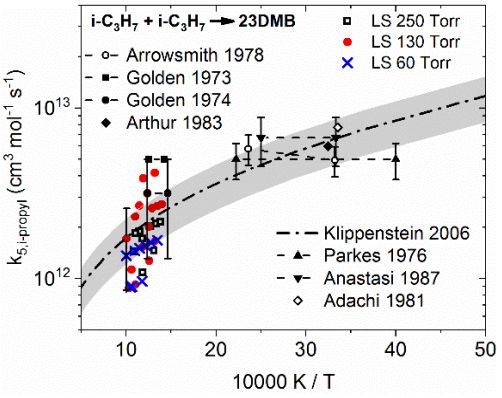

Fig. 3. Comparison of $k_{5,i\text{-propyl}}$ from the present work and selected literature results. The shaded area shows the 30% uncertainty in the Klippenstein 2006[3] value.

Many key processes in the oxidation and pyrolysis of hydrocarbons are dominated by the reactions of alkyl radicals. However, experimental studies in the critical temperature range of 600 to 1000 K are lacking especially at pressures higher than a few Torr. This temperature range is accessible to shock tubes and they could be used to expand the experimental record and provide robust tests of theoretical predictions of rate coefficients and branching ratios for reactions of alkyl radicals. However, shock tube studies of radicals typically rely on the thermal decomposition of a precursor to create the radical and many precursors dissociate by high activation energy processes. Thus, the radicals are generated at higher temperatures than desired and at temperatures where alkyl radicals rapidly dissociate, thereby precluding study of association reactions. To address this problem a broad study of the generation of alkyl radicals from the thermal dissociation of alkyl nitirites has been conducted by DFST/LS. This study builds on a previously reported joint experimental and theoretical study with Jasper on the self-reaction and dissociation of resonantly stabilized 2-methyl allyl radicals (700-1350K), that used thermal dissociation of 3-methylbut-3-enyl nitrite as a low temperature (<900 K) radical source. Alkyl nitrites have now been used to generate ethyl, n-propyl, iso-propyl, 1-butyl, 2-butyl, iso-butyl and tert-butyl radicals in the range 700-1000 K. Both dissociation of the nitrites and the subsequent reactions of the radicals were studied.

Dissociation of alkyl nitrites can be described by a generic reaction mechanism, Table1, which is initiated by scission of the weak O-NO bond and rapid dissociation of the alkoxy radical. At the lower temperatures of these studies the alkyl radicals are thermally stable and reaction 5, recombination, and reaction 6, disproportionation, dominate the secondary chemistry. For n-alkyl radicals k_6/k_5 = 0.05-0.1. As the degree of branching increases the disproportionation channel becomes increasingly dominant and for tert-butyl is heavily favored over reaction 5 (k_6/k_5~2). Several alkyl radicals dissociate by eliminating CH_3 (reaction 3). This is a relatively facile process that becomes significant at around 800 K and is competitive with the disproportionation and recombination paths. Once a population of CH_3 radicals is established then reaction 9 becomes increasingly competitive and is an important sink for both CH_3 and alkyl radicals. The ethyl radical does not eliminate CH_3 and is thermally stable until about 850K, when loss of an H-atom starts to become important which also initiates reactions 7 and 8. The secondary reactions are all strongly exothermic and make significant contributions to the observed LS signals which complicates interpretation. However, literature data and calculations of specific rate coefficients by Jasper and Sivaramakrishnan has allowed the chemical models to be sufficiently constrained to obtain accurate simulations of the LS experiments. For instance, results on the recombination of i-C_3H_7 radicals are shown in Fig. 3.The LS results are in excellent agreement with theoretical values from Klippenstein et al.[3] and the lower T and P experimental literature. The nitrites

provide not only convenient sources for studying self-reaction of radicals but also a well characterized source of radicals for reaction with other species. Furthermore, they can also be used as relatively clean sources for crating initial bursts of H atoms and CH_3 radicals at modest temperatures. Currently, this ability is being exploited to study H + 1,3-pentadiene over the range 1050-1350 K. At these temperature 1,3-pentadiene is stable in LS experiments but the temperature range is largely inaccessible to LS experiments with the traditional source of H-atoms, ethyl iodide.

C. Future work

The DFST/TOF-MS/LS studies of aromatics and resonantly stabilized radicals are being expanded to include reactions between radicals and oxygen molecules. Current studies on the self-reaction and dissociation of alkyl radicals will be completed. The well-characterized alkyl nitrites will be exploited for studying a series of radical + molecule reactions. Further work will be conducted to develop a range of sources of unsaturated and aromatic radicals. Work is continuing on the decomposition of cyclic species and results from the work on n-butyl and s-butyl radicals will help constrain a chemical kinetic model for the dissociation of cycloheptane and 1-heptene. It is anticipated that Michael's high purity shock tube will be converted to a DFST and optical diagnostics will be implemented to complement the DFSST/TOF-MS/LS experiments.

III. References

1) Somers K. P., Simmie J. M., Gillespie F et al., Combust. Flame, **2013**, 160, 2291–2318.
2) Lifshitz A., Tamburu C. and. Shashua R, J. Phys. Chem. A, **1997**, 101, 1018–1029.
3) Klippenstein S.J., Georgievskii Y. and Harding L.B., Phys. Chem. Chem. Phys., **2006**, 8 1133–1147.

IV. Publications and submitted journal articles supported by this project 2016-2018

1) Tranter R. S., Randazzo J. B., Lockhart J. P. A., Chen X. and Goldsmith C. F. 'High Temperature Pyrolysis of 2-Methyl Furan' Phys. Chem. Chem. Phys. **2018**, DOI: 10.1039/C7CP07775K.
2) Randazzo J. B., Fuller M. E., Goldsmith C. F. and Tranter R. S. 'Thermal Dissociation Of Alkyl Nitrites And Recombination Of Alkyl Radicals'**2017**, Proc. Combust. Inst. Submitted.
3) Hansen N., Tranter R. S., Randazzo J. B., Lockhart J. P. A., and Kastengren A. L. 'Investigation of Sampling-Probe Distorted Temperature Fields with X-Ray Fluorescence Spectroscopy' 2017, Proc. Combust. Inst. Submitted.
4) Lockhart J. P. A., Goldsmith C. F., Randazzo J. B., Ruscic B. and Tranter R. S. 'An Experimental and Theoretical Study of the Thermal Decomposition of C_4H_6 Isomers' J. Phys. Chem. A, **2017,** 121, 3827-3850.
5) Hansen N., Tranter R.S., Moshammer K., Randazzo J.B., Lockhart J.P.A., Fugazzi P. G., Tao T., and Kastengren A.L. '2D-Imaging Of Sampling-Probe Perturbations in Laminar Premixed Flames Using Kr X-Ray Fluorescence' Combust. Flame, **2017**, 181, 214-224.
6) Tranter R. S., Jasper A. W., Randazzo J. B., Lockhart J. P. A., and Porterfield J. P. 'Recombination and Dissociation of 2-Methyl Allyl Radicals: Experiment and Theory' Proc. Combust. Inst. **2017**, 36, 211-218.
7) Randazzo J. B., Annesley C. J., Bell K., and Tranter R. S. 'A Shock Tube Laser Schlieren Study of Cyclopentane Pyrolysis' Proc. Combust. Inst. **2017**, 36, 273-280.
8) Tranter R. S., Kastengren A. L., Porterfield J. P., Randazzo J. B., Lockhart J. P. A., Baraban J. H., and Ellison G. B.' Measuring Flow Profiles in Heated Miniature Reactors With X-ray Fluorescence Spectroscopy' Proc. Combust. Inst. **2017**, 36, 4603-4610.
9) Ossler F., Canton S. E., Seifert S., Hessler J. P., and Tranter R. S. 'Measurements of Structures and Concentrations of Carbon Particle Species in Premixed Flames by the use of *In-Situ* Wide Angle X-ray Scattering' Carbon **2016**, 96, 782-798.

HIGH PRESSURE DEPENDENCE OF GAS PHASE REACTIONS AND SEMICLASSICAL BIMOLECULAR TUNNELING APPROACHES

Albert Wagner
Chemical Sciences and Engineering Division
Argonne National Laboratory
9700 South Cass Avenue
Argonne, IL 60439
Email: wagner@anl.gov

PROJECT SCOPE

This program is aimed both at improved semiclassical tunneling processes in bimolecular reactions and at understanding pressure effects on relaxation and reaction processes in higher pressure regimes where collisions between two species may be frequently interrupted by other species.

RECENT PROGRES

High Pressure Relaxation: The pressure dependence of reaction kinetics is typically modeled by Master Equation methods that incorporate the isolated binary collision (IBC) approximation that inelastic collisions are binary events uninterrupted by collisions with other species. Since higher maximum pressures are becoming the norm in internal combustion engine design, we have developed a program to study IBC breakdown starting with an initial focus on energy relaxation. We are using molecular dynamics simulations to study the transition from the IBC regime to higher-pressure regimes for (excited OH)/(Argon bath) with the Sewell group (U. Missouri) and (excited CH_3NO_2)/(Argon bath) with the Rivera-Rivera group (Ferris State University). This simulations follow an initially vibrationally and/or rotationally excited molecule in a periodic box filled with 1000 thermal Ar atoms at 300K and pressures up to 400 atm. For these two systems, the *inter*molecular potentials are available[1] pairwise additive Exp-6 or Lennard-Jones.

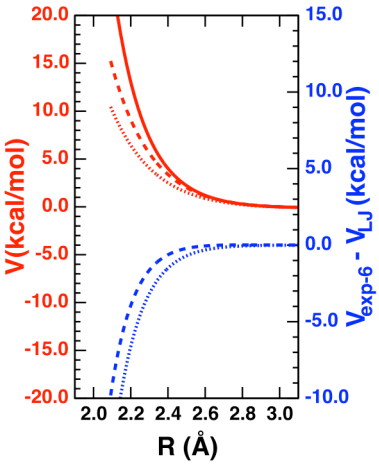

Fig. 1. Ar-H potentials vs. distance. The left (right) axis is for the red (blue) curves. The solid red curve is LJ potential. The dotted and dashed curves are for the Exp-6 (Mayo) and Exp-6 (optimized), respectively. See text.

In our OH simulations, the choice of the Ar-H pairwise potential has a qualitative effect on the relaxation. In Fig. 1, a Lennard-Jones potential (LJ) from a previous Ar/OH study[2] is compared to its Exp-6 potential produced by Mayo rules[3] and then further optimized to minimize the difference with LJ below the 300 K thermal energy of the Ar bath. The optimized potential (Exp6) differs from LJ only in a softer wall above the Ar thermal energy. Fig. 2 shows the decay of the initial OH ($v = 4$) state as a function of time for four pressures. At each pressure, the initial rate of decay is ~ 50 times slower for Exp6. The Exp6 rate when extrapolated to very low pressures is qualitatively similar to experimental measurements on OH($v = 4$) with He.[4] Since

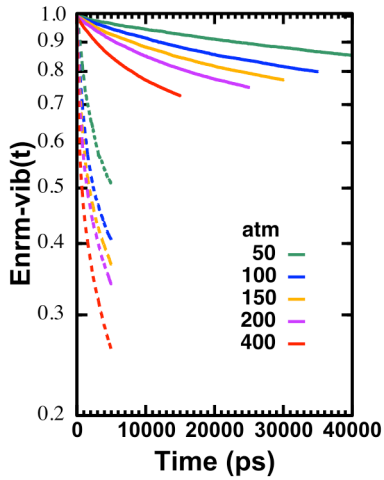

Fig. 2. Normalized excess OH vibrational energy vs. time for five pressures: Exp6 (solid), LJ (dashed) (see text).

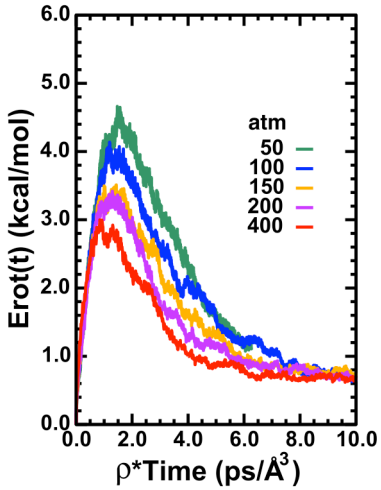

Fig. 3. OH rotational energy vs. density*time for five pressures with LJ potential (see text).

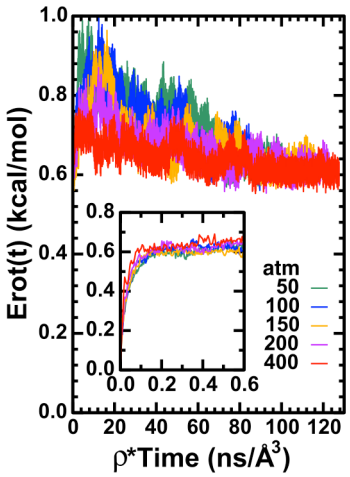

Fig. 4. OH rotational energy vs. density*time for five pressures with Exp6 potential (see text).

the light H in O-H carries all the vibrational amplitude, hyper-thermal collisions of H with Ar are clearly important and sensitive to Exp6 and LJ differences. Both potentials show curvature on a semi-log plot, indicating polyexponential decay. An exponential gap model applied to LJ results indicates this curvature is due to the anharmonicity of OH whose vibrational frequency becomes noticeably higher as vibrational energy decays. This model is now being applied to the Exp6 results. Figures 3 (LJ) and 4 (Exp6) show the rotational energy change from its initial value of zero as a function of density*time which is directly proportional to collision number. In both cases, the rotational energy overshoots the thermal value of kT (0.6 kcal/mol). Such an overshoot is indicative of OH vibrational to rotational energy internal conversion in competition with bath gas thermalization. The higher the pressure and the slower the vibrational relaxation, the more thermalization will dominate with a consequent reduction in the overshoot.

In our CH_3NO_2 simulations, we are decomposing previously published[1] vibrational and

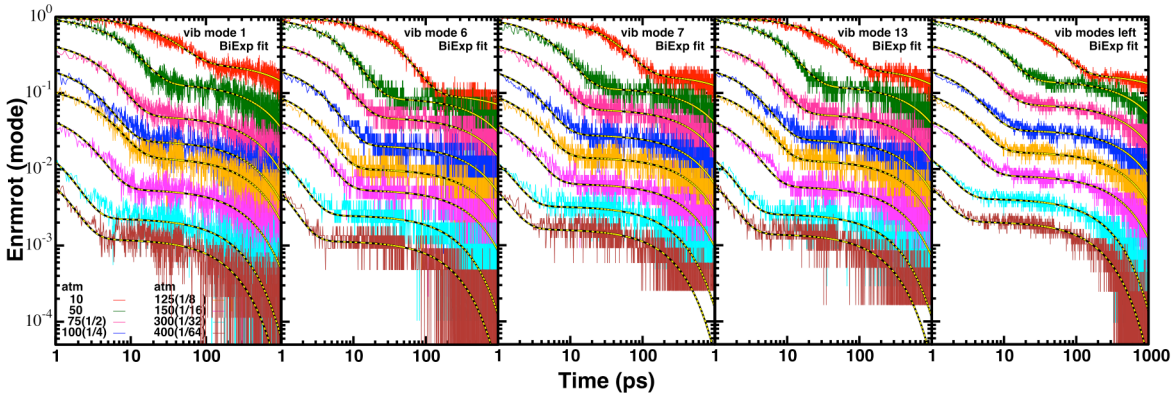

FIG. 5. The contribution of four specific vibrational modes and an aggregate of the remaining eleven vibrational modes to the normalized rotational energy as a function of time for eight pressures (curves are displaced down for each pressure for clarity).

rotational energies as a function of time into contributions from the 15 vibrational and 3

rotational normal modes. With the formulation of Rhee and Kim[5], vibrational energy is exclusively decomposed into vibrational normal modes while both the rotational and vibrational-rotational (Coriolis) energies are decomposed into primarily rotational and secondarily vibrational normal modes. Figure 5 gives the decomposition of the rotational energy into its vibrational mode contributions. This is a log-log plot that emphasizes the rapid early time decay followed by a much slower decay. The dashed yellow lines are biexponential fits of the form: $Ae^{-\alpha t} + (1-A)e^{-\beta t}$. A similar plot and fits have been generated for the analogous contributions of the three rotational modes. Figures 6 and 7 show the density (equivalently, pressure) dependence of the fit-optimized values of α (Fig. 6) and β (Fig. 7) for both the rotational mode and vibrational mode contributions. As shown in the figures, non-linear density dependence is only apparent in the smaller exponent β for later times. We are in the process of developing a map of pressure dependence of mode specific energy relaxation in its vibrational, rotational, and Coriolis forms.

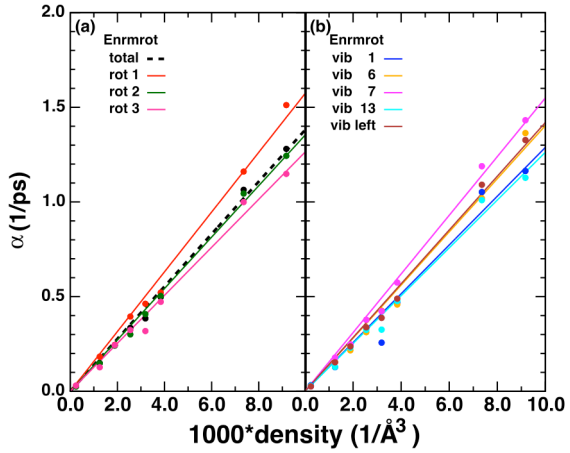

Fig. 6. For the rotational (Panel a) and vibrational (Panel b) contributions to the rotational energy, biexponential α vs. density.

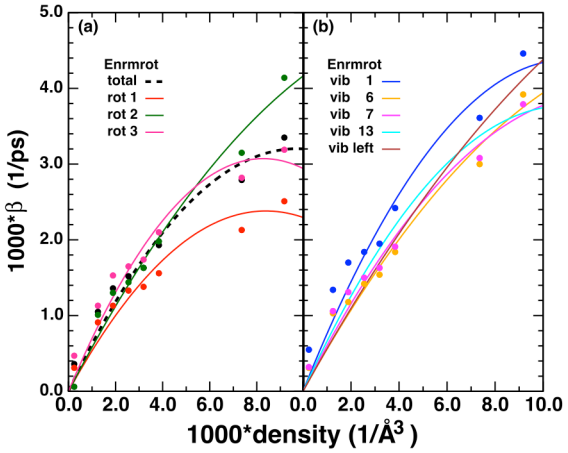

Fig. 7. For the rotational (Panel a) and vibrational (Panel b) contributions to the rotational energy, biexponential β vs. density.

Tunneling in Bimolecular Reactions: Most tunneling methods are based on reaction paths whose calculation is typically not readily parallelized. We recently developed an improved semi-classical tunneling theory[6] (iSCTST) that is based on readily parallelized, second order vibrational perturbation theory (VPT2) at the saddle point. Our approach required the construction of a composite 1D tunneling potential carrying VPT2 saddle point information and the calculated barrier heights in both directions. We have recently reviewed a large variety of bound 1D potentials with analytic quantum mechanical eigenvalues. The eigenvalues for all these potentials have a zero value and slope at the dissociation energy when treated as a function of the quantum number and measured from the bottom of the well. Assuming this is always true and using the usual semiclassical replacement of a quantum number by an imaginary semiclassical action, we can produce an analytic tunneling expression *without the construction of a potential*. Implementation of this approach is in progress.

High Temperature Partition Functions: A new topic concerns partition function which at high temperatures can become quite anharmonic for polyatomic molecules and radicals. Using the

Monte Carlo Phase Space Integrals (MCPSI) method our group has calculated on ab initio potential energy surfaces the ratio Fvib of the anharmonic to harmonic classical partition functions for 22 molecules and radicals.[7] As expected Fvib can be quite large (~2) for larger radicals. To test the accuracy of a classical Fvib, for the smaller systems, D. Bross in our group has jointly carried out exact quantum mechanical (QM) calculations of vibrational levels on the same potential energy surfaces used for MCPSI. This information results in a QM Fvib to which MCPSI Fvib is favorably compared in Fig. 9 for HO_2 and CH_2. With a VPT2 calculation of the anharmonic x matrix, MCPSI Fvib can be approximately corrected for its neglect of zero point energy. The figures shows this correction further improves the accuracy of MCPSI. Of course, unlike highly parallel MCPSI, it is not feasible to obtain a high temperature QM Fvib for large systems.

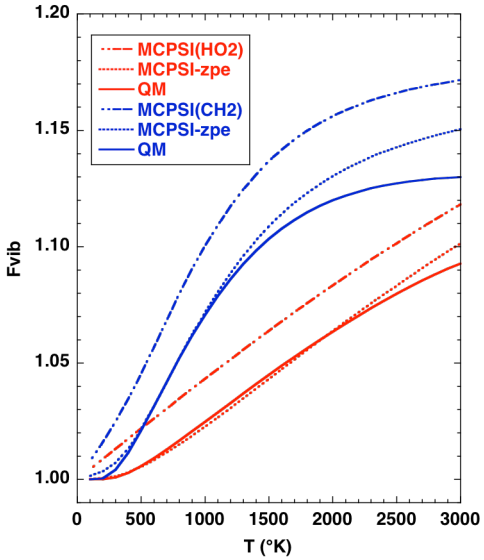

Fig. 9. for HO_2 and CH_2, QM, MCPSI, and zero-point corrected MCPSI Fvib vs. temperature.

FUTURE PLANS

For pressure dependent studies we will complete the CH_3NO_2 and OH simulations and then increase the excitation energy to allow competition between energy relaxation and unimolecular dissociation in HO_2 and also C_2H_5 (in collaboration with R. Dawes (MIST)). For bimolecular tunneling studies, we will implement and test the new version of the iSCTST tunneling approach on several reactions ($O+H_2$, OH+CO, $OH+H_2$, OH+OH, $Cl+CH_4$, and $F+H_2O$) with published VPT2 characterizations by Stanton (U. Florida) and Barker (U. Michigan). For high temperature partition function studies, we intend to apply the zero-point energy correction to all the MCPSI results in DOE-Sponsored publication #1 below.

---

[1] DOE-Sponsored publications #2 and 3 below.

[2] D. L. Thompson, *J. Phys. Chem.* **86,** 2538 (1982).

[3] S. L. Mayo, B. D. Olafson, and W. A. Goddard III, *J. Phys. Chem.* **94,** 8897 (1990).

[4] N. Kohno, J. Yamashita, Ch. Kadochiku, H. Kohguchi, and K. Yamasaki, *J. Phys. Chem. A* **117,** 3253 (2013).

[5] Y.M. Rhee and M. S. Kim, *J. Chem. Phys.* **107**, 1394 (1997).

[6] A. F. Wagner, *J. Phys. Chem. A* **117**, 13089-13100 (2013).

[7] DOE-Sponsored publication #1 below.

DOE-SPONSORED PUBLICATIONS SINCE 2015

1. A. W. Jasper, Z. B. Gruey, L.B. Harding, Y. Georgievskii, S. J. Klippenstein, A. F. Wagner, ANHARMONIC ROVIBRATIONAL PARTITION FUNCTIONS FOR FLUXIONAL SPECIES AT HIGH TEMPERATURES VIA MONTE CARLO PHASE SPACE INTEGRALS, *J. Phys. Chem.* **122**, 1727-1740 (2018).
2. J. W. Perry and A. F. Wagner, PRESSURE EFFECTS ON THE RELAXATION OF AN EXCITED HYDROPEROXYL RADICAL IN AN ARGON BATH, *Proc. Comb. Inst.* **36**, 229 (2017).
3. L. A. Rivera-Rivera, A. F. Wagner, T. D. Sewell, and D. L. Thompson PRESSURE EFFECTS ON THE RELAXATION OF AN EXCITED NITROMETHANE MOLECULE IN AN ARGON BATH, *J. Chem. Phys.* **142**, 014303 (2015).

Chemical Kinetics of Elementary Reactions

Judit Zádor
Combustion Research Facility, Mail Stop 9055, Sandia National Laboratories
Livermore, CA 94551-0969
jzador@sandia.gov

I. PROGRAM SCOPE

My program focuses on fundamental aspects of gas-phase chemical kinetics. I aim to understand and characterize the temperature and pressure dependence of uni- and bimolecular reactions using quantum chemistry and mostly statistical theories often in a master equation framework. Many of the reactions I study have relevance to combustion and atmospheric chemistry. I frequently collaborate with experimentalists. An important part of the program is that I develop methods to automatically explore reactive potential energy surfaces to systematize and significantly accelerate research in elementary chemical kinetics.

II. RECENT PROGRESS

A. The self-reaction of acetylene

Acetylene (C_2H_2) is one of the most well studied molecules in physical chemistry. In gas-phase combustion systems the interest in this molecule stems largely from its role in molecular weight growth processes: pure acetylene pyrolysis serves as a basis for the understanding of the pyrolysis of other hydrocarbons and to soot formation in general. The consensus is that above ~1500 K acetylene pyrolysis starts mainly with the homolytic fission of the C–H bond creating an ethynyl radical (C_2H) and an H atom. However, this mechanism cannot explain the weight growth taking place below ~1500 K, because the fission reaction is too slow here to initiate the chain reaction. Nevertheless, rigorous theoretical or direct experimental evidence was lacking about this hypothetical self-reaction, to an extent that even its molecular mechanism was debated in the literature, except that it should include radicals and H atom production. The C_4H_4 potential energy surface (PES) is very complex and there are multiple pathways that can contribute to the self-reaction of acetylene. The PES has been also very extensively studied in the literature because of its complexity, beauty, and fundamental nature. Our goal was to find out whether the acetylene + acetylene or the acetylene + vinylidene step is the main initiation process in acetylene pyrolysis below ~1500 K, and whether the calculated rate coefficients and branching fractions can account for the low-temperature acetylene pyrolysis observations.

We refined previously calculated quantum mechanical results to construct the PES, and constrained the full master equation for this system, which contains 4 deep wells, 5 bimolecular products, 19 transition states, and 3 shallow wells. We calculated pressure- and temperature-dependent rate coefficients in the 0.001–100 bar and 300–2500 K range. The comparison of the theoretical results to the available experimental results was found to be satisfactory.

We are now in the position to answer the decades-old question: What is the most important initiation reaction for acetylene pyrolysis, and what is the mechanism? We found that acetylene reacts with itself via the vinylidene form, formally creating methylene cyclopropene as the initial adduct, which rapidly interconverts to 1,2,3-butatriene and the lowest energy isomer, vinylacetylene. Both of these species can directly be connected to the H-atom-forming channel necessary for the chain reaction. Moreover, via the well-skipping HCCH + $:CCH_2$ → $HCCCCH_2$ + H reaction prompt H atom formation is also possible at finite pressures. Our calculations also show that the direct dimerization of acetylene is also important, especially below ~1200 K, where it is faster than the acetylene +

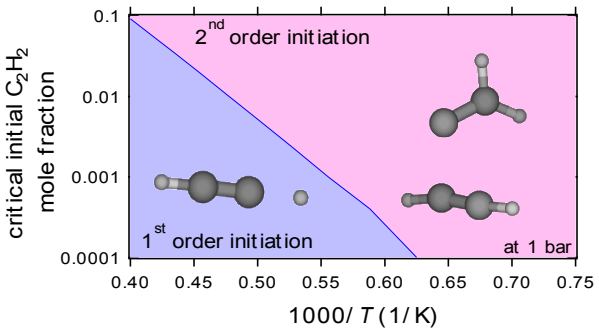

vinylidene initiation. However, this reaction largely just produces cyclobutadiene, with no energetically favorable channels for further isomerization or dissociation. Unless cyclobutadiene contributes to chain propagation in some yet unknown way, this is not a chain propagating reaction. The well-skipping HCCH + HCCH → $HCCCCH_2$ + H reaction is negligible (at most 5%) under the conditions we investigated. Therefore, we can firmly establish that an H atom driven acetylene pyrolysis mechanism is largely initiated by the acetylene + vinylidene entrance channel at low temperatures.

We can also see under what conditions the self-reaction dominates over simple bond scission to produce H atoms. Our calculations show that for dilute mixtures of acetylene (few %, typical of shock tube experiments) the unimolecular initiation dominates H-atom production more and more with increasing temperatures. However, for more concentrated acetylene mixtures the bimolecular reactions dominate even at high temperatures, especially considering that the formed vinylacetylene, not included in this comparison, will also add to the H atom balance on a slightly longer timescale, diminishing the importance of the first order initiation even further for these scenarios.

B. Automated exploration of reaction pathways

KinBot, our code that enables the automated exploration of PESs for a large number of relevant gas-phase systems is being developed currently in two projects outside the core BES funding: the Klippentein-led Exascale Computational Project PACC funded by SC/ASCR, and the Exascale Computational Catalysis (ECC) project led by me funded by SC/CCS. Within the core BES program, I apply the code to chemically interesting problems, some of which are in collaboration with my experimental colleagues.

In collaboration with Green (MIT) and Suleymanov (Cyprus Institute) we investigated the chemical pathways of a γ-ketohydroperoxide using several automated PES exploration tools. Ketohydroperoxides are important in liquid phase autoxidation and in gas phase partial oxidation and pre-ignition chemistry, but because of their low concentration, instability, and various analytical chemistry limitations, it has been challenging to experimentally determine their reactivity, and only a few pathways are known. We found 75 elementary-step unimolecular reactions of the simplest γ-ketohydroperoxide, 3-hydroperoxypropanal by a combination of density functional theory with several automated transition state search algorithms — the Berny algorithm coupled with the freezing string method (FSM), single- and double-ended growing string methods (SSM and GSM), the heuristic KinBot algorithm, and the single-component artificial force induced reaction method (SC-AFIR). The present joint approach significantly outperforms previous manual and automated transition state searches — 68 of the reactions of γ-ketohydroperoxide discovered here were previously unknown and completely unexpected. All methods found the lowest energy transition state, which corresponds to the first step of the Korcek mechanism, but each algorithm except for SC-AFIR detected several reactions not found by any of the other methods.

Analysis of the reverse reactions leading to the formation of γ-ketohydroperoxide reveals promising new chemistry with low energy barriers for reactions involving zwitterions, biradicals, including carbenes, and Criegee intermediates. Similar species are in the focus of current intense research and we showed that several of the detected reactions may be relevant in atmospheric and combustion chemistry. In particular, we studied the reaction of the simplest Criegee intermediate with vinyl alcohol in more detail, which leads to γ-ketohydroperoxide via a submerged barrier reaction with possible well-skipping to two radical products, by calculating the rate constant for this reaction at atmospheric conditions and comparing it to other possible decay processes of vinyl alcohol. As a result of our analysis, directions for subsequent chemical rate studies have been formulated exhibiting a clear example of the benefits of applying automated transition state search algorithms for the discovery of new chemical reactions. Our study highlights the complexity of chemical space exploration and the advantage of combined application of several approaches. Overall, the present work demonstrates both the power and the weaknesses of existing fully automated approaches for reaction discovery which suggest possible directions for further method development and assessment in order to enable reliable discovery of all important reactions of any specified reactant(s).

KinBot-generated PESs were also key to the analysis of MPIMS experiments measuring the low-temperature oxidation products for tetrahydrofurane, a work in collaboration with Leonid Sheps (Sandia). Although no rate coefficients were calculated in this work, our code allowed us to efficiently explore not

just the R + O_2, but also the QOOH + O_2 surfaces, and establish the lowest energy pathways. This was crucial, as we found that the second-O_2 addition reaction involves competing pathways, either producing OH or HO_2. Enumerating and comparing the key channels on the complicated multiwell surfaces is challenging, and was greatly enhanced by our tool.

III. NEW DIRECTIONS AND ONGOING WORK

A. Photoionization of methyl hydroperoxide (MHP)

In collaboration with Sztaray (U Pacific) the dissociative photoionization processes of MHP are being studied with imaging PEPICO experiments and extensive quantum-chemical and statistical rate calculations. Energy selected MHP^+ ions, within a photon energy range of 11.4–14.0 eV, dissociate into CH_2OOH^+, HCO^+, CH_3^+, and H_3O^+ ions. Formation of CH_2OOH^+ is the lowest-energy channel, through a simple bond scission dissociation. This daughter ion represents the ionized form of the smallest "QOOH" radical, $\cdot CH_2OOH$ and its thermochemistry is, therefore, of considerable interest. Statistical modeling of the experimental data gave a 0 K appearance energy of 11.650±0.003 eV for the CH_2OOH^+ ion. From this, together with the heats of formation of MHP and H, and a calculated CH_2OOH ionization energy, a mixed experimental-theoretical heat of formation of 74.5±2.6 kJ mol^{-1} is obtained for the $\cdot CH_2OOH$ "QOOH" radical.

The higher-energy fragmentation pathways are explored by quantum-chemical calculations of the potential energy surface, unveiling a complex web of possible rearrangement-dissociation processes. Ultimately, several of the energetically accessible but kinetically unfavored rearrangements are ruled out and we found that the dominant HCO^+ fragment ion is produced through a roaming transition state. Born-Oppenheimer molecular dynamics simulations confirm the entropically more favored loss of water from the rearranged molecular ion $[H_2CO\ldots H_2O]^+$, leading to an energized H_2CO^+ species, which quickly dissociates to HCO^+. At higher energies, H_3O^+ is formed in a consecutive process from the CH_2OOH^+ fragment ion, through a likely roaming transition state. With the direct C–O fission of the molecular ion leading to the methyl cation completing the picture, these theoretical dissociation pathways show excellent agreement with the experimental data and a full RRKM modeling based on the proposed mechanism needed only small tuning of the calculated transition state properties to match the experimental ion abundances.

B. Pyrolysis of pentanol

In collaboration with Van Geem (U Ghent) we investigate the unimolecular dissociation of *n*-pentanol radicals, which can be thought of as the reverse of 1-pentene + OH reaction, as a continuation of our work on OH + alkene systems. This is yet another, even larger radical system, with relevance to pyrolysis of alcohols. KinBot is used to explore the pathways, which feature mostly usual, at the same time very many isomerization and dissociation pathways, which would be very difficult and slow to study by hand. We also investigate the dependence of the capture rate coefficient into the van der Waals well on the conformation of the pentene molecule as part of this project. Investigating these larger systems with rigorous methods also helps modelers assess the validity of the rules with which they estimate the rate coefficients, and as part of this project we also put the calculated rate coefficients into a comprehensive pentanol pyrolysis model and compare the results to flow reactor experiments. Our results suggest that the rate coefficients based on the KinBot-directed AITSTME framework do matter and improve the comparison between experiment and model.

C. Spin-forbidden chemistry: cyclopentene + O

In collaboration with Osborn (Sandia) and Ramasesha (Sandia), we study the reaction of cyclopentene + O reaction initiated experimentally on the triplet surface. The ethene + O reaction, recently studied in collaboration with Jasper, Miller, and Klippenstein, is dominated by chemistry happening on the singlet surface, because ISC is efficient at the C_2H_4O initial adduct, while the barriers connected to this adduct on the triplet surface are high. The cyclopentene + O reaction, however, can proceed on the triplet surface as well due to submerged barriers belonging to the ring-opening of the initial C_5H_8O adduct and its further isomerization. Moreover, ISC is also possible via these open-chain isomers. Our work is in progress to

explore the relevant parts of the PES aided with KinBot, and to match the predicted products and their branching ratios with the measured yields.

IV. DOE SUPPORTED PUBLICATIONS, 2016-PRESENT

1. Chen, M.-W., Rotavera, B., Chao, W., Lin, J. J.-M., Zádor, J., Taatjes, C. A.: *Direct measurement of OH and HO_2 formation in R + O_2 reactions of cyclohexane and tetrahydropyran: Influence of radical ring-opening in oxidation of cyclic oxygenated hydrocarbons.* Physical Chemistry Chemical Physics, **2018** advance article.
2. Grambow, C. A., Jamal, A., Li, Y.-P., Green, W. H., Zádor, J., Suleimanov, Y. V.: *New unimolecular reaction pathways of a γ-ketohydroperoxide from combined application of automated reaction discovery methods.* Journal of the American Chemical Society, **2018** 140 1035-1048.
3. Johansson, K. O., Campbell, M. F., Elvati, P., Schrader, P. E., Zádor, J., Richards-Henderson, N. K., Wilson, K. R., Violi, A., Michelsen, H. A.: *Photoionization efficiencies of five polycyclic aromatic hydrocarbons*. Journal of Physical Chemistry A, **2017** 121 4447-4454.
4. Johansson, K. O., Zádor, J., Elvati, P., Campbell, M. F., Schrader, P. E., Richards-Henderson, N. K., Wilson, K. R., Violi, A., Michelsen, H. A.: *Critical assessment of photoionization efficiency measurements for characterization of soot-precursor species*. Journal of Physical Chemistry A, **2017** 121 4475-4485.
5. Zádor, J., Miller, J. A.: *The self-reaction of acetylene*. **2017** 121 4203-4217.
6. Rotavera, B., Savee, J. D., Antonov, I. O., Caravan, R. L., Sheps, L., Osborn, D. L., Zádor, J., Taatjes, C. A.: *Influence of oxygenation in cyclic hydrocarbons on chain-termination reactions from R + O_2: tetrahydropyran and cyclohexane*. Proceedings of the Combustion Institute, **2017** 36 597-606.
7. Al Rashidi, M. J., Thion, S., Togbé, C., Dayma, G., Mehl, M., Dagaut, P., Pitz, W. J., Zádor, J., Sarathy, S. M.: *Elucidating reactivity regimes in cyclopentane oxidation: Jet stirred reactor experiments, computational chemistry, and kinetic modeling*. Proceedings of the Combustion Institute, **2017** 36 469-477.
8. Li, X., Jasper, A. W., Zádor, J., Miller, J. A., Klippenstein, S. J.: *Theoretical kinetics of O + C_2H_4.* Proceedings of the Combustion Institute, **2017** 36 219-227.
9. Antonov, I. O.; Zádor, J.; Rotavera, B.; Papajak, E.; Osborn, D. L.; Taatjes, C. A.; Sheps, L.: *Competing reaction pathways in the low-temperature oxidation of THF*. Journal of Physical Chemistry A **2016** 119 7742–7752.
10. Miller, J. A., Klippenstein, S. J., Robertson, S. H., Pilling, M. J., Shannon, R., Zádor, J., Jasper, A. W., Goldsmith, C. F., Burke, M. P.: *"Comment on "When rate constants are not enough" by John R. Barker, Michael Frenklach, and David M. Golden"*. Journal of Physical Chemistry A, **2016** 120 306-312.

Isomer-specific spectroscopy of aromatic fuels and their radical intermediates

Timothy S. Zwier
Department of Chemistry, Purdue University, West Lafayette, IN 47907-2084
zwier@purdue.edu

Program Definition and Scope

The chemical complexity of gasoline, diesel fuels, and aviation fuels, and the fast-expanding list of potential plant-derived biofuels offer a challenge to the scientific community seeking to provide a molecular-scale understanding of their combustion, and of the incomplete combustion that leads to soot formation. Development of accurate combustion models stands on a foundation of experimental data on the kinetics and product branching ratios of individual reaction steps. Spectroscopic tools need to be developed to selectively detect and characterize the widening array of fuel components and the reactive intermediates they generate upon pyrolysis and combustion. There is growing recognition that a key component of future progress in the field is the development of detection schemes that are isomer-specific and even conformation-specific. This research program uses an array of laser-based and broadband microwave methods to carry out conformation-specific spectroscopy on key fuel components and the reactive intermediates formed during their pyrolysis and combustion.

Recent Progress

A. Conformational Preferences of alkylaromatics (ref. 7-9)

We are studying the conformation-specific spectroscopy of a series of alkylaromatics containing phenyl, naphthyl, anthracyl, acenaphthyl, and pyrene as prototypical models for diesel and aviation fuel components and representative of alkylated PAHs present in the early stages of PAH and soot formation. PAHs selectively alkylated at each of the unique sites on the PAH are being synthesized on our behalf by the Ghosh group at Purdue. We obtain conformation-specific UV and alkyl CH stretch IR spectra of each alkylated PAH using UV-UV and IR-UV double resonance methods, with the goal of understanding how the conformational preferences of the alkyl chain are affected by the substitutional position and alkyl chain length of the alkyl group, building off our work on phenylalkanes (ref. 2,7).

The alkyl CH stretch region of the infrared is a region rich in information content, but a challenge to assign, due to the ubiquitous presence of strong Fermi resonance mixing between the alkyl CH stretch and CH bend overtone levels. Conformational assignments based on a comparison of the observed alkyl CH stretch spectra with *ab initio* predictions of harmonic frequencies often fail in spectacular fashion due to these Fermi resonances, which shift and split bands to the point that comparison with harmonic calculations is fruitless. Working in collaboration with Ned Sibert (UW-Madison), we have developed a first-principles model of the alkyl CH stretch region built around a local mode Hamiltonian that explicitly takes into account anharmonic mixing via stretch-bend coupling.

We have recently submitted a manuscript (ref. 9) describing the conformational explosion that accompanies the presence of two alkyl chains on a single phenyl ring. We have recorded LIF excitation and single-conformer IR spectra of *para*-substituted diethyl, dipropyl, and dibutylbenzene. These spectra group in the UV by the number of chains (0,1, or 2) having a *gauche* orientation for the first alkyl chain dihedral. Conformers differing only in whether the two alkyl chains are on the same or opposite sides of the phenyl ring have nearly identical IR spectra, and UV spectra shifted by only a few wavenumbers. Using these experimental techniques in

conjunction with computational methods, subsets of origin transitions in the LIF excitation spectrum can be classified into different conformational families. Two conformations are resolved in p-dEthB, seven in p-dPropB and about nineteen in p-dButB. These chains are largely independent of each other as there are no new single-chain conformations induced by the presence of a second chain. Given the subtle differences in the energies of the conformers, when combined with barriers to isomerization of the alkyl chain that are also similar in size, leads to an 'egg carton' shaped potential energy surface. A cursory LIF excitation scan of *para*-dioctylbenzene shows a broad congested spectrum at frequencies consistent with interactions of alkyl chains with the phenyl π cloud.

We have also completed our study that introduced a new method for recording IR spectra of phenyl-containing molecules in the excited electronic state, recorded by detecting red-shifted fluorescence that occurs following IR excitation of the S_1 origin levels of the molecules. These spectra can have a high signal-to-noise ratio, since the IR-induced fluorescence is against zero background. We surmise that the $S_1(v)$ levels accessed by IR excitation undergo fast IVR prior to fluorescence, and therefore represent emission from an S_1 alkylbenzene with energy greater than the barriers to isomerization of the alkyl chain.

B. Chemically linked diaromatics and incipient stages of soot formation

Motivated by the need to re-consider current models of PAH dimerization in flames, we are studying the conformation-specific spectroscopy of a series of synthesized diaryl compounds involving the same prototypical PAHs linked by ethyl, propyl, and $–CH_2OCH_2-$ chains. Current models of soot formation require dimerization of PAHs as small as pyrene to account for the observed soot particle size distribution. However, the work of Sabbah *et al.*[JPCL **1**, 2962(2010)] has shown that physical dimerization of pyrene will be insignificant at flame temperatures, calling basic tenets of the model into question. We hypothesize that short chemical linkages are responsible for dimerization of smaller PAHs at flame temperatures. This hypothesis is being tested by determining the conformational preferences of the series of diarylalkane and diarylethers linked at the same unique PAH sites from part A. By combining the single-conformation spectroscopic data with theoretical modeling carried out by our collaborator Stephen Klippenstein, we can test how the relative energies and temperature-dependent populations of extended and π-stacked conformers vary with chemical linker, PAH size and shape, and substitution site.

We currently have a complete data set on the first set of molecules in this series: 1,1'-, 2,2'-, and 1,2'-dinaphthylethane, with structures shown below. We are currently working with Ned Sibert and Lyudmila Slipchenko's group to model and understand the infrared spectra and the vibronic coupling in the flexible bichromophore.

C. Mass-correlated broadband microwave spectra of intermediates formed in flash pyrolysis (ref. 6,10-12)

During the past year, we have completed a major upgrade to our chirped-pulse Fourier Transform microwave spectrometer (CP-FTMW), by incorporating into it a time-of-flight mass spectrometer (TOFMS), shown in schematic form in Figure 1. Using 118 nm light to carry out VUV single photon photoionization, we can record mass spectra that reflect the composition of the mixture of interest with little

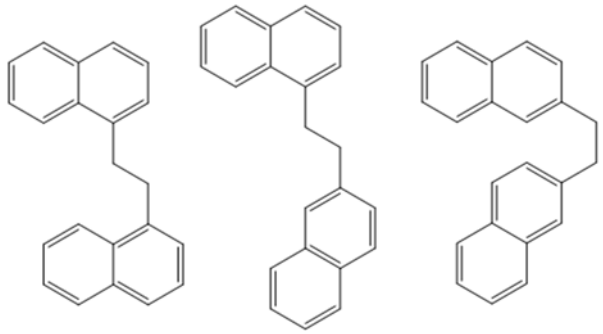

molecular fragmentation, whether it's the effluent from a flash pyrolysis source, a discharge, or a photochemical mixture. We have focused particularly to date on recording TOFMS as a function of pyrolysis source temperature, looking for correlations between the masses appearing in the mass spectrum and rotational transitions in the microwave. As Figure 2 shows, these mass-correlated microwave spectra help identify the molecular formulae of the carriers of rotational transitions. When combined with strong-field coherence breaking methods that select out of a mixture transitions due to a single component of that mixture, the combined scheme enables efficient assignment of the microwave transitions.

With the pyrolysis source, we have recorded and assigned microwave spectra due to the 2-furanyloxy radical (from 2-methoxyfuran), the phenoxy radical (from anisole and phenyl allyl ether), and *ortho*-hydroxy phenoxy radical (from guaiacol). The temperature-dependent signals of the 2-furanoxy radical from TOFMS and CP-FTMW spectra are compared in Figure 2.

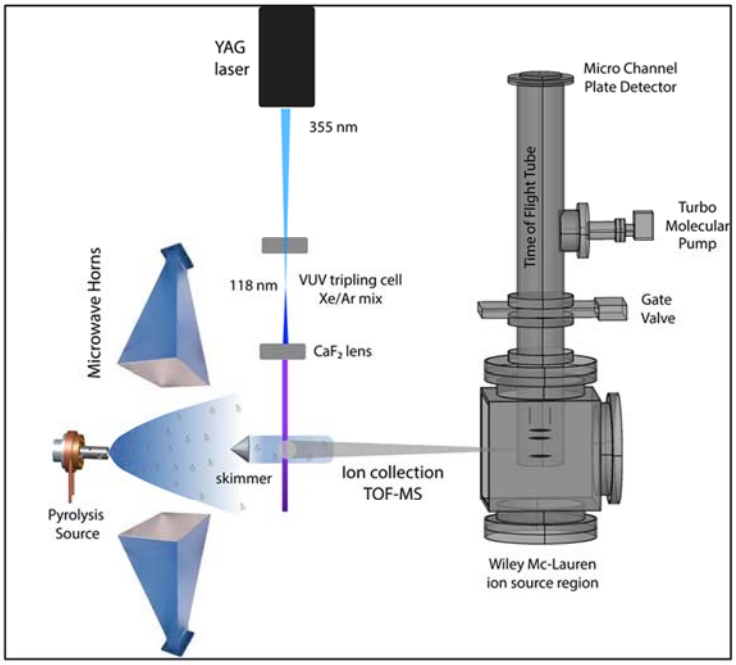

***Figure 1**. Schematic diagram of the combined CP-FTMW and TOF mass spectrometer, outfitted with a flash pyrolysis source.*

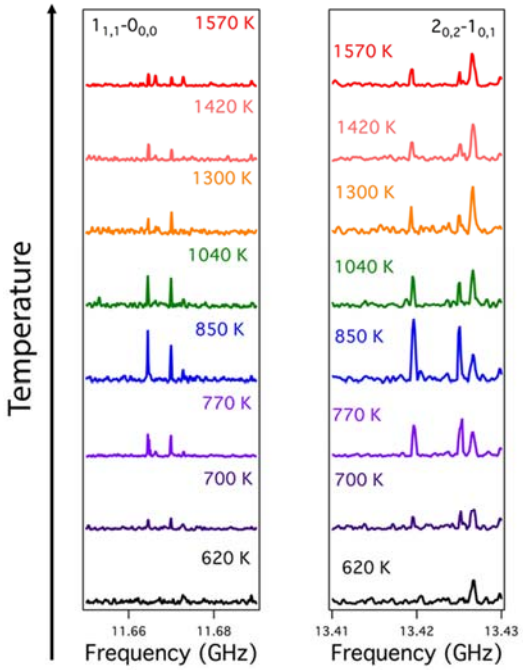

Figure2: Intensities of the $1_{1,1}$-$0_{0,0}$ and $2_{0,2}$-$1_{0,1}$ rotational transitions of the 2-furanyloxy radical as a function of the pyrolysis source temperature.

Future Work

(1) Single-conformation spectroscopy of alkylnaphthalenes and dianthracylethanes.
(2) Pyrolysis of syringol using mass-correlated, broadband microwave spectroscopy.
(3) Incorporation and initial testing of CP-FTMW/ VUV TOFMS as a tool for characterizing highly oxygenated intermediates from a stirred flow reactor, in collaboration with Nils Hansen.

Publications acknowledging DOE support, 2015-present

1. Jacob C. Dean, Nicole L. Burke, John R. Hopkins, James G. Redwine, P.V. Ramachandran, Scott A. McLuckey, and Timothy S. Zwier, "UV Photofragmentation and IR Spectroscopy of Cold, G-type β-O-4 and β–β Dilignol-Alkali Metal Complexes: Structure and Linkage-Dependent Photofragmentation", J. Phys. Chem. A **119,** 1917-32 (2015).

2. Daniel P. Tabor, Daniel M. Hewett, Sebastian Bocklitz, Joseph A. Korn, Anthony J. Tomaine, Arun K. Ghosh, Timothy S. Zwier, and Edwin L. Sibert III, "Anharmonic modeling of the conformation-specific IR spectra of ethyl, n-propyl, and n-butylbenzene", J. Chem. Phys. **144**, 224310 (2016).

3. Nathanael M. Kidwell, Deepali N. Mehta-Hurt, Joseph A. Korn, and Timothy S. Zwier, "Infrared and Electronic Spectroscopy of Jet-cooled 5-methyl-2-furanylmethyl Radical derived from the Biofuel 2,5-Dimethylfuran", J. Phys. Chem. A **120**, 6434-43 (2016).

4. A.O. Hernandez, Chamara Abeysekera, Brian M. Hays, and Timothy S. Zwier, "Broadband Multi-resonant Strong Field Coherence Breaking as a Tool for Single Isomer Microwave Spectroscopy", J. Chem. Phys. **145**, 114203 (2016).

5. Joseph A. Korn, Khadija Jawad, Daniel P. Tabor, Edwin L. Sibert III, and Timothy S. Zwier, "Conformation-specific Spectroscopy of Alkylbenzyl Radicals: α-ethylbenzyl and α−propylbenzyl radicals", J. Chem. Phys. **145**, 124314 (2016).

6. Alicia O. Hernandez-Castillo, Chamara Abeysekera, Brian M. Hays, Isabelle Kleiner, Ha Vinh Lam Nguyen, and Timothy S. Zwier, "Conformational Preferences and Internal Rotation of Methyl Butyrate by Microwave Spectroscopy", J. Mol. Spec. **337**, 51-58 (2017).

7. Daniel M. Hewett, Sebastian Bocklitz, Daniel P. Tabor, Edwin L. Sibert III, Martin Suhm, and Timothy S. Zwier, "Identifying the First Folded Alkylbenzene via Ultraviolet, Infrared, and Raman Spectroscopy of Pentylbenzene through Decylbenzene", Chem. Sci. **8**, 5305-18 (2017).

8. Daniel M. Hewett, Daniel P. Tabor, Joshua L. Fischer, Edwin L. Sibert III, and Timothy S. Zwier, "Infrared-Enhanced Fluorescence-Gain Spectroscopy: Conformation-Specific Excited-State Infrared Spectra of Alkylbenzenes", J. Phys. Chem. Lett. **8**, 5296-5300 (2017).

9. Piyush Mishra, Daniel M. Hewett, and Timothy S. Zwier, "Conformational Explosion: Understanding the complexity of short chain para-dialkylbenzene potential energy surfaces", (submitted).

10. Sean M. Fritz, A.O. Hernandez-Castillo, Chamara Abeysekera, Brian M. Hays and Timothy S. Zwier, "Conformer-specific Microwave Spectroscopy of 3-Phenyl propionitrile by Strong Field Coherence Breaking", (submitted).

11. Chamara Abeysekera, A.O. Hernandez-Castillo, John Stanton, and Timothy S. Zwier, Broadband Microwave Spectroscopy of 2-Furanyloxy Radical: Primary Pyrolysis Product of 2-Methoxyfuran, (submitted).

12. A.O. Hernandez-Castillo, Chamara Abeysekera, Sean M. Fritz, and Timothy S. Zwier, "Mass-correlated CP-FTMW spectroscopy: Structural characterization of the Phenoxy Radical", (submitted).

Participant List

38th Annual Gas Phase Chemical Physics Research Meeting
Participant List

Last Name	First Name	Organization	Email_Address
Ahmed	Musahid	Lawrence Berkeley National Laboratory	mahmed@lbl.gov
Allendorf	Sarah	Sandia National Laboratories	swallen@sandia.gov
Anderson	Scott	University of Utah	anderson@chem.utah.edu
Bellan	Josette	California Institute of Technology	Josette.Bellan@jpl.nasa.gov
Chandler	David	Sandia National Laboratories	chand@sandia.gov
Chen	Jacqueline	Sandia National Laboratories	jhchen@sandia.gov
Continetti	Robert	UC San Diego	rcontinetti@ucsd.edu
Dahms	Rainer	Sandia National Laboratories	rndahms@sandia.gov
Davis	Michael	Argonne National Laboratory	davis@tcg.anl.gov
Davis	Floyd	Cornell University	hfd1@cornell.edu
Douberly	Gary	University of Georgia	douberly@uga.edu
Ellison	Barney	CU Boulder	barney@jila.colorado.edu
Field	Robert	MIT	rwfield@mit.edu
Frank	Jonathan	Sandia National Laboratories	jhfrank@sandia.gov
Garrett	Bruce	DOE/BES	bruce.garrett@science.doe.gov
Green	William	MIT	whgreen@mit.edu
Hansen	Nils	Sandia National Laboratories	nhansen@sandia.gov
Harding	Lawrence	Argonne National Laboratory	harding@anl.gov
Hwang	Robert	Sandia National Laboratories	rqhwang@sandia.gov
Jasper	Ahren	Argonne National Laboratory	ajasper@anl.gov
Jenk	Cynthia	Argonne National Laboratory	cjenks@anl.gov
Kaiser	Ralf I.	University of Hawaii at Manoa	ralfk@hawaii.edu
Kirchhoff	William	DOE (Retired)	william.kirchhoff@att.net
Kliewer	Christopher	Sandia National Laboratories	cjkliew@sandia.gov
Klippenstein	Stephen	Argonne National Laboratory	sjk@anl.gov
Krause	Jeffrey	DOE/BES	Jeff.Krause@science.doe.gov
Laufer	Allan	NIST	allan.laufer@nist.gov
Leone	Stephen	Lawrence Berkeley National Laboratory/UC Berkeley	srl@berkeley.edu

Lester	Marsha	University of Pennsylvania	milester@sas.upenn.edu
Lucht	Robert	Purdue University	lucht@purdue.edu
Mazziotti	David	The University of Chicago	damazz@uchicago.edu
Najm	Habib	Sandia National Laboratories	hnnajm@sandia.gov
Nesbitt	David	JILA/University of Colorado	djn@jila.colorado.edu
Neumark	Daniel	Lawrence Berkeley National Laboratory/UC Berkeley	dneumark@berkeley.edu
Neuscamman	Eric	UC Berkeley	eneuscamman@berkeley.edu
Osborn	David	Sandia National Laboratories	dlosbor@sandia.gov
Parker	James	U.S. Army Research Office	james.k.parker30.civ@mail.mil
Pepiot	Perrine	Cornell University	pp427@cornell.edu
Pitz	William	Lawrence Livermore National Laboratory	pitz1@llnl.gov
Pratt	Stephen	Argonne National Laboratory	stpratt@anl.gov
Prozument	Kirill	Argonne National Laboratory	prozument@anl.gov
Ramasesha	Krupa	Sandia National Laboratories	kramase@sandia.gov
Reisler	Hanna	University of Southern California	reisler@usc.edu
Ruscic	Branko	Argonne National Laboratory	ruscic@anl.gov
Shepard	Ron	Argonne National Laboratory	shepard@tcg.anl.gov
Sheps	Leonid	Sandia National Lab	lsheps@sandia.gov
Sisk	Wade	DOE/BES	wade.sisk@science.doe.gov
Sivaramakrishnan	Raghu	Argonne National Laboratory	raghu@anl.gov
Stanton	John	University of Florida	jfstanton@gmail.com
Taatjes	Craig	Sandia National Laboratories	cataatj@sandia.gov
Tranter	Robert	Argonne National Laboratory	tranter@anl.gov
Wagner	Al	Argonne National Laboratory	wagner@anl.gov
Wilson	Kevin	Lawrence Berkeley National Laboratory	krwilson@lbl.gov
Zádor	Judit	Sandia National Laboratories	jzador@sandia.gov
Zwier	Timothy	Purdue University	zwier@purdue.edu